Identification of novel roles for the survival motor neuron (Smn) protein: implications on spinal muscular atrophy (SMA) pathogenesis and therapy

Melissa Bowerman

Thesis submitted to the Faculty of Graduate and Postdoctoral Studies in partial fulfillment of the requirements for the Ph.D. degree in Cellular and Molecular Medicine

Department of Cellular and Molecular Medicine

Faculty of Medicine

University of Ottawa

AUTHORIZATION

Table 1.1: License number (John Wiley and Sons): 2777091075798

Figure 1.1: License number (Nature Publishing Group): 2777100808504

Chapter 2: License number (Springer): 2767680639228

Chapter 3: License number (Elsevier): 2794830879257

Chapter 4: License number (Elsevier): 2767681159744

Chapter 5: License number (Oxford University Press): 2767681466415

Chapter 6: © Melissa Bowerman

Chapter 7: License number (John Wiley and Sons): 2882550407043

ABSTRACT

Spinal muscular atrophy (SMA) is the leading genetic cause of death of young children. It is an autosomal recessive disease caused by the mutation and/or the deletion within the ubiquitously expressed survival motor neuron 1 (*SMN1*) gene. SMA pathology is characterized by spinal cord motor neuron degeneration, neuromuscular junction (NMJ) defects and muscular atrophy. Upon disease onset, SMA patients progressively become paralyzed and in the most severe cases, they die due to respiratory complications. Over the years, it has become clear that SMN is a multi-functional protein with important roles in small nuclear ribonucleoprotein (snRNP) assembly, RNA metabolism, axonal outgrowth and pathfinding, mRNA transport as well as in the functional development of NMJs, skeletal muscle and cardiac muscle. However, it remains unclear which of these functions, and the respective perturbed molecular pathways, dictate SMA pathogenesis. Here, we have established Smn-depleted PC12 cells and an intermediate SMA mouse model to characterize a role for Smn in the regulation of actin cytoskeleton dynamics. We find that Smn depletion results in the increased expression of profilin IIa and active RhoA (RhoA-GTP) as well as the decreased expression of plastin 3 and Cdc42. Importantly, the inhibition of rho-kinase (ROCK), a direct downstream regulator of RhoA, significantly increased the lifespan of SMA mice and shows beneficial potential as a therapeutic strategy for SMA. In an addition, we have uncovered a muscle- and motor neuron-independent role for SMN in the regulation of pancreatic development and glucose metabolism in SMA mice and type 1 SMA patients. This finding highlights the importance of combining a glucose tolerance assessment of SMA patients with their existing clinical care management. Thus, our work has uncovered two

novel and equally important roles for the SMN protein, both of which contribute significantly to SMA pathogenesis.

TABLE OF CONTENTS

LIST OF TABLES

LIST OF FIGURES

CHAPTER 7: SMA is associated with defects in glucose metabolism and pancreatic development

CHAPTER 8: General discussion

LIST OF ABBREVIATIONS

AAL; adductor auris longus
AchR: acethylcholine receptor
AD: Alzheimer's disease
α-COP: alpha subunit of the coat protein 1
Arx: aristaless-related homeobox
AS: auricularis superior
AUC: area under the curve
BTX: alpha-bungarotoxin
Cdc42: cell division control protein 42 homolog
CNS: central nervous system
COP1: coat protein 1
cpg15: candidate plasticity-related gene 15
Dnmt1: DNA methyltransferase 1
E: embryonic day
EGFP: enhanced green fluorescent protein
EP: endplate
F-actin: filamentous actin
FBS: fetal bovine serum
FL: full-length
FMRP: fragile X mental retardation protein
G-actin: monomeric actin
GAPs: GTPase-activating proteins
GAP-43: growth associated protein 43
GAPDH: glyceraldehyde-3-phosphate dehydrogenase
GcgR: glucagon receptor
GDIs: guanine nucleotide dissociation inhibitors
GDP: guanosine-5'-diphosphate
GEFs: guanine nucleotide exchange factors
Gems: gemini of coiled bodies
GFP: green fluorescent protein
GST-PBD: (gluthathione S-transferase)-(Rac/Cdc42 p21 activated kinase 1 protein binding domain)
GST-RBD: (gluthathione S-transferase)-(Rho-GTP Rhotekin binding domain)
GTP: guanosine-5'-triphosphate
HD: Huntington's disease
HDAC: histone deacetylase
H&E: hematoxylin and eosin
hnRNP: heterogeneous nuclear ribonucleoprotein
HS: horse serum
hSMN: human survival motor neuron protein
htt: huntingtin
IGF1: insulin-like growth factor 1

IPGTT: intraperitoneal glucose tolerance test
Islet-1: insulin gene enhancer binding protein 1
KGRs: kainate glutamate receptors
K-rich: rich in lysine residues
KSRP: KH-type splicing regulatory protein
LALc: levator auris longus caudal band
LALr: levator auris longus rostral band
LIMK: LIM kinase
Lum: deep lumbricals
MLC: myosin light chain
NF: neurofilament
NGF: nerve growth factor
NLS: nuclear localization signal
NMJ: neuromuscular junction
N-WASP: neuronal Wiskott–Aldrich Syndrome protein
P: post-natal day
p-: phosphorylated
pII: profilin II
PAK5: p21-activated kinase 5
Pax4: paired box protein 4
Pax6: paired box protein 6
Pdx1: pancreatic and duodenal homeobox 1
PFA: paraformaldehyde
Pfn2: profilin 2
PI3K: phosphatidylinositol-3-kinase
P-rich: rich in proline residues
PRMT: protein arginine methyltransferase
PTEN: phosphatase and tensin homolog
Rac1: Ras-related C3 botulinum toxin substrate 1
RhoA: Ras homolog gene family, member A
ROCK: rho-kinase
SC: spinal cord
sc-AAV9: self-complimentary adeno-associated virus 9
shRNA: short-hairpin RNA
SMA: spinal muscular atrophy
SMN: survival motor neuron
SMNΔ7: SMN protein lacking exon 7
snoRNP: small nucleolar ribonucleoproteins
snRNA: small nuclear RNA
snRNP: small nuclear ribonucleoprotein
SV2: synaptic vesicle 2
T2DM: type 2 diabetes mellitus
TA: tibialis anterior
TGS1: trimethylguanosine synthetase 1

TrKA: tyrosine kinase receptor type 1
TSA: trichostatin A
TVA: transversus abdominis
U snRNP: uridine-rich small nuclear ribonucleoprotein
UTR: untranslated region
WT: wild type
YG box: tyrosine-glycine sequence

ACKNOWLEDGEMENTS

I would like to firstly thank my supervisor, Dr. Rashmi Kothary, for his continual support, guidance, motivation and mentorship throughout the years. He has taught me to work honestly and with intent, to respect everyone's individualities and to be satisfied with all results, because in the end, they do provide us with an answer to our question. Importantly, he has always been supportive of my decision to have children during my Ph.D. studies, thus allowing me pursue both my scientific career and the establishment of a family. This has allowed me to become the researcher and the person that I am today. THANK YOU!

I am also grateful to my colleagues, many of whom have become friends, who have constantly encouraged and challenged me to become a better researcher as well as made our laboratory an amazing workplace: Carrie Anderson, Ariane Beauvais, Kunal Bhanot, Justin Boyer, Dr. Patrice Cote, Yves De Repentigny, Andrew Ferrier, Sabrina Gibeault, Dr. James Knight, Samantha Kornfeld, Dr. Karen Lee, Dr. Hong Liu, John-Paul Michalski, Dr. Lyndsay Murray, Ryan O'Meara, Bruno Pinheiro, Dr. Madeline Pool, Dr. Scott Ryan, Dr. Tadasu Sato, Dr. Dina Shafey, Armin Yazdani and Dr. Kevin Young.

I would also like to thank the members of my thesis advisory committee who have helped tremendously in the guidance of my project: Drs. Valerie Wallace, Jocelyn Cote and Antonio Colavita.

I am grateful to the following funding agencies for supporting me during my graduate studies: Ontario Graduate Scholarship in Science and Technology and Canadian Institutes of Health Research.

Last but not least, I want to express my gratitude toward my partner, Geoff, and our two beautiful children Olivia and Alexandre. They are the best thing in my life and make me a better person, and thus a better researcher.

CHAPTER 1: General Introduction

SPINAL MUSCULAR ATROPHY

Spinal muscular atrophy (SMA) is the most common genetic disease resulting in infant death, affecting approximately 1 in 6000-10 000 births (Pearn 1978a; Crawford et al. 1996). It is an autosomal recessive disease characterized by severe loss of α-motor neurons in the spinal cord and muscular atrophy of the limbs and trunk leading to paralysis and ultimately death (Crawford et al. 1996).

SMA is a clinically heterogeneous disease and the various types are classified based on age of onset and severity of symptoms (**Table 1.1**). Type 0 SMA has a prenatal onset and is characterized by reduced fetal movements *in utero* and early neonatal death (Dubowitz 1999; MacLeod et al. 1999). Types I, II and III are the most common and share a childhood onset (Pearn 1980; Munsat et al. 1992). Type I SMA (Werdnig-Hoffmann disease), the most severe form, afflicts patients before 6 months of age. These type I patients are never able to sit up and usually die before 2 years of age due to respiratory distress. Patients with the milder forms type II and type III SMA (Kugelberg-Welander disease), exhibit SMA symptoms between 6 months and 17 years of age. Type II children are generally able to stand and sit but not walk, while type III individuals have the ability to walk if aided. Finally, type IV SMA is characterized by an adult onset of the disease where patients develop symptoms after the age of 30 (Pearn 1978a).

Table 1.1 Diagnostic features in the classification of spinal muscular atrophy

Table 1. Diagnostic features in the classification of spinal muscular atrophy

Type	Age at onset	Motor abilities
0	Prenatal onset	Reduced fetal movements *in utero*; some degree of spontaneous ventilation and movement at birth
I	At birth or <6 months	Never able to sit
II	<18 months	Unable to stand or walk unaided
III	>18 months	Able to walk unassisted
IV	Adult onset	Mild proximal muscle weakness

ETIOLOGY OF SPINAL MUSCULAR ATROPHY

SMA is a monogenic disease resulting from the loss-of-function of the survival motor neuron 1 (*SMN1*) gene located on human chromosome 5q13 (Lefebvre et al. 1995). The genomic sequence covers 27 kilobases (kb) and encodes a 17 kb transcript consisting of 9 exons (Burglen et al. 1996) (Lefebvre et al. 1995; Chen et al. 1998). Approximately 95% of SMA cases are due to homozygous deletions of exon 7 and/or exon 8 of *SMN1* (Wirth 2000). The remaining 5% of SMA occurrences are due to rare homozygous mutations that range from nonsense, frameshift, splice site and missense mutations (reviewed in (Wirth 2000)). While these mutations span the entire gene, the majority can be found within exons 6 and 7, a highly conserved region responsible for the self-oligomerization of the SMN protein (Hahnen et al. 1997; Talbot et al. 1997; Lorson et al. 1998b; Wirth et al. 1999).

SMN1 is highly conserved and almost all eukaryotic organisms studied to date contain a single copy of the gene (Bergin et al. 1997; Miguel-Aliaga et al. 1999; Miguel-Aliaga et al. 2000; Paushkin et al. 2000). Interestingly, a recent genomic duplication that occurred prior to the divergence of humans and chimpanzees has given rise to a second gene exclusively in humans, termed *SMN2* (Lefebvre et al. 1995; Rochette et al. 2001). The two genes have identical promoter regions and their genomic sequences are 99% identical, differing only by 5 nucleotides (Monani et al. 1999a; Monani et al. 1999b; Boda et al. 2004). Of these substitutions, a critical difference lies at position 6 of exon 7, where a C to T substitution in *SMN2* leads to the aberrant splicing of exon 7 (Lorson et al. 1999; Monani et al. 1999a). The alternative splicing of exon 7 and the subsequent production of an unstable SMNΔ7 protein is caused by the loss of an

exon splicing enhancer and/or the gain of an exon splicing silencer (Lefebvre et al. 1995; Cartegni et al. 2002; Kashima et al. 2003). Thus, the telomeric *SMN1* copy expresses the full-length SMN protein while the centromeric *SMN2* copy predominantly produces the SMNΔ7 protein (Gennarelli et al. 1995; Lefebvre et al. 1995). Deletions or mutations in *SMN1* but not *SMN2* cause all forms of SMA, however *SMN2* can modulate the severity of the disease through its copy number (Lefebvre et al. 1995). Indeed, patients affected by the milder forms of SMA generally have a higher copy number of *SMN2* (Lefebvre et al. 1997).

SMA ANIMAL MODELS

Various neuronal, muscle, fibroblast and immortalized cellular models have been used to characterize the functions of SMN in SMA pathogenesis. However, the generation of SMA animal models has been of irrefutable value for the understanding of how SMN depletion affects the *in vivo* function of interacting cells and tissues. SMA has been modeled in invertebrates such as *Caenorhabditis elegans* (Briese et al. 2009) and *Drosophila melanogaster* (Chan et al. 2003). Through the use of antisense morpholino technology, the Smn protein has been knocked down in zebrafish, a small vertebrate in which motor neuron development is well characterized and can be easily visualized (McWhorter et al. 2003). The most common used SMA models however have been generated in mice. The complete knockout of murine Smn ($Smn^{-/-}$) is embryonic lethal, highlighting its requirement for survival (Schrank et al. 1997). The heterozygous mouse ($Smn^{+/-}$) however, only displays minor motor neuron loss, which does not impact their reproductive ability or lifespan (Jablonka et al. 2000). In an attempt to generate a more severe mouse model, mice harboring two copies of the human *SMN2* BAC transgene were

backcrossed onto the *Smn* null background (*Smn*$^{-/-}$*;SMN2*) (Hsieh-Li et al. 2000; Monani et al. 2000b). This not only rescued the early embryonic lethality of the *Smn*$^{-/-}$ mice but also resulted in severe SMA mice that die within the first postnatal week. Due to its disease severity and short lifespan, the *Smn*$^{-/-}$*;SMN2* mouse model often makes it difficult to investigate developmental roles for the Smn protein as well as the potential of therapeutic strategies. Subsequently, transgenic mice expressing the SMNΔ7 protein were crossed onto the *Smn*$^{-/-}$*;SMN2* background to generate a new SMA mouse model (*Smn*$^{-/-}$*;SMN2;SMNΔ7/SMNΔ7)* that while retaining a severe phenotype, has an extended lifespan of approximately 14 days (Le et al. 2005). Both of these mouse models (commonly termed severe and *SMNΔ7*) have been extensively used as representations of type I SMA. Recent efforts have thus focused on generating animal models that would better reflect types II and III SMA. Interestingly, mimicking the human *SMN2* gene by creating a C to T substitution within the murine *Smn* gene (*Smn C>T*) lead to a mouse with a very mild pathology, corresponding to a type III/type IV SMA model (Gladman et al. 2010). This mild effect of the C to T mutation is consistent with a previous report showing that the alternative splicing of the *Smn C>T* minigene was significantly less pronounced than a construct harboring a substitution of 3 nucleotides in the exon splicing enhancer of exon 7 (*Smn2B*) (DiDonato et al. 2001). The *Smn2B* allele containing a loxP-flanked neomycin selection cassette was recently used to establish an inducible mouse model where Smn expression can be dictated by Cre recombinase (Hammond et al. 2010). Thus, while attempts were made, there remains a gap in mouse models representing types II and III SMA. Nevertheless, the existing mouse models, in combination with the other various animal and cellular models, have been invaluable in deciphering the many roles of the SMN protein.

UNCOVERING THE ROLE OF SMN IN SMA PATHOGENESIS

Smn protein localization and expression patterns

The term ubiquitous is often used to characterize the expression of the SMN protein. Indeed, the SMN protein localizes in the cytoplasm (Liu et al. 1996), neuronal growth cones (Fan et al. 2002), neuronal extensions (Fallini et al. 2010), the nucleolus (Charroux et al. 2000; Wehner et al. 2002), and in punctate nuclear structures called Gemini of coiled bodies (Gems) (Liu et al. 1996). However, upon detailed investigation, it has become clear that levels of SMN are controlled in a tissue- and temporal-specific manner. An immunoblot analysis of human tissues suggests that spinal cord, brain, liver and kidney express more SMN protein than fibroblasts, lymphocytes, skeletal and cardiac muscle (Coovert et al. 1997). A more recent report shows that while Smn mRNA and protein are present throughout mouse embryogenesis, their expression levels are significantly higher in the developing nervous system (Liu et al. 2010b). Similarly, investigation of the developing human forebrain identified a specific expression pattern of the SMN protein that was stronger in younger fetal brains than older ones (Briese et al. 2006). This temporal-change is consistent with data showing high levels of Smn protein in embryonic mouse spinal cord followed by a sudden decrease postnatally (Jablonka et al. 2000). It also appears that the cellular localization of SMN is developmentally regulated. Indeed, while SMN is found in the human central nervous system (CNS) as early as 6 weeks of embryogenesis, its localization in motor neurons temporally shifts from nuclear to cytoplasmic to axonal (Giavazzi et al. 2006). Thus, although at first glance it seems that SMN is ubiquitously expressed, the temporal expression and subcellular localization are actually tightly regulated, suggesting multiple roles for the SMN protein.

Functional domains of the SMN protein

The full-length SMN protein is 38 kDa in size (Liu et al. 1996) and contains various well-described functional domains (**Figure 1.1**). Exons 2a and 2b encode a region rich in lysine residues (K-rich) that plays a role in the binding of nucleic acids (Lorson et al. 1998a). Individually, the region encoded by exon 2b is important for both self-oligomerization and the interaction with Gemin2, a protein essential for the assembly of spliceosomal uridine-rich small nuclear ribonucleoproteins (U snRNPs) (Fischer et al. 1997; Young et al. 2000b) and contains a putative nuclear localization signal (NLS) (DiDonato et al. 1997). A Tudor domain is encoded by exon 3, which is responsible for the interaction of the SMN protein with Sm proteins, key players in the assembly of U snRNPs (Mattaj 1988; Buhler et al. 1999). Exon 5 and a portion of exon 6 encode a proline-rich (P-rich) domain that mediates the interaction of SMN with profilin (Giesemann et al. 1999; van Bergeijk et al. 2007), a small actin-binding protein. The C-terminus of the region encoded by exon 6 contains an additional self-association domain (Lorson et al. 1998b) and a triplicated tyrosine-glycine sequence (YG box) (Talbot et al. 1997), important for mRNA metabolism. Finally, the region encoded by exon 7 contains a cytoplasmic targeting signal (Zhang et al. 2003).

While the functional domains within the SMN protein have been extensively studied, their implication in SMA pathogenesis remains unclear. Le *et al*. (Le et al. 2000) addressed this question through the generation of various mutated SMN constructs that were subsequently transfected in COS-7 cells and human type I SMA fibroblasts. They showed that loss of exon 7 resulted in a reduced number of Gems, nuclear structures that are composed of SMN protein (Liu

et al. 1996). On the other hand, the deletions of the amino-terminal and exon 2a, as well as the exon 6 Y272C mutation, all lead to increased nuclear SMN accumulation. Interestingly, constructs containing exon 5 and exon 2 NLS deletions, as well as the exon 7 G279V mutation, did not have SMN localization defects. The combined deletion of exons 5 and 7, however, significantly reduced Gem numbers and increased cytoplasmic SMN content. In Smn-depleted zebrafish models, the conserved QNQKE region within exon 7, which is disrupted by the G279V mutation, was essential for normal neuronal outgrowth (Carrel et al. 2006). Thus, it appears that the domains of the SMN protein dictate its multi-functionality and makes the identification of the specific pathway responsible for the distinct SMA pathology that much more difficult to decipher.

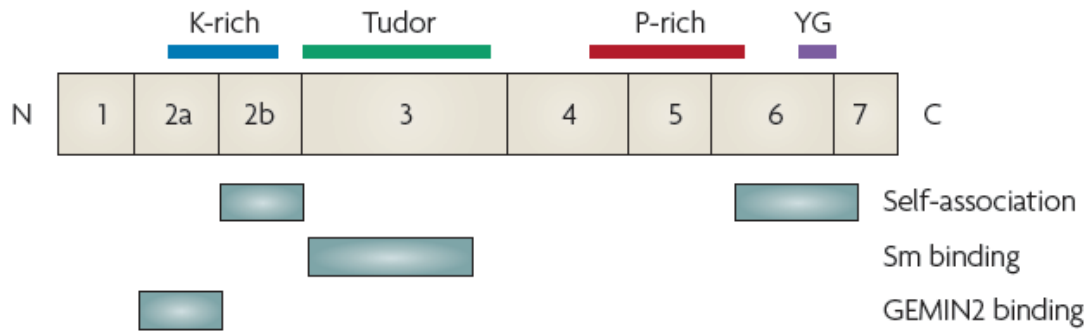

Figure 1.1 A diagram of SMN showing the exons and domains. Exon 2b encodes a domain that is important in binding Gemin 2, as well as for self-association. Both exon 2a and 2b are conserved. The K domain is rich in lysine (K-rich) and there is a Tudor domain in exon 3 that binds Sm proteins and has homology to other Tudor domains. Exon 5 and part of exon 6 contain a proline-rich (P-rich) domain that may influence profilin binding. The C-terminal domain of exon 6 contains the conserved YG box and is important for self-association.

SMN: a multifunctional protein

SMN's housekeeping role: regulation of RNA metabolism

In various cell types, the SMN protein is localized in Gems (Liu et al. 1996), punctate nuclear structures thought to mediate the cytoplasmic assembly of small nuclear ribonucleoproteins (snRNPs) (Paushkin et al. 2002). SnRNPs are the major components of the spliceosome responsible for the removal of intronic sequences from immature mRNAs (Will et al. 2001). In nuclear Gems, the SMN protein interacts with itself, Gemin2-8, Unrip and Sm proteins (Paushkin et al. 2002; Carissimi et al. 2006). This multiprotein complex mediates the cytoplasmic assembly and nuclear import of snRNPs (Paushkin et al. 2002). The Tudor domain of SMN regulates snRNP biogenesis by associating with and forming a heptameric Sm protein ring, which will subsequently interact with the Sm binding sites of specific snRNAs (Liu et al. 1997; Buhler et al. 1999; Meister et al. 2001a; Jae et al. 2011). To avoid non-specific activity of Sm proteins in the cytoplasm, they are bound to the chaperone plCLn and methylated by the protein arginine methyltransferase (PRMT) 5 and 7 (Meister et al. 2001b; Gonsalvez et al. 2007; Chari et al. 2008). SMN binds PRMT5 following the release of the methylated Sm proteins (Chari et al. 2008; Shafey et al. 2010). The SMN protein also recruits and docks trimethylguanosine synthetase 1 (TGS1), which is responsible for the 5'-cap hypermethylation of the snRNAs (Mouaikel et al. 2002; Mouaikel et al. 2003). The hypermethylation of snRNAs is required for the subsequent binding to importin-ß and snuportin, allowing for the nuclear import of the assembled and active snRNPs (Narayanan et al. 2002; Narayanan et al. 2004). Once in the nucleus, the SMN complex and snRNPs localize to Cajal bodies and/or Gems for further snRNP

maturation (Liu et al. 1996; Matera et al. 2007). Thus, the SMN protein modulates multiple crucial steps for efficient and correct snRNP biogenesis.

Given the various functional interactions between SMN and components of snRNP assembly, it has been hypothesized that Smn depletion may lead to inadequate snRNP biogenesis, and thus defects in mRNA processing. Indeed, defects in snRNP synthesis have been observed in human SMA fibroblasts (Wan et al. 2005), SMA vertebrate models (Winkler et al. 2005; Gabanella et al. 2007) and in cellular models expressing human SMN mutants (Pellizzoni et al. 1999). Disease severity in SMA mice correlate with snRNP assembly activity and a subset of UsnRNPs is specifically affected by Smn depletion (Gabanella et al. 2007). In zebrafish, the injection of purified snRNPs rescued the axonal outgrowth and pathfinding defects observed in Smn-depleted animals (Winkler et al. 2005). These studies suggest that defective snRNP assembly may indeed be responsible for SMA pathogenesis. However, a more recent study in zebrafish showed that while the expression of SMN mutants resulted in aberrant axonal morphology, they did not influence snRNP biogenesis (Carrel et al. 2006). Thus, it still remains unclear what role snRNP assembly defects play in the onset and progression of SMA.

Since snRNPs are key components of the spliceosome (Will et al. 2001), it has been hypothesized that SMA may result from inappropriate splicing of one or several mRNAs. This theory was first introduced by Pellizzoni *et al*. in an *in vitro* assay when they demonstrated that wild type SMN stimulates pre-mRNA splicing while human SMN mutants inhibited it (Pellizzoni et al. 1998). In a more recent study, analysis of brain, spinal cord and kidney tissues of SMA mice revealed that Smn deficiency causes large-scale tissue-specific pre-mRNA splicing

defects (Zhang et al. 2008). Similarly, an increase in general splicing defects was observed in fibroblasts from SMA patients (Fox-Walsh et al. 2009). These studies however were performed in models reflecting the later stages of disease progression. Baumer *et al*. thus evaluated pre-symptomatic SMA mice and found that they were devoid of any mRNA abnormalities (Baumer et al. 2009). The authors also show that the number of splicing defects increased as the disease progressed (Baumer et al. 2009). This study therefore suggests that defective mRNA splicing may be a secondary effect of SMN depletion and the subsequent cellular breakdown. While the resulting aberrantly spliced transcripts may indeed impact disease severity and or progression, no causal link has presently been made between these targets and SMA pathogenesis.

Although *SMN* is best described as a housekeeping gene that controls snRNP assembly and mRNA splicing, several reports suggest that SMN may serve other functions in the regulation of RNA metabolism. Indeed, the SMN protein associates with RNA helicase A and RNA polymerase II, implying that it may also modulate the transcription machinery (Pellizzoni et al. 2001b). In addition, SMN localizes within the nucleolus (Lefebvre et al. 2002; Wehner et al. 2002), interacting with the small nucleolar ribonucleoproteins (snoRNPs) GAR1 and fibrillarin (Jones et al. 2001; Pellizzoni et al. 2001a; Wehner et al. 2002), which are responsible for the processing of ribosomal RNAs (rRNAs) (Tyc et al. 1989; Girard et al. 1992). SMN also associates with the non-ribosomal nucleolar proteins, nucleolin and B23, both multifunctional with roles in rRNA processing. Thus, it appears that SMN may have a distinct nucleolar role in addition to its better-known functions in snRNP assembly and mRNA splicing. However, more in-depth investigations are required to better understand how the involvement of SMN in the nucleolus impacts SMA pathogenesis.

The above-mentioned roles for the SMN protein are ubiquitous and control the general pathways that maintain the normal functioning of all cells. Although extensively studied, none of these housekeeping functions, and their subsequent loss upon SMN depletion, explains the specific loss of spinal cord motor neurons that typifies SMA. There has been therefore a surge in studies examining the role of SMN specifically in neuronal cells as well as in various SMA-afflicted tissues and compartments.

A neuronal-specific role for SMN in axonal outgrowth and pathfinding

Identifying where SMN is localized in neuronal cells is a crucial step to better understand its intrinsic role in motor neurons. Smn is found in growth cones of differentiating mouse embryonal teratocarcinoma P19 cells (Fan et al. 2002). In primary neuronal cells isolated from embryonic chick forebrain and rat spinal cord, Smn localizes in granules within neurites and growth cones (Zhang et al. 2003). Interestingly, Smn expression significantly increases upon differentiation of murine neurosphere-derived neural stem cells and neuronal-like PC12 cells (van Bergeijk et al. 2007; Shafey et al. 2008). The localization and expression patterns of SMN in differentiating neuronal cells thus imply a possible role in axonal outgrowth and pathfinding.

In support of a role for SMN in axonal outgrowth, Zhang et al. showed that the cytoplasmic localization of Smn is dictated by exon 7 and that expressing a SMNΔ7 construct in neuronal cells resulted in significantly shorter neurites (Zhang et al. 2003). Smn-depleted zebrafish display severe defects in motor neuron-specific axonal growth, pathfinding and branching (McWhorter et al. 2003). Indeed, other neuronal cell types, such as interneurons and sensory neurons, were spared of any morphological defects, suggesting that motor neurons may

be more sensitive to SMN depletion (McWhorter et al. 2003). Neuronal outgrowth defects have also been observed in Smn-depleted PC12 cells and primary mouse motor neurons (Rossoll et al. 2003; van Bergeijk et al. 2007). A significant reduction in growth cone size accompanied the inability of the primary mouse motor neurons to differentiate normally (Rossoll et al. 2003). Collectively, these findings suggest that SMA pathogenesis may stem from a motor neuron-specific failure to differentiate and reach an appropriate target. However, the data from the SMA mouse models are contradictory. Analysis of embryonic day (E) 10.5 severe SMA mice showed abnormal morphology and truncation of the cranial and lumbar spinal nerves, respectively (Liu et al. 2010b). On the other hand, work from another group was unable to identify any axonal outgrowth, formation or branching defects in E10.5 to post-natal day (P) 3 severe mice (McGovern et al. 2008). Thus, it remains unclear if SMN's role in neurodevelopment is at the source of SMA pathology. Furthermore, the specific axonal outgrowth and pathfinding molecular pathways regulated by SMN have yet to be identified and are of utmost importance for our understanding of SMN's neuronal-specific function.

SMN's role in axonal transport of mRNAs

Seeing that SMN localizes in neuronal extensions and in growth cones, it has been suggested that SMN may modulate axonal transport. Bechade *et al*. were the first to visualize, using fluorescence and electron microscopy, Smn in dendrites of rat spinal cord samples (Bechade et al. 1999). They also showed that Smn associates with microtubules and thus suggested a function for SMN in dendritic transport (Bechade et al. 1999). Pagliardini *et al*. also characterized Smn localization in the spinal cord of rats and observed its interaction with

cytoskeletal components in dendrites, axons and axonal terminals (Pagliardini et al. 2000). Their work suggests that SMN may be transported along neuronal extensions and/or participate in the active transport of specific motor neuron mRNAs (Pagliardini et al. 2000). Immunofluorescence analysis further showed that Smn exhibits punctate and granular localization patterns in neurites of rat spinal cord and chick forebrain neurons (Zhang et al. 2003). Live-imaging experiments of chick forebrain neurons transfected with EGFP-SMN constructs substantiated SMN's active transport along neuronal extensions by showing rapid, bi-directional and cytoskeletal-dependent movements (Zhang et al. 2003). A more in-depth investigation of the actively transported Smn granules revealed that they contain Gemin proteins but not Sm proteins (Zhang et al. 2006; Todd et al. 2010b; Todd et al. 2010c), suggesting a function independent of snRNP assembly. Indeed, these SMN transport granules may be responsible for shuttling proteins and/or mRNAs along the axons and delivering them to the growth cones, allowing for normal motor neuron development. This hypothesis is supported by the recent report of Smn's association and co-localization with the α-subunit of the coat protein 1 (α-COP) vesicle coat protein complex within isolated murine motor neurons (Peter et al. 2011). Interestingly, the COP1 complex has been linked to the translation, localization and transport of various mRNAs (de La Vega et al. 1999; Bi et al. 2007). Importantly, the authors demonstrate that α-COP is detected in lamellipodia, growths cones and in active Smn-containing transport granules along the axons (Peter et al. 2011). These findings highlight the importance of understanding SMN's function in axonal transport as it may directly impact SMA onset and/or progression. The recent report of defects in fast anterograde axonal transport in *SMNΔ7* mice indeed suggests that altered axonal transport may underlie SMA pathogenesis (Dale et al. 2011).

One of the first identified and most studied mRNA transported by SMN along neuronal extensions is β-actin. Rossoll *et al*. made the original observation that motor neurons isolated from the severe SMA mouse model displayed decreased β-actin protein and mRNA expression in distal axons and growth cones (Rossoll et al. 2003). They hypothesized that SMN may transport β-actin along the axons via the RNA-binding heterogeneous nuclear ribonucleoprotein R (hnRNP R), which has a recognized role in mRNA processing and transport to the nerve terminal (Dreyfuss et al. 1993; Rossoll et al. 2002; Glinka et al. 2010). Indeed, hnRNP R interacts with both Smn and the 3' UTR of β-actin mRNA (Rossoll et al. 2002; Rossoll et al. 2003). Furthermore, both hnRNP and its association with Smn have been shown to be essential for the accurate axonal translocation of β-actin mRNA to growth cones (Rossoll et al. 2003; Glinka et al. 2010). Smn also associates with KH-type splicing regulatory protein (KSRP) (Tadesse et al. 2008), another β-actin interactor (Gu et al. 2002; Tadesse et al. 2008). The recently described α-COP-Smn interaction also appears to complex with β-actin mRNA (Peter et al. 2011). Although the interactions of SMN with β-actin mRNA described above support a role for SMN in the axonal transport of β-actin mRNA, they occur indirectly via various partners. Recently, a direct interaction between Smn and β-actin mRNA in the cytoplasm of the human neuroblastoma SHS5Y cell line was shown (Todd et al. 2010a). Furthermore, β-actin mRNA in SMN-containing transport granules was identified along the neurites (Todd et al. 2010a). Together, these results indicate that the disruption of β-actin mRNA localization may indeed be pathological and be integral to SMA pathogenesis. Indeed, the recent rescue of neuronal outgrowth and survival of motor neurons isolated from *SMNΔ7* mice via the depletion of phosphatase and tensin homolog (PTEN) was accompanied by the restoration of β-actin mRNA

in the growth cones (Ning et al. 2010). Thus, at the very least, β-actin mRNA localization appears to be a marker of normal neuronal development.

While much attention has been given to SMN's role in β-actin mRNA transport, other mRNAs required at the nerve terminal could also be affected by SMN depletion in the motor neuron. Via mass spectrometry analysis of endogenous Smn co-immunoprecipitates from embryonic cortical neurons, Akten *et al*., have recently identified HuD, a neuron specific RNA-binding protein (Pascale et al. 2004; Hinman et al. 2008), as a novel interacting partner (Akten et al. 2011). One of HuD's targets is the candidate plasticity-related gene 15 (cpg15), which plays a role in motor axon outgrowth, neuromuscular synaptogenesis and anti-apoptosis (Javaherian et al. 2005; Putz et al. 2005). The authors show that cpg15 associates with HuD and Smn (Akten et al. 2011). Importantly, Smn depletion decreases cpg15 mRNA expression while overexpression of cpg15 partially rescued the motor axon defects in Smn-deficient zebrafish (Akten et al. 2011). Although the role of cpg15 in SMA pathogenesis has not fully been established, these results suggest that the axonal transport of various mRNAs other than β-actin may be affected by SMN loss.

A role for SMN in the regulation of actin cytoskeletal dynamics

Since β-actin mislocalization is indeed a phenotype of Smn-depleted neurons, many research groups have further characterized how this impacts the overall regulation of actin cytoskeletal dynamics. Smn depletion in neuronal-like PC12 cells results in increased filamentous (F)-actin at the expense of monomeric (G)-actin (van Bergeijk et al. 2007). In human SHS5Y cells, the mislocalization of the SMN protein, due to the loss of α-COP, increased

the number of F-actin positive filopodia (Peter et al. 2011). Recent work by Nölle *et al*. revealed a similar increase of the F-actin component in primary motor neurons isolated from the severe SMA mice (Nolle et al. 2011). Importantly, this defect was cell-autonomous as primary fibroblasts obtained from SMA patients did not display actin organization abnormalities (Nolle et al. 2011). It therefore appears that the mislocalization of β-actin mRNA subsequently leads to the predominant reorganization of actin into filamentous fibers, thus shifting the dynamic environment of the cell.

In addition to actin itself, various actin regulators are misregulated in Smn-depleted models. Profilin IIa, the neuronal isoform of the *profilin II* gene (Di Nardo et al. 2000; Lambrechts et al. 2000), is a small actin-binding protein and key player in actin dynamics (reviewed in (Birbach 2008)). Profilin IIa interacts with the polyproline motif of the Smn protein in neuronal cellular models (Giesemann et al. 1999; Sharma et al. 2005; Nolle et al. 2011). Importantly, experiments performed in PC12 cells demonstrate that Smn's interaction with profilin IIa regulates actin polymerization by sequestering profilin IIa's negative influence on neurite sprouting and outgrowth (Da Silva et al. 2003; Sharma et al. 2005). Indeed, the neuronal differentiation defects of Smn-depleted PC12 cells were specifically rescued by the exogenous expression of an Smn construct containing the profilin-binding domain (van Bergeijk et al. 2007). Interestingly, a recent report shows that the human SMN S230L mutant abrogates the Smn-profilin IIa association (Nolle et al. 2011). Profilin IIa is also regulated by rho-kinase (ROCK) (Da Silva et al. 2003; Shao et al. 2008), an important upstream regulator of actin cytoskeletal dynamics (reviewed in (Amano et al. 2010)). Nölle *et al*. demonstrate that Smn-depleted PC12 cells display hyperphosphorylation of profilin IIa and hypophosphorylation of

ROCK downstream targets, suggesting that SMN depletion results in increased p-profilin IIa-ROCK interaction and subsequently hyperactivity of ROCK (Nolle et al. 2011). Thus, the above findings imply that SMN may also modulate actin dynamics via its functional interaction with the neuronal-specific profilin IIa.

Plastin 3 (also known as T-plastin or T-fimbrin) is an actin-bundling protein (Glenney et al. 1981; Giganti et al. 2005) that has also been implicated in SMA pathogenesis. Plastin 3 was identified as a positive modifier of SMA in asymptomatic females with symptomatic siblings carrying identical *SMN1* and *SMN2* genotypes (Oprea et al. 2008). These unaffected females displayed significantly higher levels of plastin 3 mRNA and protein in their blood (Oprea et al. 2008). Interestingly, Smn, plastin 3 and actin are found complexed together in the spinal cord of mice (Oprea et al. 2008). Furthermore, the neuronal outgrowth and differentiation defects of Smn-depleted PC12 cells and isolated motor neurons from severe SMA mice were rescued by the overexpression of plastin 3 (Oprea et al. 2008). A recent analysis of a cohort of 88 SMA patients also supports the correlation of plastin 3 expression with disease severity, albeit with a restriction to postpubertal females (Stratigopoulos et al. 2010). However, the study of four Spanish SMA families with discordant siblings did not reveal a significant increase of plastin 3 expression in the asymptomatic females (Bernal et al. 2011). Thus, while the extent of plastin 3's influence on SMA severity requires further investigation, these studies nevertheless further support the hypothesis that misregulated actin dynamics play a role in SMA pathogenesis. The proper control of the actin cytoskeleton is crucial to ensure accurate neuritogenesis, neurite elongation and branching as well as synaptic vesicle organization, mobilization and trafficking (Fifkova et al. 1982; Bray et al. 1985; da Silva et al. 2002; Shupliakov et al. 2002; Sakaba et al.

2003; Dillon et al. 2005; Cingolani et al. 2008). The phenotypic defects that typify SMA cellular and animal models may therefore stem from the misregulation of actin dynamics.

SMN's role in neuromuscular junction (NMJ) development

The NMJ is the contact point between the motor neuron and the muscle, both pathological targets of SMA. A number of recent studies has reported NMJ defects in SMA mouse models, suggesting a role for the SMN protein within this specialized compartment.

On one hand, misregulation of various pre-synaptic effectors has been observed in NMJs of SMA models. Smn-depleted zebrafish display reduced expression of synaptic vesicle 2 (SV2) (Boon et al. 2009), while SMA mouse models show an aberrant accumulation of phosphorylated neurofilament (NF) at the distal axonal innervations (Cifuentes-Diaz et al. 2002; Kariya et al. 2008; Murray et al. 2008; Kong et al. 2009; Ling et al. 2011). Furthermore, innervation of the NMJ is often partial or completely absent (Kariya et al. 2008; Murray et al. 2008; Kong et al. 2009; Ling et al. 2011). While some studies have identified a selective innervation vulnerability of motor axons associated with proximal muscles (Kariya et al. 2008; Kong et al. 2009) and a fast-synapsing phenotype (Murray et al. 2008), a recent in-depth report suggests that innervation state is independent of muscle location and fiber type (Ling et al. 2011). Nevertheless, these studies suggest that SMN plays a role in the pre-synaptic development of NMJs.

On the other hand, postsynaptic NMJ defects are also apparent in SMA models. Motor endplates from SMA mice display an overall immaturity, highlighted by their reduction in size and number of perforations (Kariya et al. 2008; Murray et al. 2008; Kong et al. 2009). Furthermore, the motor endplates of SMA mice express the embryonic acetylcholine receptor

(AchR) subunit instead of the adult AchR subunit, revealing an important developmental delay (Arnold et al. 2004; Kong et al. 2009). SMN depletion therefore also impacts the postsynaptic development of the NMJ. Further investigation will be required to understand whether the pre-synaptic and postsynaptic NMJ defects in SMA are dependent or independent of each other.

The morphological NMJ defects in SMA are further accompanied by functional consequences. Indeed, studies performed in SMA mice show abnormal synaptic transmission, a decreased probability of synaptic vesicle release and intermittent neurotransmission failures (Kariya et al. 2008; Kong et al. 2009). It therefore appears that SMN plays an important part in maintaining the normal function of the NMJ.

Whether the NMJ pathology is a primary or a secondary consequence of SMN loss remains uncertain. Denervation and NF accumulation has been observed in severe and *SMNΔ7* SMA mice prior to overt phenotypic onset and motor neuron loss (Kariya et al. 2008; McGovern et al. 2008). These findings suggest that defective NMJ innervation may be at the root of SMA pathogenesis. In contrast, a study performed in the severe SMA mouse model failed to observe any pre-synaptic or postsynaptic NMJ alterations (Murray et al. 2010b; Ling et al. 2011). The authors therefore discuss a dying-back pathology where the motor axons initially innervate the endplates but eventually retract upon disease progression and motor neuron degeneration (Murray et al. 2010b; Ling et al. 2011). While our understanding of NMJ pathology and how it influences SMA onset and progression requires further investigation, it is evident that at the very least, the NMJ defects in SMA have become a histopathological hallmark of the disease.

A non-neuronal role for SMN in skeletal muscle development

The muscular atrophy that typifies SMA has long been thought of as being a secondary consequence to the primary motor neuron degeneration. Recently, evidence from various research groups suggests that SMN may have a muscle-specific function. Indeed, Smn-depleted C2C12 myoblasts display decreased proliferation as well as defects in myoblast fusion and myotube formation (Shafey et al. 2005). This parallels a study performed in skeletal muscle obtained from type I SMA fetuses showing delayed muscle growth characterized by smaller and disorganized myotubes (Martinez-Hernandez et al. 2009). Using a tandem-affinity-purification technique, Smn-interacting partners were identified in C2C12 myoblasts (Shafey et al. 2010). These Smn-interactors were specific to various growth and differentiation stages, suggesting a dynamic function for Smn in muscle cells (Shafey et al. 2010). A recent analysis of skeletal muscle from the pre-symptomatic severe SMA mouse model reveals distinct molecular changes, also suggestive of a muscle-intrinsic role for the SMN protein (Mutsaers et al. 2011).

While initial screens and morphological analyses suggest a muscle-specific role for SMN, the functional pathways that it regulates are still being elucidated. Work performed in *Drosophila* and mice found than Smn is a sarcomeric protein that localizes to the Z-disc of skeletal and cardiac muscle, and that it interacts with the crosslinking protein α-actinin (Rajendra et al. 2007; Walker et al. 2008; Shafey et al. 2010). Other Smn-interactors such as Gemins and Unrip were present at the Z-discs while snRNPs were absent, suggesting that the sarcomeric Smn plays a role independent of snRNP assembly (Walker et al. 2008). Further investigation is required to decipher the role of SMN at the Z-disc and in SMA pathology.

Seeing that SMN displays specific localization and interaction patterns in muscle, many research groups have assessed the importance of SMN expression in muscle on SMA pathology. The phenotype of an SMA *drosophila* model was partially rescued when Smn expression was restored to embryonic and larval muscles (Chan et al. 2003). An additional study performed in *Drosophila* shows that Smn depletion in muscle produces a more severe phenotype with increased lethality compared to a neuron-specific Smn loss (Chang et al. 2008). In the severe SMA mouse model however, the increased expression of Smn in muscle provided a small improvement in lifespan while the increased expression in neurons had a greater effect on survival (Gavrilina et al. 2008). Thus, although SMN does appear to play a role in muscle, its exact contribution to SMA pathogenesis remains to be clarified.

With increasing evidence that the muscular atrophy observed in SMA may be independent of motor neuron loss, various muscle-specific therapeutic strategies have been devised, specifically aimed at targeting known pathways that regulate muscle growth. Administration of follistatin, a positive muscle growth regulator, to the *SMNΔ7* mice resulted in significant improvement in muscle mass, gross motor function and lifespan (Rose et al. 2009). However, upon targeting of myostatin, a negative regulator of muscle growth, the phenotype of the *SMNΔ7* mice was unaffected (Sumner et al. 2009). While targeting muscle-specific pathways may prove beneficial for SMA, a combination with pan-neuronal therapeutic strategies may be required for the maximization of positive effects.

A non-neuronal role for SMN in cardiac muscle

In recent years, a potential role has been suggested for SMN in the heart. In cardiac myofibrils, Smn localizes at the sarcomeric Z-discs and interacts with α-actinin (Walker et al. 2008). Analysis of the severe and *SMNΔ7* SMA mouse models revealed cardiac defects such as increased interstitial fibrosis, increased oxidative stress, arrhythmia, bradycardia, dilated cardiomyopathy and overall impaired cardiac function (Bevan et al. 2010; Heier et al. 2010; Shababi et al. 2010a). Interestingly, delivery of trichostatin A (TSA) and self-complementary adeno-associated virus 9 (sc-AAV9)-SMN, therapies with known beneficial effects on the survival of SMA mice (Avila et al. 2007; Foust et al. 2010), also ameliorated the cardiac defects (Bevan et al. 2010; Heier et al. 2010). Importantly, clinical studies on SMA patients support a cardiac function for the SMN protein (Moller et al. 1990; Burglen et al. 1995; Menke et al. 2008; Rudnik-Schoneborn et al. 2008). Indeed, Rudnik-Schoneborn *et al*. have identified a correlation between type 1 SMA patients (with only one SMN2 copy) and heart defects (Rudnik-Schoneborn et al. 2008). This correlation did not hold true in type 1 SMA patients with more than one SMN2 copy, suggesting that congenital heart defects are limited to very severe SMA pathologies (Menke et al. 2008; Rudnik-Schoneborn et al. 2008). While it remains unclear to what extent the role of SMN in the heart contributes to SMA pathogenesis, these studies raise the possibility that SMN may have additional muscle- and neuron-independent functions that could influence the overall health of SMA patients.

Objectives and Aims

Despite the described accumulating information on SMN's various roles in cells and tissues, there still lacks a direct explanation for the specific motor neuron degeneration in SMA. Indeed, the motor neuron loss may result from a specific role for SMN in motor neurons and/or be subsequent to defective NMJ and skeletal muscle development. Alternatively, SMA may be caused by aberrant snRNP activity, which would lead to defective neuronal mRNA splicing. Furthermore, as suggested by the heart studies, SMN may have additional roles in tissues and organs that may influence the health of the SMN-sensitive motor neurons and muscles. Our **hypothesis** therefore is twofold:

1. SMN depletion results in the misregulation of actin cytoskeletal dynamics, thus leading to motor neuron degeneration, muscular atrophy and NMJ pathology.

2. SMN depletion affects the function and development of non-muscle and non-neuronal tissues, thus impacting SMA pathogenesis and development of therapeutic strategies.

To address our hypothesis, we have established the following **aims**:

1. Establish and characterize clones of PC12 cells with reduced Smn expression.

2. Produce an intermediate SMA mouse model of SMA to validate findings from our PC12 cell culture.

3. Determine if the SMA phenotype can be modulated by genetically manipulating proteins or by using compounds that target the disrupted pathways identified in our cellular and animal models.

4. Characterize additional muscle- and neuron-independent functions of SMN that influence SMA pathogenesis.

Our research will allow us to identify novel functions for the SMN protein and define their implications in SMA pathogenesis. The ultimate goal of this project is to develop new therapeutic strategies to alleviate and ameliorate SMA pathology.

CHAPTER 2: Smn depletion in PC12 cells results in misregulation of regulators of actin cytoskeletal dynamics

Smn depletion alters profilin II expression and leads to upregulation of the RhoA/ROCK pathway and defects in neuronal integrity

Mélissa Bowerman, Dina Shafey and Rashmi Kothary

Published in *Journal of Molecular Neuroscience*, 2007, 32 (2), 120-131

Author Contributions

Conceived and designed the experiments: MB and RK. Performed the experiments: MB. Analyzed the data: MB. Wrote the paper: MB. Other: Designed and made the short-hairpin RNAs: DS.

ABSTRACT

Spinal muscular atrophy (SMA) is the most common genetic disease resulting in infant mortality due to severe loss of α-motor neurons. SMA is caused by mutations or deletions of the ubiquitously expressed survival motor neuron (*SMN*) gene. However, why α-motor neurons of SMA patients are specifically affected is not clear. We demonstrate here that Smn knockdown in PC12 cells alters the expression pattern of profilin II, resulting in an increase in the neuronal-specific profilin IIa isoform. Moreover, the depletion of Smn, a known interacting partner of profilin IIa, further contributes to the increased profilin IIa availability. Altogether, this leads to an increased formation of ROCK/profilin IIa complex and an inappropriate activation of the RhoA/ROCK pathway, resulting in altered cytoskeletal integrity and a subsequent defect in neuritogenesis. This study represents the first description of a mechanism underlying SMA pathogenesis and highlights new targets for therapeutic intervention for this devastating disorder.

INTRODUCTION

Spinal muscular atrophy (SMA) is the most common genetic disease resulting in infant mortality, affecting approximately 1:10 000 births (Pearn 1978b; Crawford et al. 1996). It is an autosomal recessive disease characterized by severe loss of α-motor neurons in the spinal cord and muscular atrophy of the limbs and trunk leading to paralysis and ultimately death (Crawford et al. 1996).

At the molecular level, SMA is the result of homozygous mutations or deletion of the survival motor neuron (*SMN*) gene located on human chromosome 5q13 (Lefebvre et al. 1995). *SMN* is highly conserved with almost all eukaryotic organisms studied to date having one single copy. In humans, however, the *SMN* gene is duplicated (Lefebvre et al. 1995; DiDonato et al. 1997). Deletions or mutations in *SMN1* but not *SMN2* cause all forms of SMA, however, *SMN2* modulates the severity of the disease through its copy number (Lefebvre et al. 1995; Lefebvre et al. 1997).

SMN is ubiquitously expressed, and the protein is present in both the cytoplasm and in punctate nuclear structures called Gemini of coiled bodies (Gems) (Liu et al. 1996; Young et al. 2000a). These gems are thought to play a role in RNA metabolism (Anderson et al. 2004). The Smn protein is also part of a multiprotein complex, an assemblyosome of ribonucleoproteins (RNPs) (Paushkin et al. 2002), which is composed of self-oligomerized Smn, Gemin2-8 and Sm proteins (Paushkin et al. 2002; Carissimi et al. 2006). Thus, *SMN* is considered an important housekeeping gene playing a role in fundamental cellular events such as snRNP assembly and processing of most pre-mRNAs (Pellizzoni et al. 1998; Meister et al. 2002; Paushkin et al. 2002).

Furthermore, the complete lack of SMN protein is embryonic lethal, emphasizing its necessity for survival (Jablonka et al. 2000; Monani et al. 2000a).

Why deletions or mutations in *SMN1* specifically affect the α-motor neurons in SMA patients is not understood. Efforts have therefore been made to determine the function of SMN in neuronal cell models. SMN interacts with hnRNP-R, a ribonucleoprotein located in the axons of motor neurons (Rossoll et al. 2002). Studies in mouse embryonal teratocarcinoma P19 cells showed that SMN accumulates in growth-cone-like structures during neuronal differentiation, suggesting a role in neurite outgrowth and neuromuscular maturation (Fan et al. 2002). In fact, knockdown of the Smn protein in zebrafish results in defects in motor axon outgrowth and pathfinding (McWhorter et al. 2003), while other work has shown that SMN modulates axon growth and localization of β-actin mRNA in growth cones of motor neurons through its association with hnRNP-R (Rossoll et al. 2003). An additional neuron-specific interaction of SMN protein occurs with profilin II (Giesemann et al. 1999; Sharma et al. 2005), a small actin-binding protein and key regulator of actin dynamics, which is predominantly expressed in neural tissues and co-localizes with Smn in the cytoplasm and nuclear gems (Giesemann et al. 1999) Despite this accumulation of significant data, there is presently no explanation for the specificity of motor neuron degeneration in SMA patients. Indeed, it is still unclear whether SMN has a specific role in motor neurons other than its function within the assemblyosome of RNPs or if SMA pathogenesis is caused by defective splicing of neuronal-relevant mRNAs (Eggert et al. 2006).

Here, we assess the effects of Smn knockdown in neuronal-like cells, specifically during differentiation. We used PC12 cells which, when exposed to nerve growth factor (NGF), extend

processes similar to those produced by sympathetic neurons in primary culture, and therefore are a useful model system for neurobiological and neurochemical studies (Greene et al. 1976). We provide evidence for altered expression of profilin II in Smn depleted cells which in turn leads to the upregulation of the RhoA/ROCK actin remodeling pathway and to defects in neuronal integrity. Our work highlights one potential pathway that may explain the neuron-specific defect in SMA.

MATERIALS AND METHODS

Cell culture

The rat pheochromocytoma PC12 cell lines were maintained in DMEM (Wisent) plus 10% horse serum (HS) (Invitrogen), 5% fetal bovine serum (FBS) (Sigma), 1% antibiotic/antimycotic solution (Invitrogen) and 1% MEM non-essential amino acids solution (Invitrogen). For differentiation experiments, cells were treated with DMEM plus 1% FBS, 1% antibiotic/antimycotic solution and 50 ng/ml NGF (Chemicon). Stable cell lines were maintained in media containing 1 mg/ml G418 (Invitrogen).

Antibodies and reagents

The mouse monoclonal primary antibodies used were as follows: anti-actin (1:800 (WB), 1:200 (IF); Fitzgerald), anti-SMN (1:5000; Transduction Laboratories), anti GAP-43 (1:10,000 (WB), 1:1000 (IF); Chemicon), anti-RhoA (1:200; Santa Cruz Biotechnology), anti-Cdc42 (1:250; Transduction Laboratories), and anti-Rac1 (1:200; Transduction Laboratories).

The rabbit polyclonal primary antibodies used were as follows: anti-NF (1:300; Sigma), and the anti-profilin IIa (1:10,000) was a generous gift from Dr. Walter Witke (EMBL, Monterondo, Italy).

The secondary antibodies used were as follows: horseradish peroxidase (HRP)-conjugated goat anti-mouse IgG (1:5000; Bio-Rad), HRP-conjugated goat anti-rabbit IgG (1:5000), Cy3-conjugated goat anti-mouse IgG + IgM (1:200; Jackson ImmunoResearch Laboratories), and Alexa Fluor 488 goat anti-rabbit IgG (Molecular Probes).

The Y-27632 peptide was purchased from Calbiochem.

Immunoblot analysis

Samples were run out on 10% or 15% (for RhoA and Cdc42 activity assays) SDS-polyacrylamide gels and were blotted onto PVDF membrane (Millipore). The filters were blocked in 5% nonfat milk TBST (10 mM Tris pH 8.0, 150 mM NaCl, and 0.1% Tween 20 (Sigma)), rinsed in TBST, and then incubated overnight at 4ºC in blocking solution containing the primary antibody. Subsequently, the membranes were rinsed 3 times in TBST and incubated 1 hr at room temperature with the secondary antibody. Signals were visualized using the ECL or the ECL plus detection kits (Amersham).

Immunofluorescence analysis

Immunocytochemistry was performed as previously described (DiDonato et al. 2003). Images were taken with a Zeiss Axioplan microscope, equipped with filters suitable for FITC/Cy3/Hoechst fluorescence. For each experiment, we used 3 coverslips per day and took pictures of three fields per coverslip.

Transfection of PC12 cells

For the establishment of stable PC12 cell lines with reduced Smn expression, cells were transfected with sh_Smn_519 (Supplementary Fig. 1), which was ligated in the *Bbs*I sites of the psiRNA-hHneo vector (InvivoGen) (Shafey et al. 2005). The oligonucleotide sequence for sh_Smn_519 is: 5' TCC CAA AGT AAA GCA CAC AGC AAG TCT TCA AG A GAG ACT TGC TGT GTG CTT TAC TTT T 3'. Lipofectamine transfected cells were isolated and selected with 1 mg/ml G418 (Invitrogen). Smn knockdown in cloned cells was visualized by immunoblot

analysis and quantification of protein bands was performed with the help of the Image J program, developed by Wayne Rasband (NIH). Control PC12 cell lines were transfected with the empty psiRNA-hHneo vector or sh_lacZ_1348. The oligonucleotide sequence for the sh_lacZ_1348 is: 5'TCC CAA ATC GTC TGA CCG ATG ATC CGT TCA AGA GAC GGA TCG GTC AGA CGA TTT T 3'. For rescue experiments, the C-59 clone was transfected with the full-length human SMN-GFP (hSMN-GFP).

Neuronal outgrowth and differentiation analysis

For neuritogenesis experiments, cells were plated at low density onto 10 cm culture plates coated with 0.1% of rat tail collagen Type I (Sigma). Cells were differentiated for up to 7 days. Morphometric analysis was performed as previously described (Das et al. 2004). For each experiment, we used 3 plates per day and took pictures of 3 fields per plate. The number of differentiated cells was determined by visual examination of the field and counting cells that had at least one neurite with a length equal or greater to twice the cell body diameter, and expressed as a percentage of the total cells in the field. Neurite outgrowth was determined by manually tracing a straight line following the length of the longest neurite per cell. This was done for all cells in a field that had an identifiable neurite and for which the entire neurite arbor could be visualized. Data from the three fields in each plate were pooled and each plate was designated as an "n" of one.

RhoA and Cdc42 activity assays

RBD and PBD were expressed in bacteria and purified using glutathione Sepharose 4B beads (Pharmacia). Cells used for RhoA activity assays were lysed in ice-cold lysis buffer A (50 mM Tris pH 7.6, 500 mM NaCl, 0.1% SDS, 0.5% DOC, 1% Triton X-100, 0.5 mM $MgCl_2$) supplemented with 1 mM PMSF, 0.01 mg/ml leupeptin and 0.01 mg/ml aprotinin. Cells used for Cdc42 activity assays were lysed in ice-cold lysis buffer B (50 mM Tris pH 7.6, 150 mM NaCl, 1% Triton X-100, and 0.5 mM $MgCl_2$) supplemented with 1 mM PMSF, 0.01 mg/ml leupeptin and 0.01 mg/ml aprotinin. Thirty μg of GST-RBD or GST-PBD immobilized on glutathione beads was added to equal concentrations of various cell lysates. After 30 min incubation at 4ºC, beads were washed 4 times with lysis buffer B. The bound RhoA and Cdc42 were detected by immunoblot analysis using anti-RhoA and anti-Cdc42 antibodies. Every affinity precipitation assay was performed in triplicate.

Real-time quantitative RT-PCR

RNA was extracted using the RNeasy Midi Kit (Qiagen) and quantified. Reverse transcription was performed using 0.01 μg of total RNA. All real-time PCRs were carried out using the Mx3000 Multiplex Quantitative PCR System (Stratagene). The following primers were used for RT-PCR analysis: profilin II forward (5' TTG GCA GAG CTG GGA GA 3'), profilin IIa reverse (5' CTA GAA CCC AGA GTC TCT CAA GTAT T 3'), profilin IIb reverse (5' TAG CAG CTA GAA CCC AGA GTC T 3'), GAPDH forward (5' TGA AGG GGT CGT TGA TGG 3'), GAPDH reverse (5' AAA ATG GTG AAG GTC GGT GT 3'), 18S forward (5' CGG CTA CCA CAT CCA AGG 3'), and 18S reverse (5' CTG GAA TTA CCG CGG CT 3').

The optimum primer concentration was 5 μM. All PCR amplifications were performed using FullVelocity SYBR Green QPCR Master Mix (Stratagene), with ROX as a reference dye in a 25 μl reaction volume. A standard curve for each cDNA was first generated using 2-fold serial dilutions of the respective cDNAs as templates. The PCR cycling conditions were as follows: initial denaturation at 95°C for 5 min, followed by 45 cycles of 95°C for 10 s, 59°C for 30 s (61°C for pIIb primers), and a dissociation cycle of 95°C for 1 min, 55°C for 30 s, and 95°C for 30s. Each PCR wild-type and Smn shRNA PC12 C-59 cell lysate (n = 3) was done in triplicates. Profilin IIa and IIb transcripts were normalized to GAPDH and 18S.

ROCK immunoprecipitation

For immunoprecipitations, protein G-Sepharose beads (Amersham) were washed 3 times in H_2O followed by 3 times in lysis buffer B (described above). Beads were resuspended in lysis buffer B. Equal concentrations of cell lysates were incubated overnight at 4°C with beads and anti-ROCK antibody. Bead samples containing only the cell lysate or the antibody with the lysis buffer B were used as controls. Samples were analyzed by immunoblot analysis with the profilin IIa antibody. Each immunoprecipitation was repeated three times with different cell lysates.

Statistical methods

Student's *t* test for paired variables was used to test for differences between samples and data were considered significantly different at $p < 0.05$.

RESULTS

Smn knockdown in PC12 cells by use of short hairpin (sh) RNA interference

PC12 cells were transfected with an shRNA construct targeting a specific region within the rat *Smn* transcript (**Supplementary Figure 2.1**). This construct, sh_Smn_519, has been previously described (Shafey et al. 2005). Stable clones, referred to henceforth as Smn shRNA PC12 cells, were established and maintained in G418-containing media. To determine the amount of Smn protein depletion, western blots of cell extracts were obtained and the area and intensity of the bands were integrated and normalized to the actin/Smn ratio of the wild type PC12 cell sample. Various Smn shRNA PC12 clones were obtained with an Smn reduction ranging from 34 to 85% (**Figure 2.1 A**). For subsequent experiments, we used Smn shRNA PC12 clone C-59, with an 85% Smn reduction, to examine the effects of Smn knockdown on neuronal differentiation as well as on localization and expression of cytoskeletal components. However, it should be noted that we have confirmed our findings with other Smn shRNA PC12 clones (data not shown).

Smn knockdown affects neuritogenesis

To determine the impact of Smn depletion on PC12 cell differentiation, we induced cells with NGF for up to 7 days. The cell populations examined included: wild type PC12 cells, Smn shRNA PC12 C-59 cells (85% knockdown), PC12 cells transfected with either a non-specific shRNA control, namely sh_lacZ_1348, or the empty vector psiRNA, and Smn shRNA PC12 C-59 cells transfected with the full-length human SMN-GFP (hSMN-GFP). At days 3, 5 and 7 of differentiation, we determined the percentage of differentiated cells and the average neurite

length. There were significantly fewer differentiated Smn shRNA PC12 C-59 cells at days 3, 5 and 7 when compared to wild type PC12 cells and to the various control samples (**Figure 2.1 B, C**). Importantly, the phenotype of Smn shRNA PC12 C-59 cells was rescued when these cells were transfected with hSMN-GFP (**Figure 2.1 B, C**). Similarly, the neurites of Smn shRNA PC12 C-59 cells were significantly shorter when compared to wild type cells and to control samples (**Figure 2.1 B, D**). As before, this phenotype was rescued with the hSMN-GFP (**Figure 2.1 B, D**), indicating that these defects are specific to the knockdown of Smn protein.

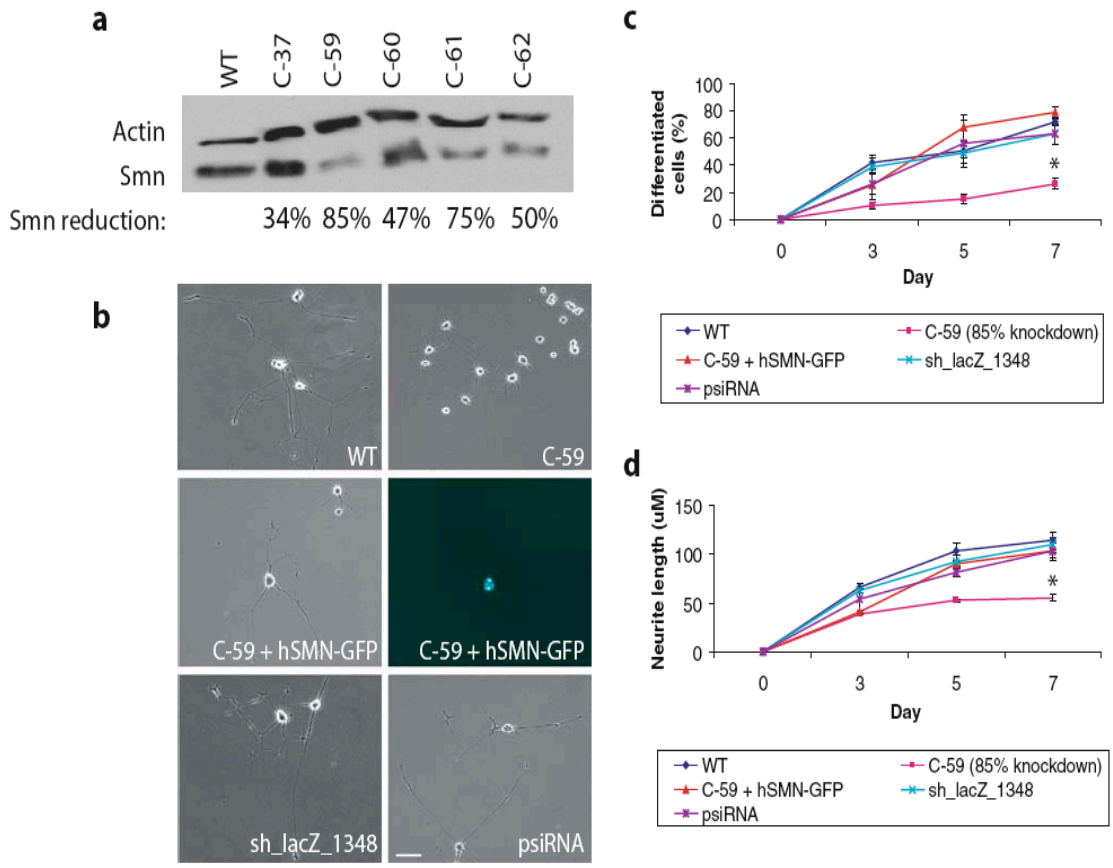

Figure 2.1. Smn knockdown in PC12 cells (via shRNA interference) affects differentiation potential and neurite outgrowth. (A) Immunoblot analysis. Smn levels were determined by blotting with an anti-Smn antibody, and anti-actin was used as a loading control. (B) Typical examples of cells at day 7 of differentiation. Smn shRNA PC12 C-59 cells, which have an 85% decrease in Smn, were compared to PC12 wild type (WT) cells, WT cells transfected with sh_lacZ_1348 and the plasmid alone (psiRNA), and C-59 cells transfected with full length hSMN-GFP. Cells were differentiated up to 7 days with NGF. WT cells and cells transfected either with sh_lacZ_1348 or the psiRNA vector alone show fully differentiated cells with long neurites. However, most Smn shRNA PC12 C-59 cells are not fully differentiated and show

shorter neurites. This phenotype is rescued with the hSMN-GFP construct. Scale bar, 50 μm. (C) Quantitative analysis of percentage of differentiated cells at days 3, 5 and 7 of differentiation. Compared to WT cells, only clone C-59 was significantly different (*, $p < 0.005$), showing a reduced number of differentiated cells. The hSMN-GFP rescued this defect. (D) Quantitative analysis of neurite length at days 3, 5 and 7 of differentiation. Only C-59 cells differed from WT cells with a significant reduction (*, $p < 0.005$) in neurite length. Introduction of hSMN-GFP into the C-59 cells rescued the defect. Data are mean +/- SE.

Neurites of Smn shRNA PC12 C-59 cells were characterized by an increased incidence of beading and/or swelling along their lengths (**Figure 2.2 A**, see also **Figure 2.3 C**), which is usually indicative of cytoskeletal perturbation and impairment of axonal transport (Nakayama et al. 2000). These beadings and/or swellings were significantly more frequent in Smn shRNA PC12 C-59 cells than in wild type PC12 cells (**Figure 2.2 B**). Once more, the transfection of Smn shRNA PC12 C-59 cells with hSMN-GFP rescued this phenotype.

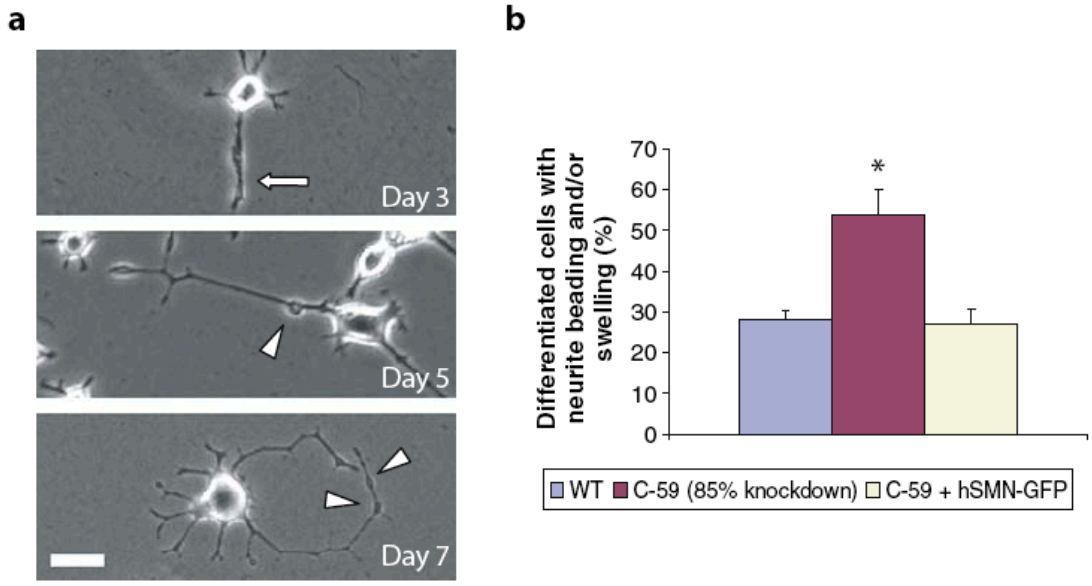

Figure 2.2. Smn knockdown in PC12 cells increases the incidence of beading and swelling along the neurites. (A) Typical examples of Smn shRNA PC12 C-59 cells at days 3, 5 and 7 of differentiation, showing terminal swelling (arrow) and beading (arrow heads) along the neurites. Scale bar, 20 μm. (B) Quantitative analysis of the percentage of differentiated cells with neurite beading and/or swelling. The Smn shRNA PC12 C-59 clone was compared to PC12 wild type (WT) cells and to C-59 cells transfected with full length hSMN-GFP. The number of C-59 cells exhibiting swelling and/or beading along their neurites was significantly greater (*, $p < 0.05$) than that of WT cells, which was rescued with hSMN-GFP. Data are mean +/- SE.

Smn knockdown affects localization and expression of cytoskeletal components

Based on the neuritogenesis defects observed in the Smn depleted PC12 cells, we performed further experiments to determine whether specific cytoskeletal components were affected in the Smn shRNA PC12 C-59 cells. Initially, we examined the expression and localization of GAP-43, an axonal-growth associated protein that plays a key role in guiding the growth of axons and modulating the formation of new connections (Benowitz et al. 1997). As well, Smn and GAP-43 have been demonstrated to co-localize, particularly in growth cones (Fan et al. 2002).

Contrary to wild type PC12 cells, where GAP-43 is concentrated at the tip of the growth cones, in Smn shRNA PC12 C-59 cells, GAP-43 accumulated in membrane ruffles around the cell body (**Figure 2.3 A**). Furthermore, the expression of GAP-43 was significantly higher at days 5 and 7 in C-59 cells (**Figure 2.3 B**). This was surprising because C-59 cells showed shorter neurites and fewer differentiated cells, and GAP-43 is an intrinsic determinant of the neuron's growth state (Benowitz et al. 1997). However, a study overexpressing caveolin-1, a negative regulator of neuronal outgrowth, also reported increased levels of GAP-43 (Gaudreault et al. 2005), suggesting that increased GAP-43 may in turn inhibit neurite extension.

Since neurite initiation and outgrowth involves coordinated changes within the actin cytoskeleton (da Silva et al. 2002), we next assessed the effects of Smn knockdown on the localization of F-actin and neurofilaments (NF). In Smn shRNA PC12 C-59 cells, NF accumulated in the beadings and/or swellings along the neurites (Fig. 3C), consistent with cytoskeletal perturbation and impairment of axonal transport. Furthermore, F-actin was

concentrated around the cell body perimeter in these cells (**Figure 2.3 C**). In fact, close to 80% of Smn shRNA PC12 C-59 cells showed this altered F-actin localization compared to about 10% in wild type PC12 cells (**Figure 2.3 D**).

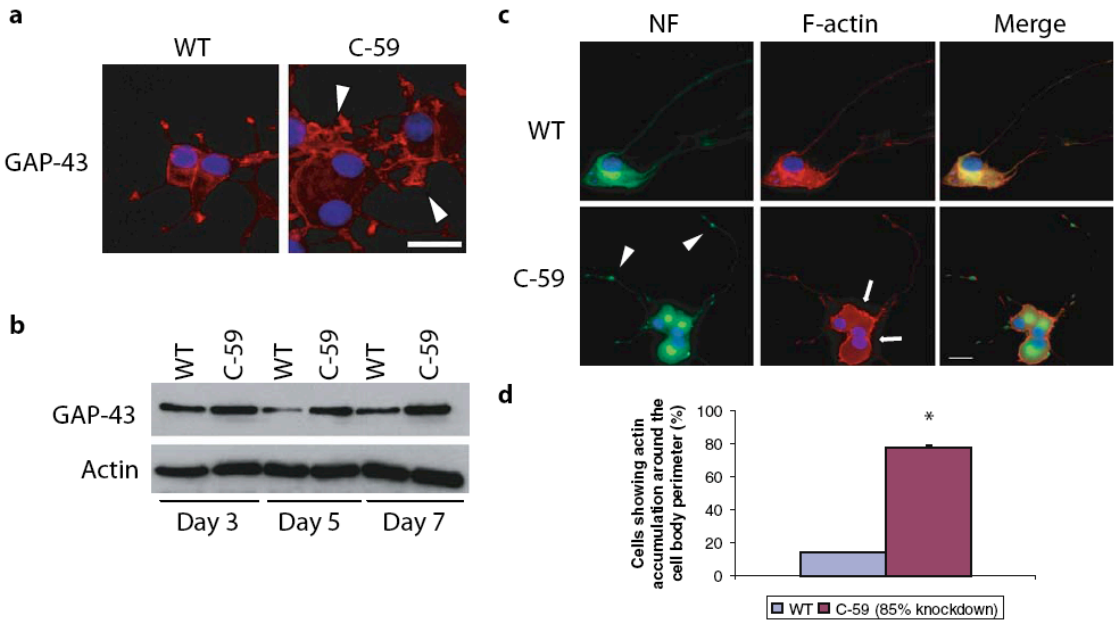

Figure 2.3. Smn knockdown in PC12 cells affects organization and expression of cytoskeletal components. (A) Typical examples of immunostaining of PC12 wild type (WT) cells and Smn shRNA PC12 C-59 cells with GAP-43 antibody at 7 days of differentiation. C-59 cells show a distinct concentration of GAP-43 in membrane ruffles (arrow heads). Scale bar, 10 μm. (B) Immunoblot analysis of GAP-43 expression at days 3, 5 and 7 of differentiation. At days 5 and 7, C-59 cells show higher levels of GAP-43 protein than WT cells. (C) Representative examples of immunostaining for neurofilament (green) and actin (red). In Smn shRNA PC12 C-59 cells, NF accumulates within the beadings/swellings in the neurites (arrow heads). There is also a buildup of F-actin along the edge of C-59 cell bodies (arrows). The right panels are a merged image. Scale bar, 20 μm. (D) Quantitative analysis of the percentage of cells showing F-actin build-up. When compared to WT cells, C-59 cells show a significantly greater (*, $p < 0.001$) number with an abnormal concentration of F-actin at the edge. Data are mean +/- SE.

Smn knockdown affects expression and activity of Rho GTPases

To assess why F-actin organization was affected in Smn shRNA PC12 C-59 cells, we focused on the signal transduction pathway linking the Rho GTPases RhoA, Rac1 and Cdc42 to the actin cytoskeleton. These proteins play an important role in neurite initiation and outgrowth by regulating actin cytoskeleton dynamics in neuronal growth cones (Luo et al. 1997; Sarner et al. 2000; Yamaguchi et al. 2001). We determined both total protein and active levels since Rho GTPases cycle between an active (GTP bound) and inactive (GDP bound) state. Of further importance is that RhoA-GTP inhibits neuronal outgrowth and differentiation, while Cdc42-GTP and Rac1-GTP promote neuronal outgrowth and differentiation (Hall 1998; Mueller 1999). There is also a requirement for concurrent Cdc42 activation and RhoA inactivation to promote neurite formation and outgrowth (Negishi et al. 2002).

In Smn shRNA PC12 C-59 cells, there was an increase in the level of total RhoA protein at days 3 and 5 of differentiation compared to wild type cells (**Figure. 2.4A**). More importantly, at day 3, when initiation of neuronal differentiation occurs, we observed a significantly greater amount of RhoA-GTP in Smn shRNA PC12 C-59 cells than in wild type cells (**Figure 2.4 A**). Interestingly, there was also a decrease in the level of total Cdc42 protein in Smn shRNA PC12 C-59 cells at days 3, 5 and 7 of differentiation compared to that in wild type cells (**Figure 2.4 B**). In terms of Cdc42 activity, Cdc42-GTP levels were high and increased with time in differentiating wild type PC12 cells (**Figure 2.4 B**). In contrast, Cdc42-GTP levels decreased by day 5 of differentiation in Smn shRNA PC12 C-59 cells (**Figure 2.4 B**). Finally, no significant differences were seen in total Rac1 protein levels in the two cells types (**Figure 2.4 C**).

Y-27632 partially rescues differentiation potential defect in Smn shRNA PC12 C-59 cells

When RhoA is in its active state, it activates its downstream effector Rho-kinase (ROCK), resulting in phosphorylation and activation of myosin light chain (MLC), F-actin accumulation and inhibition of neuronal outgrowth and differentiation (Amano et al. 1996). To therefore determine if the neuronal outgrowth and differentiation defects in Smn shRNA PC12 C-59 cells result from the observed activation of the RhoA pathway, we performed a rescue experiment with the Y-27632 peptide, which specifically inhibits ROCK (Uehata et al. 1997). Cells were differentiated in media containing 10 μM Y-27632 (Kishida et al. 2004) and assessed as above. The addition of Y-27632 did not result in an increase in the neurite length of Smn shRNA PC12 C-59 cells (**Figure 2.4 D**). However, the peptide did partially rescue the defect in differentiation potential of Smn shRNA PC12 C-59 cells (**Figure 2.4 E**). A lack of complete rescue could be explained by the fact that we observed both an increase in active RhoA and a decrease in active Cdc42 in C-59 cells. Therefore, inhibiting only the RhoA pathway, which affects neuritogenesis, cannot fully rescue neuronal outgrowth and differentiation of C-59 cells.

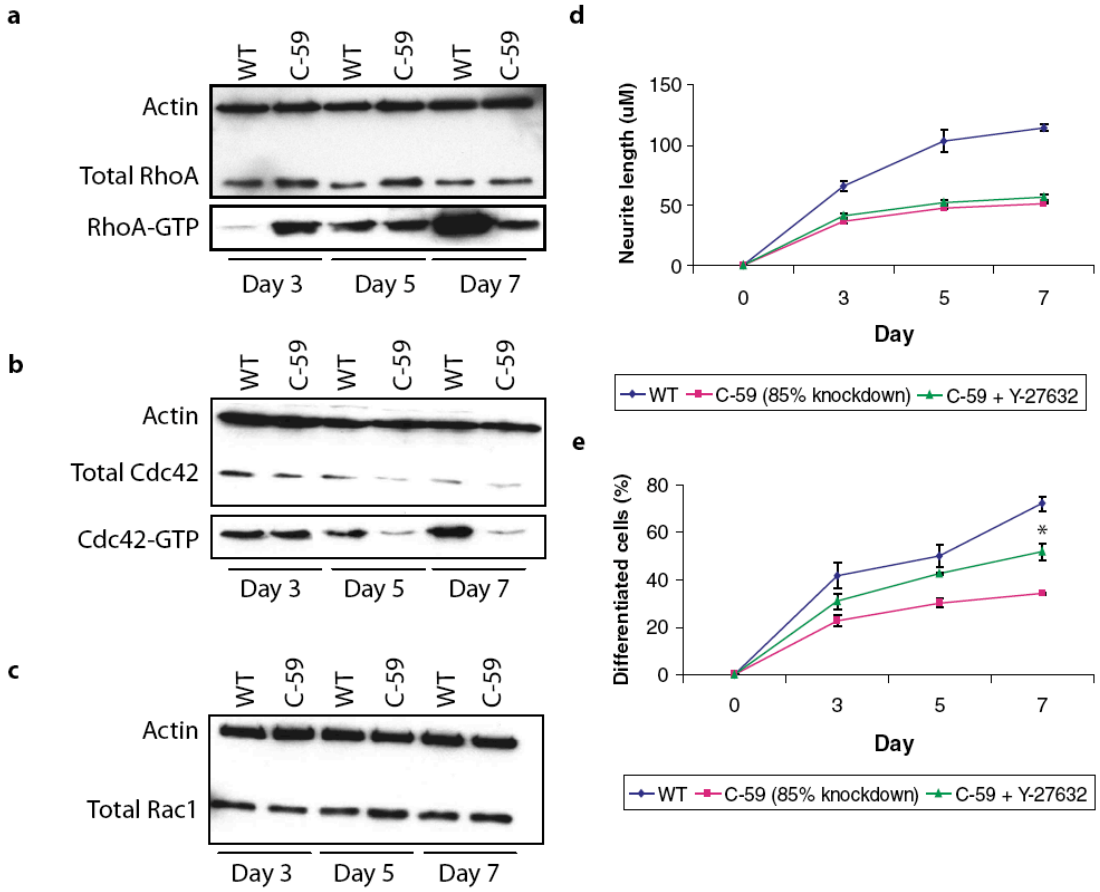

Figure 2.4. Smn knockdown in PC12 affects expression and activity of RhoA and Cdc42. In rescue experiments with the Y-27632 peptide, C-59 cells were differentiated in media supplemented with Y-27632. (A) Immunoblot analysis of total and active RhoA at days 3, 5 and 7 of differentiation. There is an increased expression of total RhoA in Smn shRNA PC12 C-59 cells at days 3 and 5 when compared to WT cells. At day 3, there is significantly more RhoA-GTP in C-59 cells while levels even out by day 5. (B) Immunoblot analysis of total and active Cdc42 at days 3, 5 and 7 of differentiation. There is a decreased expression of Cdc42 in C-59 cells at days 3, 5 and 7, when compared to WT cells. There is also a reduction in Cdc42-GTP in C-59 cells at days 5 and 7. (C) Immunoblot analysis of total Rac1 expression at days 3, 5 and 7 of differentiation. There is no difference in Rac1 levels between WT and C-59 cells. (D)

Quantitative analysis of neurite length at days 3, 5 and 7 of differentiation. Y-27632 did not rescue the defect in neurite outgrowth observed in C-59 cells. (E) Quantitative analysis of percentage of differentiated cells at days 3, 5 and 7 of differentiation. There was a partial rescue of the differentiation defect observed in C-59 cells following the addition of Y-27632 in the differentiation media (*, $p < 0.01$). Data are mean +/- SE.

Smn knockdown alters profilin II expression

The Smn complex plays a role in snRNP biogenesis and mRNA splicing (Pellizzoni et al. 1998; Meister et al. 2002; Pellizzoni et al. 2002), as well as in the assembly of the RNA polymerase II transcription/processing machinery (Pellizzoni et al. 2001b). Further, not only is there a direct correlation between the level of SMN and the ability to promote RNP assembly, but reduced assembly of U snRNPs is likely to contribute directly to SMA pathogenesis (Wan et al. 2005; Winkler et al. 2005; Eggert et al. 2006). Our goal therefore was to identify neuronal-relevant mRNAs involved in the RhoA pathway that may be affected in SMN depleted neurons. Our primary candidate was profilin IIa (pIIa), derived by alternative splicing of profilin II (Di Nardo et al. 2000; Lambrechts et al. 2000). Da Silva et al. (Da Silva et al. 2003) have shown that the RhoA/ROCK regulation of neuritogenesis involves pIIa-mediated control of actin stability. Further, profilin II binds to and co-localizes with Smn in nuclear Gems (Giesemann et al. 1999; Sharma et al. 2005). Profilin IIa is mainly expressed in neural tissues and developmentally regulated, while profilin IIb (pIIb) is the minor form and expressed in a limited number of tissues, suggesting that the alternative splicing of profilin II is tightly regulated (Lambrechts et al. 2000).

In Smn shRNA PC12 C-59 cells, there was a 6-fold increase of pIIa and pIIb transcript compared to wild type cells as assessed by real-time quantitative RT-PCR (**Figure 2.5 A**). This suggests an upregulation of profilin II transcription and/or an increase in mRNA stability as opposed to a defect in its splicing. Consistent with the RNA data, levels of pIIa protein in Smn shRNA PC12 C-59 cells were noticeably higher than in wild type cells at all stages of differentiation (**Figure 2.5 B**).

Based on previous work, it is possible that the increased availability of the neuronal profilin II isoform, pIIa, might result in increased RhoA/ROCK/pIIa complex formation, and subsequent inhibition of neuritogenesis. To test this possibility, we performed an immunoprecipitation with the ROCK antibody. Da Silva et al. (Da Silva et al. 2003) have shown that ROCK and pIIa have a physical and functional interaction and that RhoA activity is crucial for the formation of this complex. In accordance with our previous results, there is an increase in ROCK/pIIa complex in Smn shRNA PC12 C-59 cells (**Figure 2.5 C**). This result suggests that the upregulation of the RhoA/ROCK pathway, through increased availability of pIIa, plays a major role in the observed inhibition of neuronal outgrowth.

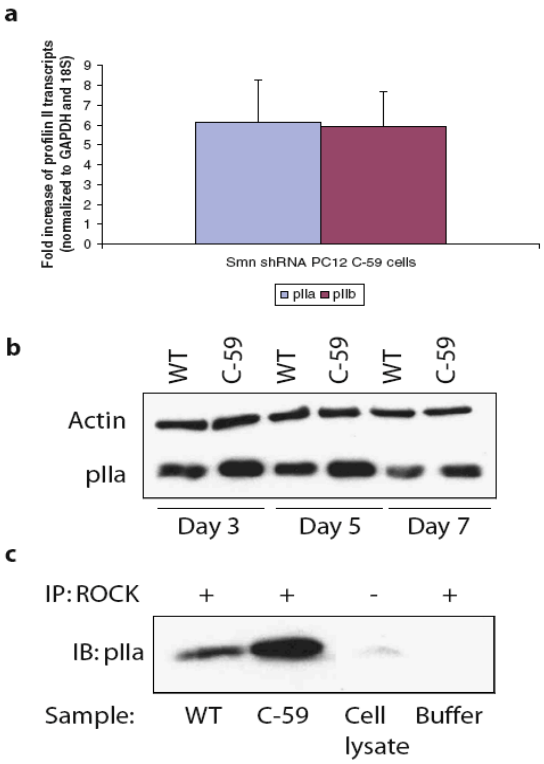

Figure 2.5. Smn knockdown in PC12 cells results in altered expression of profilin II and increased formation of ROCK/pIIa complex. (A) Real-time quantitative RT-PCR of RNA from non-differentiated wild type (WT) and Smn shRNA PC12 C-59 cells using specific primers for pIIa and pIIb transcripts. Smn shRNA PC12 C-59 cells show a 6-fold increase of profilin IIa and IIb transcripts compared to WT cells. The levels of profilin II transcripts were normalized to GAPDH and 18S levels (B) Immunoblot analysis of pIIa protein in WT and C-59 cells. At days 3, 5 and 7 of differentiation, there is more pIIa protein in C-59 cells. (C) ROCK immunoprecipitation in WT and C-59 cells at day 3 of differentiation. Detection with pIIa antibody shows that there is more ROCK/pIIa complex formed in C-59 cells than in WT cells. Data are mean +/- SE.

DISCUSSION

In the present work, we show that knockdown of Smn in PC12 cells leads to altered expression of profilin II, resulting in increased levels of the neuronal pIIa transcript and corresponding protein. The depletion of Smn, a known binding partner of pIIa (Giesemann et al. 1999; Sharma et al. 2005), further contributes to the increased availability of the pIIa protein. In fact, it has been suggested by Sharma et al. that through its interaction with pIIa, Smn may moderate the inhibitory activity of pIIa on actin polymerization. Consequently, pIIa is "free" to interact with ROCK which subsequently upregulates the RhoA/ROCK pathway, inhibiting proper neuronal outgrowth and differentiation (**Figure 2.6**). However, since pIIa presumably plays more than one role in neuronal cells, its increased availability likely perturbs other signaling pathways (**Figure 2.6**). This is confirmed by our inability to fully rescue the neuronal outgrowth and differentiation defects when exposing the Smn shRNA PC12 C-59 cells to the ROCK inhibitor Y-27632.

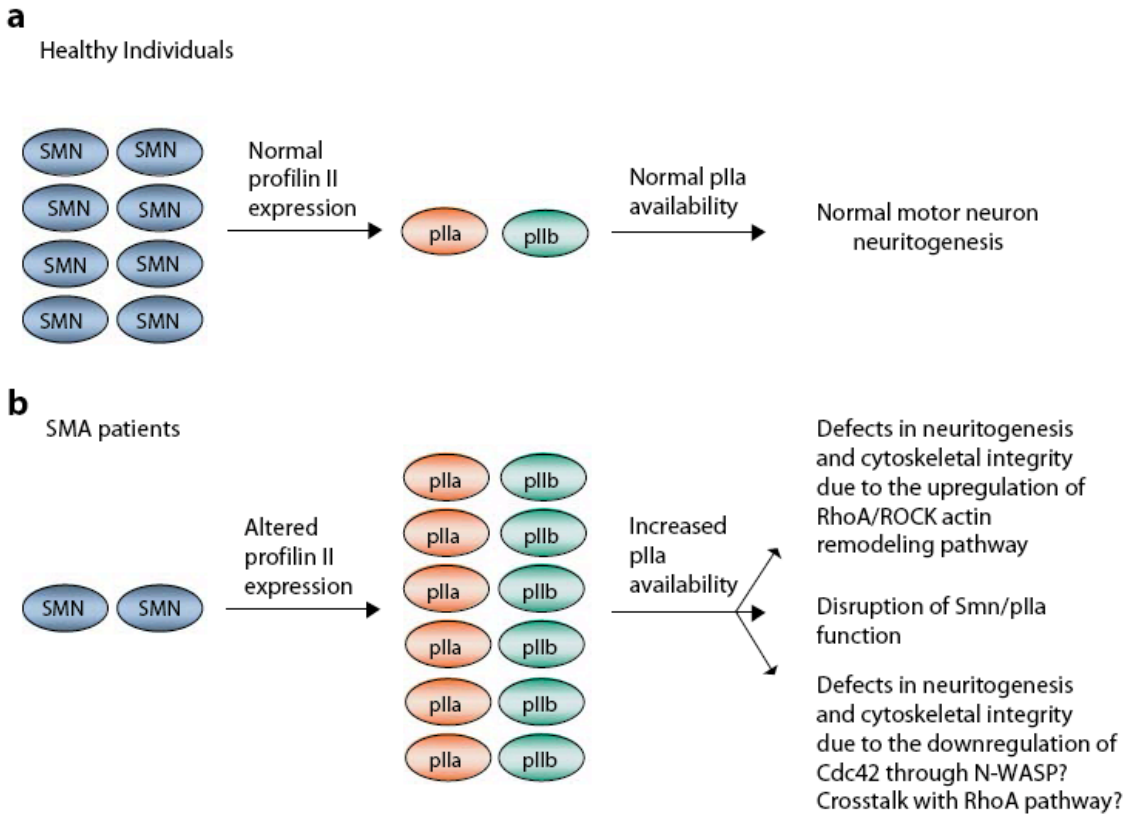

Figure 2.6. A model for SMA pathogenesis. (A) In healthy individuals, there is normal expression of functional SMN protein. This leads to correct profilin II expression, normal pIIa availability, and therefore normal motor neuron neuritogenesis. (B) In SMA patients, there is a reduced amount of functional SMN protein, which alters profilin II expression, and results in greater profilin IIa availability. The increase in pIIa would lead to an upregulation of the RhoA/ROCK pathway with subsequent defects in neuritogenesis. Other signaling pathways, such as the one involving the Smn/pIIa complex and the Cdc42 neurite formation pathway, could also be affected by this increased pIIa availability.

Indeed, it is probable that the increased pIIa availability in Smn depleted cells also affects the Cdc42 signaling pathway. We show a decrease in expression and activity of Cdc42 in the Smn knockdown PC12 cells. Profilin interacts with N-WASP, which improves Cdc42's ability to nucleate new actin filaments (Suetsugu et al. 1998; Yang et al. 2000). It is therefore possible that profilin has a different affinity for ROCK and N-WASP, and that the observed increase in profilin/ROCK complex results in a reduced availability of profilin for binding to N-WASP. Alternatively, the Cdc42 pathway could be downregulated through crosstalk with the RhoA pathway. Once activated, Cdc42 promotes neurite formation and growth by relaying signals to downstream effectors (Govek et al. 2005). One of these effectors is the p21-activated kinase (PAK) 5 (Dan et al. 2002). In neuronal N1E-115 cells, activated PAK5 inhibits RhoA activity while the overexpression of active RhoA can in turn inhibit PAK5's positive effect on neurite outgrowth (Dan et al. 2002). Thus, in addition to having a direct effect on the RhoA and Cdc42 pathways, Smn depletion may also be impacting on the crosstalk between these two pathways.

The functional interaction between Smn and pIIa may also be disturbed in the Smn depleted PC12 cells. This interaction, which is disrupted in the presence of pathogenic SMN mutations, has a greater positive effect on actin polymerization, compared to Smn and pIIa on their own (Giesemann et al. 1999; Sharma et al. 2005). Interestingly, both proteins interact with ß-actin, directly or indirectly, modulating its localization at the leading edge of cytoplasmic extensions and promoting actin polymerization (Cao et al. 1992; Suetsugu et al. 1998; Rossoll et al. 2002). The elucidation of the precise function of the Smn/pIIa interaction will shed light on the importance of its loss on SMA pathogenesis. Thus, pIIa plays multiple roles in the

differentiating neuronal cell, all of which could be affected by its increased expression, disturbing the balance required for maintaining neuronal integrity.

The first step in neuronal differentiation, neuritogenesis, occurs when nascent neurites emerge from the cell soma and eventually become an axon or a dendrite (da Silva et al. 2002). This process requires the tight regulation of actin dynamics through specific signaling pathways that are crucial for correct neuronal differentiation (Luo 2002). PC12 cells begin differentiating when exposed to NGF, which signals through the TrkA receptor. In turn, phosphatidylinositol-3-kinase (PI3K) is stimulated which increases Rac1 activity and induces transient RhoA inactivation during the first phase of neurite outgrowth (Nusser et al. 2002). Activation of PI3K is also necessary for the upregulation of the Cdc42 pathway that promotes neurite formation (Aoki et al. 2004). Our results demonstrate that PC12 cells with reduced Smn have significantly greater levels of active RhoA, specifically during the initiation phase of neuronal differentiation. This is noteworthy since a rapid and transient inactivation of RhoA during the neurite initiation phase is required for neurite outgrowth (Nusser et al. 2002), and that constitutively active RhoA during this period is sufficient to prevent neurite initiation and promote neurite retraction (Kranenburg et al. 1997; Sebok et al. 1999), consistent with the neuritogenesis defects in our Smn depleted cells. Indeed, activation of RhoA and its downstream effector ROCK hinders the NGF-induced Rac1 activation and therefore inhibit the formation of neurites (Yamaguchi et al. 2001). Further, in PC12 cells, RhoA signaling induces the formation of a thick ring-like structure of cortical actin filaments at the cell periphery (Yamaguchi et al. 2001), similar to that observed in our Smn shRNA PC12 C-59 cells. Finally, GAP-43-induced formation of filopodia depends

on Rho (Aarts et al. 1998), which could explain our findings of increased expression of GAP-43 in the Smn shRNA PC12 C-59 cells.

Our study addresses questions that had remained unanswered in regard to specificity and mechanism of SMA pathogenesis. SMN has both housekeeping and cell-specific functions. As part of the assemblyosome of RNPs, it plays a role in U snRNP assembly and pre-mRNA splicing (Pellizzoni et al. 1998; Meister et al. 2002; Paushkin et al. 2002; Pellizzoni et al. 2002). There is also a role for SMN in gene transcription through its interaction with RNA helicase A and RNA polymerase II (Pellizzoni et al. 2001b). In neuronal models, SMN modulates axon growth and localization of ß-actin mRNA in growth cones while its knockdown affects axonal outgrowth and pathfinding (Rossoll et al. 2002; McWhorter et al. 2003). Further, the interaction of Smn with the RNA-binding proteins hnRNP-R and hnRNP-Q suggest a role for Smn in RNA processing in axons of motor neurons (Rossoll et al. 2002). Pinpointing the precise affected function(s) that results in SMA has therefore not been an easy task. In our Smn knockdown PC12 cell model, we show that expression of the profilin II gene is affected, leading to increased levels of pIIa transcript and protein. Lambrechts et al. (Lambrechts et al. 2000) have demonstrated that pIIa, and not pIIb, is the major form in neural tissues. Overexpression of pIIa in hippocampal neurons leads to neuritogenesis defects (Da Silva et al. 2003) similar to those described in our study. Furthermore, unlike profilin I, which is expressed constantly during embryogenesis without increasing after birth, pIIa expression is upregulated at stage E14 of embryogenesis and continues to increase until after birth (Lambrechts et al. 2000). This expression pattern is similar to the one observed for Smn, where the highest protein levels are seen during embryo-fetal development followed by a marked decrease postnatally (Burlet et al.

1998). Thus, the altered expression of a neuronal-specific mRNA is one possible explanation of how SMN's housekeeping function can lead to a cell-specific pathology. In addition, not only are the general functions of pIIa in neuronal cells affected but the specific axonal role of the SMN/pIIa complex is also compromised. The accumulation of these defects could therefore lead to the degeneration and loss of neuronal integrity of α-motor neurons of SMA patients. Whether Smn depletion directly affects the transcription or processing of pIIa or indirectly alters splicing and/or transcription of other cytoskeletal components still needs to be addressed. Clearly, future studies will be aimed at identifying other possible neuronal-relevant mRNAs with offset expression and/or splicing patterns as well as at confirming our findings in animal models.

Our work is the first to provide evidence for specific cellular machinery and cytoskeletal components that could be involved in the neuritogenesis defects previously described for SMA. Our research provides new insight into the signaling pathways involved in the loss of α-motor neurons of SMA patients and is of utmost importance to the understanding and treatment of this neurodegenerative disorder.

ACKNOWLEDGEMENTS

We are grateful to Dr. David Picketts for critical reading of the manuscript, and the rest of the Kothary laboratory for helpful discussions. We also give thanks to Dr. Robin Parks for the sh_LacZ_1348 construct, to Dr. Jocelyn Cote for the hSMN-GFP, to Dr. Lina Dagnino for the pGEX-2T GST-RBD/PBD, and to Dr. Walter Witke for the profilin IIa antibody. This project was funded by a grant from the Canadian Institutes of Health Research (CIHR), The Muscular Dystrophy Association, and The Families of Spinal Muscular Atrophy to R.K. M.B. is a recipient of an Ontario Graduate Scholarship in Science and Technology. D.S. is a recipient of an Ontario Graduate Scholarship.

SUPPLEMENTARY FIGURES

CCCAGCCCCGTCCGTGGTAGCAGGCCATGGCGATGGGCAGCGGCGGCGCGGGCTCTGAGCAGGAAGACACCGTG
CTGTTCCGGCGTGGCACCGGCCAGAGTGATGATTCTGACATTTGGGATGATACAGCATTGATAAAAGCTTACGA
TAAAGCCGTGGCTTCCTTTAAGCATGCTCTAAAGAACGGTGACATGTGTGAAACTTCAGATAAGCCAAAAGGCA
CAGCTAGAAGAAAACCTGCTAAGAAGAATAAAAACCAAAAGAAGAATGCCACAGCTCCATTGAAACAGTGGAAA
GCTGGTGACAAATGCTCTGCCGTTTGGTCGGAAGATGGCTGCGTTTACCCAGCTACCATCACGTCAGTTGACCT
TAAGAAGAAACCTGTGTCGTGGTTTATACTGGATATGGAAACAAAGAGGAGCAAAACCTATCTGATCTGCTTTC
CCCGACCTGTGAAGTAGCTAACAATACAGAACAGAACACTCAGGAGAATGAAAGCCAAGTTTCCACAGACGACA
GTGAACACTCCTCCAGATCGCTCAG**AAGTAAAGCACACAGCAAGTC**CAAAGCTGCTCCATGGACCTCGTTTCTC
CCTCCACCTCCCCCGGTGCCCGGGGCGGGATTAGGACCAGGAAAGCCAGGTCTAAGGTTCAATGGCCCACCGCC
GCCGCCACCTCCCCCTCCCCCGTTCTTGCCGTGTTGGATGCCTCCGTTCCCTTCAGGACCACCAATAATTCCTC
CACCCCCTCCCATATCTCCCGACTGTCTGGATGACACGGATGCTCTGGGCAGTATGCTAATCTCTTGGTACATG
AGTGGTTACCACACTGGTTACTATATGGGTTTCAGACAAAATAAAAAAGAAGGAAAGAAGTGCTCACATACAAA
TTAAGAAGTTCAGCTCTCTCCCAAGGAGATGGTTTGTTGGTGTCCCTGGTCGATAAGAACAGAAGTCTCCTCGT
CACCTTTGTGGACTCTTGGCTAAGTGGTGTCATCATCAGGGTCTCCCTGTCCCGGGAGTCCATCCTGAGTCAGC
AGCAGGGCATGCATAGAGCAGCAGTTGGAGGAACCGATCAATCGATCGATCAGTGGCAGTGTGAGTGCATGGAA
GTCAGCCAAACTGTGACTGAGCACAAACGGACAATTGCAATTTTCTTAGAATGTCAAGATTTGTATTAATGCCT
TTAAAATTAAATAAAAGCCCTTTTTTGAAAAAAAAAAAAAAAAAAAAAAAAAAAAA

Supplementary Figure 2.1. Rat *Smn* cDNA (accession: AF044910) sequence and sh_Smn_519 targeted sequence (underlined and bold) used to knockdown Smn in PC12 cells.

CHAPTER 3: Establishment of an intermediate mouse model of SMA: *Smn*$^{2B/-}$

A critical Smn threshold in mice dictates onset of an intermediate spinal muscular atrophy phenotype associated with a distinct neuromuscular junction pathology

Mélissa Bowerman, Lyndsay M. Murray, Ariane Beauvais, Bruno Pinheiro and Rashmi Kothary

Published in *Neuromuscular Disorders*, 2012, 22, 263-276

Author Contributions

Conceived and designed the experiments: MB, LMM and RK. Performed the experiments: MB, LMM, AB and BP. Analyzed the data: MB, LMM and AB. Wrote the paper: MB and LMM. Other: Designed and built the "in-house" gait-analysis box: BP.

ABSTRACT

Spinal muscular atrophy (SMA) is caused by mutations/deletions within the *SMN1* gene and characterized by loss of lower motor neurons and skeletal muscle atrophy. SMA is clinically heterogeneous, with disease ranging from severe to mild. Here, we identify a critical threshold of Smn that dictates onset of SMA in the intermediate $Smn^{2B/-}$ mouse model. With about 15% normal level of Smn protein, $Smn^{2B/-}$ mice display reduced body weight, motor neuron loss and motor defects. Importantly, these mice are phenotype-free until P10 with a median life expectancy of 28 days. They show neuromuscular junction (NMJ) pathology with an inter-muscular differential vulnerability and an association between pre- and post-synaptic defects. Our work suggests that increasing Smn protein levels only minimally could be of significant benefit since $Smn^{2B/2B}$ mice are phenotypically normal. Further, the finding that NMJ pathology varies between severe and intermediate SMA mouse models, suggests that future therapies be adapted to the severity of SMA.

INTRODUCTION

Spinal muscular atrophy (SMA) is the most common genetic cause of childhood mortality and the second most common autosomal recessive disorder (Crawford et al. 1996), affecting 1:6,000-10,000 live births. SMA manifests itself by a loss of the spinal cord α-motor neurons and proximal muscular atrophy, which, in the most severe cases, results in lethality before 2 years of age (Crawford et al. 1996).

SMA is caused by homozygous deletions or mutations within the *survival motor neuron 1* (*SMN1*) gene, located on chromosome 5q13 (Lefebvre et al. 1995). Whilst the *SMN* gene is highly conserved, due to a recent duplication event, humans possess two copies of the gene: *SMN1* and *SMN2* (Lefebvre et al. 1995; DiDonato et al. 1997). The two copies are nearly identical, with one exception being a critical C to T substitution in position 6 of exon 7 in *SMN2* (Lorson et al. 1999). This silent nucleotide substitution alters the splicing code and leads to the predominant production of an unstable protein lacking exon 7, termed SMNΔ7 (Lefebvre et al. 1995). As a small amount of functional full-length (FL) SMN protein is still produced by the *SMN2* gene, the number of copies of the *SMN2* gene in SMA patients is an important modifying factor dictating disease severity (Lefebvre et al. 1997).

The inverse correlation between the amount of FL SMN protein and severity of SMA phenotype is highlighted by the heterogeneity of this monogenic disease, which is clinically classified into 5 subtypes. Type 0 infants are the most severely affected and die shortly after birth

(Dubowitz 1999; MacLeod et al. 1999). Types I, II and III SMA are characterized by a childhood onset of the disease (Pearn 1980; Munsat et al. 1992). Type I (Werdnig-Hoffmann) patients are the most severely affected and commonly die before or around 2 years of age. In types II and III (Kugelberg-Welander) children, the symptoms manifest themselves between 6 months and 17 years of age. Some individuals can stand and sit by themselves but not walk (type II) while others are able to walk if assisted (type III). Finally, type IV SMA, the least severe form, occurs in adulthood and is typified by mild weakness of the proximal muscles (Pearn 1978a).

Our understanding of how depletion of the SMN protein in all cells results in the specific neuromuscular pathology is, as yet, undefined, due to the multiple functions of SMN in the nucleus, cytoplasm, neurite and growth cone (Boyer et al. 2010). To aid our understanding of SMA pathophysiology, a number of mouse models have been developed. The initial *Smn*$^{-/-}$ mouse proved to be embryonic lethal, suggesting an essential housekeeping role for the protein (Jablonka et al. 2000). Conversely, the heterozygous *Smn*$^{+/-}$ mouse model displays a very mild phenotype and retains a normal lifespan and reproductive ability (Jablonka et al. 2000). Through the insertion of human *SMN2* transgenes, two groups were able to produce a severe SMA mouse (*Smn*$^{-/-}$*;SMN2*), which dies within the first post-natal week (Hsieh-Li et al. 2000; Monani et al. 2000b). The insertion of an additional SMN allele lacking exon 7 (*SMNΔ7*) onto the background of the severe mouse model (*Smn*$^{-/-}$*;SMN2/SMN2;SMNΔ7/SMNΔ7*) extended life span to approximately 14 days (Le et al. 2005). These severe models have been used extensively in studies aimed at identifying pathological hallmarks of SMA and for the development of therapeutic strategies (Rossoll et al. 2003; Avila et al. 2007; Murray et al. 2008; Foust et al.

2010). However, the severity of these models, demonstrated by their perinatal symptom onset and rapid phenotypic decline, makes therapeutic intervention and outcome measurements problematic. Furthermore, as recent reports suggest that the vulnerability of the neuromuscular system varies greatly over the first post-natal weeks (Li et al. 1998; Kapoukranidou et al. 2005; Murray et al. 2011), it is unclear if the positive outcomes of existing and novel therapeutic interventions will be equivalent when administered at different developmental stages. Consequently, the current mouse models may not favour the identification of drugs or compounds that might be beneficial to the milder type II, III and IV SMA patients. For these reasons, there is a pressing need for a mouse model of SMA that manifests at a later age and displays a more prolonged disease time course. In this context, there has recently been a description of a new allele of the mouse *Smn* gene, termed Smn^{2B} (DiDonato et al. 2001; Hammond et al. 2010). This allele, when present together with a null allele, gives rise to a mouse model with an intermediate phenotype (Bowerman et al. 2009; Bowerman et al. 2010; Liu et al. 2010a).

In the present work, we identify a critical threshold for the Smn protein, which dictates the onset of SMA pathology, by characterizing the $Smn^{2B/+}$ and $Smn^{2B/2B}$ mice. These mouse models have reduced levels of FL Smn protein but remain phenotypically normal. A further reduction in the level of Smn protein observed in the $Smn^{2B/-}$ mouse, leads to the characteristic pathological hallmarks of SMA observed in both patients and mouse models: muscle weakness, gait abnormalities and loss of lower motor neurons from the brain stem and spinal cord. Importantly, these mice are born indistinguishable from their normal littermates, become

symptomatic around P10 and have a median life expectancy of 28 days. We have taken advantage of this mouse model to provide a detailed analysis of neuromuscular junction pathology and reveal pre-synaptic neurofilament accumulation and denervation alongside post-synaptic shrinkage and abnormal endplate morphology. We reveal significant inter-muscular differential vulnerability with regards to denervation and provide evidence that pre-synaptic pathology is associated with post-synaptic defects. This comprehensive analysis of the neuromuscular phenotype in the intermediate $Smn^{2B/-}$ mouse model will be of value to future studies aimed at understanding the development and progression of SMA as well as aid in the identification of novel therapeutics.

MATERIALS AND METHODS

Animal models

The *Smn*$^{2B/-}$ mice were established in our laboratory and maintained in our animal facility on a C57BL/6 x CD1 hybrid background. The 2B mutation consists of a substitution of 3 nucleotides in the exon splicing enhancer of exon 7 (DiDonato et al. 2001; Hammond et al. 2010). The *Smn* knock-out allele was previously described by Schrank *et al*. (Schrank et al. 1997) and *Smn*$^{+/-}$ mice were obtained from The Jackson Laboratory. All animal procedures were performed in accordance with institutional guidelines (Animal Care and Veterinary Services, University of Ottawa).

Antibodies

The primary antibodies used were as follows: mouse anti-actin (1:800; Fitzgerald), mouse anti-Smn (1:5000; Transduction Laboratories), mouse anti-2H3 (1:250, Developmental Studies Hybridoma Bank), mouse anti-SV2 (1:250, Developmental Studies Hybridoma Bank) and rabbit anti-HB9 (1:50 Abcam). The secondary antibodies used were as follows: horseradish peroxidase (HRP)-conjugated goat anti-mouse IgG (1:5000; Bio-Rad), DyLight goat anti-mouse (1:250, Jackson), Alexa Fluor 680 goat anti-mouse (1:5000, Molecular Probes), goat anti-rabbit biotin-SP-conjugated (1:200; Dako), streptavidin-Cy3-conjugated (1:600; Jackson Immuno Research). The α-bungarotoxin (aBTX) conjugated to tetramethylrhodamine isothiocyanate was from Molecular Probes (5 μg mL^{-1}).

Immunoblot analysis

Equal amounts of brain and spinal cord samples were separated by electrophoresis on 10% SDS-polyacrylamide gels and blotted onto a nitrocellulose membrane (Amersham). For quantification of protein, the membranes were blocked in Odyssey blocking buffer (LI-COR), incubated with the actin antibody overnight at 4ºC, rinsed in PBS (0.1% Tween 20, Sigma) and incubated with the Smn antibody, anti-Smn for 2 hours at room temperature. Subsequently, the membranes were rinsed in PBS (0.1% Tween 20) and incubated for 1 hour at room temperature with an Alexa Fluor 680-conjugated secondary antibody. The infrared fluorescent signals were detected using the Odyssey Infrared Imaging System (LI-COR). Both maximal and minimal exposure times were used to ensure accurate measurements.

For qualitative representation, the membranes were blocked in 5% non-fat milk in TBST (10 mM Tris-HCl pH 8.0, 150 mM NaCl, and 0.1% Tween 20 (Sigma)), and washes were performed with TBST. Signals were visualized using the ECL or the ECL plus detection kit (Amersham). Exposure times were chosen based on the saturation of the highest amounts of protein.

RT-PCR

RNA from spinal cords was extracted with the TRIzol Reagent (Gibco) according to the manufacturer's instructions. Reverse transcription was performed using 0.5 μg of total RNA. To ensure product specificity, a nested RT-PCR was used. The following primers were used for RT-PCR analysis: 1st round: *Smn* forward (5' GAA CAG AAC ACT CAG GAG AAT GAA 3') and *Smn* reverse (5' ATG GAT GGA CTC CCA CAG C 3'); 2nd round: *Smn* forward (5' CCT CAT

TTC TTC CTC CAC CA 3') and *Smn* reverse (5' CCT ATC TCC TGA GAC AGA GC 3'). *FL Smn* mRNA/*SmnΔ7* mRNA ratios were determined by densitometry using the Image J software (NIH).

Hematoxylin and Eosin staining

Spinal cord (L1-L2 lumbar regions) and brain stem sections (5 μm) were deparaffinized in xylene and fixed in 100% ethanol. Following a rinse in water, samples were stained in hematoxylin (Fisher) for 3 minutes, rinsed in water, dipped 40 times in a solution of 0.02% HCl in 70% ethanol and rinsed in water again. The sections were stained in a 1% eosin solution (BDH) for 1 minute, dehydrated in ethanol, cleared in xylene and mounted with Permount (Fisher). Images were taken with a Zeiss Axioplan2 microscope, with a 20X objective.

Quantitative assays were performed on 3 mice for each genotype and 5 sections per mouse. Analyzed sections were at least 10 μm apart. Motor neurons were identified by their shape and size (> 10 μm in diameter) in the same designated area of the ventral horn region of the spinal cord and the designated area containing the facial nerves of the brain stem. Only motor neurons with visible nuclei were counted as to prevent double-counting.

Immunohistochemistry

For immunohistochemistry, spinal cord and brain stem sections were first deparaffinized in xylene (3 x 10 mins), fixed in 100% ethanol (2 x 10 mins), rehydrated in 95% and 75% ethanol (5 secs each) and placed 5 mins in 1 M Tris-HCl pH 7.5. Sections were then placed in

boiling sodium citrate antigen retrieval buffer (10 mM sodium citrate, 0.05% Tween 20, pH 6.0) for 20 minutes in the microwave. The sections were then rinsed 10 minutes under running cold tap water and incubated for 2 hours at room temperature (RT) in blocking solution (TBLS (10% NaN_3), 20% goat serum, 0.3% Triton X-100). This was followed by an overnight incubation at 4ºC with the primary antibody. Subsequently, sections were washed 3 times with PBS, incubated 1 hour at RT with the secondary antibody and washed 3 times with PBS. Hoechst (1:1000) was added to the last PBS wash followed by the slides being mounted in Fluorescent Mounting Medium (Dako). Images were taken with a Zeiss confocal microscope, with a 20X objective, equipped with filters suitable for Cy3/Hoechst fluorescence.

Neuromuscular junction immunohistochemistry

Muscles were labelled by immunohistochemistry to allow quantification of neuromuscular innervation as described previously (Murray et al. 2008). Briefly, muscles were immediately dissected from recently sacrificed mice and fixed in 4% paraformaldehyde (Electron Microscopy Science) in PBS for 15 minutes. Post-synaptic acetylcholine receptors (AChRs) were labelled with aBTX for 10 min. Muscles were then blocked in 4% bovine serum albumin (BSA)/1% TritonX in PBS for 30 min before incubation overnight in primary antibodies and visualized with DyLight-conjugated secondary antibodies. Muscles were then whole-mounted in Dako Fluorescent mounting media. Images were taken with a Zeiss confocal microscope

Gait measurements

Gait assessment was performed using an in-house gait box (**Supplementary Figure 3.1**). The front paws of the mice were marked with red ink while the back paws were marked with blue ink. The mice were then placed at the larger end of the gait box with a light shone through to encourage the mice to walk towards the opposite end, leaving their imprints on a piece of white paper. Subsequently, stride length (distance from right heel strike to next right heel strike), step length (distance from right heel strike to left heel strike) and stride width (perpendicular distance between back paws) were measured.

Pen-test

Balance and strength were assessed using the pen-test as described (Willmann et al. 2011) Mice were placed on a suspended pen at different time-points (postnatal days (P) 12, 14, 17 and 21). The latency to fall from the pen was measured with a plateau of 30 seconds. At each time-point, individual mice were placed three consecutive times.

Electron microscopy

Tibial nerve preparations were dissected and pinned out on dental wax before being immersion-fixed in 0.1 M cacodylate buffer containing 4% formaldehyde and 2.5% glutaraldehyde for 4 hours before post-fixation in 1% osmium tetroxide for 45 minutes. Preparations were dehydrated in ascending alcohol series (50%, 70%, 90%, 100% x 2) and acetone. Preparations were embedded in Spur monomer. Ultra-thin sections (75-90 nm) were cut

and collected on mesh grids, stained with uranyl acetate and lead citrate. Sections were viewed in a Hitachi H7100 transmission electron microscope (TEM).

Statistical methods

For the Kaplan-Meier survival analysis, the log-rank (Mantel-Cox) test was used and survival curves were considered significantly different at $P<0.05$. For the remaining statistical analyses, the Student's one-tail or two-tail *t* test for paired variables, the Kruskal Wallis with Dunn multiple comparison post hoc test and the Mann Whitney U test were used to test for differences between samples and data were considered significantly different at $P< 0.05$.

RESULTS

Absence of an SMA phenotype in mice with significantly decreased levels of Smn protein

Recent reports have described the genetic knock-in and characterization of the *Smn2B* allele in the mouse (Hammond et al. 2010). In short, the *Smn2B* allele consists of the substitution of 3 nucleotides in the exon splicing enhancer (ESE) within exon 7 of the murine *Smn* gene. This mutation promotes the excision of exon 7 and the production of the SmnΔ7 protein, thus replicating the splicing pattern of the human *SMN2* gene (DiDonato et al. 2001). Subsequent mice homozygous for the *Smn2B* mutation were termed $Smn^{2B/2B}$.

RNA analysis of brains and spinal cords of one month old mice revealed that the *SmnΔ7* transcript is present in both homozygous ($Smn^{2B/2B}$) and heterozygous mice ($Smn^{2B/+}$) (**Figure 3.1 A**). The *SmnΔ7* transcript was not observed in wild type samples (**Figure 3.1 A**). Quantification shows that there is significantly more *SmnΔ7* transcript in both the brains and spinal cords of $Smn^{2B/2B}$ mice when compared to the $Smn^{2B/+}$ mice (**Figure 3.1 B**; $P = 0.0005$ and 0.02, respectively). This increase in *SmnΔ7* transcript at the expense of the *FL Smn* transcript is accompanied by a decrease in Smn protein. Compared to wild type levels, the brains of $Smn^{2B/+}$ and $Smn^{2B/2B}$ mice retain 70% and 25% FL Smn, respectively, while the spinal cords of $Smn^{2B/+}$ and $Smn^{2B/2B}$ mice retain 78% and 36% FL Smn, respectively (**Figure 3.1 C and Table 3.1**). Thus, the presence of one or both Smn^{2B} alleles is sufficient to reduce Smn expression.

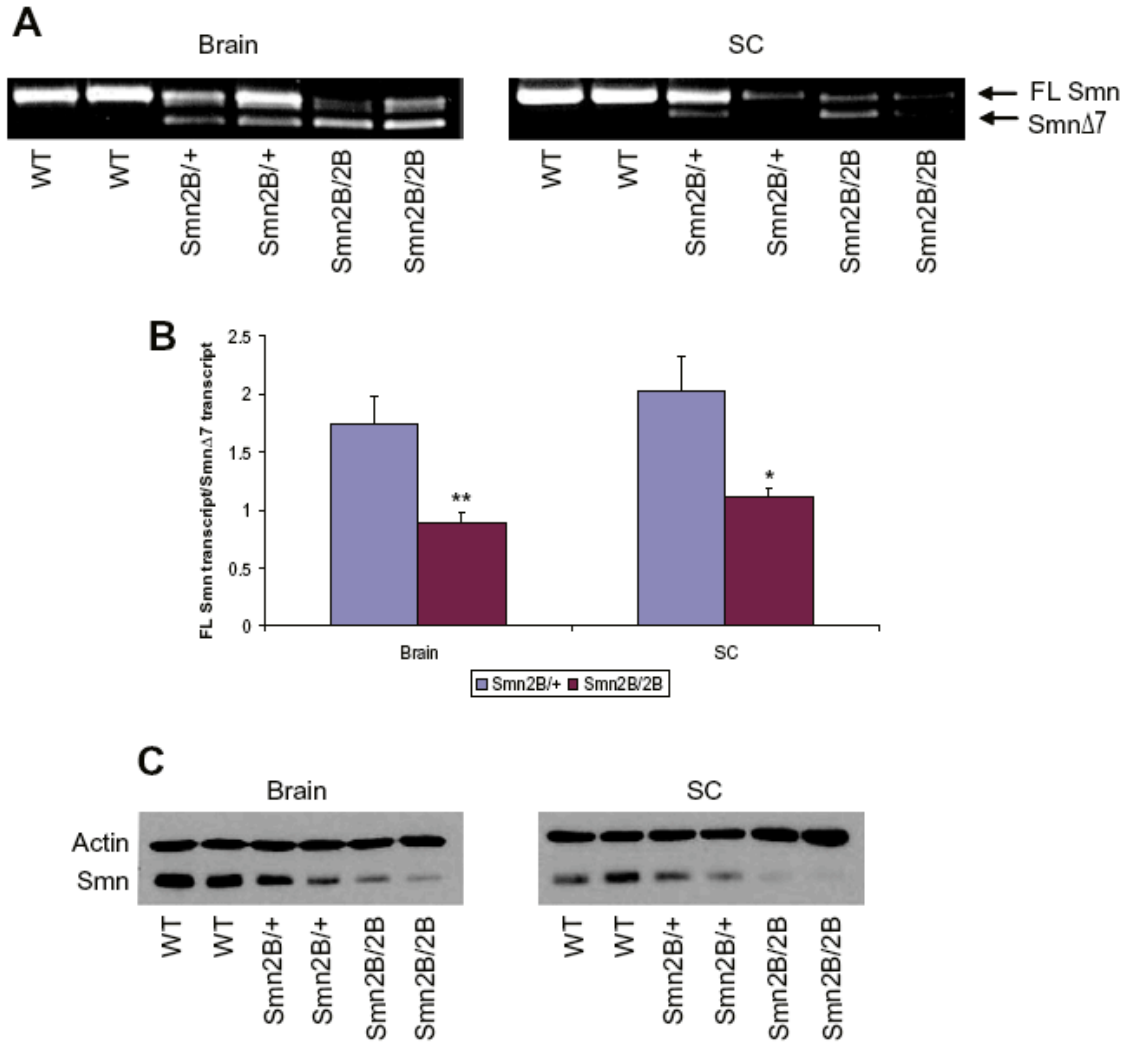

Figure 3.1. The *Smn*$^{2B/+}$ and *Smn*$^{2B/2B}$ mice have increased *SmnΔ7* transcript and decreased FL Smn protein. A) Nested RT-PCR shows that the brains and spinal cords (SC) of one month old *Smn*$^{2B/+}$ and *Smn*$^{2B/2B}$ mice express the *SmnΔ7* transcript with a concordant decrease in the expression of the *FL Smn* transcript. WT = wild type. B) Quantification of *FL Smn* transcript/*SmnΔ7* mRNA shows that the brains and spinal cords of *Smn*$^{2B/2B}$ mice express significantly more *SmnΔ7* mRNA than the *Smn*$^{2B/+}$ mice (**P = 0.0005 and *P = 0.002, respectively; n = 4 mice per genotype. Data are mean +/- S.D). C) Immunoblot analysis shows

that the brains and spinal cords of one month old *Smn*$^{2B/+}$ and *Smn*$^{2B/2B}$ mice have reduced levels of FL Smn protein. Actin served as a loading control. Representative images were chosen based on the saturation of the highest amounts of protein. For quantification (see **Table 3.1**), both maximal and minimal exposure times were used to ensure accurate measurements.

Table 3.1. Percentage of full-length Smn protein relative to the brains and spinal cords of wild type mice

	$Smn^{2B/+}$	$Smn^{2B/2B}$	$Smn^{2B/-}$
Brain	69.96 % +/- 26.66 [a]	25.25 % +/- 10.68	8.99 % +/- 1.83 [b]
Spinal Cord	78.41 % +/- 25.22	36.24% +/- 6.73	24.51% +/- 9.83 [c]

[a] Data are mean +/- SDEV (n = 5 for each genotype)
[b] The Smn levels in the brains of $Smn^{2B/-}$ mice are significantly lower compared to $Smn^{2B/+}$ and $Smn^{2B/2B}$ mice ($P = 0.0004$ and 0.005 respectively).
[c] The Smn levels in the spinal cords of $Smn^{2B/-}$ mice are significantly lower compared to $Smn^{2B/+}$ and $Smn^{2B/2B}$ mice ($P = 0.001$ and 0.03 respectively).

Interestingly, the *Smn*$^{2B/2B}$ mouse has a normal lifespan and reproductive ability, and is indistinguishable from its wild type littermates. Similar growth curves and performances on the pen-test (see Methods) between wild type and *Smn*$^{2B/2B}$ mice further support the absence of an overt phenotype in the latter group (**Figure 3.2 A, B**). Since the existing *Smn*$^{+/-}$ mild SMA mouse model shows a very late onset of motor neuron loss (Jablonka et al. 2000), we analyzed the brain stems and spinal cords (L1-L2 lumbar regions) of six month old wild type, *Smn*$^{2B/+}$ and *Smn*$^{2B/2B}$ mice (**Figure 3.2 C**). Hematoxylin and eosin staining was used to identify motor neurons based on their morphology, size (> 10 μm diameter), and location. There was no reduction in the number of motor neuron cell bodies in heterozygous or homozygous mice, when compared to wild type littermates (**Figure 3.2 C, D**). Similar results were obtained in one year old mice (data not shown). It has previously been suggested that neuromuscular junction (NMJ) defects precede motor neuron loss in SMA pathology (Murray et al. 2008). We thus analyzed NMJs in the transversus abdominis (TVA), a muscle known to be vulnerable in other SMA mouse models (Murray et al. 2008), in 8 month old wild type and *Smn*$^{2B/2B}$ mice. Gross morphological analysis of muscle innervation revealed no evidence of denervation, with *Smn*$^{2B/2B}$ NMJs displaying a mature morphology, which was indistinguishable from wild type controls. (**Figure 3.2 E**). Thus, while the *Smn*$^{2B/2B}$ mice have significantly reduced *FL Smn* mRNA and protein, they do not display any of the neuromuscular hallmarks of SMA.

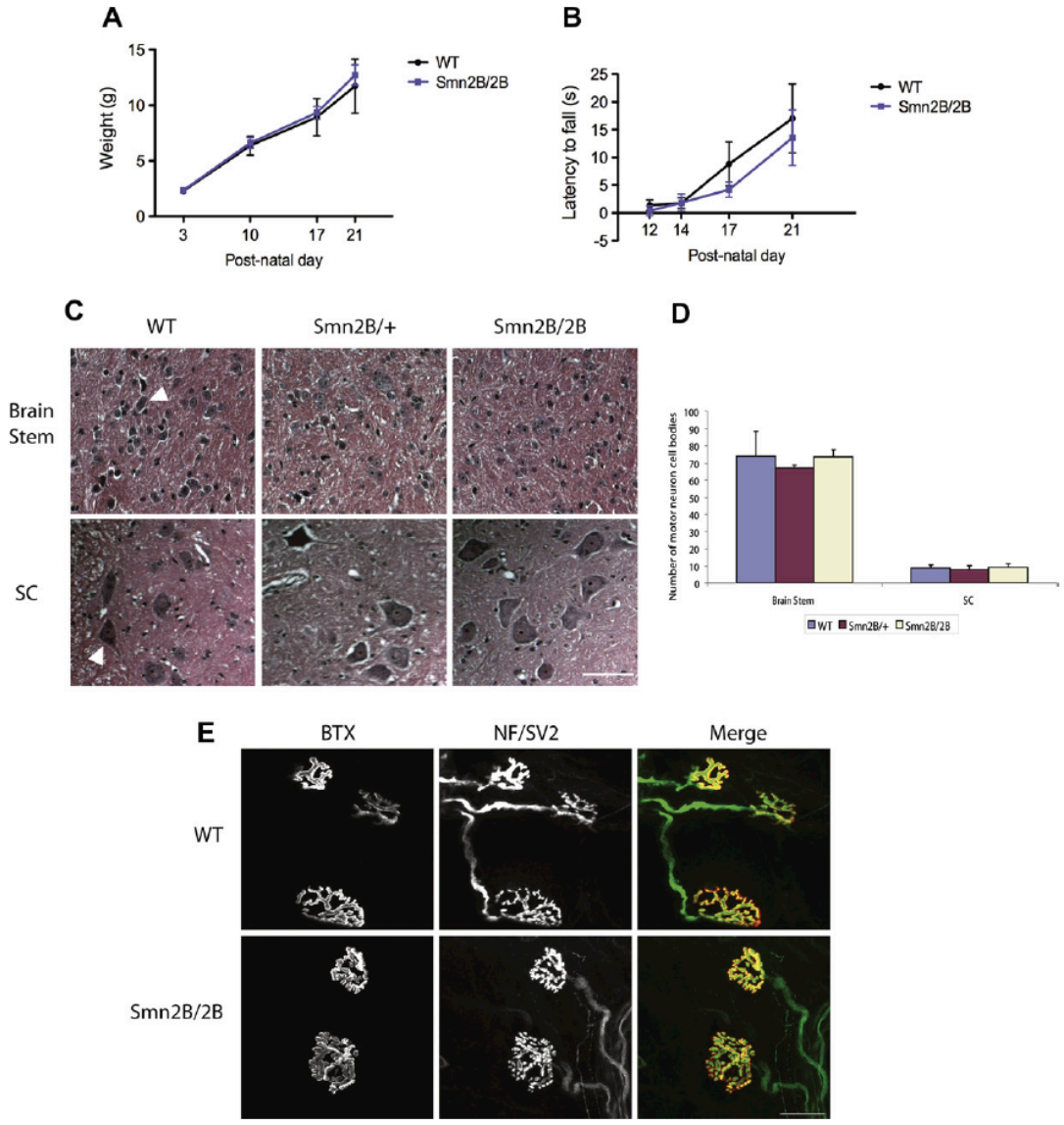

Figure 3.2. Absence of an SMA phenotype in *Smn*$^{2B/2B}$ mice**.** A) Weight curve showing similar growth profile between wild type (WT) and *Smn*$^{2B/2B}$ mice (n = 24/11 mice per WT/ *Smn*$^{2B/2B}$)**.** B) Performance of WT (n = 10) and *Smn*$^{2B/2B}$ (n = 11) mice on the pen-test at post-natal days (P) 12, 14, 17 and 21. Both groups had similar performances on the pen-test, displaying indistinguishable strength and balance (n=10/11 11 mice per WT/ *Smn*$^{2B/2B}$). C) Representative images of hematoxylin and eosin stained sections from the brain stems and the ventral horn

region of the lumbar (L1-L2) spinal cords (SC) of WT, *Smn*$^{2B/+}$ and *Smn*$^{2B/2B}$ mice. A typical large motor neuron cell body is indicated by an arrowhead. Scale bar = 100 μm D) Quantification shows that there is no difference between the number of motor neurons in WT (n = 4), *Smn*$^{2B/+}$ (n = 6) and *Smn*$^{2B/2B}$ (n= 6) mice, in both the brain stems and spinal cords (n = 4/6/6 mice per WT/*Smn*$^{2B/+}$/Smn$^{2B/2B}$, Data are mean +/- S.D). E) Representative confocal micrographs of neuromuscular junction morphology in the transversus abdominis of 8 month old WT and *Smn*$^{2B/2B}$ mice (green/NF/SV2: neurofilament/synaptic vesicle protein 2; red/BTX: rhodamine-conjugated bungarotoxin). Scale bar = 20 μm.

These results demonstrate that despite having significantly reduced levels of Smn transcript and protein, the *Smn*$^{2B/2B}$ mouse displays no overt motor phenotype or motor neuron loss, even up to 1 year of age. This suggests that SMA severity is more so influenced by a threshold or a narrow range of FL SMN protein rather than being defined by a linear function. The *Smn*$^{2B/2B}$ mice were subsequently crossed with *Smn*$^{+/-}$ mice to produce *Smn*$^{2B/-}$ mice, to achieve a greater reduction of Smn protein (down to approximately 15% of wild type levels) and to determine if this would lead to the development of a phenotype reminiscent of SMA.

Smn$^{2B/-}$ mice: an intermediate model for SMA

The Smn$^{2B/-}$ *mouse model displays an intermediate SMA phenotype*

As previously reported (Bowerman et al. 2009; Bowerman et al. 2010; Liu et al. 2010a), The *Smn*$^{2B/-}$ mouse model (**Figure 3.3 A**) begins to display neuromuscular pathology, as evidenced by an observable physical weakness, tremors and ambulating abnormalities at approximately two weeks of age. This is emphasized by a significant arrest in weight-gain observed in these mice at P17 and onwards (**Figure 3.3 B**) and a median life expectancy of 28 days (**Figure 3.3 C**). The *Smn*$^{2B/-}$ mice also display the SMA pathological hallmark of motor neuron loss in the brain stem and ventral horn region of the lumbar spinal cord (L1-L2) (**Figure 3.3 D, E**).

Interestingly, a small cohort of *Smn*$^{2B/-}$ mice survives beyond 60 days, although still displaying the characteristic neuromuscular pathology. The reasons for these outliers remain unclear, however we suggest it is at least partly attributable to Smn-independent disease modifiers and/or intrinsic genetic background differences (Oprea et al. 2008).

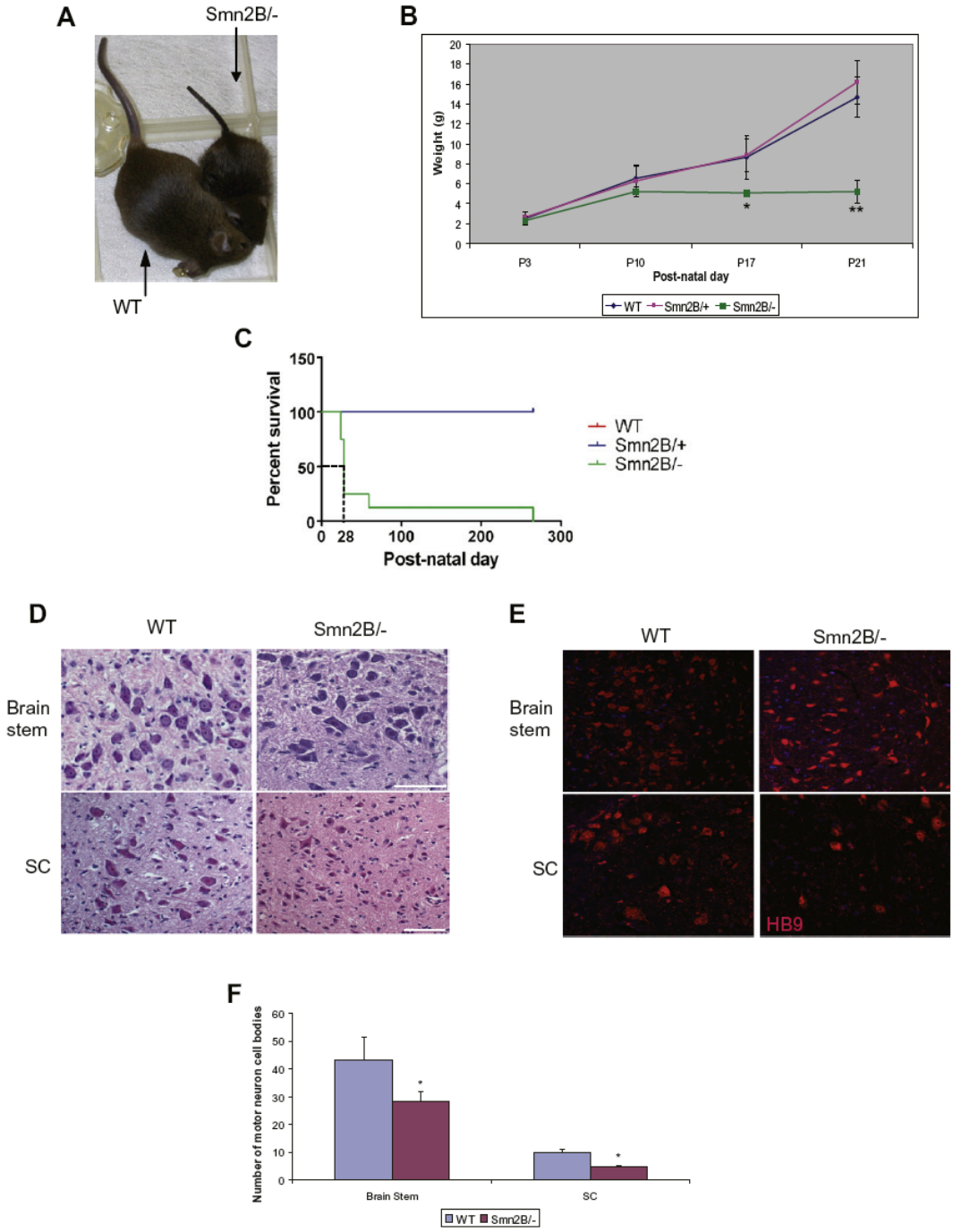

Figure 3.3. The *Smn*$^{2B/-}$ mice display an intermediate SMA phenotype. A) Representative image of a wild type (WT) and a *Smn*$^{2B/-}$ mouse at three weeks of age. B) Weight curve of WT, *Smn*$^{2B/+}$ and *Smn*$^{2B/-}$ mice from post-natal day (P) 0 to 21. Up until P10, the weight of *Smn*$^{2B/-}$ mice is

comparable to that of WT mice. Afterwards, at P17 and P21, the $Smn^{2B/-}$ mice are significantly smaller than WT mice. The weight of $Smn^{2B/+}$ mice was comparable to that of WT mice. (*P = 0.03 and **P = $8E^{-15}$; n = 5/15/8 mice per WT/$Smn^{2B/+}$/$Smn^{2B/2B}$; Data are mean +/- S.D). C) The Kaplan-Meier survival curve shows that the lifespan of $Smn^{2B/-}$ mice is significantly decreased compared to WT and $Smn^{2B/+}$ mice (P = 0.0007), with median life expectancy of 28 days. D) Representative images of hematoxylin and eosin stained sections from the brain stem and the ventral horn root region of the lumbar spinal cord of WT and $Smn^{2B/-}$ mice. A typical large motor neuron cell body is indicated by an arrowhead. Scale bar = 100 μm. E) Representative images of HB9 (red) staining of brain stem and the ventral horn root region of the lumbar spinal cord of WT and $Smn^{2B/-}$ mice. Arrowhead depicts a typical large motor neuron body. Scale bar = 50 μm. F) There is a significant loss of motor neurons in the brain stem and the spinal cord of $Smn^{2B/-}$ mice when compared to WT mice (*P = 0.04 and *P = 0.002, respectively).

The $Smn^{2B/-}$ mouse model has a critical reduction of Smn mRNA and protein

We next analyzed Smn mRNA and protein levels in the brains and spinal cords of the $Smn^{2B/-}$ mice at one month of age, a time point at which all mice display a severe motor phenotype. Whilst one month old wild type mice predominantly produced *FL Smn* transcript, RT-PCR analysis shows that both the brains and the spinal cords of $Smn^{2B/-}$ mice predominantly produce the *SmnΔ7* transcript (**Figure 3.4 A**). This is further supported by their significantly reduced *FL Smn* transcript/*SmnΔ7* transcript ratios when compared to $Smn^{2B/+}$ mice (**Figure 3.4 B**; $P = 0.02$ (brain) and 0.01 (spinal cord)).

The observed decrease in *FL Smn* transcript is accompanied by a dramatic decrease in Smn protein in both the brains and spinal cords of $Smn^{2B/-}$ mice when compared to $Smn^{2B/+}$ and wild type littermates (**Figure 3.4 C**). To better quantify the decrease in Smn protein, we performed immunoblot analysis on tissue lysate from 5 mice of each genotype using the Odyssey system (see Methods). The results are summarized in **Table 3.1**. When compared to the $Smn^{2B/+}$ and $Smn^{2B/2B}$ mice, the brains and spinal cords of $Smn^{2B/-}$ contained significantly less Smn protein, with an approximate 10% and 25% residual FL Smn protein, respectively (**Table 3.1**; $P = 0.005$ and 0.03, respectively). Interestingly, there is only an approximately 15% (brain) and a 10% (spinal cord) difference between the phenotypically normal $Smn^{2B/2B}$ mice and the SMA $Smn^{2B/-}$ mouse model.

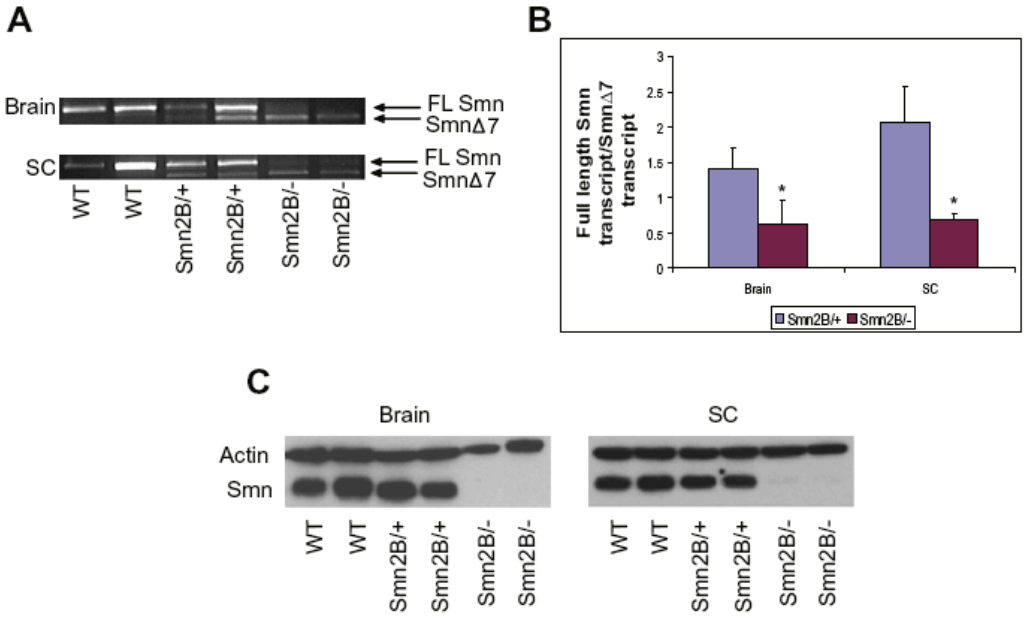

Figure 3.4. The *Smn*$^{2B/-}$ mice have increased *SmnΔ7* transcript and decreased FL Smn protein levels. A) Nested RT-PCR shows that the brains and spinal cords of *Smn*$^{2B/-}$ mice predominantly express the *SmnΔ7* transcript compared to *Smn*$^{2B/+}$ and wild type (WT) mice. B) Quantification of *FL Smn* transcript/*SmnΔ7* transcript ratios shows that *Smn*$^{2B/-}$ mice (n = 3) mice express significantly more *SmnΔ7* transcript than *Smn*$^{2B/+}$ mice (n = 4) in both the brain and spinal cord (**P* = 0.02 and **P* = 0.01, respectively; n = 4/3 mice per *Smn*$^{2B/+}$/Smn$^{2B/-}$; data are mean +/- S.D). C) Immunoblot analysis shows that the *Smn*$^{2B/-}$ brains and spinal cords have decreased FL Smn protein levels compared to *Smn*$^{2B/+}$ and WT mice. Representative images were chosen based on the saturation of the highest amounts of protein. For quantification (see **Table 3.1**), both maximal and minimal exposure times were used to ensure accurate measurements.

The $Smn^{2B/-}$ mice display neuromuscular defects

Gait analysis was used to assess signs of neuromuscular dysfunction in the $Smn^{2B/-}$ mice (Burgess et al. 2010). For this experiment, an in-house gait box (**Supplementary Figure 3.1**) was used. Stride length, step length and stride width were all significantly shorter in $Smn^{2B/-}$ mice when compared to wild type and $Smn^{2B/+}$ littermates (**Figure 3.5 A, B**). To eliminate the possibility that the difference in these measurements is simply due to the overall smaller size of the $Smn^{2B/-}$ mice, we compared the stride length/stride width ratios and this analysis revealed a significant decrease in $Smn^{2B/-}$ mice (**Figure 3.5 C**). Therefore, whilst smaller body size is likely to have an impact upon stride size, neuromuscular dysfunction is also a significant contributing factor to this phenotype.

We next used the pen-test (see Methods) as a gross assessment of the balance and strength of the $Smn^{2B/-}$ mice at P12, 14, 17 and 21. Both wild type and $Smn^{2B/+}$ mice were able to stay on the pen longer and were statistically indistinguishable from each other (**Figure 3.5 D**). On the other hand, at P14, 17 and 21, $Smn^{2B/-}$ mice showed a significantly poorer performance, never being able to balance or hold themselves on the pen (**Figure 3.5 D**; $P = 0.0002$, 0.004 and $1.75E^{-05}$, respectively). This, in combination with the arrest in weight gain observed in these mice, suggests that the $Smn^{2B/-}$ mice are significantly weaker than their $Smn^{2B/+}$ and wild type littermates.

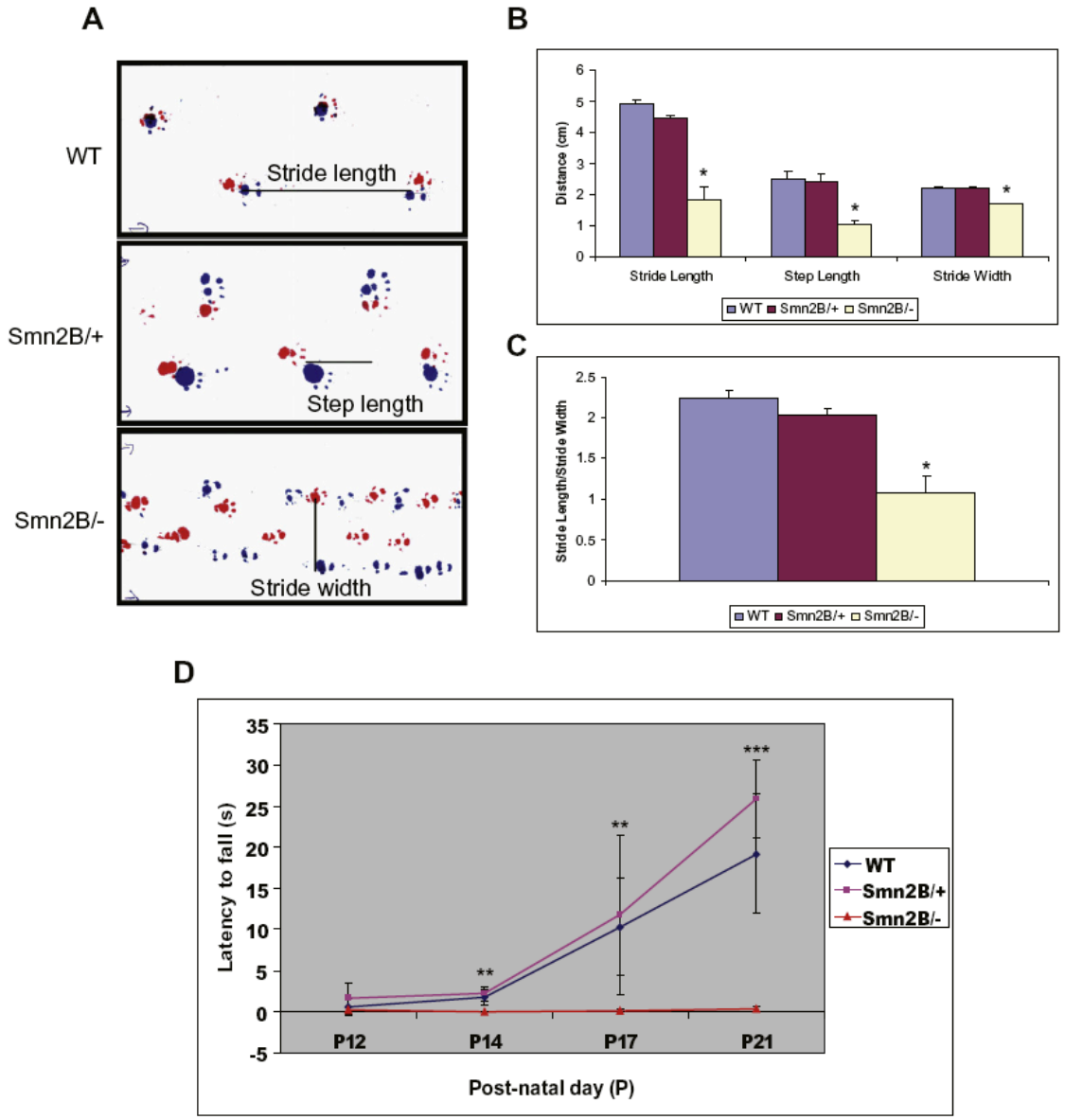

Figure 3.5. The *Smn*$^{2B/-}$ mice display locomotor defects. A) Representative examples of wild type (WT), *Smn*$^{2B/+}$ and *Smn*$^{2B/-}$ mouse paw prints used for gait analysis (red = front paws, blue = back paws). The stride length was defined as the distance from the right heel strike to next right heel strike, step length as the distance from right heel strike to left heel strike and stride width as the perpendicular distance between back paws. B) Quantification shows that stride length, step

length and stride width of $Smn^{2B/-}$ mice are significantly shorter than WT mice (*P = 0.002, *P = 0.005 and *P = 0.001, respectively). $Smn^{2B/+}$ mice were similar to WT. (n = 3 mice per genotype; data are mean +/- S.D). C) The stride length/stride width ratio of $Smn^{2B/-}$ mice is significantly smaller than that of $Smn^{2B/+}$ and WT mice (*P = 0.008). D) Performance of wild type (WT), $Smn^{2B/+}$ and $Smn^{2B/-}$ mice on the pen-tests at post-natal days (P) 12, 14, 17 and 21. At P14, P17 and P21, $Smn^{2B/-}$ mice are significantly weaker than WT mice, effectively unable to balance and/or grip to remain on the suspended pen (**P = 0.0002, **P = 0.0004 and ***P = $1.75E^{-05}$, respectively).

Axonal loss and degeneration in $Smn^{2B/-}$ mice

It has been suggested that SMA pathology occurs in a distal to proximal manner, with synapses and axons being affected prior to overt motor neuron loss (Murray et al. 2008). We thus examined motor neurons distally through the electron microscopic analysis of the tibial nerve, which innervates the distal portion of the hind limb and foot, including the deep lumbrical muscles. Most $Smn^{2B/-}$ axons appeared healthy with organized microtubules, intact mitochondria and compact myelin sheaths (**Figure 3.6 A**). However, a subset of axons displayed a degenerative morphology, as evidenced by unraveling of the myelin sheath and associated shrinkage of the axon within (**Figure 3.6 A**). Quantification of the number of degenerating axons revealed a trend towards an increase in $Smn^{2B/-}$ nerves compared to $Smn^{2B/+}$ controls (**Figure 3.6 B**). As expected, due to the loss of motor neuron cell bodies, $Smn^{2B/-}$ nerves revealed a statistically significant decrease in the number of axons per nerve (**Figure 3.6 C**). Together, this data suggest that increased axonal degeneration leads to a reduction in axons number in the $Smn^{2B/-}$ mouse model.

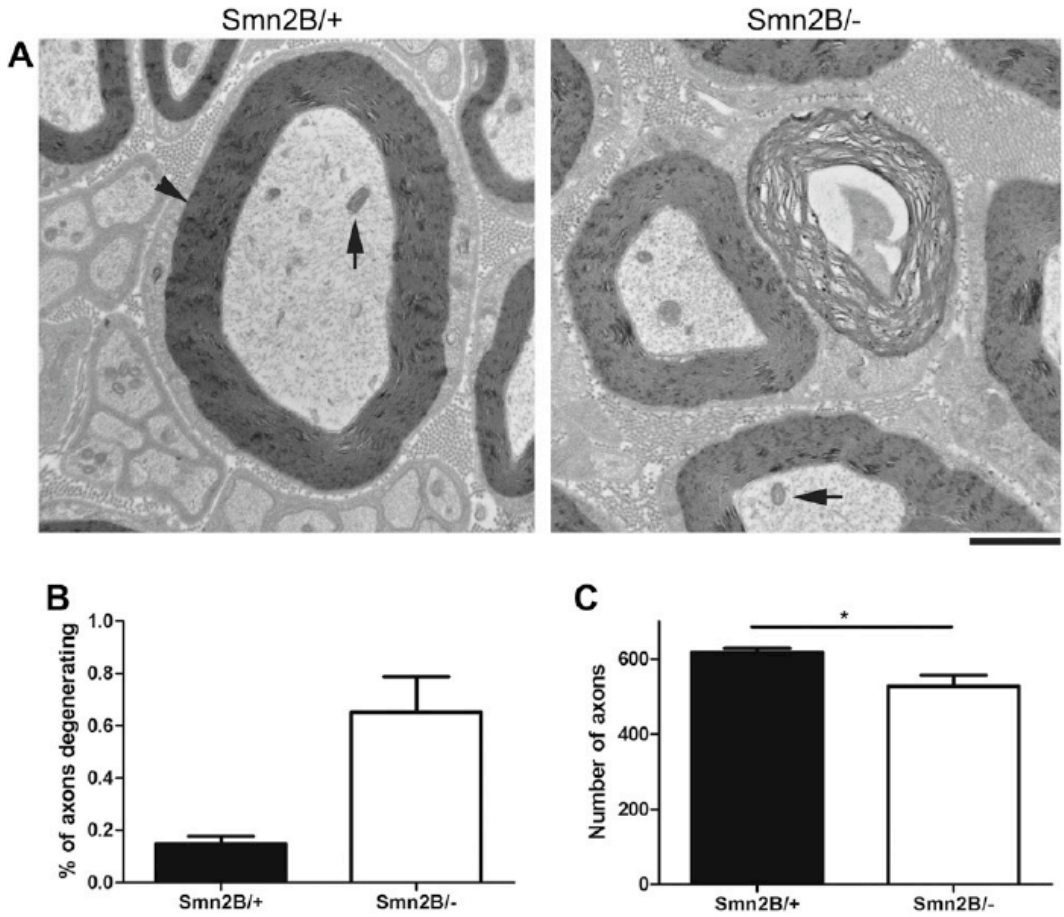

Figure 3.6. Axonal loss and degeneration in the tibial nerve of *Smn*$^{2B/-}$ mice. A) Representative electron micrographs from *Smn*$^{2B/+}$ and *Smn*$^{2B/-}$ tibial nerves at post-natal (P) day 21. In *Smn*$^{2B/+}$ mice, axons generally appeared healthy with intact mitochondria (arrow) and compact myelin sheathes (arrowhead) while *Smn*$^{2B/-}$ mice displayed some degenerating axons, as evidenced by unravelling of the myelin sheath and degeneration of the associated axon. B) Quantification of the percentage of degenerating axons revealed an increase in the *Smn*$^{2B/-}$ tibial nerve, although this number failed to reach statistical significance. (n = 3 nerves/mice per genotype; data are mean +/- SD. C) Quantification of the number of axons revealed a significant reduction in the tibial nerve of *Smn*$^{2B/-}$ mice compared to *Smn2*$^{B/+}$ (*P = 0.0454; n = 3 nerves/mice per genotype; data are mean +/- SD).

Neuromuscular junction pathology in $Smn^{2B/-}$ mice

Previous work on more severe mouse models of SMA indicates that neuromuscular junctions (NMJs) are early and important pathological targets (Kariya et al. 2008; Murray et al. 2008; Kong et al. 2009; Murray et al. 2010c). We therefore assessed NMJ connectivity and morphology in a range of thin or small muscles positioned throughout the body, allowing a comprehensive analysis of NMJ pathology. In addition to their useful anatomical features, these muscles were also selected as they have been extensively characterized in both the *$Smn^{-/-}$;SMN2/SMN2* and *$Smn^{-/-}$;SMN2/SMN2;SMNΔ7/SMNΔ7* mouse models (Murray et al. 2008; Murray et al. 2010a; Murray et al. 2010b). This therefore allows direct comparison of the features of NMJ pathology in distinct muscle groups between different mouse models. Here, $Smn^{2B/-}$ mice were compared to $Smn^{2B/+}$ littermates, as the latter displayed NMJ morphology indistinguishable from wild type mice.

In accordance with previous reports on the severe SMA mouse models, we observed NMJ loss in $Smn^{2B/-}$ mice, although the extent of denervation varied between different muscles (**Figure 3.7 A, B**). Consistent with previous reports in the more severe SMA mouse models (Murray et al. 2008), the muscle most severely affected was the transversus abdominis (TVA) (**Figure 3.7 B**). Conversely, contrary to the previously described selective vulnerability of the Levator Auris Longus caudal band (LALc) (Murray et al. 2008), here we show the selective vulnerability of the LAL rostral band (LALr) (**Figure 3.7 B**).

In addition to denervation, we observed significant accumulation of neurofilament (NF) at the NMJ, as evidenced by large swellings within the pre-synaptic terminal, which were absent in control littermates (**Figure 3.7 C**). Although the significance of these swellings is unclear, this observation is again consistent with reports from other mouse models of SMA (Cifuentes-Diaz et al. 2002; Kariya et al. 2008; Murray et al. 2008).

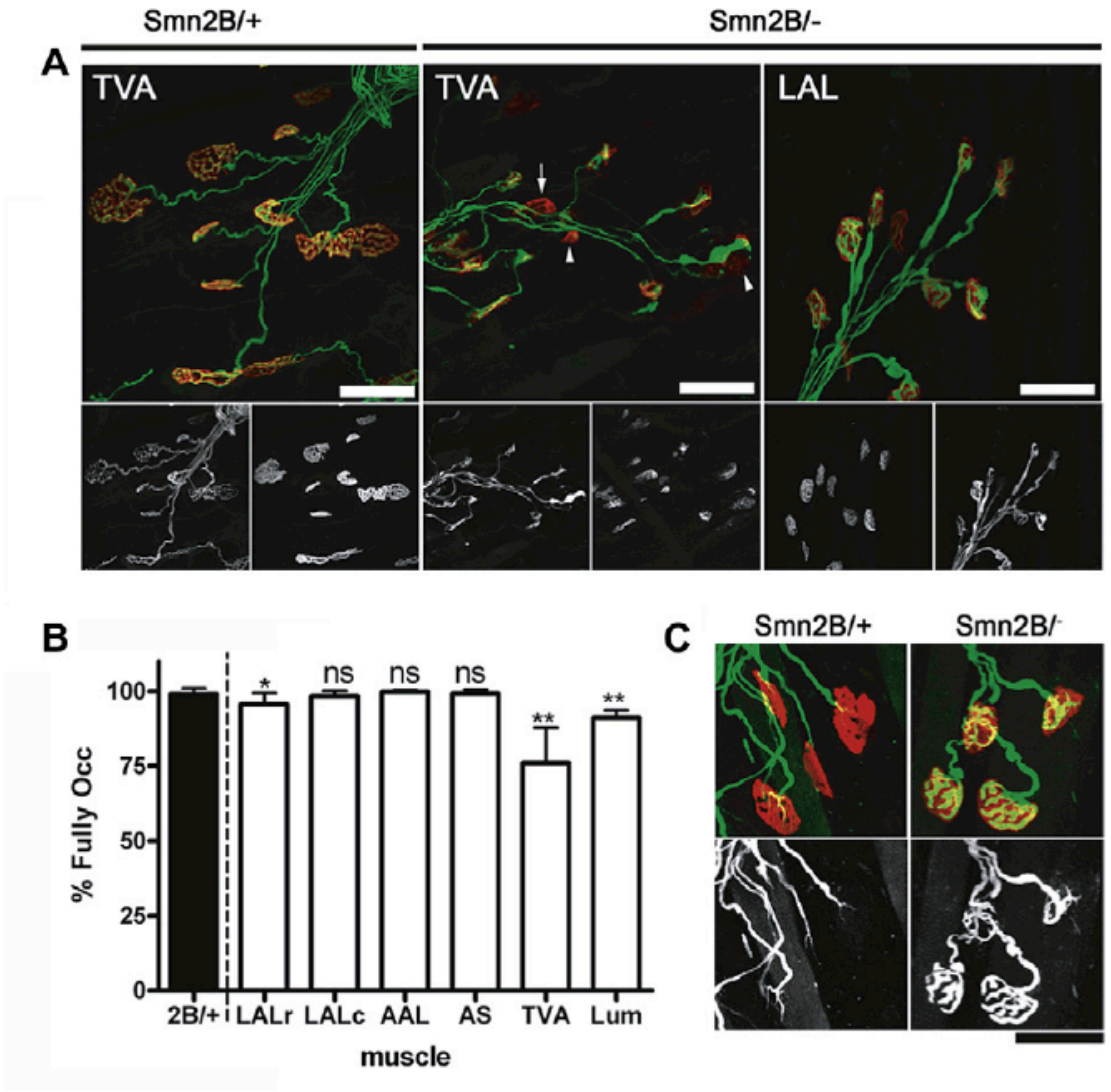

Figure 3.7. Denervation and neurofilament accumulation at the pre-synaptic terminal of *Smn*$^{2B/-}$ mice. A) Representative confocal micrographs showing neuromuscular junctions from P21 control *Smn*$^{2B/+}$ and *Smn*$^{2B/-}$ mice from the transversus abdominis (TVA) and Levator Auris Longus (LAL) muscle (green/lower left: neurofilament/synaptic vesicle protein 2; red/lower right: rhodamine-conjugated bungarotoxin). Note the presence of completely (arrow) and partially denervated (arrowhead) motor endplates in the TVA muscle as evidenced by AChR labelling in the absence of a pre-synaptic terminal. Scale bar = 20 μm. B) Quantification of the

percentage of fully occupied endplates in a range of muscles situated throughout the body (TVA, transversus abdominis; LALr, Levator Auris Longus rostral band; LALc, Levator Auris Longus caudal band; AAL, Adductor Auris Longus, AS, Auricularis Superior; Lum, Deep Lumbricals) compared to the TVA muscle in $Smn^{2B/+}$ (2B/+) mice. Significant denervation was observed in TVA, LALr and Lumbricals *(**P = 0.0002, *P = 0.0027, **P = 0.0003 respectively), whilst LALc, AS and AAL remain spared. (n =3/5 $Smn^{2B/+}$/$Smn^{2B/-}$ mice respectively; data are mean +/- S.D.). C) Confocal micrographs showing neuromuscular junctions from P21 control $Smn^{2B/+}$ and $Smn^{2B/-}$ mice from the Levator Auris Longus (LAL) muscle (green/lower panel: neurofilament 165; red: rhodamine-conjugated bungarotoxin). Neurofilament accumulations are present throughout the pre-synaptic terminal in $Smn^{2B/-}$ mice, which are absent in control littermates ($Smn^{2B/+}$). Scale bar = 20 μm.

We also observed post-synaptic changes including shrinkage of the motor endplate area (**Figure 3.8 A, B**) and immature endplate morphology, where the endplates of *Smn*$^{2B/-}$ mice did not take on the adult pretzel-like appearance (**Figure 3.8 A, C**). Endplates were morphologically classified as: perforated (adult morphology), bright bands (presence of bright lines of AChRs but absence of perforations), or disorganized (random dispersal of AChRs). Characterization of endplates within the LAL muscle of *Smn*$^{2B/-}$ mice revealed that they have significantly less perforated endplates (<15%) compared to *Smn*$^{2B/+}$ control littermates (>80%) (**Figure 3.8 C**).

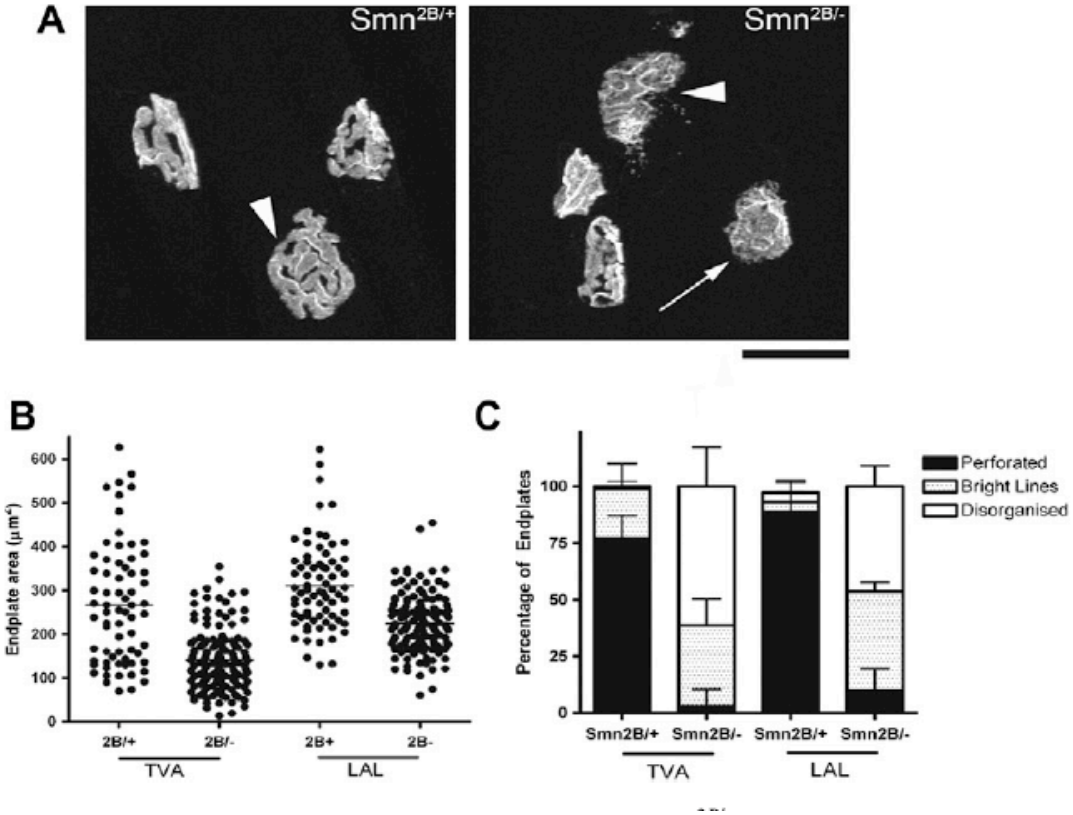

Figure 3.8. Post-synaptic shrinkage and maturations defects in the motor endplate of *Smn*$^{2B/-}$ mice. A) Representative confocal micrographs showing endplates (EP) labelled with rhodamine conjugated bungarotoxin (BTX) from P21 control *Smn*$^{2B/+}$ and *Smn*$^{2B/-}$ mice from the LAL muscle. Compared to the characteristic perforated adult morphology (arrowhead in *Smn*$^{2B/+}$ panel), the endplates of *Smn*$^{2B/-}$ mice appear less mature displaying either bright bands of AChR without any perforations (arrowhead in *Smn*$^{2B/-}$ panel) or disorganized AChRs (arrow in *Smn*$^{2B/-}$ panel). Scale bar = 20 µm. B) Scatterplot showing endplate areas in *Smn*$^{2B/+}$ and *Smn*$^{2B/-}$ in the TVA and LAL muscles. There is a significant decrease in endplate area in *Smn*$^{2B/-}$ mice ($P < 0.0001$; n = 3 mice per genotype). C) Percentage of endplates with each of the described morphologies (see panel A) in *Smn*$^{2B/+}$ and *Smn*$^{2B/-}$ LAL and TVA muscles. (n = 3 mice per genotype; data are mean +/- S.D.)

The individual contributions of the motor neuron and the muscle to the origin and progression of SMA pathology is currently unclear. To address this question, we investigated the correlation, if any, between pre- and post-synaptic pathology in $Smn^{2B/-}$ mice (**Figure 3.9**). Endplates were categorized as described above (perforated, bright lines, disorganized), while pre-synaptic classification was based on the degree of NF accumulation (**Figure 3.9 A, B**). Our first observation was that neither endplate morphology nor pre-synaptic pathology impact the size of the endplate (**Figure 3.9 C, D**). This is consistent with previous findings in more severe mouse models of SMA (Murray et al. 2008) and suggests that the endplate shrinkage may be linked to the overall smaller size of the mouse rather than with pathology. Conversely, we find that there is a trend for increased NF accumulation to be associated with morphologically abnormal endplates, and vice versa (**Figure 3.9 E, F**). This suggests that there is a potential association between pre- and post-synaptic pathology. Further work dedicated to elucidating the developmental time course of pre- and post-synaptic abnormalities will be key in identifying the primary contributor to SMA pathology.

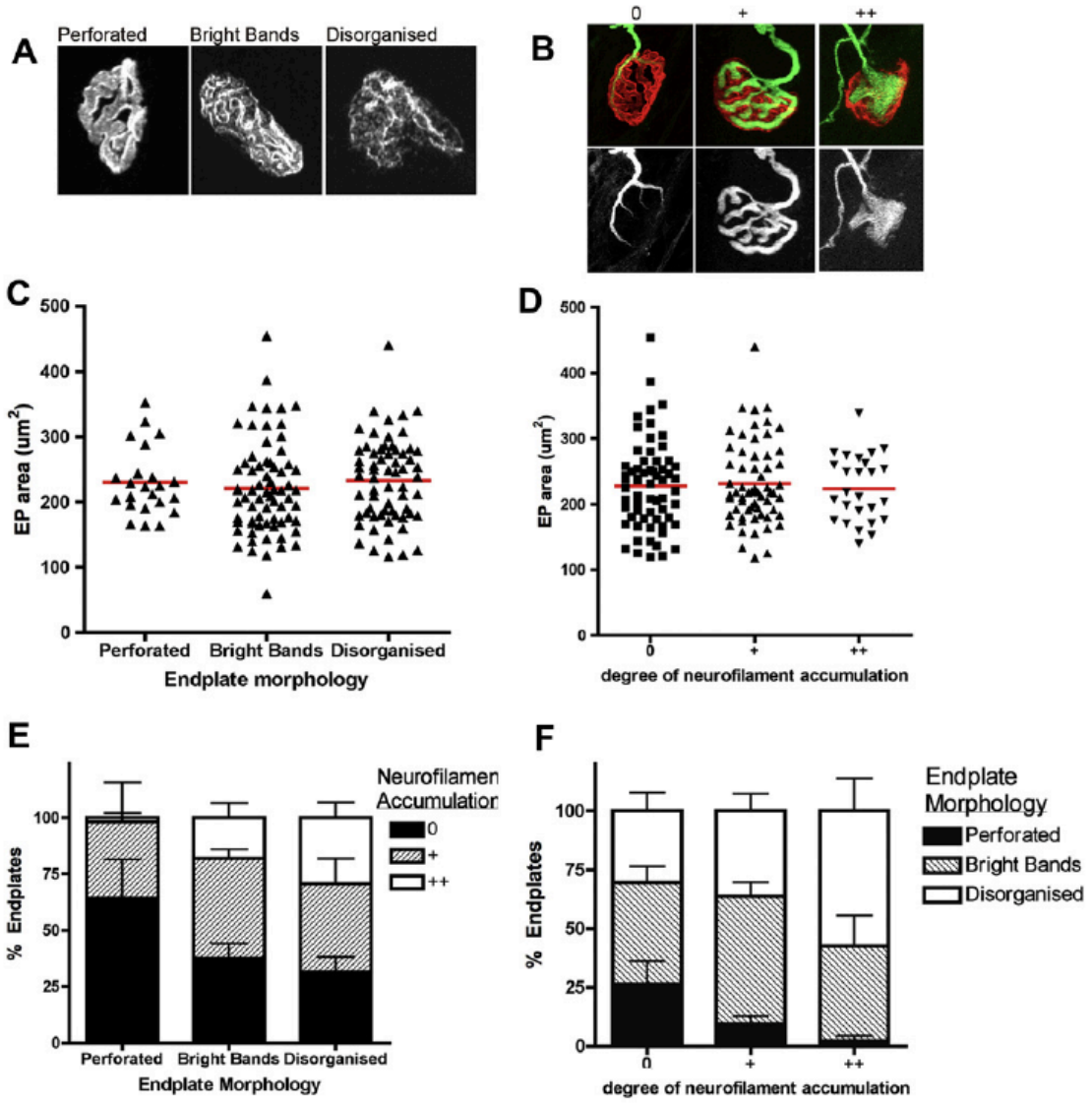

Figure 3.9. Correlation of neurofilament accumulation and endplate morphology, but not endplate size in *Smn*$^{2B/-}$ mice. A) Representative confocal micrographs displaying endplates (EP) with perforated, bright bands or disorganised phenotype (see Fig. 8a). B) Representative confocal micrographs (green/lower panel: neurofilament 165; red: rhodamine-conjugated bungarotoxin) displaying NMJs with a varying degree of neurofilament accumulation (0, no evidence of neurofilament accumulation; +, thickening of terminal arborisations; ++, spheroids

of neurofilament accumulation covering whole terminal). C and D) Scatterplots of endplate area in *Smn*$^{2B/-}$ LAL muscles sorted by EP morphology (C) or level of neurofilament accumulation (D). Endplate atrophy is not associated with endplate morphology or pre-synaptic accumulations of neurofilament (n = 3 muscles). E and F) Endplates of *Smn*$^{2B/-}$ LAL muscles show a trend towards an association of increased neurofilament accumulation with a less developed morphology (E) and a trend towards an association of less developed endplates with increased levels of neurofilament accumulation (F) (n = 3 muscles).

DISCUSSION

In the present work, we have utilized a recently introduced intermediate SMA mouse model, termed *Smn*$^{2B/-}$ (Bowerman et al. 2009; Bowerman et al. 2010; Liu et al. 2010a), to gain a better understanding of pathology associated with decreased Smn protein levels. This model has an observable SMA phenotype that arises after two weeks of life and has a median life expectancy of 28 days. In agreement with the more severe mouse models of SMA, these mice display significant reduction in body weight, abnormalities in locomotion and gait, and a significant reduction in the number of motor neuron cell bodies and axonal loss. In depth analysis of NMJ pathology reveals significant denervation and pre-synaptic accumulation of neurofilaments, alongside post-synaptic shrinkage and abnormal morphology.

Threshold requirement for Smn protein

It is interesting to note that a 15% and a 10% difference of residual FL Smn protein in the brains and spinal cords, respectively, between *Smn*$^{2B/2B}$ and *Smn*$^{2B/-}$ mice dictates absence or presence of an SMA phenotype. This is in agreement with previous studies reporting that the insertion of 3 or 4 copies of the human *SMN2* transgene onto the *Smn*$^{-/-}$ background is sufficient to rescue the phenotype of the severe *Smn*$^{-/-}$*;SMN2*/*SMN2* model that contains only two copies of *SMN2* transgene (Hsieh-Li et al. 2000; Monani et al. 2000b). However, we cannot exclude the beneficial effect of an increased production of the SmnΔ7 protein in the *Smn*$^{2B/2B}$ mouse, as Le *et al*. have previously shown that the truncated protein can extend the lifespan of the severe SMA mouse model (Le et al. 2005).

It is also important to note the possibility that the sequence change in the *Smn2B* allele may alter the function of the resulting full-length Smn protein. This could influence the efficiency of the protein and dictate the required Smn threshold identified in our study. However, the only full-length Smn protein expressed in the phenotypically normal $Smn^{2B/2B}$ mouse contains the sequence change, suggesting that the mutation creating the *Smn2B* allele does not negatively affect the function of the ensuing protein.

Nevertheless, the observations presented here are encouraging for therapeutic strategies aimed at increasing the levels of SMN protein and/or mRNA, as it appears, at least in mice, that only a small increase above the threshold limit is required for a normal phenotype and lifespan. This is also important in our understanding of the role of Smn in cellular development and maintenance.

Comparison of NMJ pathology in $Smn^{2B/-}$ mice to other SMA models

Previous analyses of more severe mouse models of SMA have revealed that NMJs are both early and significant pathological targets (Kariya et al. 2008; Murray et al. 2008; Kong et al. 2009). The present study represents the first description of NMJ pathology in an intermediate mouse model that lives beyond two weeks of age. Since NMJ vulnerability can change drastically after the first two post-natal weeks (Murray et al. 2011), the $Smn^{2B/-}$ mouse model has allowed for a better understanding of NMJ pathology in SMA.

The analysis of NMJ pathology described here was performed in a range of differentially vulnerable muscles that have previously been extensively described in more severe SMA mouse models (Murray et al. 2008; Murray et al. 2010a). This has allowed us to directly compare NMJ vulnerability between models. We reveal significant denervation of the TVA muscle, a slow twitch postural muscle. This is consistent with reports from other mouse models in which this muscle was severely affected (Murray et al. 2008). Interestingly, we did not note the same selective vulnerabilities previously described within the cranial muscles groups. As this selective vulnerability may be due to differential developmental phenotypes (Murray et al. 2008), the later onset of the SMA phenotype in the *Smn*$^{2B/-}$ mouse model may therefore be responsible for altering the vulnerability of the cranial muscle NMJs.

In the present study, we noted significant accumulations of neurofilaments (NFs) at the NMJ and shrinkage of the motor endplate area, features observed in both severe mouse models and human patients (Cifuentes-Diaz et al. 2002; Kariya et al. 2008; Murray et al. 2008). Although NF accumulation is not necessarily detrimental to the NMJ, they might be indicative of pathological molecular defects in the motor neuron. However, since we show a correlation between NF accumulation and abnormal post-synaptic morphology, NF accumulation may suggest a functionally defective NMJ. As for the endplates, their shrinkage was not associated with pre-synaptic pathology, suggesting that this characteristic is more likely attributable to the overall smaller size of the mouse.

Future uses of the $Smn^{2B/-}$ mouse model

We propose that, due to its later symptomatic onset and prolonged disease progression, the $Smn^{2B/-}$ mouse model will help us gain a better understanding of SMA pathology. Furthermore, these same characteristics will help in the development and identification of *SMN2*-independent therapies that are to begin after birth. The $Smn^{2B/-}$ mice have already allowed for a better understanding of the effect of Smn depletion on eye development, profilin IIa expression and plastin 3 expression (Bowerman et al. 2009; Liu et al. 2010a). Furthermore, they have been used to show that rho-kinase inhibition is a potential therapeutic strategy for SMA (Bowerman et al. 2010).

ACKNOWLEDGEMENTS

We are grateful to the Kothary laboratory for helpful discussions. This project was funded by a grant from the Canadian Institutes of Health Research (CIHR), and The Muscular Dystrophy Association to R.K. M.B. is a recipient of a Frederick Banting and Charles Best CIHR Doctoral Research Award, L.M.M is a recipient of a Multiple Society of Canada Postdoctoral Fellowship, and R.K. is a recipient of a University Health Research Chair from the University of Ottawa.

SUPPLEMENTARY FIGURES

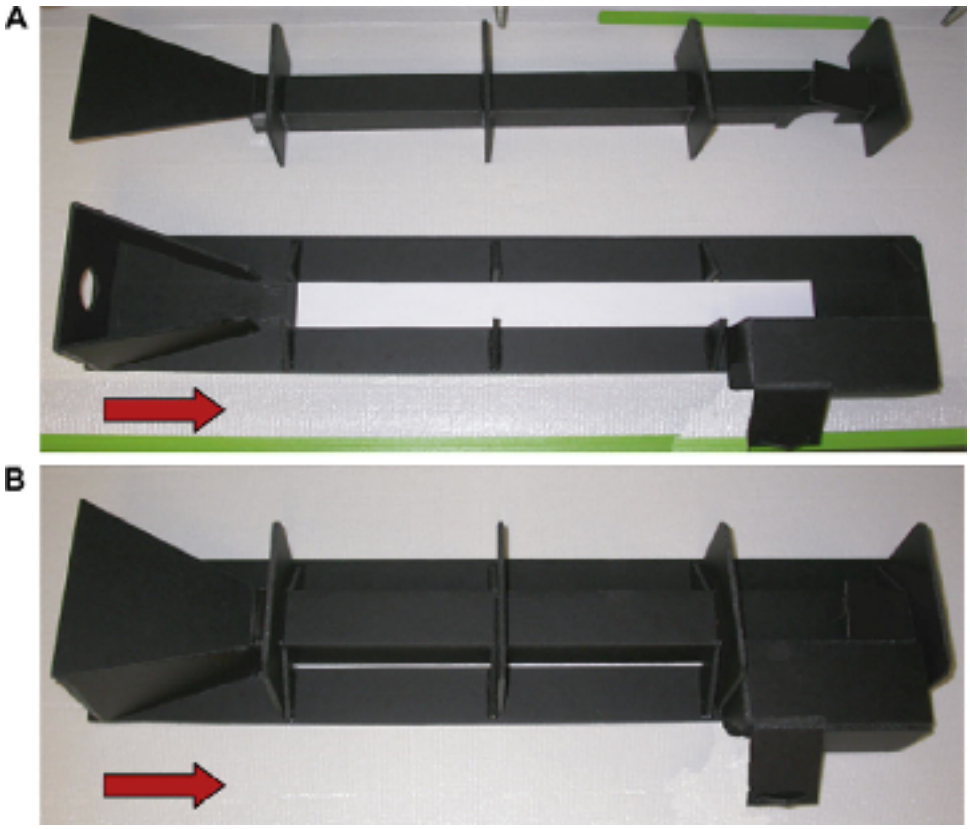

Supplementary Figure 3.1. In-house gait analysis box. A) Inside view of the gait analysis box. Mouse paws were inked red (front) and blue (back), and animals made to walk from the "funnel" end of the box toward the other end (direction as depicted by the red arrow), leaving imprints on the white piece of paper. A flashlight was placed in the hole in the "funnel" end to entice the mice to walk towards the other end. B) Closed-view of the gait analysis box, as used in the experimental analysis of gait and locomotion. The red arrow depicts the directionality of the walking mouse.

CHAPTER 4: Genetic interaction between Smn, profilin IIa and plastin 3

SMN, profilin IIa and plastin 3: a link between the deregulation of actin dynamics and SMA pathogenesis

Mélissa Bowerman, Carrie L. Anderson, Ariane Beauvais, Pietro Pilo Boyl, Walter Witke and Rashmi Kothary

Published in *Molecular and Cellular Neuroscience*, 2009, 42 (1), 66-74

Author Contributions

Conceived and designed the experiments: MB and RK. Performed the experiments: MB, CLA and AB. Analyzed the data: MB. Wrote the paper: MB. Other: provided the profilin IIa antibody and the profilin knock-out mouse: PPB and WW.

ABSTRACT

Spinal muscular atrophy (SMA) is the most common human genetic disease resulting in infant mortality. SMA is caused by mutations or deletions in the ubiquitously expressed survival motor neuron 1 (*SMN1*) gene. Why SMA specifically affects motor neurons remains poorly understood. We have shown that Smn deficient PC12 cells have increased levels of the neuronal profilin IIa protein, leading to an inappropriate activation of the RhoA/ROCK pathway. This suggests that misregulation of neuronal actin dynamics is central to SMA pathogenesis. Here, we demonstrate an increase in profilin IIa and a decrease in plastin 3 protein levels in a SMA mouse model. Furthermore, knock-out of profilin II upregulates plastin 3 expression in a Smn-dependent manner. However, the depletion of profilin II and the restoration of plastin 3 are not sufficient to rescue the SMA phenotype. Our study suggests that additional regulators of actin dynamics must also contribute to SMA pathogenesis.

INTRODUCTION

Spinal muscular atrophy (SMA) is the number one genetic killer of children under two years of age, affecting approximately 1 in 10,000 live births (Pearn 1978b; Crawford et al. 1996). It is an autosomal recessive disorder defined by severe loss of α-motor neurons in the spinal cord (Crawford et al. 1996). The motor neuron degeneration subsequently causes muscular atrophy of the limbs and trunk, which leads to paralysis and in severe cases, death (Crawford et al. 1996). SMA is caused by homozygous deletions or mutations of the ubiquitously expressed survival motor neuron 1 (*SMN1*) gene (Lefebvre et al. 1995). The *SMN* gene is highly conserved and although all eukaryotic organisms studied to date have only one copy of the gene, humans have two (Lefebvre et al. 1995; DiDonato et al. 1997). The telomeric copy, *SMN1*, produces the full-length protein while the duplicated centromeric copy, *SMN2*, expresses a truncated isoform with a deletion of the C terminal exon 7, termed Δ7SMN (Lefebvre et al. 1995). The excision of exon 7 is caused by a C to T substitution in the *SMN2* gene at position 6 of exon 7 (Lorson et al. 1999). This leads to the loss of an exon splicing enhancer and/or the gain of a exon splicing silencer, which promotes exon 7 skipping of the *SMN* gene (Cartegni et al. 2002; Kashima et al. 2003). Since the *SMN2* gene produces a small amount of functional full-length protein, it can modulate the severity of SMA in a copy number-dependent manner (Lefebvre et al. 1995).

The 38 kDa SMN protein is part of a multiprotein complex, composed of self-oligomerized SMN, Gemin2-8, Unrip and Sm proteins (Paushkin et al. 2002; Carissimi et al. 2006; Gabanella et al. 2007). This complex is responsible for the assembly of small nuclear ribonucleoproteins (snRNPs) and thus, regulates the processing of most pre-mRNAs and

ribosomal RNAs (Paushkin et al. 2002; Carissimi et al. 2006; Gabanella et al. 2007). Consequently, many investigations have focused on the housekeeping role of SMN in mRNA splicing and its relevance in SMA pathogenesis. A correlation between snRNP assembly activity in the spinal cord of SMA mice and severity of the disease has been demonstrated (Gabanella et al. 2007). Also, Smn deficiency causes tissue-specific pre-mRNA splicing defects in the spinal cord, brain and kidney in a SMA mouse model, suggesting that SMA is a general splicing disease (Zhang et al. 2008). However, no causal link has yet been made between the identified aberrantly spliced targets and SMA pathogenesis. Thus, the question of motor neuron specific death in SMA remains unresolved and suggests additional mechanisms outside of pre-mRNA processing are involved.

Other studies propose a specific role for Smn in neuronal cells. Work in P19 cells, zebrafish, and neurosphere-derived neural stem cells of severe SMA mice show a role for Smn in neurite outgrowth, neuronal differentiation, axonal pathfinding and neuromuscular maturation (Fan et al. 2002; McWhorter et al. 2003; Shafey et al. 2008). Motor neurons isolated from severe SMA mouse models have normal survival but reduced axonal growth. β-actin mRNA and protein staining is reduced in distal axons and growth cones (Rossoll et al. 2003). Interestingly, Smn interacts and co-localizes in the cytoplasm, in neurite-like extensions, and in nuclear gems with the neuronal specific protein profilin II, a small actin-binding protein and key regulator of actin dynamics (Giesemann et al. 1999; Sharma et al. 2005). More recently, Smn has been attributed a role in neuromuscular junction (NMJ) development (Kariya et al. 2008; McGovern et al. 2008; Kong et al. 2009). Indeed, pre-synaptic defects such as poor terminal arborization, intermediate filament aggregates, denervation, and impaired synaptic vesicle release have been

identified in SMA mouse models (Kariya et al. 2008; McGovern et al. 2008; Kong et al. 2009). All of these observations therefore suggest a role for Smn in neurodevelopment and/or neuromaintenance. In fact, during the maturation of the human central nervous system, there is a progressive shift from nuclear to cytoplasmic and then to axonal localization of SMN (Giavazzi et al. 2006).

We have shown that Smn knockdown in PC12 neuronal cells leads to defects in neuritogenesis caused by alterations in cytoskeletal integrity (Bowerman et al. 2007). Furthermore, we have provided evidence that these defects are mediated via an increased expression of profilin IIa and an inappropriate activation of the RhoA/ROCK pathway. In the present study, we characterize profilin IIa expression in an intermediate SMA mouse model as well as evaluate the effect of profilin II knock-out on the SMA phenotype. We provide evidence for modulation of actin-binding and actin-regulating proteins in a Smn-dependent manner, highlighting the perturbed actin cytoskeletal pathway as an important player in SMA pathogenesis.

RESULTS

Profilin IIa expression in an intermediate SMA mouse model

Our previous findings indicate that there is increased profilin IIa mRNA and protein in Smn-depleted PC12 cells (Bowerman et al. 2007). This in turn had a negative impact on neuronal outgrowth and neurite formation. To extend this analysis to an *in vivo* context, we wanted to assess profilin IIa protein levels in an intermediate SMA mouse model, termed $Smn^{2B/-}$ (unpublished data, (DiDonato 2007)). This knock-in transgenic mouse line has a recombined allele harboring mutations within exon 7 of the endogenous *Smn* gene. The 2B allele has 3 nucleotides substituted within the exon splicing enhancer (ESE) of exon 7. This change leads to the alternative splicing of the *Smn* transcript in a predominant manner, resulting in the production of Δ7Smn mRNA (DiDonato et al. 2001). By comparison, the normal wild type mouse *Smn* gene is never alternatively spliced. The $Smn^{2B/-}$ mice have a phenotype that arises shortly after two weeks of age and at three weeks of age they are significantly smaller than their wild type littermates. The lifespan of $Smn^{2B/-}$ mice is shorter than its wild type littermates with the majority dying by one month of age. RNA analysis shows a significantly smaller ratio of full-length Smn/Δ7Smn transcript while Smn protein expression is significantly reduced in all tissues, with only approximately 15% of the full-length protein still present. The $Smn^{2B/-}$ mice also exhibit a reduction in the number of motor neurons in the brain stem and spinal cord at P21 (close to the end stage of disease), concordant with existing SMA mouse models (Hsieh-Li et al. 2000; Jablonka et al. 2000; Monani et al. 2000a). Therefore, these mice represent an intermediate

SMA mouse model that can be used to investigate potential pathogenic molecular pathways prior to and at the onset of disease.

We performed immunohistochemistry to get an appreciation of profilin IIa levels within the spinal cord and brain stem of SMA mice. SMI32, an antibody specific for phosphorylated neurofilaments of axonal bodies, was used to specifically identify neuronal cells (**Figure 4.1 A**). Upon quantitative analysis, we observed a significant reduction in the number of neurons (SMI32-positive) in the brain stem and spinal cord of *Smn*$^{2B/-}$ mice (**Figure 4.1 B**). However, interestingly, we only observed a decrease in the number of profilin IIa-positive cells in the brain stem but not in the spinal cord of *Smn*$^{2B/-}$ mice (**Figure 4.1 B**). Further quantification indicates that there is no change in the percentage of profilin IIa-positive motor neurons (identified morphologically by size and shape) (**Figure 4.1 C**). This suggests that the motor neuron pool is not specifically affected by the observed changes in the number of profilin IIa-positive neurons. Qualitative assessment initially suggested an increase in profilin IIa signal intensity in the SMI32-positive cells in both brain stem and spinal cord of the *Smn*$^{2B/-}$ mice (**Figure 4.1 A**). However, quantitative measurement of profilin IIa immunofluorescence shows that SMI32-positive motor neurons (identified morphologically by size and shape) in the spinal cord but not the brain stem of *Smn*$^{2B/-}$ mice have a greater signal intensity compared to wild-type and *Smn*$^{2B/+}$ mice (**Figure 4.1 D**) (refer to Materials and Methods for quantitative assays). Immunoblot analysis shows that there is no difference in profilin IIa protein levels in the brain and spinal cord of *Smn*$^{2B/-}$ mice when compared to wild type mice (**Figure 4.1 D**). This suggests that within the spinal cord of our SMA mouse model, the increase in profilin IIa expression is cell-autonomous and not a general event in the entire tissue. Since SMA mice are characterized by a significant

loss of spinal cord motor neurons, a cell-specific increase in profilin IIa expression may thus be muted in whole tissue lysate composed of more than one cell type. As previously mentioned, overexpression of profilin IIa in hippocampal neurons has been shown to negatively regulate neuritogenesis (Da Silva et al. 2003). In addition, it has been proposed that interaction of Smn with profilin IIa could regulate actin dynamics by modulating the inhibitory effect of profilin IIa (Sharma et al. 2005). As such, the increase in profilin IIa in the motor neurons within the spinal cord of $Smn^{2B/-}$ mice might be having an overall negative effect on these neurons.

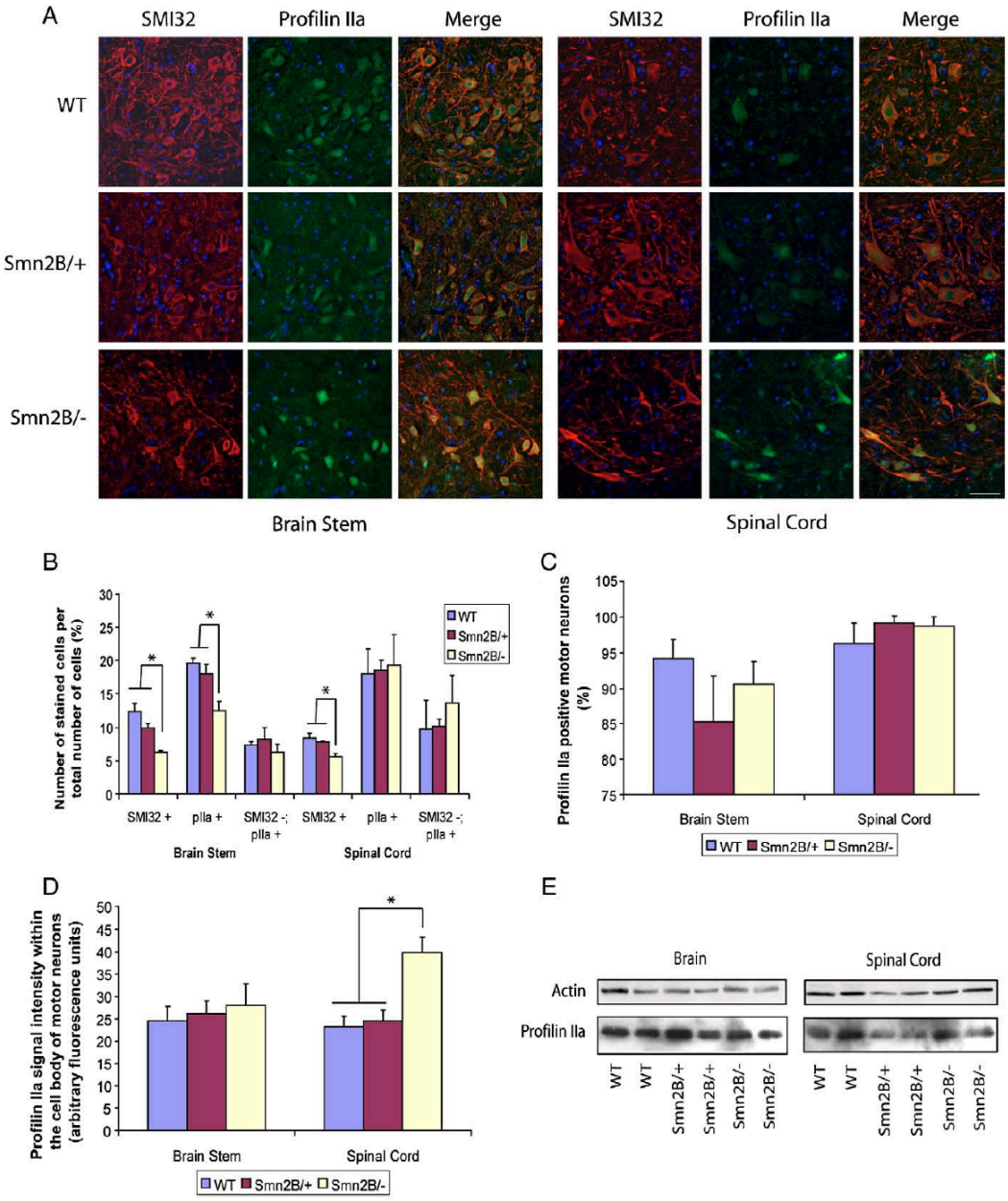

Figure 4.1. Immunohistochemistry and immunoblot analysis of profilin IIa protein levels in brain and spinal cord of wild type (WT), *Smn*$^{2B/+}$ and *Smn*$^{2B/-}$ mice at 3 weeks of age. A) Representative examples of profilin IIa (green) and SMI32 (red) staining in brain stem and spinal cord. B) Quantification of SMI32-positive, profilin-IIa positive and SMI32-negative/profilin IIa-

positive cells in brain stem and spinal cord. There are significantly fewer SMI32- and profilin IIa-positive cells in the brain stem of *Smn*$^{2B/-}$ mice when compared to WT. In the spinal cord however, only SMI32-positive cells in *Smn*$^{2B/-}$ mice are reduced in number when compared to WT. C) Quantification of profilin IIa-positive motor neurons in the brain stem and spinal cord. The motor neuron pool of the *Smn*$^{2B/-}$ mice are not specifically affected by the changes observed in profilin IIa-positive neurons. D) Quantification of profilin IIa staining intensity within the cell body of motor neurons. Profilin IIa signal is increased in the spinal cord motor neurons of the *Smn*$^{2B/-}$ mice but not in the brain stem motor neurons. E) Immunoblot analysis of whole tissue lysates indicates no apparent difference in profilin IIa levels in the brain or spinal cord of *Smn*$^{2B/-}$ mice**.** (Data are mean +/- S.E., scale bar: 50 μm)

Plastin 3 levels are decreased in the brain and spinal cord of SMA mice

Plastin 3, also known as T-plastin and T-fimbrin, is expressed in solid tissues, including the spinal cord (Bretscher 1981; Lin et al. 1988). It is an actin-bundling protein that organizes actin filaments into complex networks but also has an independent role in actin stabilization (Bretscher 1981; Gimona et al. 2002; Giganti et al. 2005). Furthermore, plastin 3 has recently been identified as a protective gender-specific modifier of SMA, forming a large complex with SMN and actin (Oprea et al. 2008). In the latter study, it was reported that female patients missing the *SMN1* gene were asymptomatic and exhibited significantly higher levels of expression of plastin 3 in lymphoblast cells when compared to their SMA-affected siblings (Oprea et al. 2008). Furthermore, it was demonstrated that plastin 3 is important for axonogenesis since its overexpression rescued the axon length and outgrowth defects associated with Smn-depletion in motor neurons derived from SMA mouse embryos and in zebrafish (Oprea et al. 2008). Here, we assessed plastin 3 levels within the brain and spinal cord of the $Smn^{2B/-}$ mice compared to their wild type littermates. Upon immunoblot analysis of mice at the phenotype stage (P21), we found that plastin 3 levels were reduced in the brain and spinal cord of $Smn^{2B/-}$ mice (**Figure 4.2 A**). Densitometric analysis shows that the ratio of plastin 3 over actin is significantly greater in both the brain and spinal cord of wild type mice compared to $Smn^{2B/-}$ mice (**Figure 4.2 B**). Plastin 3 expression was also assessed qualitatively by immunohistochemistry (**Figure 4.2 C**). Quantitative measurement of plastin 3 immunofluorescence in SMI32-positive motor neurons (identified morphologically by size and shape) indicates a significant decrease in plastin 3 signal intensity in both the brain stem and spinal cord of $Smn^{2B/-}$ mice (**Figure 4.2 D**) (refer to Materials and Methods for quantitative

assays). Since both plastin 3 and profilin II have been identified as Smn and actin interactors, we next investigated the effect of profilin II knock-out on the expression of plastin 3 and on the phenotype of the SMA mouse model (Giesemann et al. 1999; Sharma et al. 2005; Oprea et al. 2008).

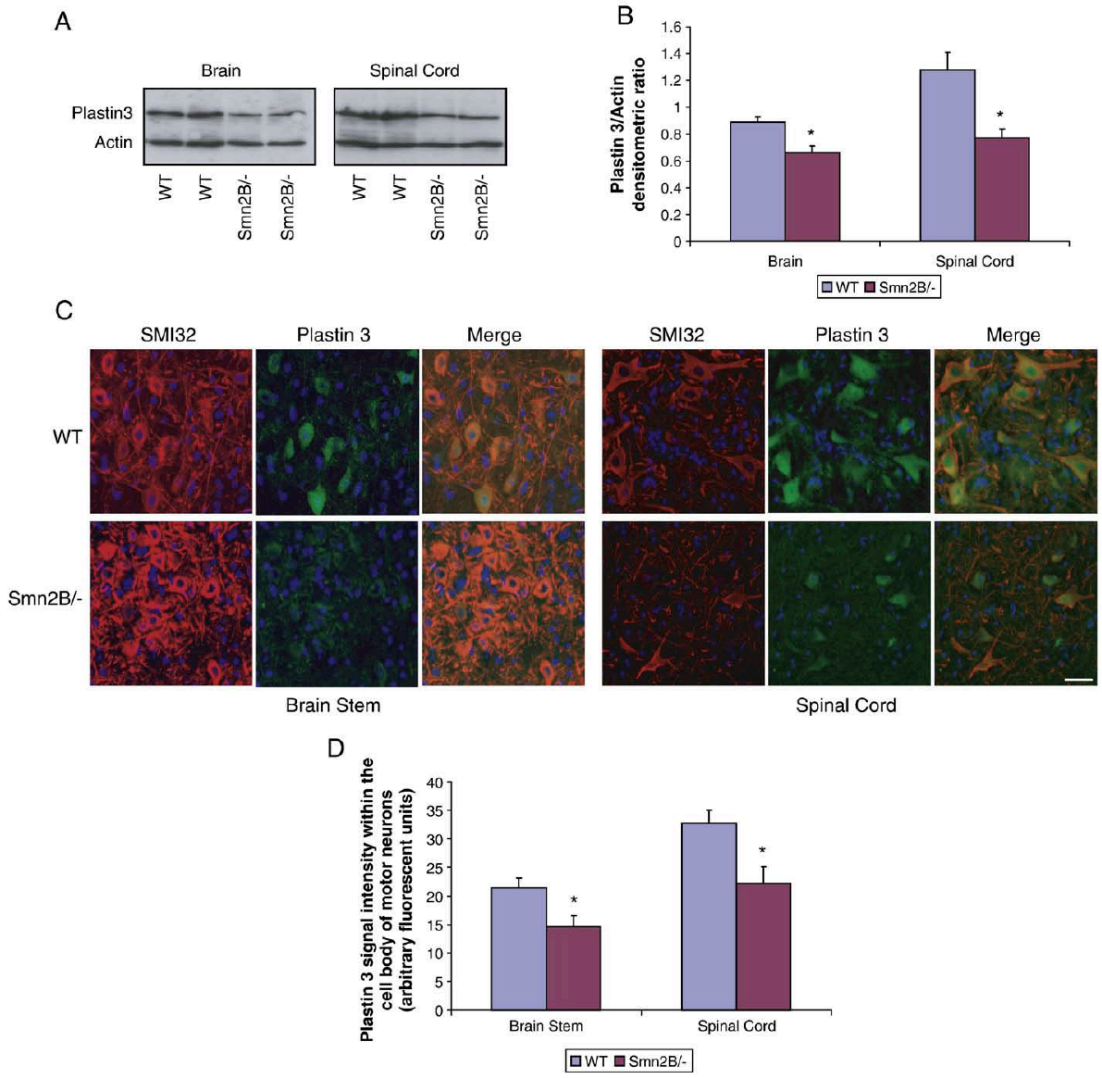

Figure 4.2. Immunohistochemistry and immunoblot analysis of plastin 3 protein levels in brain and spinal cord of wild type (WT) and *Smn*$^{2B/-}$ mice at 3 weeks of age. A) Immunoblot analysis shows reduced expression of plastin 3 in both the brain and spinal cord of *Smn*$^{2B/-}$ mice**.** B) Quantitative analysis shows that plastin 3/actin ratios are significantly higher in both the brain and spinal cord of WT mice. C) Representative examples of plastin 3 (green) and SMI32 (red) staining in brain stem and spinal cord. D) Quantification of plastin 3 staining intensity within the

cell body of motor neurons. Plastin 3 signal is decreased in both the spinal cord motor and brain stem neurons of the *Smn*$^{2B/-}$ mice. (Data are mean +/- S.E., scale bar: 50 μm)

Profilin IIa modulates plastin 3 in a Smn-dependent manner

A recent study showed an increase in the fraction of F-actin and a subsequent decrease in the fraction of G-actin in Smn-depleted PC12 cells (van Bergeijk et al. 2007). In addition, a C-terminal fragment of SMN (SMN235-294-EGFP) rescued the neuronal outgrowth defects in the Smn-depleted PC12 cells (van Bergeijk et al. 2007). This fragment contains part of the proline-rich motif responsible for profilin binding, suggesting that the rescue may be due to the decrease in available profilin IIa. To test whether reducing the available profilin levels would impact on plastin 3 levels and/or have a beneficial effect on SMA mice, we crossed the $Smn^{2B/-}$ mice with a profilin II (*pfn2*) knockout mouse model (Pilo Boyl et al. 2007). The $pfn2^{-/-}$ mice are completely viable and are characterized by a block in synaptic actin polymerization and increased synaptic excitability (Pilo Boyl et al. 2007). Although the *profilin II* knock-out mouse targets both profilin IIa and IIb isoforms, profilin IIa is the predominant isoform within the CNS (Lambrechts et al. 2000).

Heterozygous or homozygous knock-out of profilin II in the $Smn^{2B/-}$ mouse background led to the restoration of plastin 3 levels in both the brain and spinal cord, suggesting a modulation of plastin 3 by profilin IIa (**Figure 4.3 A**). To determine if this modulation was dependent on the reduction of Smn, we compared plastin 3 levels in mice that were wild type for the *Smn* gene. In this case, heterozygous or homozygous knock-out of *profilin II* did not upregulate plastin 3 levels (**Figure 4.3 B**). In fact, it seems that in presence of the wild type *Smn* allele, knock-out of profilin II led to a slight reduction in plastin 3 levels. Thus, the modulation of plastin 3 by profilin IIa is dependent on the levels of the Smn protein. Further, analysis of

mice at pre-phenotype age (P10) also reveals a drop in the levels of plastin 3 in brain and spinal cord of $Smn^{2B/-};pfn2^{+/+}$ mice (**Figure 4.3 C**). At this stage, subsequent restoration of plastin 3 upon heterozygous or homozygous *profilin II* knock-out was only observed in the spinal cord (Figure 3C). However, this observed upregulation of plastin 3 expression in P10 mice is more variable and less dramatic that what was observed at P21 (**Figure 4.3 A, C**) Our immunohistochemistry results indicate that the number of profilin IIa positive neuronal cells was reduced in the brain stem of $Smn^{2B/-}$ mice while it was unchanged within the spinal cord (**Figure 4.1 B**). Furthermore, there is a significant increase in profilin IIa signal intensity within the motor neurons of the spinal cord but not the brain stem of the $Smn^{2B/-}$ mice (**Figure 4.1 D**). Thus, the neurons within the spinal cord might be more sensitive and/or responsive to a decrease in profilin IIa levels. That plastin 3 and profilin IIa expression are affected prior to onset of disease suggests that the deregulation of profilin IIa and plastin 3 is not simply a secondary effect of motor neuron degeneration, and that it is contributory to SMA pathogenesis.

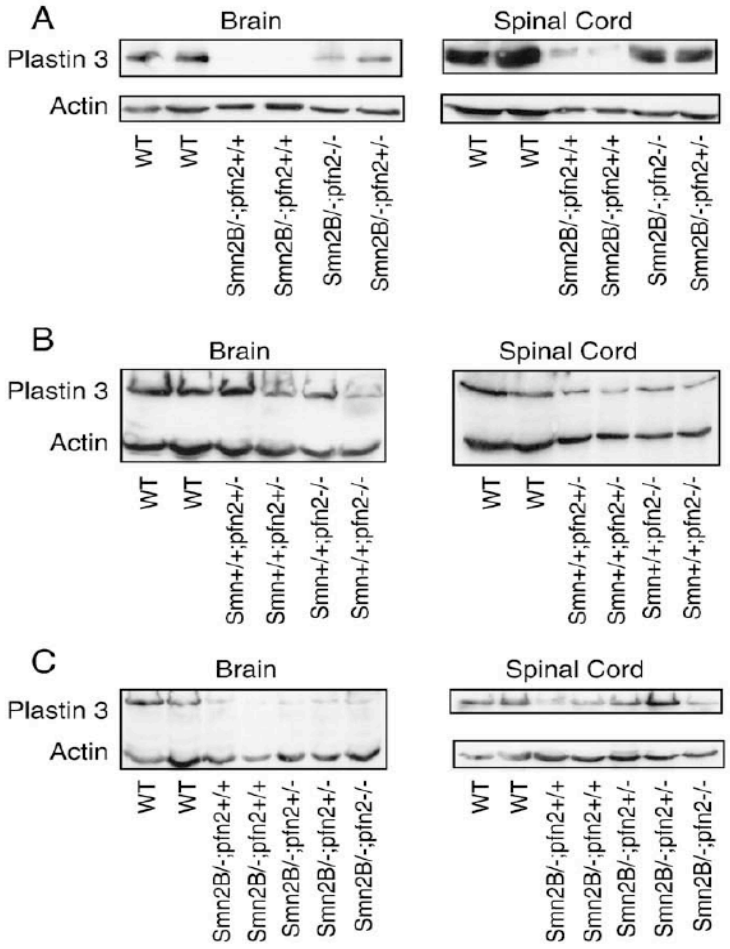

Figure 4.3. Immunoblot analysis of Smn and plastin 3 protein levels in brain and spinal cord of wild type (WT) and SMA mice at phenotype (P21) and pre-phenotype (P10) stages. A) In the brain and spinal cord of P21 $Smn^{2B/-};pfn2^{+/+}$ mice, there is a dramatic decrease in plastin 3 levels when compared to wild type mice. Plastin 3 levels are restored after the heterozygous or homozygous knock-out of *profilin II*. B) When *Smn* alleles are wild type, *profilin II* knock-out does not upregulate plastin 3 expression. Instead, there seems to be a slight decrease of plastin 3 expression. C) In both brain and spinal cord of P10 $Smn^{2B/-};pfn2^{+/+}$ mice, plastin 3 expression is

reduced when compared to wild type mice. In the brain, plastin 3 expression is not affected by *profilin II* knock-out while it appears to be restored in the spinal cord.

Downregulation of profilin II and upregulation of plastin 3 do not rescue the SMA phenotype

Heterozygous or homozygous knock-out of the profilin II allele, which resulted in the restoration of plastin 3 levels in the brain and spinal cord of $Smn^{2B/-}$ mice, had no negative or positive effect on the phenotype of these mice. Indeed, weight at 3 weeks of age and survival curve are not significantly different from the $Smn^{2B/-}$ mice harboring normal levels of profilin II (**Figure 4.4 A, B**). Since the $Smn^{2B/-}$ mice and other SMA mouse models are characterized by motor neuron loss within the brain stem and spinal cord, we performed histological analysis to determine if profilin II reduction had any effect on this pathology. As expected from the absence of any phenotypic rescue, there were significantly fewer motor neurons in the brain stem and spinal cord of $Smn^{2B/-};pfn2^{+/-}$ mice compared to wild type littermates (**Figure 4.5**) (refer to Materials and Methods for quantitative assay). Indeed, the weight loss, survival rate and overt neuromuscular phenotype observed in these mice suggest that motor neuron degeneration is not prevented through depletion of profilin II.

Although most of the $Smn^{2B/-}$ mice die around 4 weeks of age, we occasionally observe mice that survive well beyond that time point (**Figure 4.4 B**). However, while these mice survive longer, they still show signs of neurodegeneration such as gross phenotype (weight, hind-limb weakness, curvature of the spine and abnormal gait) as well as loss of brain stem and spinal cord motor neurons (unpublished observations). The fact that a few littermates of the same genotype exhibit an improved survival suggests the existence of beneficial genetic modifiers. This hypothesis is further supported by the identification of siblings of affected SMA patients

that carry identical *SMN1* mutation and *SMN2* copy number that are asymptomatic for the disease (Cobben et al. 1995; Hahnen et al. 1995).

Thus, although we have observed a cell-autonomous increase in profilin IIa protein levels and a decrease in plastin 3 levels in SMA mice, motor neuron degeneration still occurs when profilin IIa is reduced. This suggests that there might be additional contributing factors, possibly other regulators of actin dynamics, to the loss of motor neurons.

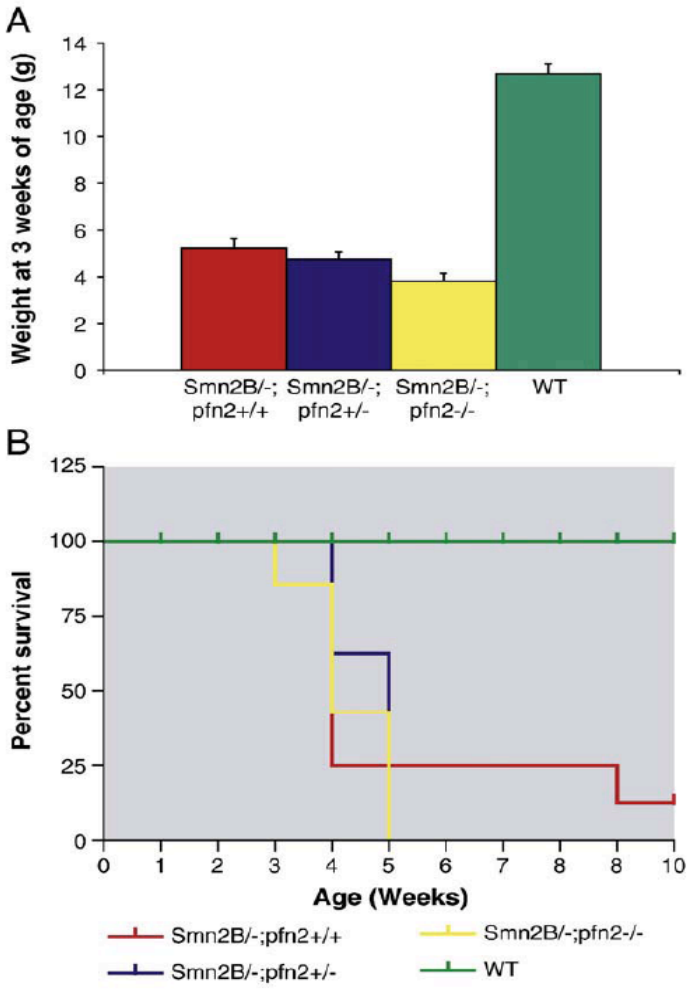

Figure 4.4. Weight and survival analysis of the effect of *profilin II* knock-out in $Smn^{2B/-}$ mice. A) Weight analysis at 3 weeks of age indicates that neither heterozygous nor homozygous knock-out of *profilin II* rescues the growth defect in $Smn^{2B/-}$ mice (Data are mean +/- S.E.). B) Kaplan-Meier survival curves of $Smn^{2B/-};pfn2^{+/+}$ (n = 8), $Smn^{2B/-};pfn2^{+/-}$ (n = 8), $Smn^{2B/-};pfn2^{-/-}$ (n = 7) and wild type (WT) (n = 10) mice. Survival analysis shows no improvement in the lifespan of $Smn^{2B/-}$ mice when *profilin II* is knocked out (P = 0.88, log-rank test).

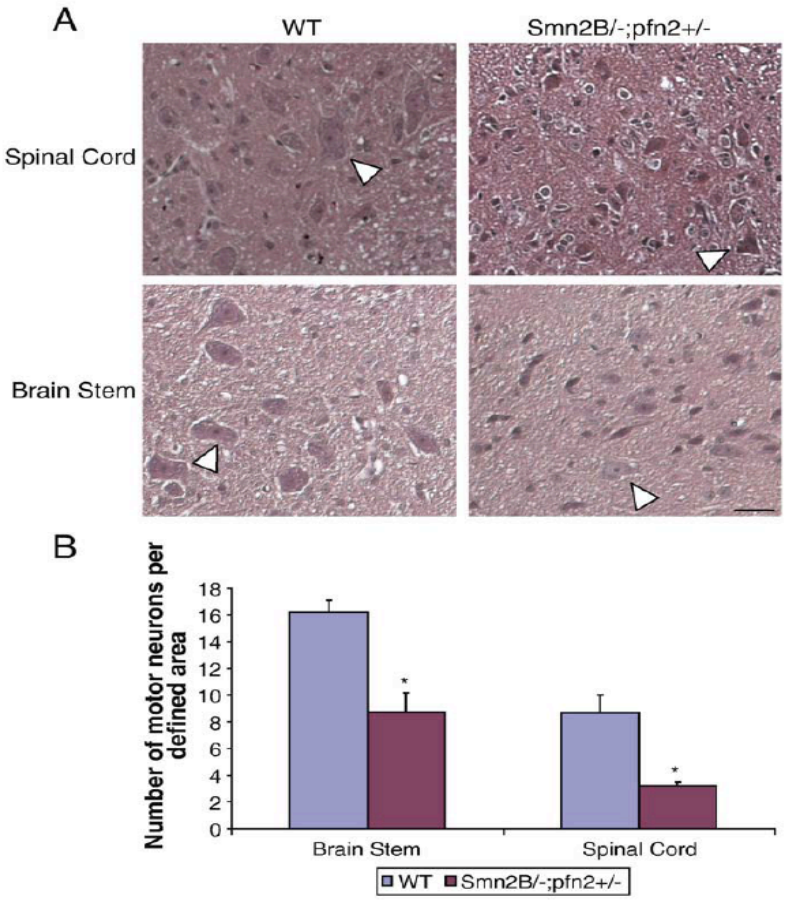

Figure 4.5. Hematoxylin and eosin staining of sections from the spinal cord and brain stem of 3 week old wild type (WT) and *Smn*$^{2B/-}$;*pfn2*$^{+/-}$ mice. A) Representative examples of motor neuron staining (arrowheads) in the brain stem and spinal cord. B) Quantification of the number of motor neurons per defined area shows a significant difference between wild type and *Smn*$^{2B/-}$;*pfn2*$^{+/-}$ mice in the brain stem and the spinal cord. (Data are mean +/- S.E., scale bar: 50 μm)

DISCUSSION

In the present work, we have shown a cell-autonomous increase in the level of profilin IIa within neuronal cells of the spinal cord of an intermediate SMA mouse model. Accompanying this was a decrease in the level of plastin 3 in the brain and the spinal cord. These results suggest that disruption of actin cytoskeletal dynamics is a central event in SMA pathogenesis. Also of interest was that heterozygous or homozygous knock-out of the *profilin II* gene restored plastin 3 levels in a Smn-dependent fashion. This occurred prior to and at the onset of disease in our SMA mouse model. However, this was not sufficient for the rescue of the SMA phenotype in these mice suggesting that additional factors are likely to be involved in the pathogenesis of SMA.

Recent studies have suggested that Smn plays a crucial role in neuromaintenance. Indeed, although axonal outgrowth and pathfinding are completely unperturbed in a severe SMA mouse model, there is evidence for subsequent loss of axonal occupation of the neuromuscular junction (NMJ), impairment of the maturation of acetylcholine receptors, improper terminal arborization, accumulation of intermediate filament aggregates, and a reduction in vesicle release (Kariya et al. 2008; McGovern et al. 2008; Kong et al. 2009). Interestingly, actin is the most abundant cytoskeletal protein found within the synapses of mature neurons (Matus et al. 1982; Hirokawa et al. 1989). At the pre-synaptic terminal, actin has been implicated in the maintenance and regulation of synaptic vesicle pools, the mobility of vesicles, neurotransmitter release, and axonal vesicle trafficking (Cole et al. 2000; Sakaba et al. 2003; Dillon et al. 2005; Jordan et al. 2005; Shtrahman et al. 2005; Darcy et al. 2006). Thus, the exquisite regulation of actin dynamics at the synapse by a multitude of actin-binding and actin-regulating proteins is necessary for

adequate NMJ maturation and function. In cultured motor neurons of a severe SMA mouse model, β-actin mRNA and protein levels are dramatically reduced in distal axons and growth cones (Rossoll et al. 2003). This perturbation in the actin cytoskeleton could in itself explain the eventual degeneration of NMJs in the severe SMA mice (Kariya et al. 2008; McGovern et al. 2008).

Nevertheless, other important regulators of actin dynamics at the synapse could also contribute to the synaptic defects observed at the NMJs of the severe SMA mice (Kariya et al. 2008; McGovern et al. 2008). The *profilin II* knock-out mouse is characterized by a block in synaptic actin polymerization and an increase in neurotransmitter release, suggesting a role for profilin IIa in the regulation of the actin-mediated vesicle exocytosis and neuronal excitability (Pilo Boyl et al. 2007). It could therefore be hypothesized that an increase of profilin IIa would have the opposite effect, that is, an inhibition of neurotransmitter release which would consequently lead to motor neuron degeneration and loss of NMJs. Interestingly, Kong *et al*. (Kong et al. 2009) have recently provided evidence for perturbed synaptic transmission in a severe SMA mouse model. Since synaptic transmission was not assessed in our *profilin II* knock-out mice, we can only hypothesize that increased profilin IIa levels in the spinal cord neurons of SMA mice contributes to the impairment of vesicle release at the NMJ. Nevertheless, it is clear that a simple reduction of profilin II in our intermediate SMA mouse model is not sufficient to rescue the SMA phenotype. It is therefore possible that other regulators of actin dynamics are affected in SMA neuronal cells.

Analysis of brain and spinal cord tissue revealed a relative decrease of plastin 3 levels in the intermediate SMA mouse model. Surprisingly, plastin 3 levels were restored after heterozygous or homozygous deletion of *profilin II*. Furthermore, plastin 3 expression appeared to decrease rather than increase when *profilin II* knock-out occurred in the presence of the wild type *Smn* gene. This suggests that profilin IIa modulates plastin 3 expression in a Smn-dependent manner. Upon overexpression of plastin 3 in Smn-depleted PC12 cells or motor neurons from E13.5 SMA embryos, a significant rescue of axon length has been reported, suggesting that a similar overexpression of plastin 3 *in vivo* might ameliorate the SMA phenotype (Oprea et al. 2008). However, at least in the context of our model, an increase in plastin 3 levels does not ameliorate the SMA phenotype. It is possible that the positive impact of plastin 3 in cellular models may not translate to an improvement of the pathology of SMA mice since it has been suggested that the NMJs are properly formed, followed by subsequent motor neuron degeneration (Kariya et al. 2008; McGovern et al. 2008). On the other hand, our results indicate that prior to disease onset, the modulation of plastin 3 expression by profilin IIa only occurs in the spinal cord. Thus, there might be an early requirement during development for plastin 3 and the late upregulation observed here is not sufficient to rescue the SMA phenotype. To assess the importance and relevance of plastin 3, future experiments should address the effects of early upregulation on SMA pathogenesis.

We have provided evidence for modulation of actin-binding and actin-regulating proteins in a Smn-dependent manner, highlighting the perturbed actin cytoskeletal pathway as an important player in SMA pathogenesis (see model in **Figure 4.6**). However, we have to assume that in addition to profilin IIa and plastin 3, other components of actin dynamics are also affected

in SMA, which would explain why the simple downregulation of profilin IIa or upregulation of plastin 3 is not sufficient on its own to ameliorate the SMA phenotype. In this regard, we have shown an increase in active RhoA and a decrease in active Cdc42 in Smn-depleted PC12 cells, resulting in altered cytoskeletal integrity (Bowerman et al. 2007). Interestingly, both profilin IIa and plastin 3 are downstream effectors of RhoA and Cdc42 (Dutartre et al. 1996; Gertler et al. 1996; Nakagawa et al. 1996; Suetsugu et al. 1998; Yang et al. 2000; Da Silva et al. 2003; Giganti et al. 2005; Shao et al. 2008). Considering the continuous and vast amount of crosstalk that occurs between pathways involved in actin dynamics, we hypothesize that other actin-binding and actin-regulating proteins will also be affected by Smn depletion. It would therefore be of value to assess if major upstream regulators of actin dynamics are perturbed in the SMA mouse model. Also, it is not clear if the expression of profilin IIa and plastin 3 are primarily affected by the loss of their interacting partner, Smn, by the localized disruption of actin dynamics, or by both (Giesemann et al. 1999; Sharma et al. 2005; Oprea et al. 2008).

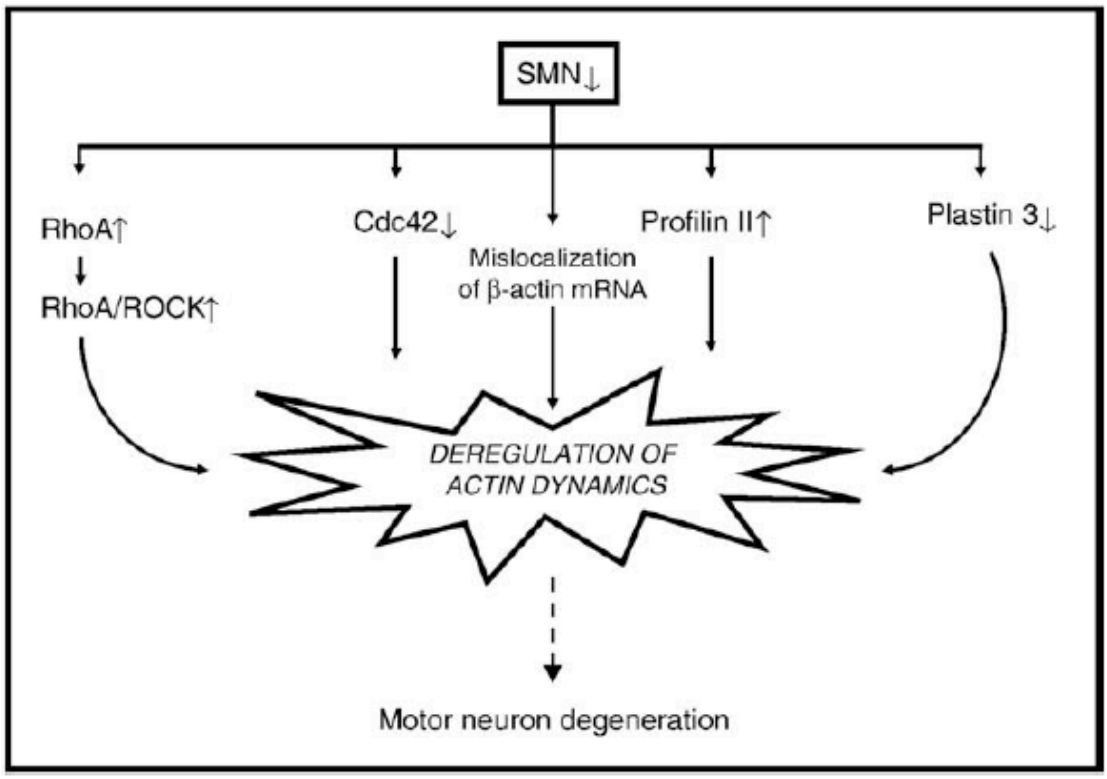

Figure 4.6. Simplified model of how SMN depletion impacts the regulators of actin cytoskeletal dynamics and thereby resulting in motor neuron degeneration.

A question debated in the SMA field is whether SMN has a distinct and unique role in neurons, thereby explaining why motor neurons are predominantly affected in SMA (Briese et al. 2005). We believe that SMN plays a crucial role in neuronal cells by regulating actin dynamics and that motor neurons are especially sensitive to the deregulation of this process. It has been suggested that the properties of a particular synapse might determine the importance of actin dynamics and activity of actin-regulating proteins within it (Reviewed in (Dillon et al. 2005; Cingolani et al. 2008). Indeed, perturbation of actin cytoskeletal dynamics at central synapses inhibits neurotransmitter release while small synapses are not affected by a disruption of actin dynamics (Cole et al. 2000; Schnell et al. 2001; Sakaba et al. 2003). Our present results indicate that there are intrinsic differences between neuronal cells of the brain and spinal cord, influencing how they are affected by modulation of actin-regulating proteins. Thus, the increased sensitivity of the large synapses of motor neurons to the tight control of actin cytoskeletal dynamics could explain why they are primarily affected in SMA.

MATERIALS AND METHODS

Antibodies

The mouse monoclonal primary antibodies used were as follows: anti-actin (1:800; Fitzgerald), anti-SMI32 (1:1000; Cedar Lane Laboratories), and anti-Smn (1:5000; Transduction Laboratories). The rabbit polyclonal primary antibodies used were as follows: anti-plastin 3 (1:200 (IB). 1:50 (IF); Santa Cruz Laboratories) and anti-profilin IIa (1:10,000 (IB), 1:500 (IF)) as described (Di Nardo et al. 2000).

The secondary antibodies used were as follows: horseradish peroxidase (HRP)-conjugated goat anti-mouse IgG (1:5000; Bio-Rad), HRP-conjugated goat anti-rabbit IgG (1:5000), Cy3-conjugated goat anti-mouse IgG + IgM (1:200; Jackson ImmunoResearch Laboratories), and Alexa Fluor 488 goat anti-rabbit IgG (1:100; Molecular Probes).

Animal models

The $Smn^{2B/-}$ mice were established in our laboratory and maintained in our animal facility on a C57BL/6 x CD1 hybrid background (unpublished data, (DiDonato 2007)). The 2B mutation consists of a substitution of 3 nucleotides in the exon splicing enhancer of exon 7 (DiDonato et al. 2001). The *Smn* knock-out allele was previously described by Schrank *et al*. (Schrank et al. 1997) and $Smn^{+/-}$ mice were obtained from The Jackson Laboratory. The *profilin 2* knock-out mice have been described previously (Pilo Boyl et al. 2007) and are on a C57Bl/6 background. All animal procedures were performed in accordance with institutional guidelines.

Immunohistochemistry

Brain stems and spinal cords of mice (P21) were quickly dissected and placed in a 4% paraformaldehyde solution overnight at 4ºC, followed by a second overnight incubation at 4ºC in a 30% sucrose solution. Finally, samples were frozen over liquid nitrogen in a 1:1 solution of OCT (Tissue Tek) and 30% sucrose, and stored at -80ºC until they were sectioned at 10 μm thickness using a cryostat.

Immunohistochemistry was performed by incubating sections for 2 hours at room temperature (RT) in blocking solution (TBLS (10% NaN_3), 20% goat serum, 0.3% Triton X-100 (Sigma-Aldrich)). This was followed by an overnight incubation at 4ºC with the first primary antibody. Subsequently, sections were washed 3 times with PBS, incubated 1 hour at RT with the secondary antibody and washed 3 times with PBS. These steps were then repeated for the second primary antibody. After the last PBS wash, sections were incubated 5 minutes with Hoechst (1:10,000) and then washed a final 3 times in PBS before being mounted in Fluorescent Mounting Medium (Dako).

Images were taken with a Zeiss Axioplan microscope, with a 20X objective, equipped with filters suitable for FITC/Cy3/Hoechst fluorescence. To ensure an unbiased approach to our qualitative and quantitative assessments, all images were taken at the same exposure time and chosen based on SMI32/Cy3 immunofluorescence.

Quantitative assays were performed on 3 mice of each genotype and 5 sections per mouse. Analyzed sections were at least 30 μm apart. SMI32-, profilin IIa- and plastin 3-positive cells were counted in the entire section of the brain stem and in the ventral horn of the spinal

cord and were divided over the total of Hoechst-positive nuclei. SMI32-positive motor neurons were identified morphologically by size and shape. Profilin IIa and plastin 3 signal intensity analysis of these same sections was performed using the Image J software. An area surrounding the cell body of motor neurons was a given a densitometry value of arbitrary fluorescence units followed by background subtraction.

Hematoxylin and eosin staining

Brain and spinal cord sections of P21 mice were first deparaffinized in xylene and then fixed in 100% ethanol. Following a rinse in water, they were stained in hematoxylin (Fisher) for 3 minutes, rinsed in water, dipped 40 times in a solution of 0.02% HCl in 70% ethanol and rinsed in water again. The sections were next stained in a 1% eosin solution (BDH) for 1 minute, dehydrated in ethanol, cleared in xylene and mounted with Permount (Fisher). Images were taken with a Zeiss Axioplan2 microscope, with a 20X objective.

Quantitative assays were performed on 3 mice for each genotype and 5 sections per mouse. Analyzed sections were at least 30 μm apart. Motor neurons were identified by their shape and size in the same designated area of the brain stem sections and in the ventral horn of the spinal cord sections.

Immunoblot analysis

Equal amounts of brain and spinal cord samples of P21 and P10 mice were separated by electrophoresis on 10% SDS-polyacrylamide gels and blotted onto a PVDF membrane (Millipore). The membranes were blocked in 5% nonfat milk in TBST (10 mM Tris-HCl pH 8.0, 150 mM NaCl, and 0.1% Tween 20 (Sigma)), incubated overnight at 4°C with the first primary

antibody, rinsed in TBST and incubated again overnight at 4ºC with the second primary antibody. Then, membranes were incubated at room temperature with the secondary antibodies, 1 hour for each one, with TBST washes in between. Signals were visualized using the ECL or the ECL plus detection kit (Amersham).

Ratios of plastin 3 over actin were performed using the Image J software on 4 different samples per genotype. Each band was given a densitometry value followed by background subtraction.

Statistical methods

Student's *t* test for paired variables was used to test for differences between samples and data were considered significantly different at $p < 0.05$. For the Kaplan-Meier survival analysis, the log-rank test was used and survival curves were considered significantly different at $p<0.05$.

ACKNOWLEDGEMENTS

We are grateful to Dr. David Picketts for critical reading of the manuscript, and the rest of the Kothary laboratory for helpful discussions. We also give thanks to Dr. Christine DiDonato for initiating the SMA mouse model project in our laboratory and her collaboration with us throughout the characterization and establishment of the *Smn*$^{2B/-}$ mice. This project was funded by a grant from the Canadian Institutes of Health Research (CIHR), and The Muscular Dystrophy Association to R.K. M.B. is a recipient of an Ontario Graduate Scholarship in Science and Technology and a CIHR Doctoral Research Award.

CHAPTER 5: Targeting the RhoA pathway via the Y-27632 ROCK inhibitor as a therapeutic strategy for SMA

Rho-kinase inactivation prolongs survival of an intermediate SMA mouse model

Mélissa Bowerman, Ariane Beauvais, Carrie L. Anderson and Rashmi Kothary

Published in *Human Molecular Genetics*, 2010, 19 (8), 1468-78

Author Contributions

Conceived and designed the experiments: MB and RK. Performed the experiments: MB, CLA and AB. Analyzed the data: MB. Wrote the paper: MB.

ABSTRACT

Spinal muscular atrophy (SMA) is an inherited disease resulting in the highest mortality of children under the age of two. SMA is caused by mutations or deletions in the survival motor neuron 1 (*SMN1*) gene, leading to aberrant neuromuscular junction development and the loss of spinal cord α-motor neurons. Here, we show that Smn depletion leads to increased activation of RhoA, a major regulator of actin dynamics, in the spinal cord of an intermediate SMA mouse model. Treating these mice with Y-27632, which inhibits ROCK, a direct downstream effector of RhoA, dramatically improves their survival. This lifespan rescue is independent of Smn expression and is accompanied by an improvement in the maturation of the neuromuscular junctions and an increase in muscle fiber size in the SMA mice. Our study presents evidence linking disruption of actin cytoskeletal dynamics to SMA pathogenesis and for the first time, identifies RhoA effectors as viable targets for therapeutic intervention in the disease.

INTRODUCTION

Spinal muscular atrophy (SMA) is an autosomal recessive disease caused by homozygous mutations and or deletions of the survival of motor neuron 1 (*SMN1*) gene (Pearn 1978b; Lefebvre et al. 1995). Affecting 1:10 000 live births, it is the number one inherited killer of children below the age of two (Pearn 1978b; Crawford et al. 1996). The depletion of the SMN protein results in the loss of α-motor neurons in the spinal cord, muscular atrophy of the limbs and trunk, paralysis and, in the most severe cases, fatality (Crawford et al. 1996). Recent studies in SMA mouse models suggest that the loss of motor neurons and muscular atrophy of SMA patients is preceded by and may be due to defects in neuromuscular junction (NMJ) maturation and function (Kariya et al. 2008; McGovern et al. 2008; Kong et al. 2009). Indeed, analysis of myotubes from SMA type I (severe) patients shows an absence of nicotinic acetylcholine receptor aggregation, an essential initial step for proper NMJ formation (Arnold et al. 2004).

While the *SMN* gene is evolutionarily conserved and all eukaryotic organisms have only one copy of the gene, humans have two copies (Lefebvre et al. 1995; DiDonato et al. 1997). *SMN1* is the telomeric copy while *SMN2* is a duplicated centromeric copy on chromosome 5q (Lefebvre et al. 1995). The critical difference within the *SMN2* gene is a C to T substitution at position 6 of exon 7 (Lorson et al. 1999). This substitution results in the loss of an exon splicing enhancer and/or the gain of an exon splicing silencer, which promotes exon 7 skipping and production of an unstable truncated protein, termed Δ7SMN (Lefebvre et al. 1995; Cartegni et al. 2002; Kashima et al. 2003). Although, the Δ7SMN protein is the major product of the *SMN2* gene, a small amount of full-length SMN protein (~ 10%) is still produced (Lefebvre et al. 1995).

Thus, the number of *SMN2* copies present in SMA patients can modulate the severity of the disease (Lefebvre et al. 1995).

Therapeutic approaches to SMA have included neuronal cell replacement and increasing SMN expression via gene therapy (Azzouz et al. 2004; Corti et al. 2008). Alternatively, others have attempted to alter the splicing pattern and/or the transcription of the *SMN2* gene to produce more full-length SMN mRNA and ultimately protein (Riessland et al. 2006; van Bergeijk et al. 2006; Avila et al. 2007; Mattis et al. 2008; Williams et al. 2009). While these approaches have resulted in improvement in weight, motor function and motor neuron loss in SMA mouse models, the increase in survival have to date been modest (Azzouz et al. 2004; Avila et al. 2007; Corti et al. 2008; Williams et al. 2009). More importantly, although encouraging, most of these approaches are still a long way from clinical translation.

To date no SMA therapeutic strategy has addressed the cellular and molecular pathways that are dysregulated as a result of the infraphysiologic levels of SMN observed in the disorder. We have previously shown that Smn depletion in PC12 cells is characterized by an increase in profilin IIa (small actin binding protein) (Carlsson et al. 1977) availability, and an increase in total and active RhoA (Luo et al. 1997; Bowerman et al. 2007). The defects in these cells include perturbation of neuronal differentiation and integrity (Bowerman et al. 2007). Furthermore, we have also identified a cell-autonomous increase in profilin IIa and a decrease in plastin 3 (actin-bundling protein) (Bretscher 1981) levels in neuronal cells of an intermediate SMA mouse model (Bowerman et al. 2009). While knocking out profilin II restored plastin 3 levels, it neither improved survival and weight, nor did it reduce motor neuron degeneration in

these SMA mice (Bowerman et al. 2009). One explanation for the failure of profilin IIa and plastin 3 reconstitution to ameliorate the SMA phenotype may be because they are end-point effectors of the actin cytoskeletal dynamics signaling pathways. It is indeed possible that more upstream regulators of actin dynamics are misregulated due to Smn depletion, and other targets in addition to profilin IIa and plastin 3 would therefore also be affected.

In the present study, we investigate the effect of Smn depletion on upstream regulators of actin dynamics in the $Smn^{2B/-}$ intermediate SMA mouse model (Bowerman et al. 2007; Bowerman et al. 2009). We show an increased activation of RhoA, a major regulator of actin dynamics, in the spinal cord of this SMA mouse model. More importantly, we demonstrate that the pharmacological inhibition of Rho-kinase, a direct downstream effector of active RhoA, dramatically increases the survival and neuromuscular junction maturation in these mice. This is the greatest increase in lifespan of an SMA mouse model reported to date; the fact that it was achieved through the use of a synthetic compound that modulates the RhoA pathway highlights the importance of the regulation of actin cytoskeletal dynamics in SMA pathogenesis. Our study thus holds significant promise for a novel therapeutic approach for this incurable disorder.

RESULTS

Abnormal RhoA activation in the $Smn^{2B/-}$ SMA mouse model

We have previously reported that Smn-depleted PC12 cells have increased total and active RhoA, a critical regulator of actin cytoskeletal dynamics (Luo et al. 1997; Bowerman et al. 2007). To determine if a similar effect was observed *in vivo*, we took advantage of an intermediate SMA mouse model that we have recently described (Bowerman et al. 2009). Briefly, this line has a three nucleotide substitution mutation within exon 7 of the endogenous mouse *Smn* gene. This change leads to the alternative splicing of *Smn*, resulting in a marked shift from full length SMN mRNA to *Δ7Smn* mRNA (DiDonato et al. 2001). This new allele is termed Smn^{2B}. $Smn^{2B/-}$ mice (which have ~15% Smn protein levels) present features of SMA after the second week of life. Upon disease onset, they become significantly smaller than their wild type littermates and exhibit motor neuron loss in the ventral horn region of the spinal cord. The majority of $Smn^{2B/-}$ mice die by one month of age.

Here, we analyzed spinal cord extracts of wild type and $Smn^{2B/-}$ mice at three stages. Postnatal days (P) 0 and 10 were considered to be pre-phenotype stage as $Smn^{2B/-}$ mice were indistinguishable from their wild type littermates, while P21 was considered to be phenotype stage. Total RhoA levels in the spinal cords of the $Smn^{2B/-}$ mice did not show significant changes when compared to wild type, however there was sample to sample variability, particularly at P21 (**Figure 5.1 A, B**). In contrast, while at P0, the active RhoA levels are unchanged (1.68% +/- 15%), we observe a consistent increase of RhoA-GTP in the spinal cords of $Smn^{2B/-}$ mice at P10 (82% +/- 10%) and P21 (84% +/- 3%) (**Figure 5.1 A, B**). This is of importance since it is the

GTP-bound RhoA that dictates its effects and the activated signaling pathways within the cell. These results suggest that RhoA activity in the spinal cord is altered when Smn is depleted. Indeed, whereas RhoA-GTP levels in the spinal cord of *Smn*$^{2B/-}$ mice are unchanged at birth, they consistently increase prior to and at onset of disease.

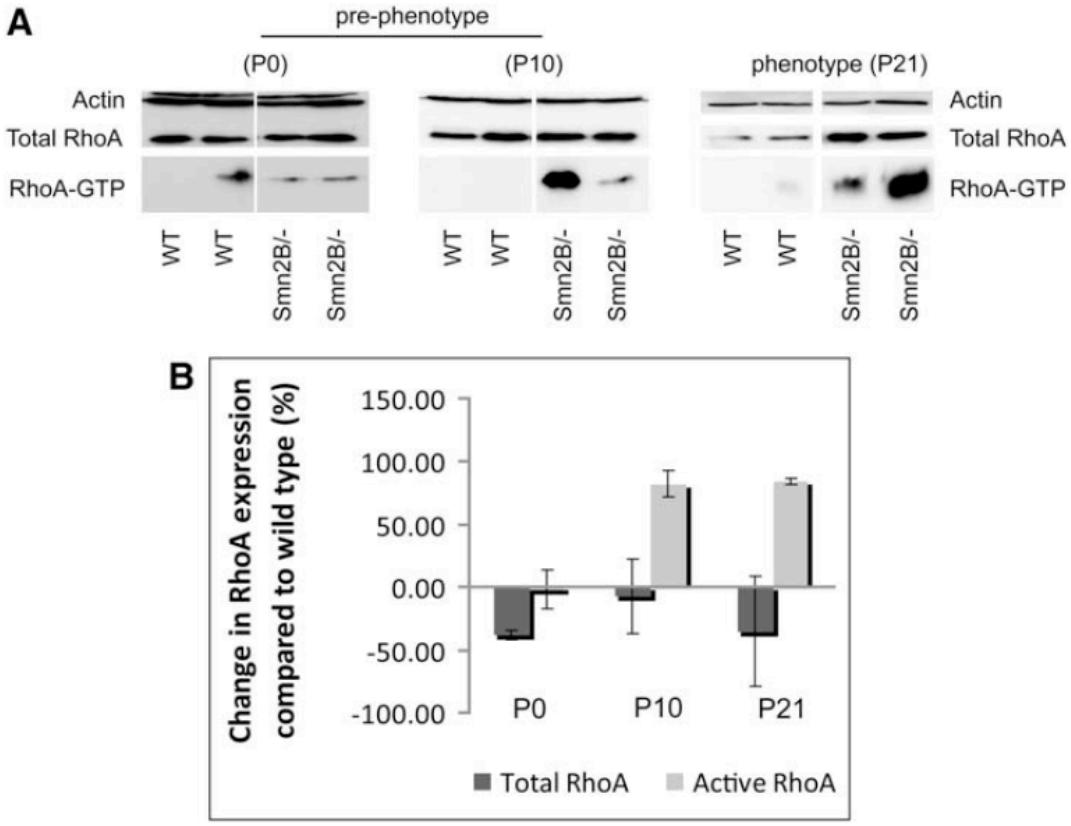

Figure 5.1. Total and active RhoA in spinal cords of wild type (WT) and *Smn*$^{2B/-}$ mice. A) The spinal cords of *Smn*$^{2B/-}$ mice at pre-phenotype (P10) and phenotype (P21) stages have an increase in RhoA-GTP (active) levels compared to WT mice. B) RhoA-GTP/actin ratios of *Smn*$^{2B/-}$ mice (n = 3) were compared to WT (n = 3). RhoA-GTP levels are increased in the spinal cords of *Smn*$^{2B/-}$ mice at P10 and P21 while total RhoA levels are more variable and not significant (data are mean +/- S.E).

Y-27632 administration improves survival of $Smn^{2B/-}$ mice

As a therapeutic strategy, we decided to target the signaling pathway of active RhoA in the spinal cord of the $Smn^{2B/-}$ mice. Y-27632 is a synthetic compound that inhibits Rho-kinase (ROCK) (Uehata et al. 1997), a direct downstream effector of RhoA-GTP (Amano et al. 1996), by competing with its ATP binding site (Ishizaki et al. 2000). We have previously demonstrated that Y-27632 partially rescues the neuronal differentiation defects in Smn-depleted PC12 cells (Bowerman et al. 2007). We thus set out to assess if the increased activation of RhoA in the spinal cord of the $Smn^{2B/-}$ mice could contribute to the observed SMA phenotype and reduced lifespan of this mouse model. The Y-27632 compound was administered to wild type, $Smn^{2B/+}$ (normal littermates) and $Smn^{2B/-}$ mice at a concentration of 1 mg/kg twice daily or 30 mg/kg once daily starting at P3 and ending at P21. Control groups were given the peptide vehicle (water). Neither treatment regime prevented the weight loss of the $Smn^{2B/-}$ mice that occurs at about P10 and beyond (**Figure 5.2 A**). Concordantly, treatment of $Smn^{2B/-}$ mice with the lower dose did not improve their lifespan although the trend was towards improvement (**Figure 5.2 B**, $P = 0.2981$). Remarkably, $Smn^{2B/-}$ mice treated with the higher dose exhibited a dramatic rescue in survival (**Figure 5.2 B**, $P = 0.018$). Indeed, the mice survived far beyond their normal lifespan and expired between 14 and 33 weeks of age. These mice move about the cage, albeit with a slight neurological phenotype (see movie in **Supplementary Figure 5.1 A**). In contrast, vehicle-treated $Smn^{2B/-}$ mice display a much more severe neurological phenotype and refrain from moving about the cage (see movie in **Supplementary Figure 5.1 B**). Finally, Y-27632 administration did not negatively impact weight or survival of $Smn^{2B/+}$ littermates (**Figure 5.2 A, B**). Overall, these

results show that treatment of *Smn*$^{2B/-}$ mice with the higher dose of Y-27632 significantly increases their lifespan.

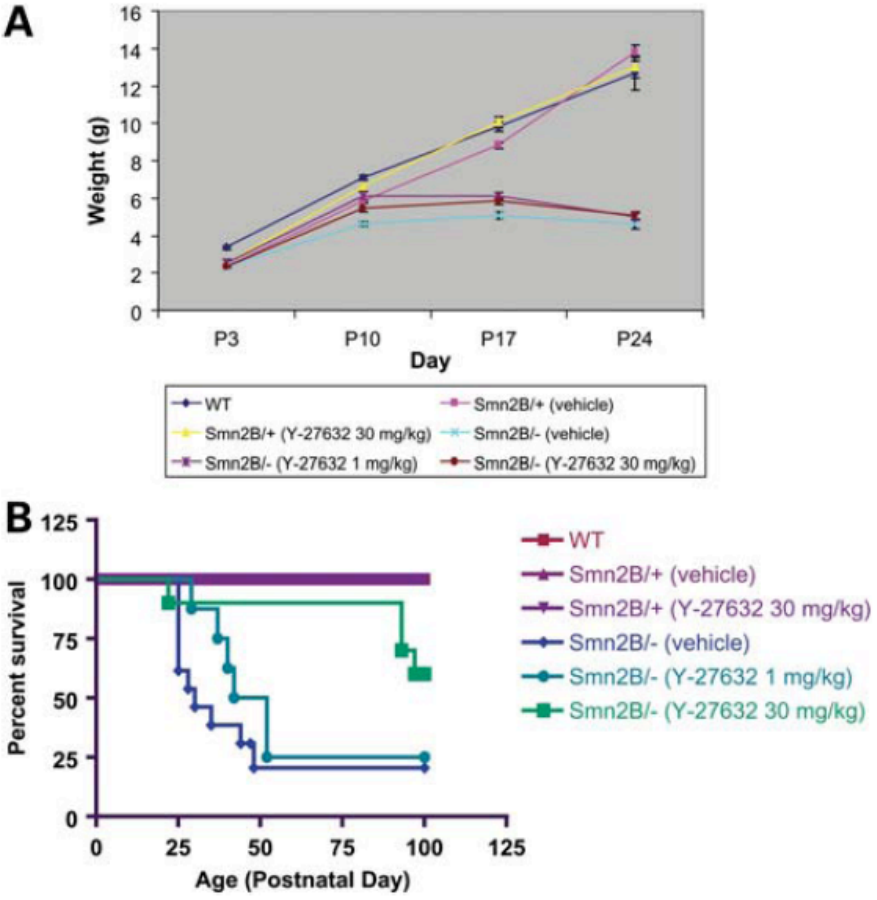

Figure 5.2. Weight and survival analysis of wild type (WT), *Smn*$^{2B/+}$ and *Smn*$^{2B/-}$ mice treated with low and high doses of Y-27632 or vehicle (water). The different groups analyzed were: untreated WT mice (n = 9), vehicle-treated *Smn*$^{2B/+}$ mice (n = 24), 1 mg/kg Y-27632-treated *Smn*$^{2B/+}$ mice (n = 12), 30 mg/kg Y-27632-treated *Smn*$^{2B/+}$ mice (n = 10), vehicle-treated *Smn*$^{2B/-}$ mice (n = 12), 1 mg/kg Y-27632-treated *Smn*$^{2B/-}$ mice (n = 8) and 30 mg/kg Y-27632-treated *Smn*$^{2B/-}$ mice (n = 10). A) Administration of 1 mg/kg or 30 mg/kg of Y-27632 does not attenuate the weight loss observed in vehicle-treated *Smn*$^{2B/-}$ mice (data are mean +/- S.E.). B) Treatment

of *Smn*$^{2B/-}$ mice with 30 mg/kg Y-27632 dramatically improves lifespan compared to vehicle-treated *Smn*$^{2B/-}$ mice ($P = 0.018$).

To determine if the Y-27632 compound had a similar effect on a severe SMA mouse model, we administered the compound to the *Smn*$^{-/-}$*;SMN2* mice that die within the first postnatal week (Monani et al. 2000b). Pregnant females were administered either 30 mg/kg of Y-27632 or vehicle starting at gestational day E14. Once born, pups were administered Y-27632 by gavage daily starting at P3. We observed no significant improvement in the lifespan of *Smn*$^{-/-}$*;SMN2* mice treated with the Y-27632 compound (**Figure 5.3**, $P = 0.42$), perhaps because the severity of the disease in this mouse model was too extreme to benefit from the treatment.

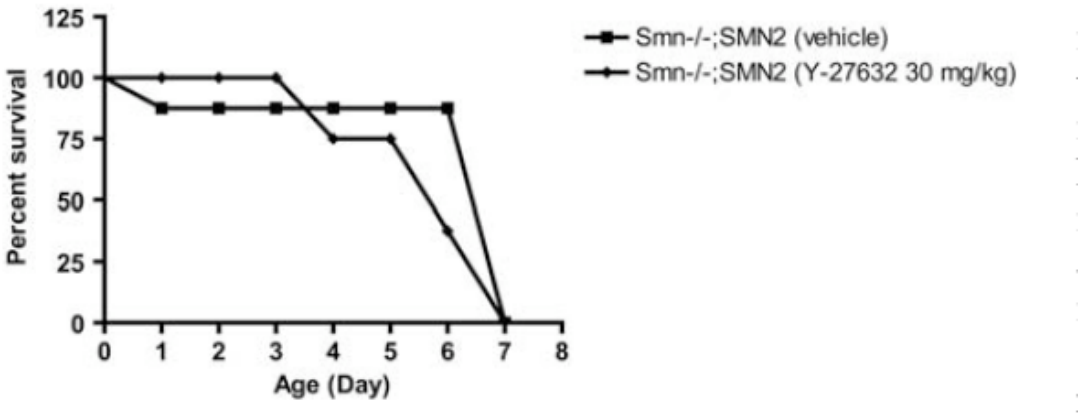

Figure 5.3. Administration of Y-27632 (30 mg/kg) to a severe SMA mouse model (*Smn*$^{-/-}$*;SMN2*) does not improve lifespan. The different age-matched groups analyzed were: vehicle-treated *Smn*$^{-/-}$*;SMN2* (n = 3) and Y-27632-treated *Smn*$^{-/-}$*;SMN2* (n = 3). There was no significant difference between the survival curves of both groups ($P = 0.42$).

Y-27632 inhibits ROCK activity but does not alter Smn expression in the spinal cord of $Smn^{2B/-}$ mice

To ensure that Y-27632 was present and active following gavage, we analyzed downstream effectors of ROCK within spinal cord protein extracts of treated animals. Activated ROCK phosphorylates LIM kinase (LIMK), which subsequently leads to the phosphorylation of cofilin (Maekawa et al. 1999; Sumi et al. 1999). The spinal cords of P10 $Smn^{2B/-}$ mice treated with 30 mg/kg of Y-27632 for one week (P3 to P10) show a decrease in both phosphorylated LIMK and phosphorylated cofilin compared to untreated $Smn^{2B/-}$ mice (**Figure 5.4 A**). Total LIMK and cofilin protein, however, were unchanged (**Figure 5.4 A**). We can thus conclude that the Y-27632 compound reaches the spinal cord and appropriately inhibits ROCK activity.

One possible explanation for the observed improvement in survival of the $Smn^{2B/-}$ mice is that Y-27632 increases Smn protein or mRNA levels. However, our analysis shows that Smn protein levels did not change in the spinal cords of $Smn^{2B/-}$ mice treated with 30 mg/kg of Y-27632 compared to untreated $Smn^{2B/-}$ mice (**Figure 5.4 B**). Additionally, administration of Y-27632 (30 mg/kg) did not alter the ratio of full-length *Smn* to *Δ7Smn* mRNAs ($P = 0.56$; **Figure 5.4 C, D**). These results suggest that the increased lifespan of $Smn^{2B/-}$ mice treated with 30 mg/kg of Y-27632 is due to its direct effect on ROCK inhibition and not because of an unanticipated increase in Smn expression.

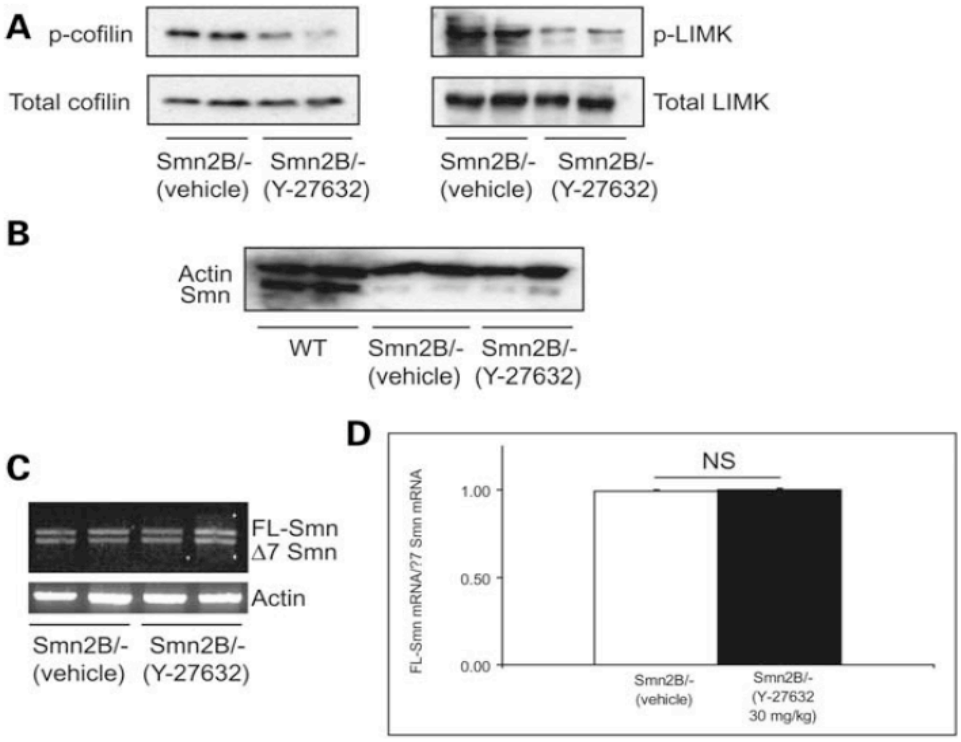

Figure 5.4. Y-27632 inhibits ROCK activity but does not alter Smn expression in spinal cords of *Smn*$^{2B/-}$ mice. A) Spinal cords of *Smn*$^{2B/-}$ mice treated with 30 mg/kg of Y-27632 show decreased levels of phospho-LIMK and phospho-cofilin compared to vehicle-treated *Smn*$^{2B/-}$ mice. LIMK and cofilin are usually phosphorylated by ROCK, the Y-27632 target. Total levels of LIMK and cofilin were unchanged between both treated and untreated *Smn*$^{2B/-}$ mice. B) The spinal cords of *Smn*$^{2B/-}$ mice treated with 30 mg/kg of Y-27632 did not show increased expression of Smn protein when compared to vehicle-treated *Smn*$^{2B/-}$ mice. C) The spinal cords of *Smn*$^{2B/-}$ mice treated with 30 mg/kg of Y-27632 did not show an increase in full-length (FL) Smn mRNA when compared to vehicle-treated *Smn*$^{2B/-}$ mice. D) Quantification of FL Smn mRNA/Δ7 Smn mRNA ratios

shows no significant differences between vehicle- and Y-27632-treated *Smn*$^{2B/-}$ mice (P = 0.56) (data are mean +/- S.E)

Y-27632 improves neuromuscular junction maturation in $Smn^{2B/-}$ mice

Recent studies have identified a role for Smn in the maturation of neuromuscular junctions (NMJs) with poor terminal arborization, denervation, impaired synaptic vesicle release and decreased NMJ size all observed in SMA mouse models. We thus elected to examine the impact of Y-27632 treatment on this structure, comparing NMJs in the tibialis anterior (TA) muscle of P21 wild type (untreated) and $Smn^{2B/-}$ mice (untreated and treated). Alpha-bungarotoxin was used to identify NMJs, and SV2 and SMI312 antibodies were used to identify the synaptic vesicles and neurons, respectively. Although the NMJs of $Smn^{2B/-}$ mice treated with 30 mg/kg of Y-27632 were smaller than those of wild type mice (**Figure 5.5 A, B**, $P = 0.027$), they were significantly larger than those observed in untreated $Smn^{2B/-}$ mice (**Figure 5.5 A, B**, $P = 0.015$). The percentage of NMJs with mature terminals was next quantified using sophisticated folds and perforations as criteria for NMJ maturity (Sanes et al. 2001). Specifically, only the terminals in which SV2 and SMI312 staining showed full endplate occupancy as well as multiple perforations and folds were considered as being mature NMJs. Once again, although not equivalent to that observed in wild type (**Figure 5.5 A, C**, $P = 0.0054$), NMJ maturation is markedly improved in treated $Smn^{2B/-}$ mice when compared to untreated mice (**Figure 5.5 A, C**, $P = 0.018$). The improvement in NMJ maturation is in accordance with other studies implicating Y-27632 in axonal sprouting and regeneration (Hirose et al. 1998; Fournier et al. 2003; Chan et al. 2005). Our results suggest that the beneficial effect of Y-27632 on the lifespan of $Smn^{2B/-}$ mice is due to a direct improvement in NMJ maturation.

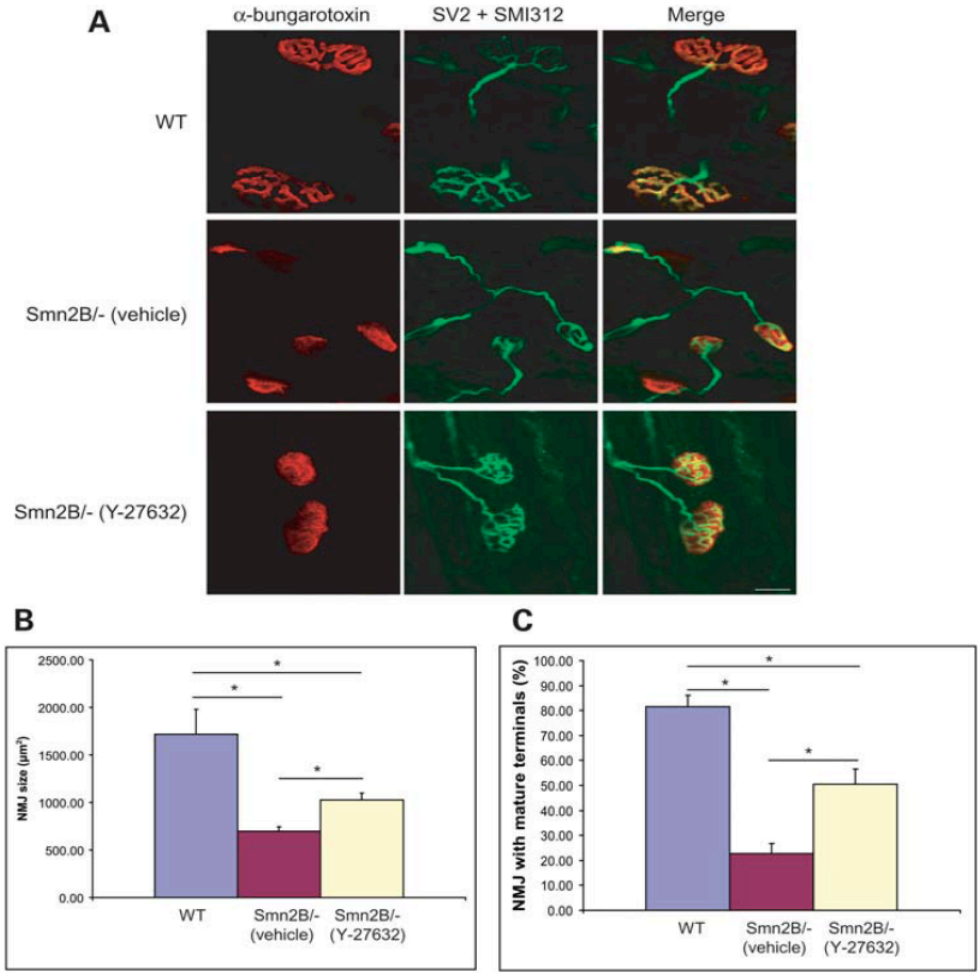

Figure 5.5. Analysis of neuromuscular junction (NMJ) maturity in the tibialis anterior (TA) muscle of postnatal day 21 (P21) wild type and *Smn*$^{2B/-}$ mice. The different age-matched groups analyzed were: untreated WT (n = 4), vehicle-treated *Smn*$^{2B/-}$ mice (n = 3) and 30 mg/kg Y-27632-treated *Smn*$^{2B/-}$ mice (n = 5). A) Representative images showing the NMJs of WT and untreated and treated *Smn*$^{2B/-}$ mice. NMJs were stained with alpha-bungarotoxin (red), the axons with SMI312 (green) and the synaptic vesicles with SV2 (green) (scale bar, 50 μm). B) Quantification of NMJ size. The NMJs of *Smn*$^{2B/-}$ mice treated with 30 mg/kg of Y-27632 are

significantly larger compared to vehicle-treated *Smn*$^{2B/-}$ mice ($P = 0.015$). However, the NMJs of treated *Smn*$^{2B/-}$ mice are still significantly smaller than WT NMJs ($P = 0.027$) (data are mean +/- S.E.). C) The percentage of NMJs with mature terminals is significantly greater in *Smn*$^{2B/-}$ mice treated with 30 mg/kg Y-27632 than with the vehicle ($P = 0.018$). However, NMJs of treated *Smn*$^{2B/-}$ mice still remain more immature than WT NMJs ($P = 0.0054$) (data are mean +/- S.E.).

Y-27632 increases muscle fiber size

To complement the weight and NMJ analyses, we investigated the effect of Y-27632 on the muscle fiber size of the tibialis anterior (TA) of P21 mice. The muscle fibers of $Smn^{2B/-}$ mice were significantly smaller than their WT littermates (**Figure 5.6 A, B**, $P = 0.0021$). Surprisingly, while the vehicle- and Y-27632-treated $Smn^{2B/-}$ mice did not differ in weight (**Figure 5.2 A**), mice that were administered the Y-27632 compound displayed a significant increase in muscle fiber size (**Figure 5.6 A, B**, $P = 0.0007$). The percentage of centrally located nuclei of vehicle-treated $Smn^{2B/-}$ mice was not significantly different from WT or Y-27632-treated $Smn^{2B/-}$ mice (**Figure 5.6 C**, $P = 0.37$ and 0.8, respectively).

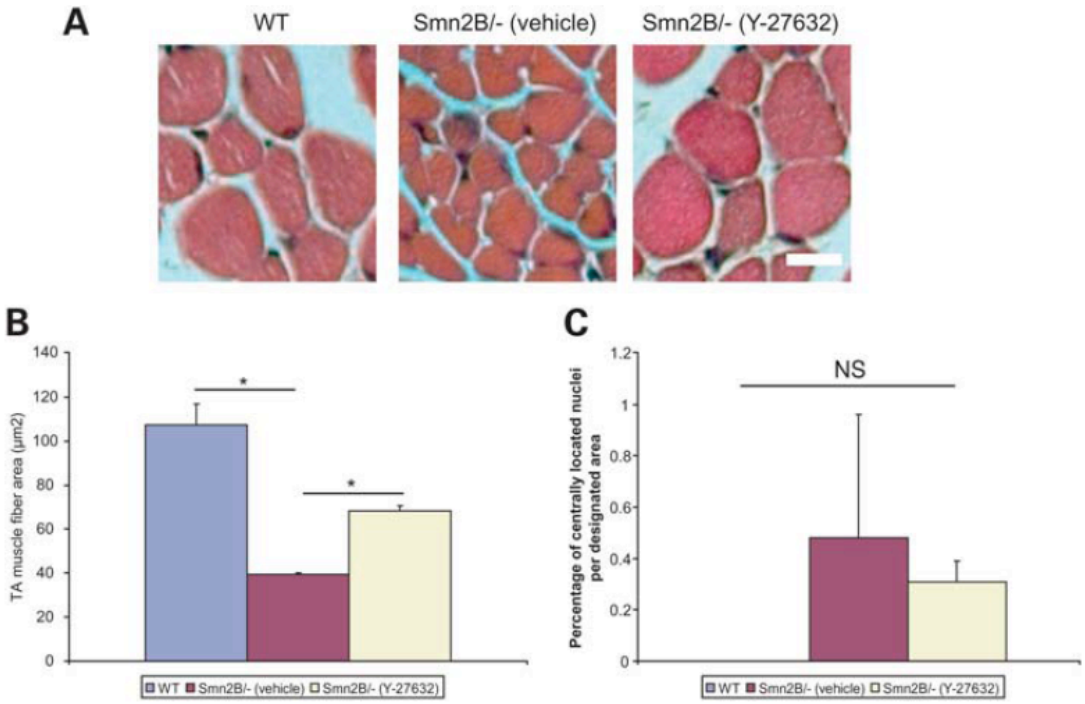

Figure 5.6. Treatment of *Smn*$^{2B/-}$ mice with Y-27632 (30 mg/kg) increases fiber diameter in tibialis anterior (TA) muscle. The different age-matched groups analyzed were: untreated wild type (WT) (n = 3), vehicle-treated *Smn*$^{2B/-}$ mice (n = 3) and Y-27632-treated *Smn*$^{2B/-}$ mice (n = 3). A) Representative images showing hematoxylin and eosin staining of muscle fibers within a designated area of the TA muscle. (scale bar, 10 µm). B) Quantification of the cross-sectional area of TA muscle fibers. Vehicle-treated *Smn*$^{2B/-}$ mice have significantly smaller muscle fibers than their WT littermates ($P = 0.0021$). Administration of the Y-27632 compound significantly increased the muscle fiber size of *Smn*$^{2B/-}$ mice ($P = 0.0007$). C) Quantification of the percentage of muscle fibers displaying a centrally located nuclei. There was no significant difference (NS) between WT and vehicle-treated *Smn*$^{2B/-}$ mice ($P = 0.37$) or between vehicle- and Y-27632-treated *Smn*$^{2B/-}$ mice ($P = 0.8$).

Y-27632 does not increase the number of motor neurons in the ventral horn region of the spinal cord

Since the *Smn*$^{2B/-}$ mice are characterized by a loss of spinal cord motor neurons (Bowerman et al. 2009), we wanted to assess if an improvement in NMJ maturation translated to a protection of these neurons from degeneration. Wild type mice had significantly more motor neurons than vehicle-treated *Smn*$^{2B/-}$ mice (**Figure 5.7 A, B**, $P = 0.002$). Treatment with the Y-27632 compound did not prevent the loss of motor neurons in the *Smn*$^{2B/-}$ mice (**Figure 5.7 A, B**, $P = 0.12$). This inability of the Y-27632 treatment to rescue such a pathological feature of SMA is most likely due to the fact that the Y-27632 is acting via an Smn-independent pathway. Thus, neuronal degeneration and/or denervation may still occur through other intrinsic pathways directly affected by the loss of the Smn protein. Indeed, administration of the Y-27632 may only strengthen the remaining NMJs and thus, enable the treated mice to survive longer.

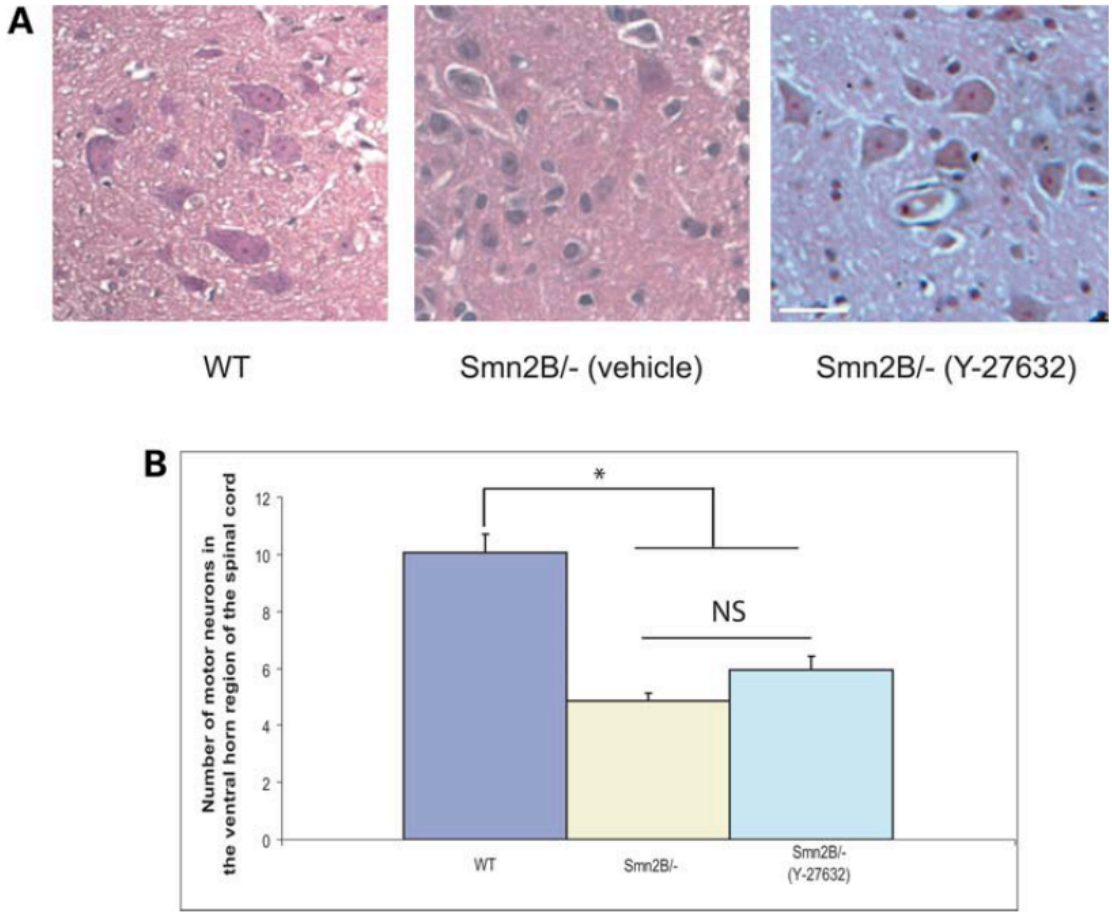

Figure 5.7. Y-27632 (30 mg/kg) administration does not protect from motor neuron loss in *Smn*$^{2B/-}$ mice. The different groups analyzed were: untreated wild type (n = 3), vehicle-treated *Smn*$^{2B/-}$ (n = 3) and Y-27632-treated *Smn*$^{2B/-}$ mice (n = 3). A) Representative images showing hematoxylin and eosin staining of the motor neurons in the ventral horn region of the spinal cord for each group (scale bar, 50 μm). B) Quantification of the number of motor neurons within the ventral horn region of the spinal cord. While untreated *Smn*$^{2B/-}$ mice show significantly fewer motor neurons than their WT littermates (P = 0.002), treatment of the SMA mice with Y-27632 did not have a positive impact on the number of motor neurons (P = 0.12) (data are mean +/- S.E.).

DISCUSSION

In this study, we show that the level of active RhoA (RhoA-GTP) is increased in the spinal cords of the *Smn*$^{2B/-}$ intermediate SMA mouse model. Inactivation of ROCK, a direct downstream effector of RhoA-GTP (Amano et al. 1996), via administration of Y-27632 (30 mg/kg), results in the most significant increase in the lifespan of SMA mice reported to date. Significantly, treatment with Y-27632 did not increase Smn RNA or protein levels suggesting the modulation of an event or events downstream of SMN depletion. Importantly, *Smn*$^{2B/-}$ mice treated with Y-27632 displayed larger NMJs and a greater percentage of mature NMJ terminals when compared to untreated *Smn*$^{2B/-}$ mice. Recent work in mouse models has suggested that SMA could be a motor neuron synaptopathy (Kariya et al. 2008; McGovern et al. 2008; Kong et al. 2009). As well, perturbed NMJ formation has been reported in myotubes from severe SMA patients (Arnold et al. 2004). Consistent with these observations, we propose that disrupted RhoA regulation in an SMN depleted neuron contributes to a failure of the NMJs to fully mature. The correcting of RhoA/ROCK signaling with Y-27632 represents one promising means of ameliorating NMJ formation and function, with a consequent improvement in lifespan.

RhoA is a small GTPase that plays an important role in the regulation of actin cytoskeletal dynamics (Luo et al. 1997). By signaling through various pathways, RhoA mediates neuronal growth, formation, polarization, regeneration, branching, pathfinding, guidance and retraction (reviewed in (Govek et al. 2005; Luo et al. 2005)). Furthermore, dysregulation of RhoA has been implicated in mental retardation, amyotrophic lateral sclerosis and lissencephaly (Boettner et al. 2002; Ramakers 2002; Kholmanskikh et al. 2003). The depletion of Smn in

motor neurons leads to defects in β-actin mRNA and protein localization (Rossoll et al. 2003). This defect may then result in anomalous signaling between the actin cytoskeletal signaling pathways and RhoA. Furthermore, an abnormal upregulation of RhoA-GTP also results in defects in actin localization (Yamaguchi et al. 2001). Previous studies have shown that the Y-27632 compound leads to actin rearrangements through the decreased phosphorylation of cofilin (Wang et al. 2009), promoting the advancement and enlargement of the neuronal growth cone and increasing (Rosner et al. 2007; Schaefer et al. 2008) the activity of voltage-gated calcium channels (Piccoli et al. 2004). The effects of the RhoA/ROCK inhibitor on the actin dynamics in neurons have thus been well characterized.

RhoA-GTP activates ROCK through phosphorylation (Amano et al. 1996), which in turn leads to the activation and phosphorylation of LIMK (Maekawa et al. 1999). Interestingly, in *Drosophila*, LIMK normally functions as a suppressor of synaptic sprouting and growth at the NMJ (Ang et al. 2006). Thus, increased RhoA activation in the spinal cord motor neurons of the $Smn^{2B/-}$ mice and a subsequent increase in LIMK activity may explain the smaller NMJs and the fewer mature terminals observed in these mice (**Figure 5.8**). The inactivation of ROCK through the administration of Y-27632 decreased the levels of phosphorylated LIMK. This reduction in phosphorylated LIMK would therefore suppress its inhibitory effect on growth and sprouting at the NMJ. A critical improvement in NMJ maturation and function, would thus lead to a subsequent enhancement in the lifespan of SMA mice. Studies attempting to alleviate the phenotype and lethality of rodent models of SMA and amyotrophic lateral sclerosis, another fatal neurodegenerative disease, also show that improvement of NMJ innervation is associated with increased survival (Gifondorwa et al. 2007; Suzuki et al. 2008; Tsai et al. 2008).

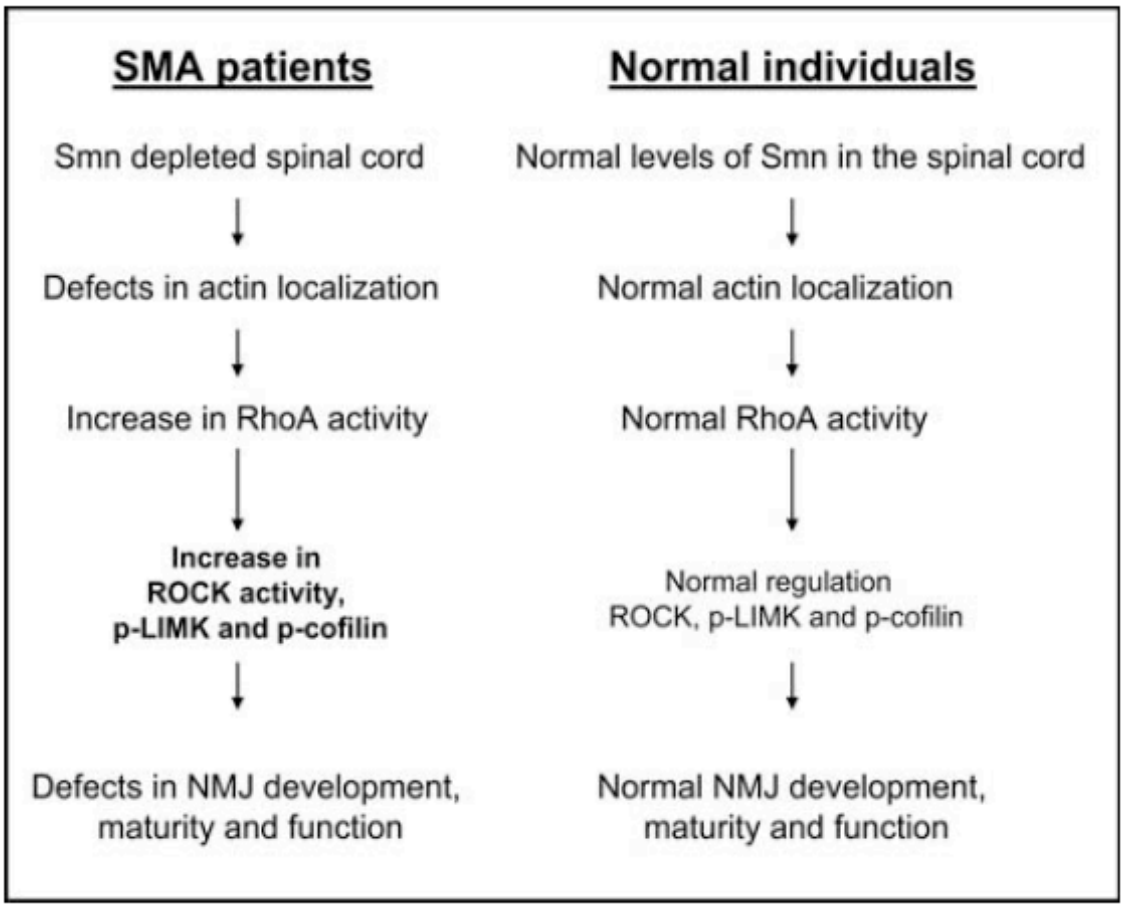

Figure 5.8. A model of how SMN depletion may affect RhoA activity in spinal cords and neuromuscular junction (NMJ) maturation. In SMA patients, a depletion in SMN results in abnormal localization and distribution of actin, which alters regulation of the actin cytoskeletal signaling pathways. A major upstream regulator of actin dynamics, RhoA, is thus misregulated, and its activity increases in the spinal cord. RhoA-GTP phosphorylates and activates ROCK, which in turn phosphorylates and activates cofilin and LIMK. An abnormal increase in p-LIMK suppresses synaptic sprouting and growth at the NMJ. This would eventually lead to the denervation and or/degeneration of the motor neurons within the ventral horn region of the spinal cord.

Interestingly, while Y-27632 administration dramatically ameliorates the survival of the *Smn*$^{2B/-}$ mice, it does not fully rescue the neurological phenotype. Indeed, we observed no improvement in the weight loss phenotype or age of onset of the disease in these mice. Further, the motor neuron loss in the ventral horn region of the spinal cord was not prevented. Given that the Y-27632 compound acts via an Smn-independent pathway, loss of the Smn protein itself might have residual pathogenic effects. Indeed, Smn has been shown to have roles in mRNA splicing and axonal transport (Paushkin et al. 2002; Rossoll et al. 2003). These functions might still be perturbed due to the persistent Smn depletion in the Y-27632-treated SMA mice. An alternative explanation for the inability of the Y-27632 to completely rescue the phenotype of the *Smn*$^{2B/-}$ mice is its simple incapacity to fully restore the maturity of NMJs. Indeed, although the NMJs of treated *Smn*$^{2B/-}$ mice are significantly larger and more mature than those of untreated *Smn*$^{2B/-}$ mice, they still remain significantly smaller and less mature than wild type NMJs. The improvement in NMJ maturation without a concomitant rescue in motor neuron and muscle fiber pathology therefore suggests that the Y-27632 treatment improves the functionality of the remaining NMJs without preventing motor neuron denervation and/or degeneration.

Surprisingly, *Smn*$^{2B/-}$ mice that received the Y-27632 compound displayed larger TA muscle fibers than their vehicle-treated counterparts. An increase in muscle fiber cross-sectional area without being accompanied by an increase in strength can occur, such as in instances of sarcoplasmic hypertrophy (Kraemer 2006). Why this occurs in the TA muscles of treated *Smn*$^{2B/-}$ mice is most likely due to the secondary effects of the systemically delivered Y-27632 compound. Indeed, activated ROCK has been shown to negatively impact the differentiation and fusion of skeletal myoblasts (Castellani et al. 2006) (Nishiyama et al. 2004; Fortier et al. 2008).

More importantly, the ROCK inactivation in skeletal myoblasts through Y-27632 administration results in enhanced differentiation, myoblast fusion, and an increase in myotube size (Nishiyama et al. 2004; Castellani et al. 2006). Thus, in addition to the effects observed in the spinal cord and NMJs of the *Smn*$^{2B/-}$ mice, the Y-27632 compound may also act on inactivating ROCK in skeletal muscle thereby enhancing differentiation and fusion, resulting in an increase in muscle fiber size. Whether this is consequential in the improved survival observed in the Y-27632-treated mice remains uncertain due to the absence of a concomitant increase in weight.

While administration of the Y-27632 compound significantly improved the survival of the *Smn*$^{2B/-}$ mice, an intermediate SMA mouse model, it had no beneficial effect on the most severe SMA mouse model, *Smn*$^{-/-}$*;SMN2* (Monani et al. 2000b). We have shown that the Y-27632 compound acts via an Smn-independent pathway, most likely by improving NMJ maturity. The rodent NMJ undergoes dramatic physical and molecular changes during the first two postnatal weeks (reviewed in (Sanes et al. 1999)). As the *Smn*$^{-/-}$*;SMN2* mice expire within the first week of life, the beneficial effect of the Y-27632 compound on NMJ maturation and size likely does not have time to occur in this severe SMA mouse model. Severe and intermediate mouse models of SMA, akin to human SMA types I, II and III, are very different in phenotype and severity of disease. In the present case in particular, the beneficial effect of Y-27632 in our intermediate mouse model is not due to "Smn" rescue but rather due to a "biological" rescue, bypassing the Smn defect altogether. These findings highlight the fact that treatment modalities for the different severities of SMA will have to be different. Indeed, it is most likely that for SMA, the "one size fits all" approach will not be tenable.

Although we have identified RhoA as a major player in the disruption of actin cytoskeletal dynamics in the *Smn*$^{2B/-}$ mouse model, we cannot exclude the involvement of other actin regulators. Indeed, our work in Smn-depleted PC12 cells shows a decrease in total and active Cdc42, another small Rho GTPase (Luo et al. 1997; Bowerman et al. 2007). Investigation of the *in vivo* effects of Smn depletion on Cdc42 expression would help elucidate if SMA pathogenesis is due to a more general disruption of actin cytoskeletal dynamics. Nevertheless, we show that abnormal activation of the RhoA pathway in the spinal cord of an intermediate SMA mouse model leads to some of the hallmarks of SMA pathogenesis. We are the first to provide evidence that the modulation of disrupted actin cytoskeletal dynamics dramatically improves the survival of SMA mice. The present work provides novel avenues for therapeutic approaches to treat this devastating disease.

MATERIALS AND METHODS

Antibodies

The mouse monoclonal primary antibodies used were as follows: anti-actin (1:800; Fitzgerald), anti-SMI312 (1:1000; Covance), anti-SV2 (1:100; Developmental Studies Hybridoma Bank), anti-RhoA (1:200 (IB), 1:5 (IF); Santa Cruz), and anti-Smn (1:5000; Transduction Laboratories). The rabbit polyclonal primary antibodies used were as follows: anti-LIMK (1:500; Cell Signaling), anti-phospho-LIMK (1:250; Cell Signaling), anti-cofilin (1:500; Chemicon); anti-phospho-cofilin (1:250; Chemicon) and anti NF (N4142) (1:200; Sigma).

The secondary antibodies used were as follows: horseradish peroxidase (HRP)-conjugated goat anti-mouse IgG (1:5000; Bio-Rad), HRP-conjugated goat anti-rabbit IgG (1:5000), Alexa Fluor 555 goat anti-mouse (1:100; Molecular Probes) and Alexa Fluor 488 goat anti-rabbit IgG (1:100; Molecular Probes).

The alpha-bungarotoxin Alexa Fluor 555 conjugate (1:10) was from Invitrogen.

Animal models

The $Smn^{2B/-}$ mice were established in our laboratory and maintained in our animal facility on a C57BL/6 x CD1 hybrid background (Bowerman et al. 2009). The 2B mutation consists of a substitution of 3 nucleotides in the exon splicing enhancer of exon 7 (DiDonato et al. 2001). The *Smn* knock-out allele was previously described by Schrank *et al*. (Schrank et al. 1997) and $Smn^{+/-}$ mice were obtained from The Jackson Laboratory. The $Smn^{-/-}$;*SMN2* mice (Monani et al. 2000b) are maintained on a FVB/N background and were obtained from The Jackson Laboratory. All

animal procedures were performed in accordance with institutional guidelines (Animal Care and Veterinary Services and Ethics, University of Ottawa).

Y-27632 experimental procedure

The Y-27632 compound (Calbiochem) was diluted in water and administered by a modified oral gavage procedure (Butchbach et al. 2007) to *Smn*$^{2B/-}$ and *Smn*$^{2B/+}$ mice from P3 to P21. The *Smn*$^{-/-}$*;SMN2* mice were given the compound by administering it by gavage to pregnant females at gestational day E14 and by reinstating gavage to the pups at P3. *Smn*$^{2B/-}$ and *Smn*$^{2B/+}$ animals received low (1 mg/kg, twice daily) or high (30 mg/kg, once daily) doses of Y-27632 while vehicle-treated animals received water. *Smn*$^{-/-}$*;SMN2* pups and their mothers received only the higher dose (30 mg/kg). Survival and weight were monitored daily.

Immunoblot analysis

Equal amounts of spinal cord samples of P0, P10 and P21 mice were separated by electrophoresis on 10% SDS-polyacrylamide gels and blotted onto a PVDF membrane (Millipore). The membranes were blocked in 5% nonfat milk in TBST (10 mM Tris-HCl pH 8.0, 150 mM NaCl, and 0.1% Tween 20 (Sigma)), incubated overnight at 4ºC with the first primary antibody, rinsed in TBST and incubated again overnight at 4ºC with the second primary antibody. Then, membranes were incubated at room temperature with the secondary antibodies, 1 hour for each one, with TBST washes in between. Signals were visualized using the ECL or the ECL plus detection kit (Amersham).

RhoA activity assay

Rhotekin-Rho-GTP binding domain GST (GST-RBD) beads were from Cytoskeleton. Thirty μg of GST-RBD beads was added to one hundred μg of spinal cord lysates. After a 1 hour incubation at 4ºC, beads were washed three times with lysis buffer B (50 mM Tris pH 7.6, 150 mM NaCl, 1% Triton X-100, and 0.5 mM $MgCl_2$) supplemented with 1 mM PMSF, 0.01 mg/ml leupeptin and 0.01 mg/ml aprotinin. The bound RhoA-GTP was detected by immunoblot analysis using an anti-RhoA antibody. The average increase or decrease of total and active RhoA was quantified by densitometry comparisons of the RhoA-GTP/actin and total RhoA/actin ratios of 3 mice per genotype using the Image J software.

RT-PCR

RNA from spinal cords was extracted with the TRIzol Reagent (Gibco) according to the manufacturer's instructions. Reverse transcription was performed using 0.5 μg of total RNA. The following primers were used for RT-PCR analysis: Smn forward (5' GCA CAG CCA GAA GAA AAC CT 3'), Smn reverse (5' CGA CAC GCA CAC TCC ACT 3'), actin forward (5' CCG TCA GGC AGC TCA TAG CTC TTC 3') and actin reverse (5' CTG AAC CCT AAG GCC AAC CGT 3'). FL Smn mRNA/Δ7 Smn mRNA ratios were determined by densitometry using the Image J software.

Immunohistochemistry of neuromuscular junctions

Dissected whole tibialis anterior (TA) muscles of P21 mice were dissected and fixed in 4% paraformaldehyde (PFA). Following the removal of connective tissue, the TA muscles were

incubated with alpha-bungarotoxin Alexa Fluor 555 conjugate for 20 min at room temperature (RT). The TA muscles were then incubated in methanol at -20ºC for 5 min, followed by an overnight incubation at 4ºC with the SV2 and SMI312 antibodies. Incubation with the secondary antibodies was performed the following day at RT for 1 hour. Finally, two to three thin filets per stained TA were cut and mounted in Fluorescent Mounting Medium (Dako). All filets were single sections of the surface of the TA muscle. Images were taken with a Zeiss confocal microscope, with a 20X objective, equipped with filters suitable for FITC/Cy3/fluorescence. For the blind quantification analysis, a minimum of 90 NMJs were analyzed for each genotype/treatment group. The Zeiss AxioVision software was used to calculate the area of NMJs. Maturity of the NMJs was determined by the sophisticated complexity of folds displayed by the terminals.

Hematoxylin and eosin staining

Spinal cord sections and TA muscle sections were first deparaffinized in xylene and then fixed in 100% ethanol. Following a rinse in water, samples were stained in hematoxylin (Fisher) for 3 minutes, rinsed in water, dipped 40 times in a solution of 0.02% HCl in 70% ethanol and rinsed in water again. The sections were next stained in a 1% eosin solution (BDH) for 1 minute, dehydrated in ethanol, cleared in xylene and mounted with Permount (Fisher). Images were taken with a Zeiss Axioplan2 microscope, with a 20X objective.

Quantitative assays were performed on 3 mice for each genotype and 5 sections per mouse. Analyzed sections were at least 10 μm apart. Motor neurons were identified by their shape and size in the same designated area of the ventral horn region of the spinal cord sections.

The area of muscle fiber within designated regions of the TA muscle sections was measured using the Zeiss AxioVision software.

Statistical methods

For the Kaplan-Meier survival analysis, the log-rank test was used and survival curves were considered significantly different at $p<0.05$.

For the remaining statistical analyses, the Student's two-tail *t* test for paired variables was used to test for differences between samples and data were considered significantly different at $p< 0.05$.

ACKNOWLEDGEMENTS

We are grateful to Drs. Valerie Wallace and Alex MacKenzie for critical reading of the manuscript, and the rest of the Kothary laboratory for helpful discussions. This project was funded by a grant from the Canadian Institutes of Health Research (CIHR), and The Muscular Dystrophy Association to R.K. M.B. is a recipient of a Frederick Banting and Charles Best CIHR Doctoral Research Award, and R.K. is a recipient of a University Health Research Chair from the University of Ottawa.

SUPPLEMENTARY DATA

Supplementary Figure 5.1. *Smn*$^{2B/-}$ mice treated with 30 mg/kg of Y-27632 show improved gait and movement. A) A movie of four treated *Smn*$^{2B/-}$ mice (four months of age) displaying the agility and ability to freely walk and move around the cage while still displaying a minor neurological phenotype. B) A movie of an untreated *Smn*$^{2B/-}$ mouse at three weeks of age (endpoint) displaying a severe neurological phenotype and reduced motor functions. Alongside it can be seen a *Smn*$^{2B/+}$ littermate displaying a normal gait and phenotype.

CHAPTER 6: Targeting the RhoA pathway via the clinically approved ROCK inhibitor Fasudil as a therapeutic strategy for SMA

Fasudil improves survival and promotes skeletal muscle development in a mouse model of spinal muscular atrophy

Melissa Bowerman, Lyndsay M. Murray, Justin G. Boyer, Carrie L. Anderson, Rashmi Kothary

Published in *BMC Medicine*, 2012, 10 (24), doi:10.1186/1741-7015-10-24

Author contributions

Conceived and designed the experiments: MB, LMM and RK. Performed the experiments: MB, LMM and CLA. Analyzed the data: MB and LMM. Initial characterization of misregulated myogenin expression in SMA skeletal muscle: JGB. Wrote the paper: MB and LMM.

ABSTRACT

Background: Spinal muscular atrophy (SMA) is the leading genetic cause of infant death. It is caused by mutations/deletions of the survival motor neuron 1 (*SMN1*) gene and is typified by the loss of spinal cord motor neurons, muscular atrophy, and in severe cases, death. The SMN protein is ubiquitously expressed and various cellular- and tissue-specific functions have been investigated to explain the specific motor neuron loss in SMA. We have previously shown that the RhoA/Rho kinase (ROCK) pathway is misregulated in cellular and animal SMA models, and that inhibition of ROCK with the chemical Y-27632 significantly increased the lifespan of a mouse model of SMA. In the present study, we evaluated the therapeutic potential of the clinically approved ROCK inhibitor Fasudil. **Methods:** Fasudil was administered by oral gavage from post-natal day 3 to 21 at a concentration of 30 mg/kg twice daily. The effects of Fasudil on lifespan and SMA pathological hallmarks of the SMA mice were assessed and compared to vehicle-treated mice. For the Kaplan-Meier survival analysis, the log-rank test was used and survival curves were considered significantly different at $p<0.05$. For the remaining analyses, the Student's two-tail *t* test for paired variables and one-way ANOVA were used to test for differences between samples and data were considered significantly different at $p< 0.05$. **Results:** Fasudil significantly improves survival of SMA mice. This dramatic phenotypic improvement is not mediated by an up-regulation of Smn protein or via preservation of motor neurons. However, Fasudil administration results in a significant increase in muscle fiber and postsynaptic endplate size, and restores normal expression of markers of skeletal muscle development, suggesting that the beneficial effects of Fasudil could be muscle-specific. **Conclusions:** Our work underscores the importance of muscle as a therapeutic target in SMA

and highlights the beneficial potential of ROCK inhibitors as a therapeutic strategy for SMA and for other degenerative diseases characterized by muscular atrophy and postsynaptic immaturity.

INTRODUCTION

As the leading genetic cause of infant deaths, spinal muscular atrophy (SMA) is a devastating and incurable neuromuscular disorder (Pearn 1978a; Crawford et al. 1996). SMA affects 1 in 6,000-10,000 births and results from deletions or mutations in the survival motor neuron 1 (*SMN1*) gene (Pearn 1978a; Lefebvre et al. 1995; Crawford et al. 1996). The primary pathological hallmark of SMA is the loss of lower motor neurons from the spinal cord and corresponding muscular atrophy with subsequent paralysis and in most severe cases, death (Pearn 1978a; Crawford et al. 1996).

The complete loss of the SMN protein is embryonic lethal (Jablonka et al. 2000). In humans however, a recent duplication event in chromosome 5 has given rise to the centromeric *SMN2* gene (Lefebvre et al. 1995). While both *SMN1* and *SMN2* genes differ by only a few nucleotides, a critical C to T substitution lies within position 6 of *SMN2* exon 7 (Lorson et al. 1999; Monani et al. 1999a). This silent mutation results in the aberrant splicing of exon 7, giving rise to the biologically unstable SMNΔ7 protein (Lefebvre et al. 1995; Lorson et al. 1999). Although the *SMN2* gene produces predominantly the SMNΔ7 protein, a small amount of full-length SMN is still produced (Lefebvre et al. 1995). Thus, the number of *SMN2* gene copies in SMA patients is a key modifier of disease severity (Lefebvre et al. 1995; Coovert et al. 1997; Lefebvre et al. 1997).

One of the major hurdles in SMA is to understand how the loss of a ubiquitously expressed protein leads to the specific loss of spinal cord motor neurons. Work from various research groups has identified distinct roles for SMN in neurodevelopment, neuromaintenance,

RNA metabolism, at the neuromuscular junction (NMJ) and in skeletal muscle (reviewed in (Boyer et al. 2010)). As of yet however, none of these various functions of the SMN protein have been recognized as being solely responsible for SMA pathogenesis.

Work from our laboratory has shown that Smn depletion in cellular and mouse models results in altered expression and localization of a number of regulators of actin cytoskeletal dynamics (Bowerman et al. 2007; Bowerman et al. 2009; Bowerman et al. 2010). Indeed, analysis of spinal cords from SMA mice revealed a significant increase in active RhoA (RhoA-GTP) (Bowerman et al. 2010), a major upstream regulator of the actin cytoskeleton (Luo et al. 1997). RhoA-GTP signaling in neuronal cells modulates various cellular functions such as growth, neurite formation, polarization, regeneration, branching, pathfinding, guidance and retraction (reviewed in (Govek et al. 2005; Luo et al. 2005)). Our previous work demonstrated that administration of the ROCK inhibitor Y-27632 (Amano et al. 1996), lead to dramatic increase in survival in a mouse model of intermediate SMA (Bowerman et al. 2010). Recently Nölle *et al*. demonstrated that knockdown of Smn in PC12 cells affects the phosphorylation state of downstream effectors of ROCK, supporting the value of the ROCK pathway as a therapeutic target for SMA pathogenesis (Nolle et al. 2011).

In the present work, we have treated SMA mice with Fasudil, a ROCK inhibitor approved for U.S. clinical trials. We show that Fasudil dramatically improves the lifespan and increases muscle fiber size in $Smn^{2B/-}$ SMA mice. Furthermore, we report for the first time that ROCK inhibition restores normal expression of markers of skeletal muscle development in SMA mice. Our study highlights the beneficial effects of ROCK inhibition not only for SMA pathogenesis

but also for any degenerative disease that has NMJ and skeletal muscle development defects. Importantly, as Fasudil is currently used in U.S. FDA-approved clinical trials for other disorders, re-purposing it is an exciting, and feasible therapeutic approach for the treatment of SMA.

MATERIALS AND METHODS

Animal models

The *Smn*$^{2B/-}$ mice were established in our laboratory and maintained in our animal facility on a C57BL/6 x CD1 hybrid background. The 2B mutation consists of a substitution of 3 nucleotides in the exon splicing enhancer of exon 7 (DiDonato et al. 2001; Hammond et al. 2010). The *Smn* knock-out allele was previously described by Schrank *et al*. (Schrank et al. 1997) and *Smn*$^{+/-}$ mice were obtained from The Jackson Laboratory. All animal procedures were performed in accordance with institutional guidelines (Animal Care and Veterinary Services, University of Ottawa).

Fasudil administration

Fasudil (LC Laboratories) was diluted in water and administered by a modified oral gavage procedure (Butchbach et al. 2007) to *Smn*$^{2B/-}$ and *Smn*$^{2B/+}$ mice from P3 to P21. The three Fasudil dosage regimens were as follows: low dose (30 mg/kg once daily), medium dose (30 mg/kg twice daily), and high dose (30 mg/kg twice daily from P3-P6; 50 mg/kg twice daily from P7-P13; 75 mg/kg twice daily from P14-P21). Vehicle-treated animals received water. Survival and weight were monitored daily.

Antibodies

The primary antibodies used were as follows: mouse anti-actin (1:800; Fitzgerald), mouse anti-Smn (1:5000; BD Transduction Laboratories), rabbit anti-phosphorylated cofilin (1:250;

Chemicon), rabbit anti-cofilin (1:500; Millipore), rabbit anti-phosphorylated cofilin 2 (1:500; Cell Signaling), rabbit anti-cofilin 2 (1:500; Millipore), mouse anti-myogenin (1:250; BD Transduction Laboratories), rabbit anti-HB9 (1:50; Abcam), mouse anti-2H3 (1:250; Developmental Studies Hybridoma Bank) and mouse anti-SV2 (1:250; Developmental Studies Hybridoma Bank). The secondary antibodies used were as follows: horseradish peroxidase (HRP)-conjugated goat anti-mouse IgG (1:5000; Bio-Rad), HRP-conjugated goat anti-rabbit IgG (1:5000; Bio-Rad), DyLight goat anti-mouse (1:250; Jackson), goat anti-rabbit biotin-SP-conjugated (1:200; Dako), streptavidin-Cy3-conjugated (1:600; Jackson Immuno Research) and Alexa Fluor 680 goat anti-mouse (1:5000; Molecular Probes). The α-bungarotoxin (BTX) conjugated to tetramethylrhodamine isothiocyanate was from Molecular Probes (5 μg/mL).

Immunoblot analysis

Equal amounts of spinal cord and tibialis anterior (TA) muscle tissue extracts were separated by electrophoresis on 10% SDS-polyacrylamide gels and blotted onto nitrocellulose membranes (Amersham). The membranes were blocked in 5% non-fat milk in TBST (10 mM Tris-HCl pH 8.0, 150 mM NaCl, and 0.1% Tween 20 (Sigma)). Membranes were incubated overnight at 4ºC with primary antibody, followed by a 1 hour incubation with the secondary antibody. All washes were performed with TBST. Signals were visualized using the ECL or the ECL plus detection kit (Amersham). Exposure times were chosen based on the saturation of the highest amounts of protein.

Hematoxylin and eosin staining

Spinal cord (L1-L2 lumbar regions) and TA muscle sections (5 μm) were deparaffinized in xylene and fixed in 100% ethanol. Following a rinse in water, samples were stained in hematoxylin (Fisher) for 3 minutes, rinsed in water, dipped 40 times in a solution of 0.02% HCl in 70% ethanol and rinsed in water again. The sections were stained in a 1% eosin solution (BDH) for 1 minute, dehydrated in ethanol, cleared in xylene and mounted with Permount (Fisher). Images were taken with a Zeiss Axioplan2 microscope, with a 20X objective.

Quantitative assays were performed on 3 mice for each genotype and 5 sections per mouse. Motor neurons were identified by their shape and size (> 10 μm in diameter) in the same designated area of the ventral horn region of the spinal cord. Every 5th section was analyzed and the subsequent totals were multiplied by 5 to give an estimate of total motor neuron number. Only motor neurons with visible nuclei were counted so as to prevent double-counting. For TA quantitative assays, the area of muscle fiber within designated regions of the TA muscle sections was measured using the Zeiss AxioVision software.

Immunohistochemistry

For immunohistochemistry, spinal cord sections were first deparaffinized in xylene (3 x 10 min), fixed in 100% ethanol (2 x 10 min), rehydrated in 95% and 75% ethanol (5 sec each) and placed 5 min in 1 M Tris-HCl pH 7.5. Sections were then placed in boiling sodium citrate antigen retrieval buffer (10 mM sodium citrate, 0.05% Tween 20, pH 6.0) for 20 minutes in the

microwave. The sections were then rinsed 10 minutes under running cold tap water and incubated for 2 hours at room temperature (RT) in blocking solution (TBLS (10% NaN_3), 20% goat serum, 0.3% Triton X-100). This was followed by an overnight incubation at 4^{o}C with the primary antibody. Subsequently, sections were incubated 1 hour at RT with the biotinylated rabbit antibody followed by a 1 hour incubation at RT with streptavidin-Cy3. All washes were done with PBS. Hoechst (1:1000) was added to the last PBS wash followed by the slides being mounted in Fluorescent Mounting Medium (Dako). Images were taken with a Zeiss confocal microscope, with a 20X objective, equipped with filters suitable for Cy3/Hoechst fluorescence.

Neuromuscular junction immunohistochemistry

TVA and TA muscle sections were labeled by immunohistochemistry to allow quantification of neuromuscular innervation as described previously (Murray et al. 2008; Bowerman et al. 2010). Briefly, TVA muscles were immediately dissected from recently sacrificed mice and fixed in 4% paraformaldehyde (Electron Microscopy Science) in PBS for 15 minutes. Post-synaptic acetylcholine receptors were labeled with αBTX for 10 min. Muscles were then permeabilized in 2% TritonX for 30 minutes and blocked in 4% bovine serum albumin/1% TritonX in PBS for 30 min before incubation overnight in primary antibodies and visualized with DyLight-conjugated secondary antibodies. Whole TA muscles were dissected and fixed in 4% paraformaldehyde. Following the removal of connective tissue, the TA muscles were incubated with αBTX Alexa Fluor 555 conjugate for 20 min at RT. Whole TVA muscle and a thin filet of TA muscle were mounted in Dako Fluorescent mounting media. Images were taken with a Zeiss confocal

microscope equipped with filters suitable for FITC/Cy3/fluorescence. Categorization of pre- and postsynaptic morphologies was performed as previously reported (Bowerman et al. 2012a).

Pen test

Balance and strength were assessed using the pen test as described (Willmann et al. 2011). Mice were placed on a suspended pen at different time-points (P12, 14, 17 and 21). The latency to fall from the pen was measured with a plateau of 30 seconds. At each time-point, individual mice were assessed three consecutive times.

Statistical Methods

All statistical analyses were performed using the GraphPad Prism software. For the Kaplan-Meier survival analysis, the log-rank test was used and survival curves were considered significantly different at $p<0.05$. When appropriate, the Student's two-tail *t* test for paired variables and one-way ANOVA were used to test for differences between samples and data were considered significantly different at $p< 0.05$.

RESULTS

Fasudil increases lifespan of $Smn^{2B/-}$ mice

The Smn^{2B} allele harbors a sequence change in the exon splicing enhancer of exon 7 of the murine *Smn* gene, leading to the predominant production of the SmnΔ7 protein (DiDonato et al. 2001; Hammond et al. 2010). The Smn^{2B} allele in combination with the knockout allele results in an intermediate SMA mouse model ($Smn^{2B/-}$) with a median lifespan of 30 days that displays motor neuron loss, neuromuscular defects and immature NMJs (Bowerman et al. 2012a). We have previously shown that the ROCK inhibitor Y-27632 dramatically improved the lifespan of $Smn^{2B/-}$ mice (Bowerman et al. 2010). Since Y-27632 has not been approved for clinical use, we set out to determine if the ROCK inhibitor, Fasudil, which has been approved for U.S clinical trials (Yamaguchi et al. 2006), would have similar beneficial effects on the $Smn^{2B/-}$ mice.

Treating the $Smn^{2B/-}$ mice by gavage twice daily (30 mg/kg dose) from post-natal day (P) 3 to P21 lead to a significant increase in lifespan when compared to vehicle-treated $Smn^{2B/-}$ mice (Figure 1A). Indeed, 57% of Fasudil-treated $Smn^{2B/-}$ mice survived over 300 days while the median survival of vehicle-treated $Smn^{2B/-}$ mice is 30.5 days (**Figure 6.1 A**). A lower dose of Fasudil had no effect while a higher dose was accompanied by a non-negligible toxicity (**Supplementary Figure 6.1**). Interestingly, both vehicle- and Fasudil-treated $Smn^{2B/-}$ mice showed a similar arrest in weight gain after P10 (**Figure 6.1 B**). When assessing strength and balance via the pen test (Willmann et al. 2011), both vehicle- and Fasudil-treated $Smn^{2B/-}$ mice had short latencies to fall from the pen (**Figure 6.1 C**). Thus, while Fasudil significantly increased the lifespan of the $Smn^{2B/-}$ mice, it did not influence the weight loss or the

neuromuscular weakness that typifies this SMA mouse model (Bowerman et al. 2012a). However, when comparing mice past weaning age, we find that Fasudil-treated *Smn*$^{2B/-}$ mice are better groomed, move about more freely in the cage and display a less severe neurological phenotype than vehicle-treated *Smn*$^{2B/-}$ mice (**Supplementary Figure 2**). Additionally, despite their initial compromised body size and neuromuscular function, surviving Fasudil-treated *Smn*$^{2B/-}$ females are able to reproduce, as exemplified by a female that was euthanized because of dystocia (**Figure 6.1 A**). The dystocia-linked death, however, highlights the breeding limitations in these aging Fasudil-treated mice that still exhibit an SMA neuromuscular phenotype.

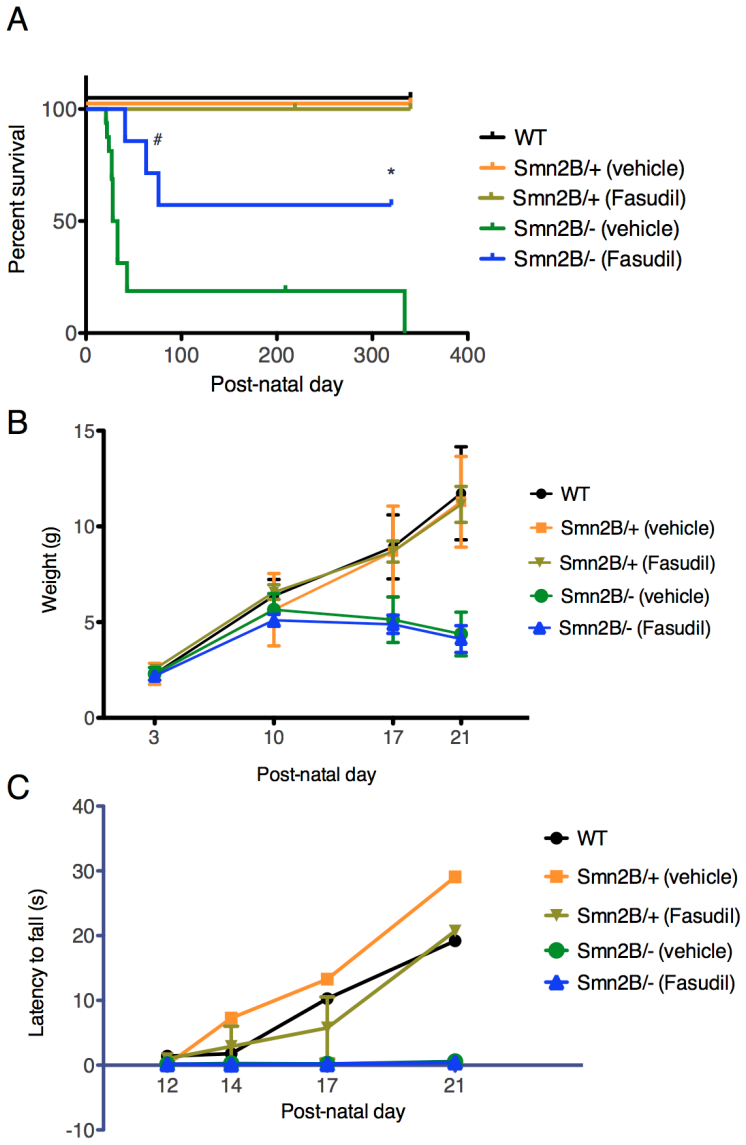

Figure 6.1. Fasudil increases lifespan of *Smn*$^{2B/-}$ mice, independent of weight gain and pen test performance. Fasudil (30 mg/kg twice daily) or vehicle (water) was administered by gavage from post-natal (P) day 3 to P21. The different groups analyzed were: untreated wild type (WT) (n = 10), vehicle-treated *Smn*$^{2B/+}$ (n = 8), Fasudil-treated *Smn*$^{2B/+}$ (n = 9), vehicle-treated *Smn*$^{2B/-}$ (n = 16) and Fasudil-treated *Smn*$^{2B/-}$ (n = 7). A) Fasudil significantly increases lifespan of *Smn*$^{2B/-}$ mice when compared to vehicle-treated *Smn*$^{2B/-}$ mice (*P = 0.0251; # indicates death due to dystocia).

Administration of Fasudil does not have adverse effects on the lifespan of normal littermates. B) Fasudil does not prevent the arrest in weight gain that occurs in vehicle-treated *Smn*$^{2B/-}$ mice onwards of P10. C) Fasudil does not improve the performance of *Smn*$^{2B/-}$ mice on the pen test when compared to vehicle-treated *Smn*$^{2B/-}$ mice.

Fasudil activity in the spinal cord does not prevent motor neuron loss in $Smn^{2B/-}$ mice

The main goal of using Fasudil as a therapeutic strategy is to compensate for the increased levels of RhoA-GTP in the spinal cords of the $Smn^{2B/-}$ mice (Bowerman et al. 2010). In order to investigate the mechanisms by which Fasudil exerts its beneficial effects, we investigated its activity and impact on motor neuron loss in the spinal cord. Spinal cord extracts from P21 Fasudil-treated $Smn^{2B/-}$ mice showed a reduction in phosphorylated cofilin, a downstream effector of ROCK (Maekawa et al. 1999; Sumi et al. 1999), when compared to vehicle-treated SMA mice (**Figure 6.2 A**), demonstrating that oral administration of Fasudil efficiently delivers the drug to the CNS and leads to an efficient inhibition of ROCK activity.

To investigate if the beneficial effects of Fasudil administration are mediated through an increase in Smn expression, we compared Smn protein levels in P21 spinal cords of wild type, vehicle-treated and Fasudil-treated $Smn^{2B/-}$ mice. This comparison shows that Fasudil does not lead to a significant upregulation of Smn expression (**Figure 6.2 B**) and further suggests that Fasudil acts via an Smn-independent pathway to improve the survival of $Smn^{2B/-}$ mice.

As a major hallmark of SMA is loss of lower motor neuron cell bodies from the spinal cord, we assessed the effect of Fasudil on the motor neuron loss previously characterized in the $Smn^{2B/-}$ mouse model (Bowerman et al. 2009; Bowerman et al. 2012a). Quantification of the number of motor neuron cell bodies in the ventral horn region of L1-L2 lumbar spinal cord sections revealed similar significant reductions in both vehicle- and Fasudil-treated $Smn^{2B/-}$ mice compared to wild type controls (**Figure 6.2 C, D**). This implies that the beneficial effects observed following Fasudil administration are not mediated via a preservation of motor neuron

cell bodies. It is therefore possible that Fasudil acts on other SMA-afflicted tissues and/or compartments that subsequently influence the functionality of the surviving motor neurons.

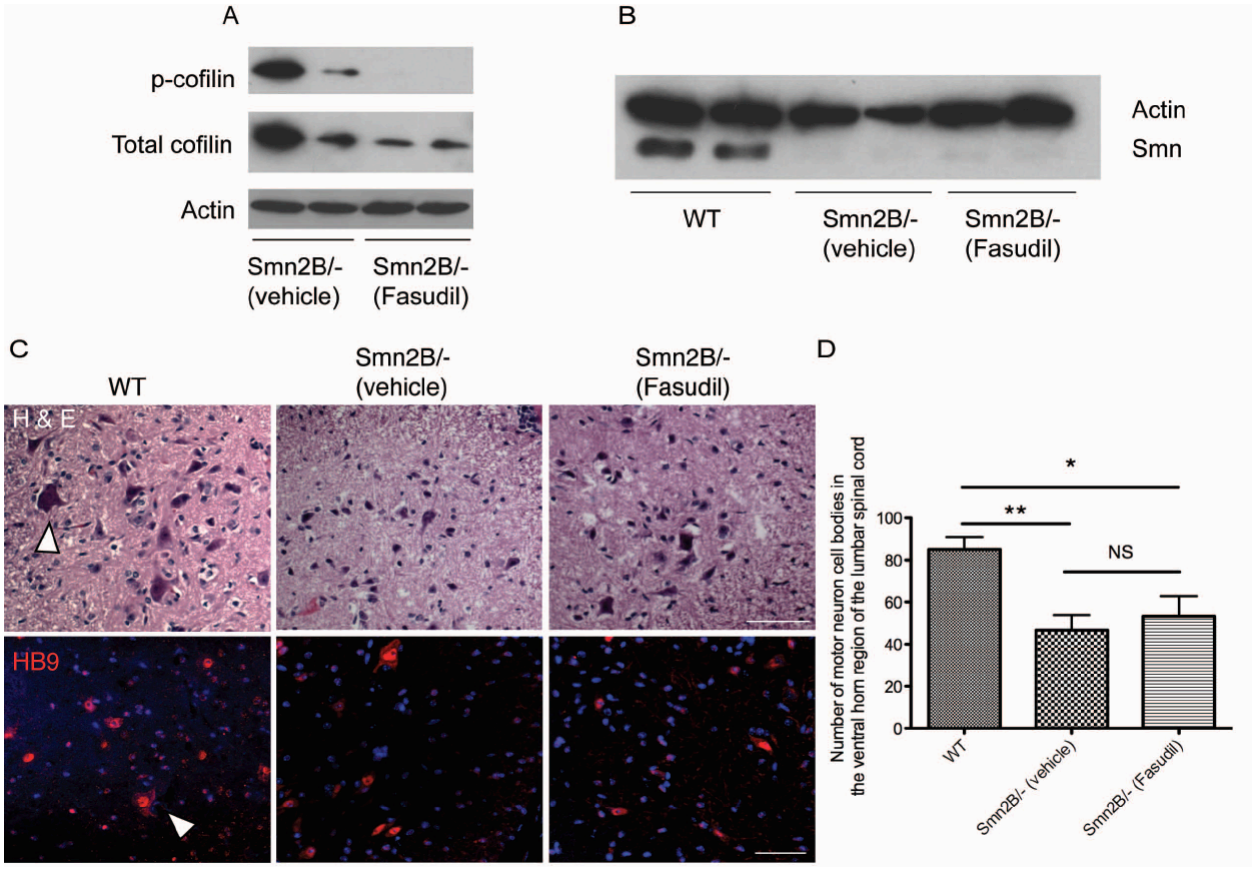

Figure 6.2. Fasudil activity in the spinal cord is Smn-independent and does not prevent motor neuron loss in the ventral horn region. A and B) Spinal cords were obtained from P21 untreated wild type (WT), vehicle-treated *Smn*$^{2B/-}$ and Fasudil-treated *Smn*$^{2B/-}$ mice. A) Immunoblot analysis shows that spinal cords treated with the rho-kinase (ROCK) inhibitor Fasudil have decreased levels of p-cofilin, a known substrate of ROCK. B) Immunoblot analysis shows that Fasudil does not increase Smn protein levels in the spinal cords of *Smn*$^{2B/-}$ mice. C and D) Spinal cord sections were analyzed from P21 untreated wild type (WT) (n = 3), vehicle-treated *Smn*$^{2B/-}$ (n = 3) and Fasudil-treated *Smn*$^{2B/-}$ (n = 3) mice. C) Representative images of hematoxylin and esoin (H&E)- and HB9-stained spinal cord sections. Arrowhead depicts a typical large motor neuron. Scale bar = 50 μm. D) Quantification of motor neurons within the ventral horn region of the

spinal cord shows that Fasudil does not prevent the motor neuron loss that occurs in vehicle-treated *Smn*$^{2B/-}$ mice (*$P < 0.05$; **$P < 0.01$; NS = not significant; data are mean +/- s.d.).

Fasudil increases skeletal muscle fiber size

In addition to motor neuron degeneration, SMA is also typified by muscular atrophy (Pearn 1978a; Crawford et al. 1996). In recent years, several intrinsic pathologies and defective molecular pathways have been reported in SMA muscle ((Walker et al. 2008; Martinez-Hernandez et al. 2009; Mutsaers et al. 2011) and JGB, unpublished data). Furthermore, we have previously demonstrated that the ROCK inhibitor Y-27632 lead to an increase in the TA myofiber size of $Smn^{2B/-}$ mice (Bowerman et al. 2010). We thus investigated the effect of Fasudil on skeletal muscle and show that TA muscles from Fasudil-treated P21 $Smn^{2B/-}$ mice display significantly larger myofibers than vehicle-treated $Smn^{2B/-}$ mice (**Figure 6.3 A, B**). Indeed, both wild type and Fasudil-treated $Smn^{2B/-}$ mice show similar myofiber sizes (**Figure 6.3 A, B**). To determine whether this increase in muscle fiber size was SMA-dependent, we also compared TA muscles of vehicle- and Fasudil-treated $Smn^{2B/+}$ phenotypically normal littermates. This revealed no significant difference in myofiber size (**Figure 6.3 C, D**), thus suggesting that Fasudil acts on muscle-specific molecular pathways that are distinctly perturbed in the SMA mice.

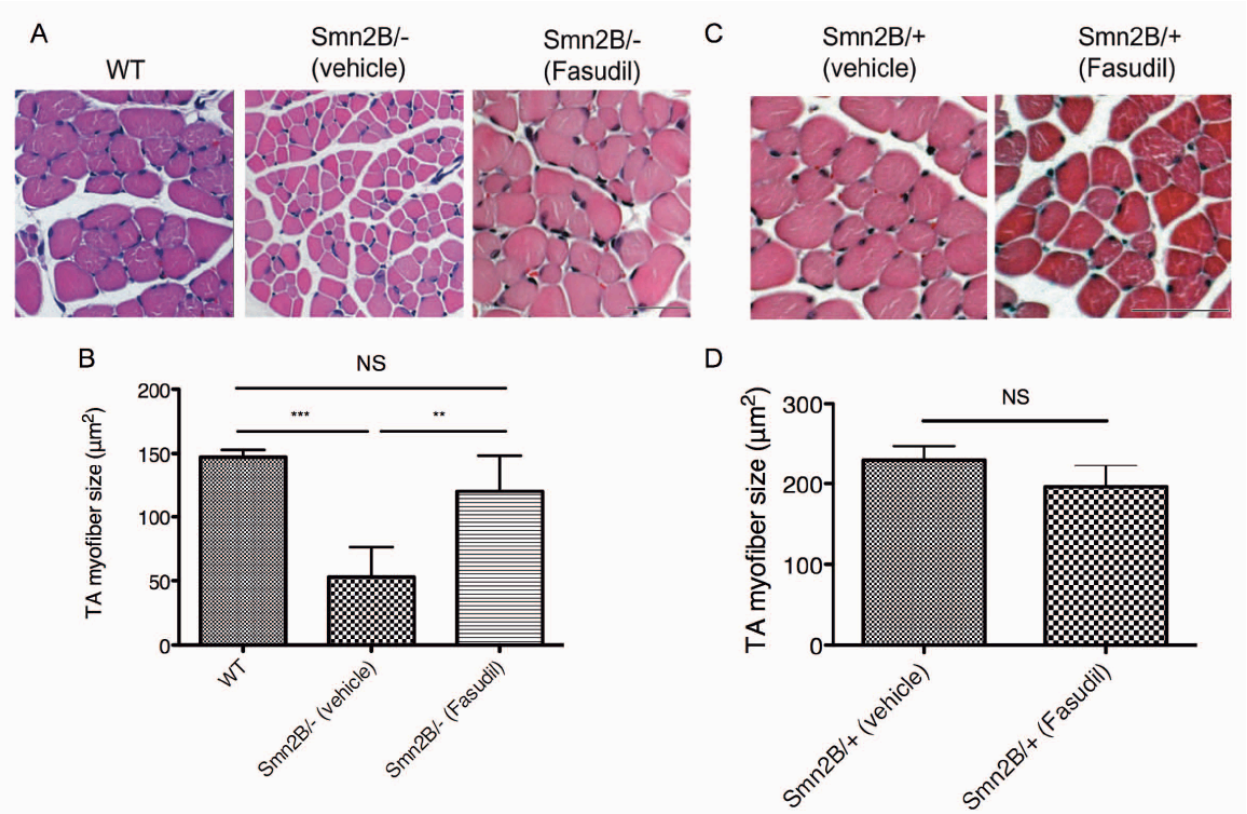

Figure 6.3. Fasudil increases tibialis anterior (TA) myofiber size. TA muscles were isolated from P21 untreated wild type (WT) (n = 3), vehicle-treated $Smn^{2B/+}$ (n = 3), Fasudil-treated $Smn^{2B/+}$ (n = 3), vehicle-treated $Smn^{2B/-}$ (n = 6) and Fasudil-treated $Smn^{2B/-}$ (n = 6) mice. A) Representative images of cross-sections of WT, or vehicle- and Fasudil-treated $Smn^{2B/-}$ TA muscles stained with hematoxylin and eosin. Scale bar = 50 µm. B) Quantification shows that Fasudil-treated $Smn^{2B/-}$ TA muscles display significantly larger myofibers than vehicle-treated $Smn^{2B/-}$ mice. (**P < 0.01; ***P < 0.001; NS = not significant; data are mean +/- s.d.). C) Representative images of cross-sections of vehicle- and Fasudil-treated $Smn^{2B/+}$ TA muscles stained with hematoxylin and eosin. Scale bar = 50 µm. D) Quantification shows that Fasudil does not significantly increase the myofiber size of $Smn^{2B/+}$ normal mice (NS = not significant; data are mean +/- s.d.).

Fasudil-treated muscles display restored myogenin expression

To assess if Fasudil was active in skeletal muscle, we examined factors downstream of ROCK signaling. Cofilin 2 is a skeletal muscle-specific actin-regulating protein and downstream effector of activated ROCK (Ono et al. 1994; Arber et al. 1998). We thus determined the impact of administrating Fasudil by gavage on skeletal muscle by evaluating p-cofilin 2 levels in vehicle- and Fasudil-treated TA muscles from P21 mice. Interestingly, the TA muscles from $Smn^{2B/-}$ mice have significantly higher levels of p-cofilin 2 protein than wild type muscles (**Figure 6.4 A, B**), suggesting that the RhoA/ROCK pathway is also misregulated in skeletal muscle. Fasudil decreases p-cofilin 2 levels in $Smn^{2B/-}$ muscle to wild type levels, indicating that it is active in the TA muscle and restores the normal ROCK/p-cofilin 2 levels (**Figure 6.4 A, B**). We also show that Fasudil does not upregulate Smn expression in the TA muscles of $Smn^{2B/-}$ mice (**Figure 6.4 C**). Thus, consistent with the spinal cord analysis (**Figure 6.2 B**), it appears that the beneficial effects of Fasudil in skeletal muscle are most likely Smn-independent.

Recent work from our laboratory suggests that hindlimb muscles from P21 $Smn^{2B/-}$ mice display defects in muscle development, as evidenced by the misregulation of myogenin (JGB, unpublished data), a transcription factor that plays a well-characterized role in myogenesis (Hasty et al. 1993). We thus investigated whether Fasudil had any impact on myogenin levels. Analysis of TA muscles from P21 mice confirms the increased levels of myogenin in skeletal muscle of $Smn^{2B/-}$ mice compared to wild type controls (**Figure 6.4 D, E**). Importantly, Fasudil administration leads to a significant decrease in myogenin levels in $Smn^{2B/-}$ mice (**Figure 6.4 D, E**). In fact, myogenin levels in Fasudil-treated TA muscles are restored to wild type levels. Thus,

Fasudil can restore the normal level of myogenin and suggests that it may increase muscle size by restoring the normal development of skeletal muscle.

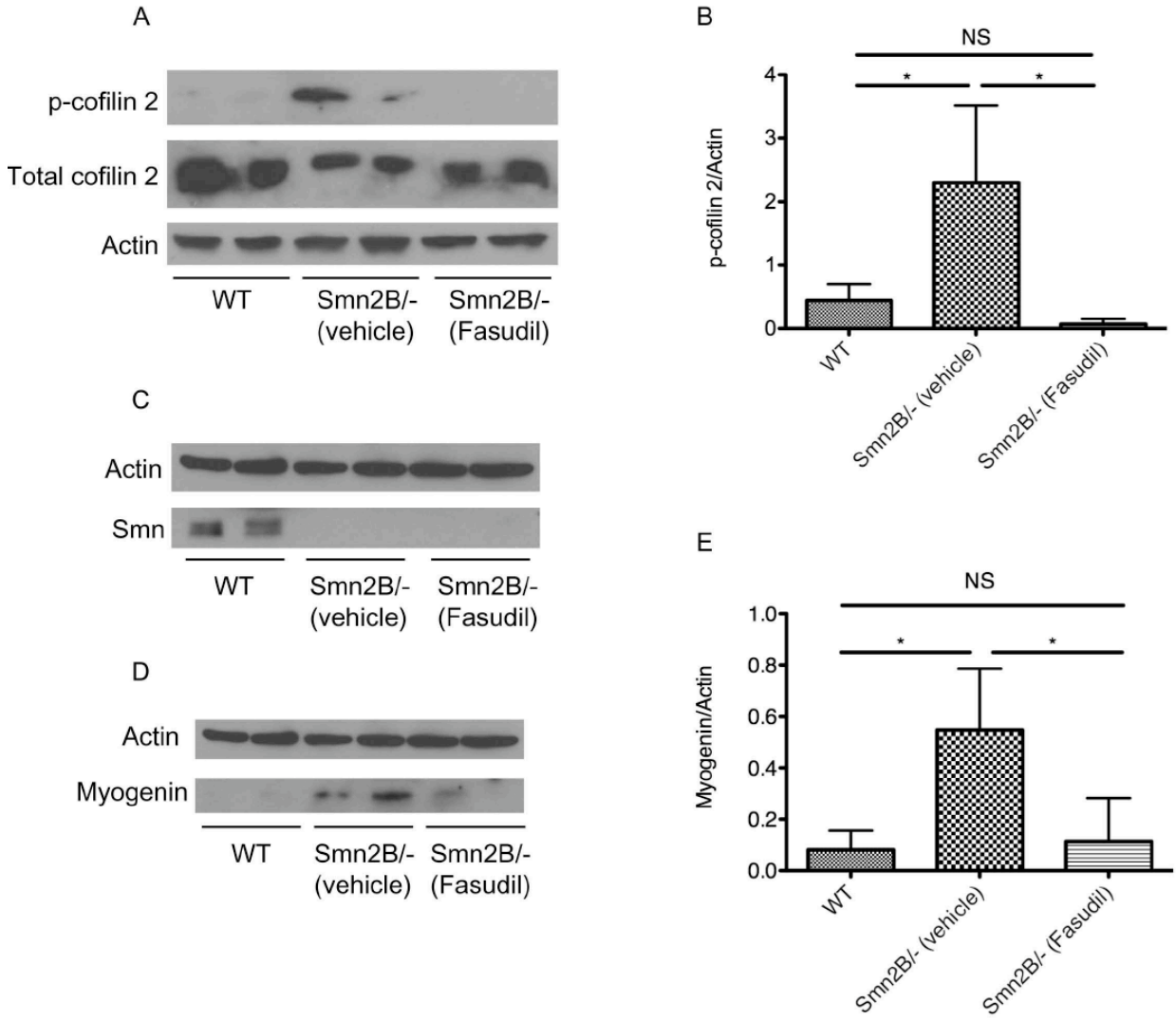

Figure 6.4. Fasudil administration inhibits ROCK in skeletal muscle and restores normal myogenin expression levels. Tibialis anterior (TA) muscles were isolated from P21 untreated wild type (WT) (n = 4), vehicle-treated *Smn*$^{2B/-}$ (n = 4) and Fasudil-treated *Smn*$^{2B/-}$ (n = 4) mice. A) Immunoblot analysis of p-cofilin 2, a muscle-specific downstream substrate of ROCK, shows that its levels are increased in the TA muscles of *Smn*$^{2B/-}$ mice compared with wild type. Furthermore, this experiment shows that Fasudil inhibits ROCK in the TA muscle of *Smn*$^{2B/-}$ mice, and reduces the p-cofilin 2 levels to wild type levels. B) Quantification shows that wild

type TA muscles have significantly less p-cofilin 2 than vehicle-treated *Smn*$^{2B/-}$ TA muscles, and that Fasudil is active in skeletal muscle and restores p-cofilin 2 to normal levels. (*$P < 0.05$; NS = not significant; data are mean +/- s.d.). C) Immunoblot analysis shows that Fasudil does not increase Smn protein levels in the TA muscles of *Smn*$^{2B/-}$ mice. D) Immunoblot analysis shows that Fasudil results in a decrease in myogenin protein levels in Fasudil-treated *Smn*$^{2B/-}$ TA muscles when compared to vehicle-treated *Smn*$^{2B/-}$ mice. E) Wild type muscle has significantly less myogenin than vehicle-treated *Smn*$^{2B/-}$ TA muscles. Fasudil administration to *Smn*$^{2B/-}$ mice restores myogenin to normal levels (*$P < 0.05$; NS = not significant; data are mean +/- s.d.).

Fasudil does not ameliorate the pre-synaptic phenotype of NMJs from $Smn^{2B/-}$ mice

We have previously identified pre-synaptic pathology at the NMJ in the transversus abdominis (TVA) of the $Smn^{2B/-}$ mice, as evidenced by a loss of pre-synaptic inputs and accumulation of neurofilaments (Bowerman et al. 2012a). To determine if the reduction in muscle pathology observed following Fasudil administration could be secondary to reduced pathology at the NMJ, we performed an in-depth analysis. This analysis was performed on P21 late-symptomatic mice in the TVA muscle, which has previously been shown to display marked NMJ loss and pre-synaptic abnormalities at this time point (Bowerman et al. 2012a). The degree of pre-synaptic swelling, identified by neurofilament (NF) and synaptic vesicle 2 (SV2) staining, was classified into four categories based on morphology (type 1: normal, no pre-synaptic swelling observed; type 2: swollen, pre-synaptic terminal arborization is thickened compared to type 1; type 3: spheroid accumulations, spherical swellings accumulate over the NMJ; type 4: spheroid covers endplate (EP), spherical accumulations obscure the entire endplate) (**Figure 6.5 A**). While over 80% of wild type terminals displayed a 'normal' pre-synaptic morphology, in both vehicle- and Fasudil-treated $Smn^{2B/-}$ mice we observed a high level of pre-synaptic swelling, with over 50% of EPs displaying morphologies classified as types 2-4 (**Figure 6.5 B**). Quantification of the number of fully innervated NMJs shows a significant decrease in both vehicle- and Fasudil-treated $Smn^{2B/-}$ mice when compared to wild type, with no significant difference observed between vehicle- and Fasudil-treated SMA mice (**Figure 6.5 C**). Thus, it appears, at least in P21 animals, that Fasudil does not ameliorate the pre-synaptic phenotype observed in $Smn^{2B/-}$ mice. This suggests that the improvement in muscle pathology we observe

after Fasudil administration is unlikely to be mediated through the NMJ, and that it likely is having a direct affect on the muscle.

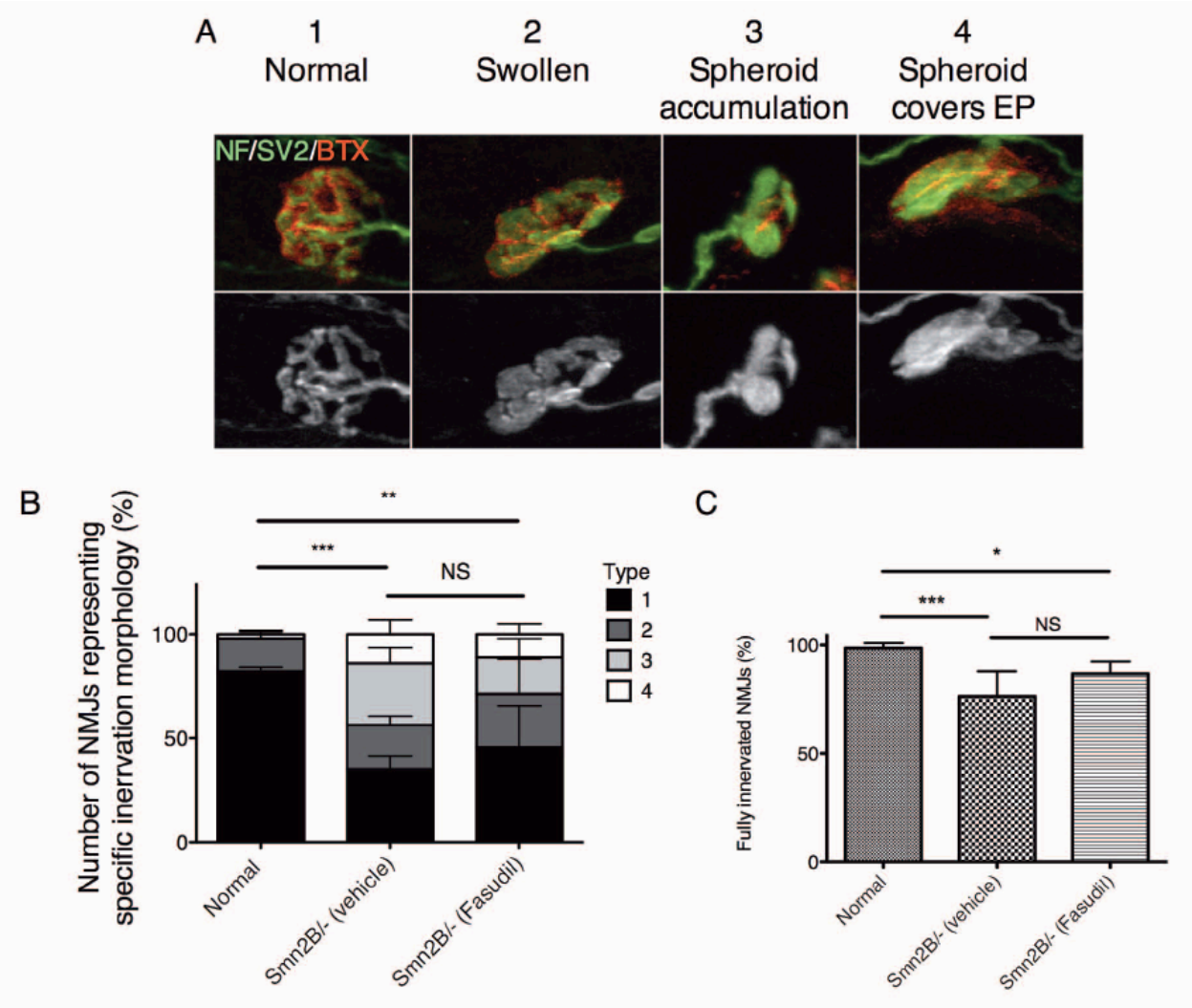

Figure 6.5. Fasudil does not improve pre-synaptic NMJ phenotype of *Smn*$^{2B/-}$ mice. Pre-synaptic morphology was analyzed in the transversus abdominis (TVA) muscle of P21 untreated normal littermates (n = 3), vehicle-treated *Smn*$^{2B/-}$ (n = 6) and Fasudil-treated *Smn*$^{2B/-}$ (n = 4) mice. A) Representative images of NMJs depicting the pre-synaptic morphology categories: normal (type 1), swollen (type 2), spheroid accumulation (type 3) and spheroids covers the endplate (EP) (type 4). (Neurofilament (NF) and synaptic vesicle protein 2 (SV2): green; EP: red (BTX)). B) Quantification of the pre-synaptic morphology shows that normal littermates have significantly more 'normal' (type 1) NMJs than both vehicle- and Fasudil-treated *Smn*$^{2B/-}$ mice (**$P < 0.01$;

***P < 0.001; NS = not significant; data are mean +/- s.d.). C) Quantification of the fully innervated NMJs shows that both vehicle- and Fasudil-treated $Smn^{2B/-}$ muscles display significantly fewer fully innervated NMJs than normal littermates, with no significant difference between vehicle or Fasudil treated $Smn^{2B/-}$ mice (*P <0.05; ***P < 0.001; NS = not significant; data are mean +/- s.d.).

Fasudil increases endplate area of $Smn^{2B/-}$ NMJs

We have previously shown that Y-27632 administration significantly increases the endplate area of NMJs within the tibialis anterior (TA) skeletal muscle (Bowerman et al. 2010). We thus assessed the effect of Fasudil on endplate size in both the TA and the TVA of P21 mice. Fasudil-treated $Smn^{2B/-}$ mice had significantly larger TA and TVA endplate areas than vehicle-treated $Smn^{2B/-}$ mice (**Figure 6.6**). Interestingly, this increase in endplate area was weight-independent, since both vehicle- and Fasudil-treated $Smn^{2B/-}$ mice display similar weight curves (**Figure 6.1 B**). Our results suggest that while Fasudil does not ameliorate the pathology evident at the pre-synaptic compartment of P21 $Smn^{2B/-}$ NMJs (**Figure 6.5**), there is a dramatic increase in the size of the post-synaptic compartment of NMJs within both muscles investigated (**Figure 6.6**). Together, these results are consistent with the beneficial effects of Fasudil being primarily mediated by the muscle and not the motor neuron

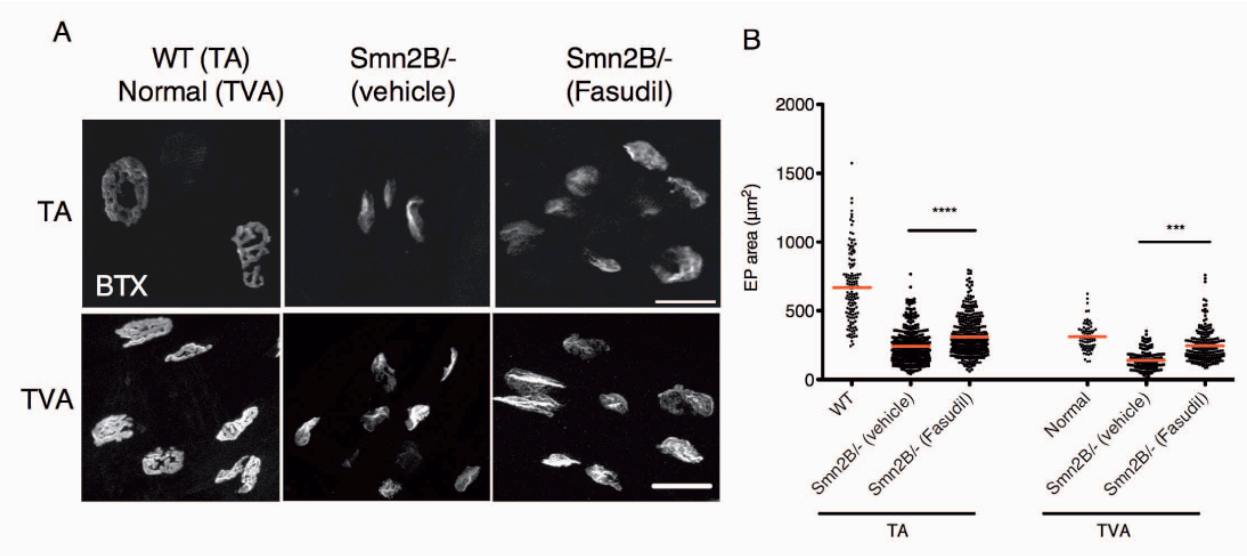

Figure 6.6. Fasudil increases endplate (EP) area in the tibialis anterior (TA) and transversus abdominis (TVA) muscles. Muscles were isolated from P21 untreated wild type (WT) (n = 3), untreated normal littermates (n = 3), vehicle–treated $Smn^{2B/-}$ (n = 4) and Fasudil-treated $Smn^{2B/-}$ mice (n = 3). A) Representative images of TA and TVA EPs stained with α-bungarotoxin (BTX). Scale bars = 25 μm (TA) and 30 μm (TVA). B) Quantification of EP area shows that Fasudil-treated $Smn^{2B/-}$ TA and TVA muscles display significantly larger EPs when compared to vehicle-treated $Smn^{2B/-}$ muscles. (***$P < 0.001$; ****$P < 0.0001$; data are mean +/- s.d.).

Increased NMJ maturation is observed in aging Fasudil-treated $Smn^{2B/-}$ mice

Although we saw no improvement in pre-synaptic NMJ pathology in P21 $Smn^{2B/-}$ mice, we wanted to evaluate the effect of Fasudil over time on NMJ pathology. NMJs from the TVA muscle of P21 Fasudil-treated $Smn^{2B/-}$ mice were compared to those of 6 month old Fasudil-treated $Smn^{2B/-}$ mice. Interestingly, we observed a marked decrease in pre-synaptic pathology in 6 month old mice compared to P21 mice, as evidenced by an increase in the percentage of fully occupied endplates (**Figure 6.7 A, B**). This was accompanied by a dramatic increase in endplate maturation (**Figure 6.7 C, D**). We therefore suggest that although there was no initial improvement in the morphological aspects on NMJ pathology, given sufficient time, Fasudil administration allows for the improved maturation of NMJs in $Smn^{2B/-}$ mice.

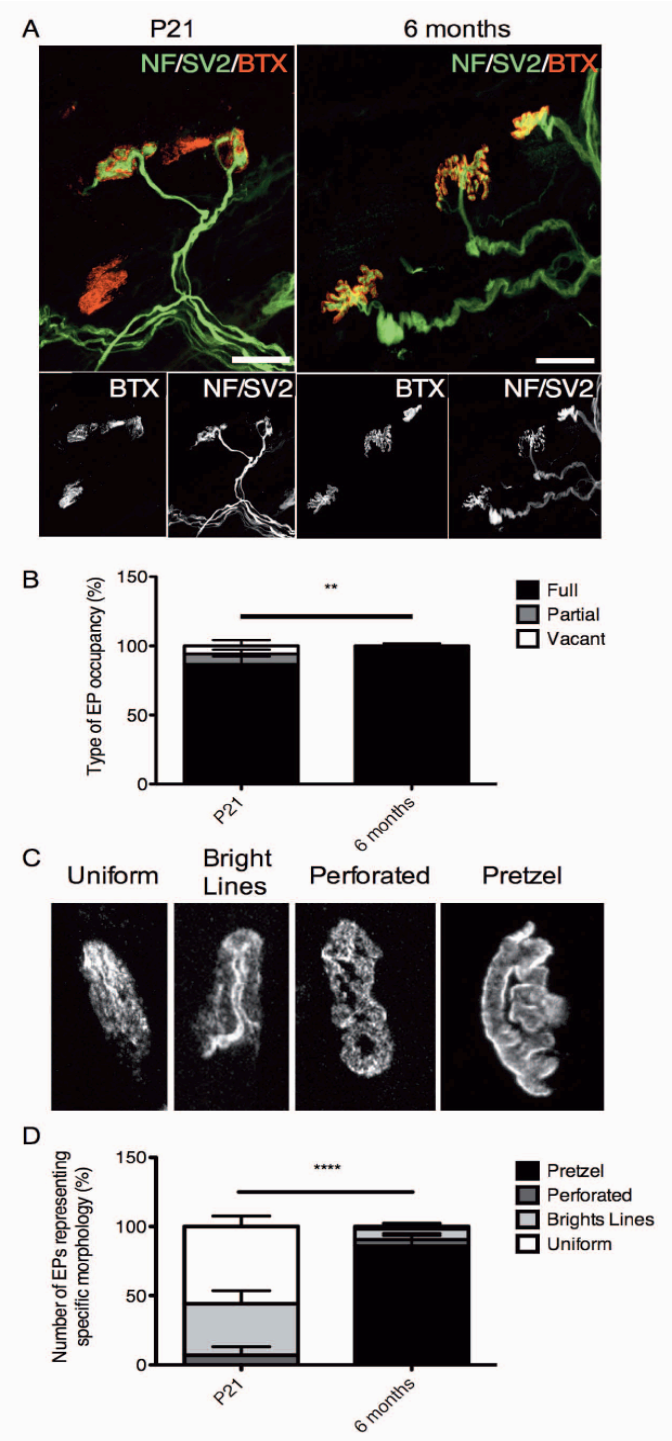

Figure 6.7. Aging Fasudil-treated *Smn*$^{2B/-}$ mice display mature NMJs. Transversus abdominis (TVA) muscles were isolated from P21 (n = 6) and 6 month old (n = 4) Fasudil–treated *Smn*$^{2B/-}$

mice. A) Representative images of TVA muscles from P21 and 6 month old Fasudil-treated *Smn*$^{2B/-}$ mice. (Neurofilament (NF) and synaptic vesicle protein 2 (SV2): green; EP: red (BTX)). Scale bar = 30 μm. B) Type of EP occupation were categorized and quantified as fully occupied (where the pre-synaptic terminal completely covers the EP), partial (where the pre-synaptic terminal partially covers the EP), or vacant (where no pre-synaptic terminal is present at an EP). Surviving 6 month old Fasudil-treated *Smn*$^{2B/-}$ mice display significantly more fully occupied EPs than P21 Fasudil-treated *Smn*$^{2B/-}$ mice (**$P = 0.0096$; data are mean +/- s.d.). C) Representative images of EP morphology categorization from mature to immature: pretzel, perforated, bright lines and uniform. EPs are visualized with BTX. D) Quantification shows that 6 month old Fasudil-treated *Smn*$^{2B/-}$ mice display significantly more mature pretzel-shaped EPs than P21 Fasudil-treated *Smn*$^{2B/-}$ mice (****$P < 0.0001$); data are mean +/- s.d.).

DISCUSSION

Previous work has implicated the RhoA/ROCK pathway in SMA pathogenesis (Bowerman et al. 2007; Bowerman et al. 2010; Nolle et al. 2011). In the present study, we demonstrate that targeting the ROCK pathway with the inhibitor Fasudil significantly increases the lifespan of the *Smn*$^{2B/-}$ SMA mice. The increased survival is independent of Smn expression, weight gain, pen test performance and pre-synaptic NMJ phenotype. We find however, that Fasudil benefits post-synaptic pathology and muscle development. Importantly, the results obtained from other Fasudil clinical trials, are proof-of-principle of its feasibility and availability as a therapeutic approach for the treatment of SMA. Future SMA clinical endeavors should therefore consider assessing the beneficial potential of ROCK inhibitors.

Smn protein levels remained significantly low in both Fasudil-treated spinal cord and muscle samples of SMA mice. These findings are important when considering therapeutic avenues for SMA. There are presently many strategies being developed to increase the expression of SMN, such as gene therapy, modulation of transcription and splicing of *SMN2*, and the use of various histone deacetylase (HDAC) inhibitors (reviewed in (Chuang et al. 2009; Shababi et al. 2010b; Passini et al. 2011)). Although these therapeutic approaches show promising results, they remain in pre-clinical stages and may not be as efficient if administered to mid to late symptomatic patients (Le et al. 2011). It is therefore crucial to understand the pathological molecular pathways that are affected upon SMN loss and how these can be modulated to attenuate their degenerative effects. Along with other research groups, we have shown that the RhoA/ROCK pathway is indeed perturbed in SMA cellular and animal models

and that its targeting leads to a significant beneficial outcome (Bowerman et al. 2007; Bowerman et al. 2010; Nolle et al. 2011).

We had previously identified the upregulation of RhoA-GTP in the spinal cords of *Smn*$^{2B/-}$ mice (Bowerman et al. 2010). The misregulated RhoA/ROCK pathway in the spinal cord was therefore the primary target of our Fasudil therapeutic strategy (Bowerman et al. 2010). Interestingly, we have observed that Fasudil does not prevent the motor neuron loss that occurs in the *Smn*$^{2B/-}$ mice. In fact, the most apparent effects of Fasudil appear to be the restoration of normal skeletal muscle growth and development, as well as increased postsynaptic endplate area. A number of recent reports suggest that the SMN protein may have a muscle-intrinsic role that influences SMA pathology ((Walker et al. 2008; Martinez-Hernandez et al. 2009; Mutsaers et al. 2011) and JGB, unpublished data). Active RhoA has previously been shown to positively regulate the expression of myogenin (Takano et al. 1998; Dhawan et al. 2004). Furthermore, work performed in avian and murine myoblasts shows that inhibition of ROCK promotes exit from the cell cycle and subsequent terminal differentiation (Castellani et al. 2006). Indeed, myoblasts treated with the ROCK inhibitor Y-27632 display increased differentiation, cell fusion and myotube formation (Castellani et al. 2006). Fasudil's inhibition of the RhoA/ROCK pathway most likely restores the normal skeletal muscle developmental program of *Smn*$^{2B/-}$ mice via modulation of myoblast differentiation and fusion, as well as myogenin expression. The Fasudil-dependent increase in myofiber size could lead to the subsequent increase in endplate size. Indeed, a positive correlation has previously been established between myofiber size and motor endplate size (Waerhaug et al. 1974). Furthermore, various reports suggest that postsynaptic

differentiation and formation is initially muscle-dependent and motor axon-independent (Lin et al. 2001; Yang et al. 2001). Our study therefore highlights two important points. Firstly, therapeutic strategies that improve skeletal muscle and endplate growth should be considered when developing therapies for SMA. Secondly, ROCK inhibition may have positive outcomes in other pre-clinical disease models characterized by muscle atrophy and NMJ pathology.

Intriguingly, the dramatic increase in skeletal muscle myofiber size of Fasudil-treated $Smn^{2B/-}$ mice is not accompanied by changes in weight or strength, when compared to vehicle treated $Smn^{2B/-}$ mice. Previous studies have reported this phenomenon, providing a variety of potential explanations. In cases of sarcoplasmic hypertrophy, the non-contractile myofiber components expand while muscular strength remains unchanged (Kraemer 2006). Further, the characterization of a postnatal myogenin knockout mouse model revealed normal skeletal muscle size albeit with a 30% weight loss compared to control littermates (Knapp et al. 2006). The authors suggest that this phenotype is caused by a slower growth rate and perturbed energy homeostasis (Knapp et al. 2006). Finally, Rehfeldt *et al*. showed that mice homozygous for the *Compact myostatin* mutation (*C/C*) display muscular hyperplasia and increased muscle weight but with a reduction in overall body weight (Rehfeldt et al. 2005). The authors also identify a reduction in the number of capillaries per muscle in the *C/C* mice, subsequently impacting oxidative metabolism (Rehfeldt et al. 2005). Interestingly, recent work in the severe SMA mouse model demonstrated a significant decrease in the capillary bed density within skeletal muscle (Somers et al. 2011). Thus, the findings mentioned above highlight the fact that an increase in muscle size and or weight does not necessarily positively correlate with an increase in

body weight. Regardless, the restoration of myofiber growth and skeletal muscle development by Fasudil, in the absence of weight gain, appears to be sufficient to providing therapeutic benefits to the $Smn^{2B/-}$ mice.

In recent years, it has been postulated that SMA may be a die-back neuropathy, where the motor axons initially reach the endplate but subsequently retract as disease progresses (Kariya et al. 2008; Murray et al. 2009; Ling et al. 2011). This hypothesis suggests that synapses are selectively vulnerable in SMA, with synapse loss preceding cell body degeneration. In addition, it has been suggested that neurons undergo compartmental degeneration, where the soma, axons and synapses of neurons possess specific and compartmentalized mechanisms of degeneration (Gillingwater et al. 2001; Gillingwater et al. 2003; Coleman 2005). It therefore follows that therapeutics which target distal compartments of the cell, such as the synapse or axon, can be protective to the cell body. In our study, we show that while Fasudil administration has little impact upon the initial loss of motor neurons, it dramatically increases myofiber and endplate size in SMA mice. We therefore suggest that this improvement in postsynaptic parameters stabilizes the synaptic connections and subsequently protects the remaining motor neurons. Consistent with this observation, the surviving synapses constitute NMJs that will eventually develop and mature normally. Given the tight correlation between endplate maturation and neuromuscular activity (reviewed in (Sanes et al. 1999)), Fasudil may indirectly improve NMJ transmission, subsequently ameliorating motor endplate maturation. Alternatively, considering the crucial role of the actin cytoskeleton in the redistribution of AChRs during postsynaptic remodeling (Dobbins et al. 2006; Cartaud et al. 2011), Fasudil's modulation of actin dynamics

could directly restore normal AChR clustering. Clearly, the understanding and identification of Fasudil's influence on NMJ maturation in SMA mice requires further investigation. Nevertheless, our work highlights the applicability of the compartmental degeneration hypothesis to SMA pathogenesis and the potential of therapies aimed at preventing synaptic degeneration.

ROCK has evolved as an important therapeutic target in various models of cardiovascular disease, spinal cord injury and glaucoma (reviewed in (Wierzbowska et al. 2010; Cadotte et al. 2011; Satoh et al. 2011)). Furthermore, the approved in U.S. clinical trials ROCK inhibitor Fasudil has shown beneficial effects in patients with vasospastic angina (Masumoto et al. 2002), stable effort angina (Shimokawa et al. 2002), general heart failure (Kishi et al. 2005), and pulmonary hypertension (Fukumoto et al. 2005). It has now become evident that the pathogenic misregulation of the RhoA/ROCK pathway in various Smn-depleted cellular and animal models can also be modulated by the ROCK inhibitors Y-27632 and Fasudil, leading to significant positive outcomes (Bowerman et al. 2007; Bowerman et al. 2010; Nolle et al. 2011).

CONCLUSIONS

The administration of Fasudil to SMA mice significantly increases their lifespan without an obvious increase in Smn expression and preservation of spinal cord motor neurons. In fact, Fasudil improves postsynaptic and skeletal muscle development. Our work underscores the importance of muscle as a therapeutic target in SMA and highlights the beneficial potential of ROCK inhibitors as a therapeutic strategy for SMA and for other degenerative diseases characterized by muscular atrophy and postsynaptic immaturity.

ACKNOWLEDGEMENTS

We are grateful to the Kothary laboratory for helpful discussions. This project was funded by a grant from the Canadian Institutes of Health Research (CIHR), and The Muscular Dystrophy Association (USA) to RK. MB and JGB are recipients of a Frederick Banting and Charles Best CIHR Doctoral Research Award, LMM is a recipient of a Multiple Sclerosis Society of Canada Postdoctoral Fellowship, and RK is a recipient of a University Health Research Chair from the University of Ottawa.

SUPPLEMENTARY DATA

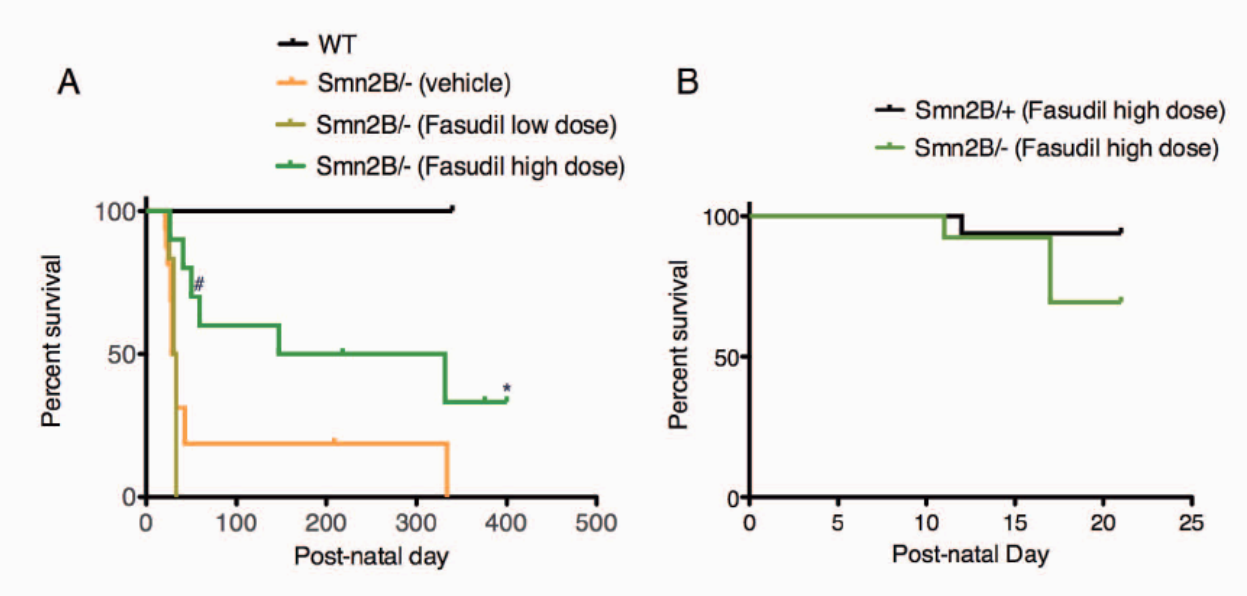

Supplementary Figure 6.1. Effect of low and high doses of Fasudil. A low dose of Fasudil (30 mg/kg once daily), a high dose of Fasudil (30 mg/kg twice daily from P3-P6; 50 mg/kg twice daily from P7-P13; 75 mg/kg twice daily from P14-P21), or vehicle (water) was administered by gavage. The different groups analyzed were: untreated wild type (WT) (n = 10), Fasudil (high dose)-treated *Smn*$^{2B/+}$ (n = 16), vehicle-treated *Smn*$^{2B/-}$ (n = 16), Fasudil (low dose)-treated *Smn*$^{2B/-}$ (n = 6) and Fasudil (high dose)-treated *Smn*$^{2B/-}$ (n = 10) mice. A) Survival curves show that the low Fasudil dosage regimen had no effect while the high Fasudil dosage regimen significantly increases the lifespan of *Smn*$^{2B/-}$ mice when compared to vehicle-treated *Smn*$^{2B/-}$ mice (*P = 0.03; # indicates death due to malocclusion of the teeth). B) Survival curve shows that the high Fasudil dosage regimen has non-negligible toxic effects on both *Smn*$^{2B/-}$ mice and the normal *Smn*$^{2B/+}$ littermates.

Supplementary Figure 6.2. *Smn*$^{2B/-}$ mice treated with Fasudil show improved gait and movement. A movie of aging Fasudil- (left mouse) and vehicle-treated (right mouse) *Smn*$^{2B/-}$ mice (two months of age). The Fasudil-treated mouse displays the agility and ability to freely walk and move around the cage while still displaying a minor neurological phenotype. The vehicle-treated *Smn*$^{2B/-}$ mouse displays a severe neurological phenotype and reduced motor functions.

CHAPTER 7: SMA is associated with defects in glucose metabolism and pancreatic development

FOREWORD

During the course of our investigation on the role of SMN in the regulation of actin dynamics, we encountered several anecdotal observations pointing to a possible function for SMN in glucose metabolism. The first one was during the establishment of the *Smn*$^{2B/-}$ mouse model, where we had a subset of mice that had reduced levels of Smn without displaying an SMA phenotype. During an aging study to determine if these mice would eventually develop SMA symptoms, we were informed that all of them had become diabetic. At the time, as we were more interested in a neuromuscular phenotype, we did not pursue this surprising observance. A few years later, based on their own hypotheses, Drs. John Woulfe and Fraser W. Scott performed preliminary experiments on the pancreas of the *Smn*$^{2B/-}$ mice and detected morphological abnormalities. While they did communicate their findings with us, neither them nor us went further with this line of investigation. Finally, we recently attempted to modulate the misregulated Cdc42 pathway by administering resveratrol to our mice (Su et al. 2005; Azios et al. 2007). Instead of providing any benefits, resveratrol significantly decreased the lifespan of the *Smn*$^{2B/-}$ mice, suggesting that this natural compound may be exacerbating an underlying phenotype. Seeing that resveratrol is frequently used in metabolic studies due to its effect on glucose metabolism (Szkudelski et al. 2011), we concluded that it was time for us to finally undertake an in-depth assessment of glucose homeostasis in our SMA mice. Hence the following study.

Glucose metabolism and pancreatic defects in Spinal Muscular Atrophy

Melissa Bowerman, Kathryn J. Swoboda, John-Paul Michalski, Gen-Sheng Wang, Courtney Reeks, Ariane Beauvais, Kelley Murphy, John Woulfe, Robert A. Screaton, Fraser W. Scott, and Rashmi Kothary

Accepted for publication in *Annals of Neurology*, 2012

Author Contributions

Conceived and designed the experiments: MB, JPM, GSW, RAS, FWS and RK. Performed the experiments: MB, KJS, JPM, CR and AB. Analyzed the data: MB, KJS, JPM and RAS. Wrote the paper: MB and KJS. Other: provided human pancreas samples: KJS and KM.

ABSTRACT

Objective: Spinal muscular atrophy (SMA) is the number one genetic killer of young children. It is caused by mutation or deletion of the survival motor neuron 1 (*SMN1*) gene. While SMA is primarily a motor neuron disease, metabolism abnormalities such as metabolic acidosis, abnormal fatty acid metabolism, hyperlipidemia and hyperglycemia have been reported in SMA patients. We thus initiated an in-depth analysis of glucose metabolism in SMA. Methods: Glucose metabolism and pancreas development was investigated in the $Smn^{2B/-}$ intermediate SMA mouse model and type 1 SMA patients. Results: Here, we demonstrate in an SMA mouse model a dramatic cell fate imbalance within pancreatic islets, with a predominance of glucagon-producing α cells at the expense of insulin-producing β cells. These SMA mice display fasting hyperglycemia, hyperglucagonemia and glucose resistance. We demonstrate similar abnormalities in pancreatic islets from deceased children with the severe infantile form of SMA in association with supportive evidence of glucose intolerance in at least a subset of such children. Interpretation: Our results indicate that defects in glucose metabolism may play an important contributory role in SMA pathogenesis.

INTRODUCTION

Spinal muscular atrophy (SMA) is a neuromuscular disorder affecting 1 in 6,000-10,000 live births. SMA is a leading inherited cause of death in children under two years of age (Pearn 1978b; Crawford et al. 1996). Homozygous deletions and/or mutations of the survival motor neuron 1 (*SMN1)* gene are responsible for over 95% of cases of this devastating autosomal recessive disease (Pearn 1978b; Lefebvre et al. 1995). Pathological and clinical manifestations of SMA are largely due to loss of motor neurons in the spinal cord and brainstem, resulting in generalized muscular atrophy, weakness, respiratory insufficiency, and in more than 50% of cases, death in infancy or early childhood (Crawford et al. 1996).

The *SMN* gene is essential for survival and a complete depletion of the protein results in early developmental lethality (Jablonka et al. 2000). In humans, the loss of the telomeric *SMN1* gene is compensated by the presence of the duplicated centromeric *SMN2* gene (Lefebvre et al. 1995). While the two genes differ by several nucleotides, the functional difference lies within a C to T substitution at position 6 of exon 7 in *SMN2* (Lorson et al. 1999). This silent mutation causes aberrant splicing of the *SMN2* gene and the production of an unstable protein, termed SMNΔ7, due to the excision and loss of exon 7 (Lefebvre et al. 1995; Lorson et al. 1999). This alteration in splicing most likely results from the loss of an exon splice enhancer and/or the gain of an exon splice silencer (Lefebvre et al. 1995; Cartegni et al. 2002; Kashima et al. 2003). While the major product of the *SMN2* gene is the SMNΔ7 protein, the full-length SMN protein is still produced in small quantities (~10%) (Lefebvre et al. 1995). As such, SMA severity is

heavily modulated by the number of *SMN2* copies present in patients (Lefebvre et al. 1995; Lefebvre et al. 1997).

While the pathological hallmark of SMA is motor neuron loss, recent reports have identified additional defects in the muscle (Walker et al. 2008), at the neuromuscular junction (Murray et al. 2008) and in the heart (Bevan et al. 2010; Heier et al. 2010; Shababi et al. 2010a). In the present work, we report for the first time glucose metabolism and pancreatic developmental defects in an SMA mouse model and human SMA patients. Our results demonstrate a progressive loss of the insulin-producing β cells and a corresponding increase in the number of the glucagon-producing α cells in pancreatic islets. This altered cell fate is accompanied by glucose clearance defects in the SMA mice during fasting and following an acute glucose tolerance test. In addition, pathology specimens from human SMA type I infants demonstrates similar abnormalities in pancreatic islet cell morphology and distribution. These observations in the SMA mouse model, and the corresponding parallels in human tissues, indicate that these findings may indeed be relevant to the human condition.

These novel findings have two major implications. Firstly, the observed defects in glucose metabolism and pancreatic development may be contributing additional stressors, which impact motor neuron loss, muscle function and survival in SMA. Secondly, as SMA patients are living longer due to improved assistive technology, further studies to assess the metabolic consequences of impaired glucose metabolism and its potential impact on their clinical course will be of utmost importance.

MATERIALS AND METHODS

Antibodies

The primary antibodies used were as follows: guinea pig anti-insulin (1:50; Dako), mouse anti-glucagon (1:200; Abcam), rabbit anti-Ki67 (1:50; Leica Microsystems), rabbit anti-phospho-AKT (Ser 473) (1:500; Cell Signaling) and rabbit anti-AKT (1:500; Cell Signaling). The secondary antibodies used were as follows: donkey anti-guinea pig biotin-SP-conjugated (1:200; Jackson Immuno Research), streptavidin-Cy3-conjugated (1:600; Jackson Immuno Research), Alexa Fluor 488 goat anti-mouse (1:500; Molecular Probes), Alexa Fluor 555 goat anti-rabbit (1:500; Molecular Probes) and HRP-conjugated goat anti-rabbit IgG (1:5000; Bio-Rad).

Animal models

The $Smn^{2B/-}$ mice were established in our laboratory and maintained in our animal facility on a C57BL/6 x CD1 hybrid background (Bowerman et al. 2009). The 2B mutation consists of a substitution of 3 nucleotides in the exon splicing enhancer of exon 7 (DiDonato et al. 2001). The *Smn* knock-out allele was previously described by Schrank *et al*. (Schrank et al. 1997) and $Smn^{+/-}$ mice were obtained from The Jackson Laboratory. All animal procedures were performed in accordance with institutional guidelines (Animal Care and Veterinary Services and Ethics, University of Ottawa).

Human samples

Pediatric control pancreatic samples were collected by KJS and KM in a de-identified fashion from children who died for reasons other than SMA. For the type I SMA pancreatic samples,

informed consent was obtained from the parents of the patients to perform a research autopsy under IRB 8751, reviewed and approved by the University of Utah Institutional Review Board. The autopsies were performed in collaboration with pathologists at each of the USA institutions involved (Primary Children's Medical Center and the Medical Examiner's Office, Salt Lake City, Utah; Cook Children's Medical Center, Ft Worth, Texas; Children's Hospital of Atlanta Scottish Rite, Atlanta, Georgia). Ages for the human pancreatic samples were as follows: 4, 5, 15 and 36 months for the controls samples and 18 (#177), 35 (#195), 28 (#206), 33 (#217), 15 (#251) and 7 months (#351) for the SMA samples.

Immunohistochemistry of pancreas sections

Whole pancreas were dissected out of P7, P10, P15 and P21 mice and placed overnight in 4% paraformaldehyde. Tissues were embedded in paraffin and cut at a thickness of 4 μm. For immunohistochemistry, pancreas sections were first deparaffinized in xylene (3 x 10 min), fixed in 100% ethanol (2 x 10 min), rehydrated in 95% and 75% ethanol (5 sec each) and placed 5 min in 1 M Tris-HCl pH 7.5. The pancreas sections were then incubated for 2 hours at room temperature (RT) in blocking solution (TBLS (10% NaN_3), 20% goat serum, 0.3% Triton X-100). This was followed by an overnight incubation at 4ºC with the primary antibodies. Subsequently, sections were washed 3 times with PBS, incubated 1 hour at RT with the secondary antibodies and then washed 3 times with PBS. Hoechst (1:1000) was added to the last PBS wash followed by the slides being mounted in Fluorescent Mounting Medium (Dako). Images were taken with a Zeiss confocal microscope, with a 20X objective, equipped with filters suitable for FITC/Cy3/Hoechst fluorescence.

Immunoblot analysis

Equal amounts of protein extracts from liver samples of random-fed P21 mice were separated by electrophoresis on 10% SDS-polyacrylamide gels and blotted onto a PVDF membrane (Millipore). The membranes were blocked in 5% nonfat milk in TBST (10 mM Tris-HCl pH 8.0, 150 mM NaCl, and 0.1% Tween 20 (Sigma)), and incubated overnight at 4ºC with the first primary antibody. The membranes were then incubated at room temperature with the secondary antibody for 1 hour, followed by three TBST washes. Signals were visualized using the ECL or the ECL plus detection kit (Amersham).

TUNEL assay

Whole pancreas were removed from P10 mice and immediately flash frozen over liquid nitrogen in a 1:1 solution of OCT (Tissue Tek) and 30% sucrose, and stored at -80ºC until they were sectioned at 10 μm thickness using a cryostat. Sections were processed for cell death detection terminal deoxynucleotidyl transferase-mediated dUTP nick end labelling (TUNEL, Roche), following manufacturer's instructions. After co-staining for insulin, the slides were mounted in Fluorescent Mounting Medium (Dako) and images were taken with a Zeiss confocal microscope, with a 20X objective, equipped with filters suitable for FITC/Cy3/Hoechst fluorescence.

Glucose tests

All blood glucose readings were done using the OneTouch®Ultra2® glucometer. Random fed P7, P15 and P21 mice were evaluated at the same time of day for non-fasting

glucose levels. For fasting glucose levels, P7, P15 and P21 mice were fasted for 6 hours, at which point glucose levels were read. A maximum of 6 hours was allowed for fasting either due to the age of the mice (P7 and P15) or to the severe diseased state of the SMA mice (P21).

The intraperitoneal glucose tolerance test (IPGTT) was performed on P15 and P21 mice fasted for 6 hours. They were then administered a 20% glucose solution (2 g glucose/kg body weight) through IP-injection. Glucose levels were measured at 0, 15, 30, 90 and 120 min in blood samples collected from the tail vein.

Measurement of insulin and glucagon serum levels

Serum was collected from random-fed P7, P15, and P21 mice as well as P21 mice 30 min post-IPGTT. Insulin and glucagon levels were measured using the mouse Bio-Plex Pro™ diabetes magnetic bead-based immunoassay (Bio-Rad) following manufacturer's instructions. Data acquisition and analysis were done using the Bio-Plex 200 Luminex-based reader and the accompanying Bio-Plex Manager software.

Pancreatic islet isolation

Islets were isolated from anaesthetized P15 mice by perfusion of the pancreatic bile duct with collagenase XI (Sigma). The islets were then purified by two rounds of manual selection using a dissecting microscope, and cultured in RPMI + 11 mM glucose as described in Fu, A. *et al* (Fu et al. 2009).

RT-PCR

RNA extraction from P15 islets was done using the RNeasy® Mini Kit and QIAshredder™ (Qiagen), following the manufacturer's instructions. Reverse transcription was performed using equal amounts of total RNA. The following primers were used for RT-PCR analysis: Pdx1 forward (5' AGG TCA CCG CAC AAT CTT GCT 3'), Pdx1 reverse (5' CTT TCC CGA ATG GAA CCG A 3'), Pax6 forward (5' AAC AAC CTG CCT ATG CAA CC 3'), Pax6 reverse (5' ACT TGG ACG GGA ACT GAC AC 3'), NeuroD forward (5' GTC CCA GCC CAC TAC CAA TT 3'), NeuroD reverse (5' CGG CAC CGG AAG AGA AGA TT 3'), Islet1 forward (5' ATG ATG GTG GTT TAC AGG CTA AC 3'), Islet1 reverse (5' TCG ATG CTA CTT CAC TGC CAG 3'), Insulin forward (5' CGA GGC TTC TTC TAC ACA CC 3'), Insulin reverse (5' GAG GGA GCA GAT GCT GGT 3'), Glucagon forward (5' CCA CTC ACA GGG CAC ATT CA 3'), Glucagon reverse (5' GTC CCT GGT GGC AAG ATT GT 3'), Actin forward (5' CCG TCA GGC AGC TCA TAG CTC TTC 3') and Actin reverse (5' CTG AAC CCT AAG GCC AAC CGT 3').

Statistical analysis

All statistical analyses were done with the Graphpad Prism software. When appropriate, a Student's two-tail *t* test or a two-way ANOVA followed by a Bonferroni multiple comparison test was used. Data were considered significantly different at $P < 0.05$.

RESULTS

Over the years, published data indicates that SMA patients can display a host of metabolic abnormalities, particularly in the setting of a catabolic state (Quarfordt et al. 1970; Dahl et al. 1975; Tein et al. 1995; Crawford et al. 1999). However, in addition to previously reported abnormalities including metabolic acidosis, abnormal fatty acid metabolism and hyperlipidemia, we have noted significant hyperglycemia on several occasions when our SMA patients received an infusion of intravenous glucose or underwent prolonged fasting, particularly during a catabolic state associated with illness (unpublished observations, KJS and KM). This encouraged us to initiate a collaboration to perform an in-depth analysis of glucose metabolism in a previously characterized intermediate SMA mouse model, $Smn^{2B/-}$ (Bowerman et al. 2009). These mice express approximately 15% residual full-length Smn protein, display the characteristic motor neuron loss, neuromuscular junction defects and muscular atrophy of SMA resulting in a median lifespan of 1 month (Bowerman et al. 2009; Bowerman et al. 2010). Additionally, we looked for evidence in support of such abnormalities in human subjects participating in an ongoing clinical study.

SMA mice are glucose intolerant

We first compared random-fed (non-fasting) and fasting glucose levels of wild type (WT) and $Smn^{2B/-}$ mice at three different time points: post-natal (P) day 7, 15 and 21. These time points represent pre-phenotype (P7), early phenotype (P15) and late phenotype (P21) stages of SMA in this mouse model. At P7 and P15, both WT and $Smn^{2B/-}$ mice have normal glycemia in non-fasting states (**Figure 7.1 A, B**). As would be expected, the glucose levels in WT mice are

significantly decreased following a six hour fast (**Figure 7.1 A, B**). However, fasting *Smn*$^{2B/-}$ mice are hyperglycemic (**Figure 7.1 A, B**), suggesting an inability to properly metabolize glucose. At P21, the glucose metabolism defects are amplified by a subpopulation of *Smn*$^{2B/-}$ mice with higher fasting than non-fasting glucose levels (**Figure 7.1 C**), suggesting a combination of hypoglycemia in the random fed state and an inability to metabolize glucose. Interestingly, the more severe *SMNΔ7* SMA mouse model, also displays hypoglycemia upon reaching end stage of the disease (Butchbach et al. 2010). At P21, although reduced, the WT fasting glucose levels are not significantly decreased compared to non-fasting levels (**Figure 7.1 C**), probably due to an insufficient fasting period. However, due to the severe diseased state of the SMA mice at P21, a longer fasting period was neither possible nor allowable.

To determine the ability of fasting *Smn*$^{2B/-}$ mice to metabolize glucose in an acute setting, we performed an intraperitoneal glucose tolerance test (IPGTT). At P15, the glucose clearance curve of the *Smn*$^{2B/-}$ mice is similar to that of WT mice (**Figure 7.1 D**). Further, the area under the curves (AUCs) of WT and *Smn*$^{2B/-}$ mice is not significantly different (**Figure 7.1 E**), suggesting that there is no change in the overall glucose tolerance of P15 SMA mice. However, when IPGTT curves are individually recorded, some irregularities become apparent in P15 *Smn*$^{2B/-}$ mice. For instance, a precipitous drop in glucose levels followed by a slow increase was observed in one animal (**Figure 7.1 F**), while another followed the normal WT curve until the glucose levels began to rise in the later stages of the IPGTT (**Figure 7.1 F**). When quantifying the change in glucose levels from 60 to 90 minutes and 60 to 120 minutes, we find that *Smn*$^{2B/-}$ mice display an increase while the WT mice show a decrease (**Figure 7.1 G**). The IPGTT was next repeated in P21 *Smn*$^{2B/-}$ and control mice. At this time point, the *Smn*$^{2B/-}$ mice show signs of

glucose intolerance with glucose levels significantly higher than WT levels at 30 and 60 minutes following the glucose IP (**Figure 7.1 H**). Importantly, the AUCs of *Smn*$^{2B/-}$ mice are significantly greater than those of WT mice (**Figure 7.1 I**). Thus, it appears that at an early age SMA mice have fasting glucose clearance defects, which progressively develops into glucose intolerance.

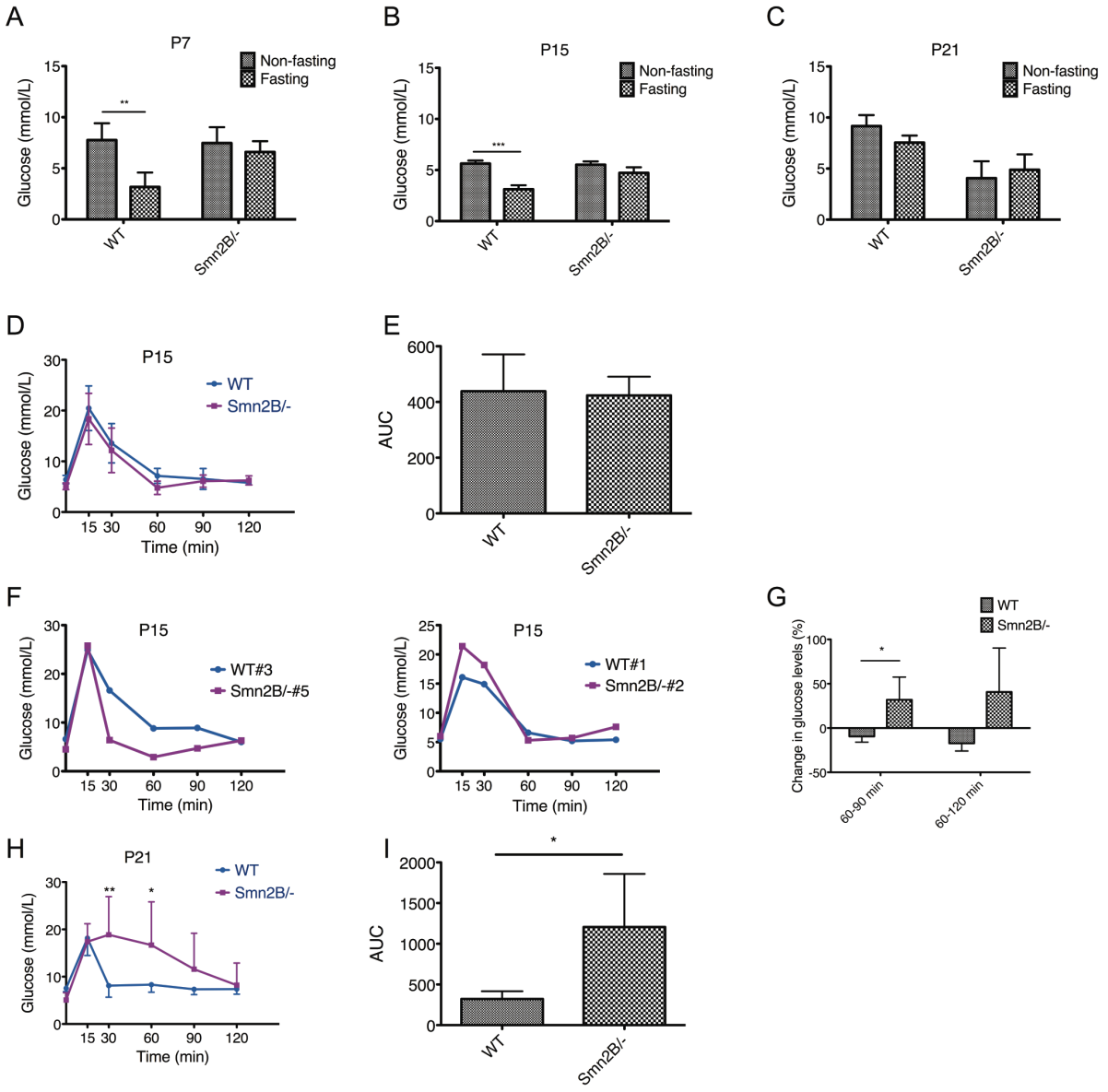

Figure 7.1. Glucose intolerance in *Smn*$^{2B/-}$ mice. A, B and C) Serum glucose levels in post-natal day (P) 7, P15 and P21 random-fed and fasted wild type (WT) (n = 4 (P7), 5 (P15) and 5 (P21)) and *Smn*$^{2B/-}$ mice (n = 3 (P7), 5 (P15) and 11 (P21)). At all time points, fasted WT mice show reduced glucose levels while fasted *Smn*$^{2B/-}$ mice are hyperglycemic. At P21, random-fed *Smn*$^{2B/-}$ mice show signs of hypoglycemia. (Data are mean +/- s.d.; two-way ANOVA; $^{**}P < 0.01$;

***$P < 0.001$). D) Intraperitoneal glucose tolerance test (IPGTT) curves of P15 wild type (WT) (n = 3) and $Smn^{2B/-}$ (n = 5) mice show similar patterns. (Data are mean +/- s.d.). E) Quantification of the IPGTT area under the curve (AUC) shows no difference between P15 WT and $Smn^{2B/-}$ mice. (Data are mean +/- s.d.). F) Individual comparisons of IPGTT curves between P15 WT and $Smn^{2B/-}$ mice show irregularities in the curves of the SMA mice. $Smn^{2B/-}$ #5 displayed a precipitous drop in glucose levels followed by a slow increase, while $Smn^{2B/-}$ #2 followed the normal WT curve until the glucose levels began to rise after 60 min. G) Quantification of the change in glucose levels from 60 to 90 minutes and 60 to 120 minutes demonstrates an increase in the $Smn^{2B/-}$ mice and a decrease in the WT mice. (Data are mean +/- s,d,; t-test; *$P = 0.021$ (60-90 min); $P = 0.059$ (60-120 min)). H) IPGTT curves of P21 WT (n = 5) and $Smn^{2B/-}$ (n = 10) mice show increased glucose levels at 30 min and 60 min in SMA mice, indicative of glucose intolerance. (Data are mean +/- s.d.; t-test; **$P = 0.002$; *$P = 0.018$). I) Quantification of the IPGTT AUC of P21 mice shows a significant increase in the AUC of the $Smn^{2B/-}$ mice when compared to WT, suggesting defective glucose clearance. (Data are mean +/- s.d.; t-test; *P = 0.011).

SMA mice display reduced β cell and increased α cell numbers

Since the pancreatic islets are one of the key players responsible for the maintenance and regulation of blood glucose, we next performed immunohistochemical analysis to assess the cellular profile. Double-labeling of insulin-producing β cells and glucagon-producing α cells revealed a significant decrease in number of β cells and a significant increase in α cells in the pancreas of $Smn^{2B/-}$ mice relative to WT controls (**Figure 7.2 A, B, C**). As early as P7 there is a small shift in pancreatic cell composition while at P15, the $Smn^{2B/-}$ islets are predominantly composed of α cells (**Figure 7.2 A, B, C**). The increase in α cells appears to plateau at P15, as the percentage of glucagon-positive cells per islet is similar in P21 $Smn^{2B/-}$ islets (**Figure 7.2 A, B, C**). The observed decrease in β cells in $Smn^{2B/-}$ islets also corresponds to an overall decrease in β cell mass (**Figure 7.2 D, E**). The reduced β cell mass is apparent at all three time points (P7, P15 and P21), irrespective of β cell composition of the islets (**Figure 7.2 D, E**). Thus, a loss of β cells and an increase in α cells within $Smn^{2B/-}$ pancreatic islets corresponds to a functional inability to metabolize glucose, at both pre-phenotype and phenotype stages.

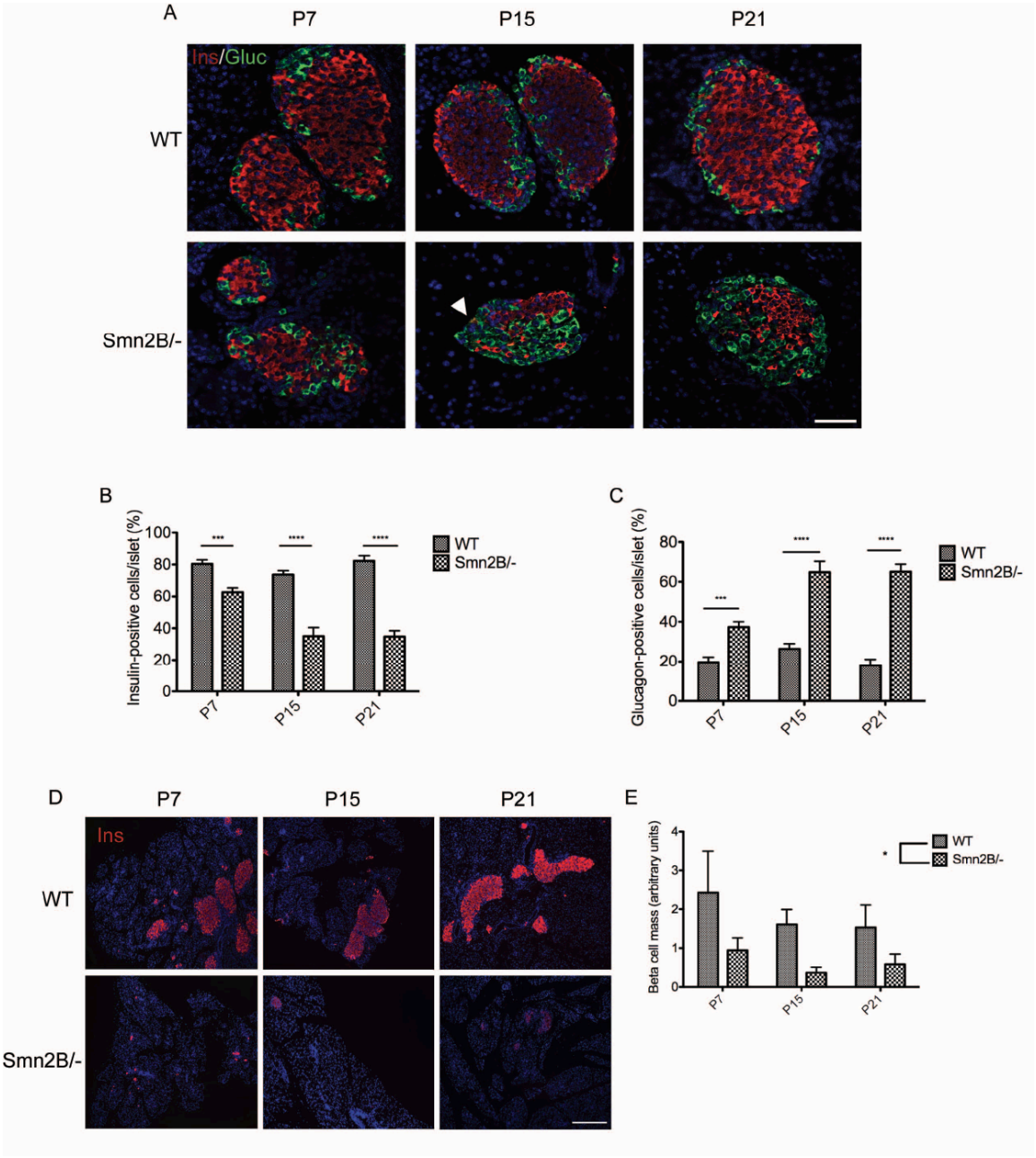

Figure 7.2. Pancreatic defects in *Smn*$^{2B/-}$ mice. A) Representative cross-sections of P7, P15 and P21 pancreatic islets of WT and *Smn*$^{2B/-}$ mice. Islets were co-labeled for insulin (red; β cells), glucagon (green; α cells) and Hoechst (blue; nuclei). Arrowhead shows a yellow cell in an *Smn*$^{2B/-}$ islet, positive for both insulin and glucagon. Scale bar = 50 μm. B) Quantification of the percentage of insulin-positive cells per islet shows a significant decrease of β cells in *Smn*$^{2B/-}$

islets (n = 3 mice) at all time-points when compared to WT islets (n = 3 mice). (Data are mean +/- s.d.; two-way ANOVA; ***$P < 0.001$; ****$P < 0.0001$). C) Quantification of the percentage of glucagon-positive cells per islet shows a significant increase of α cells in *Smn*$^{2B/-}$ islets (n = 3 mice) at all time points relative to WT (n = 3 mice). (Data are mean +/- s.d.; two-way ANOVA; ***$P < 0.001$; ****$P < 0.0001$). D) Representative images of P7, P15 and P21 pancreatic cross-sections of WT and *Smn*$^{2B/-}$ mice. Sections were stained for insulin (red; β cells) and Hoechst (blue; nuclei). Scale bar = 100 μm. E) Quantification of the β cell mass (β cell area/whole pancreatic section area). The *Smn*$^{2B/-}$ mice (n = 3 mice per time point) display a significant reduction in β cell mass compared to WT mice (n = 3 mice per time point). (Data are mean +/- s.d.; t-test; *$P = 0.021$).

SMA mice have hyperglucagonemia and increased insulin sensitivity

We next assessed if the loss of ß cells and the gain of α cells in *Smn*$^{2B/-}$ mice is reflected in the overall blood insulin and glucagon levels. Serum was collected from random-fed P7, P15 and P21 WT and *Smn*$^{2B/-}$ mice. In addition, sera from P21 mice were analyzed thirty minutes following a glucose injection, as this time point corresponds to the greatest observed difference in glucose levels between WT and *Smn*$^{2B/-}$ mice in the IPGTT.

Serum glucagon levels from *Smn*$^{2B/-}$ mice were significantly higher than those observed in WT mice at all time points (**Figure 7.3 A**), suggesting that both pre-phenotype and phenotypic SMA mice are hyperglucagonemic. Interestingly, insulin levels were similar at all time points between *Smn*$^{2B/-}$ and WT mice (**Figure 7.3 B**), indicating the functional competence of the remaining insulin-producing β cells in *Smn*$^{2B/-}$ islets.

Since P21 *Smn*$^{2B/-}$ mice are glucose intolerant, we next addressed whether they displayed signs of insulin resistance. To do this, we measured levels of phosphorylated AKT (p-AKT) in the liver, as reduced levels are indicative of insulin resistance (reviewed in (Taniguchi et al. 2006)). Livers from P21 random-fed *Smn*$^{2B/-}$ mice displayed higher levels of p-AKT when compared to WT livers (**Figure 7.3 C, D**), suggesting instead a hypersensitivity to insulin. The absence of insulin resistance in the livers of *Smn*$^{2B/-}$ mice is consistent with their normal levels of insulin, as the pancreas typically responds to insulin resistance by increasing its insulin production (reviewed in (Shanik et al. 2008)).

Thus, the above results suggest that a critical consequence of the increased number of α cells within *Smn*$^{2B/-}$ islets is hyperglucagonemia while, in contrast, loss of β cells within *Smn*$^{2B/-}$ islets does not significantly impact upon insulin levels.

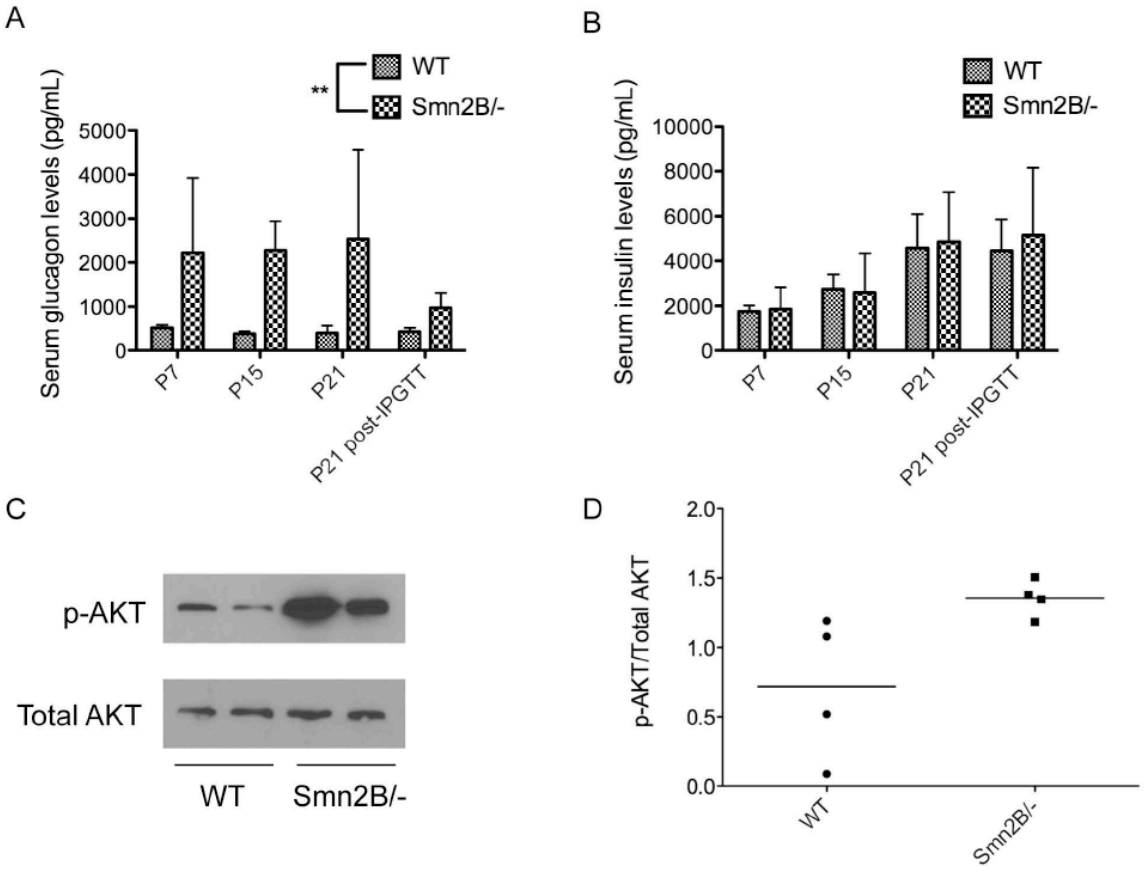

Figure 7.3. *Smn*$^{2B/-}$ mice have normoinsulinemia, hyperglucagonemia and increased insulin sensitivity. A and B) Serum glucagon (A) and insulin (B) levels in random-fed P7, P15, P21 and P21 30 min post-IPGTT wild type (WT) (n = 3 (P7), 4 (P15), 7 (P21) and 4 (P21 30min)) and *Smn*$^{2B/-}$ (n = 4 (P7), 3 (P15), 3 (P21) and 6 (P21 30 min)) mice. While insulin levels were similar between both groups (B), glucagon levels were significantly higher in the *Smn*$^{2B/-}$ mice when compared to WT (A). (Data are mean +/- s.d.; t-test; $^{**}P = 0.0042$). C) Representative immunoblot of p-AKT and total AKT in extracts of random-fed livers of P21 WT and *Smn*$^{2B/-}$ mice. D) Quantification of the p-AKT/total AKT ratios shows a trend ($P = 0.0536$) towards

increased p-AKT in *Smn*$^{2B/-}$ livers (n = 4 mice) compared to WT (n = 4 mice), indicative of increased insulin sensitivity.

Pancreatic islets in SMA mice do not have increased apoptotic or proliferative cells

To determine if the loss of β cells in pancreas from $Smn^{2B/-}$ mice was due to increased apoptosis, we performed a TUNEL assay on P10 tissue. This time point was chosen as it bridges the minimal loss in β cells observed at P7 and the maximal loss observed at P15. Very few apoptotic cells were observed in either WT or $Smn^{2B/-}$ pancreatic islets (**Figure 7.4 A**). Indeed, both the number of TUNEL-positive islets and the number of TUNEL-positive cells per islet were similarly low in both groups (**Figure 7.4 B, C**). We next assessed if the increase in α cells in $Smn^{2B/-}$ islets was due to an increase in proliferation. Double-labeling of glucagon and Ki67, a proliferation marker, was performed on sections from pancreas of P10 WT and $Smn^{2B/-}$ mice (**Figure 7.4 D**). The number of islets containing Ki67-positive glucagon-positive cells was comparable between wild type and $Smn^{2B/-}$ (**Figure 7.4 E**). Therefore, the decrease in β cells and increase in α cells in $Smn^{2B/-}$ pancreatic islets are neither a result of increased β cell apoptosis nor an increase in α cell proliferation.

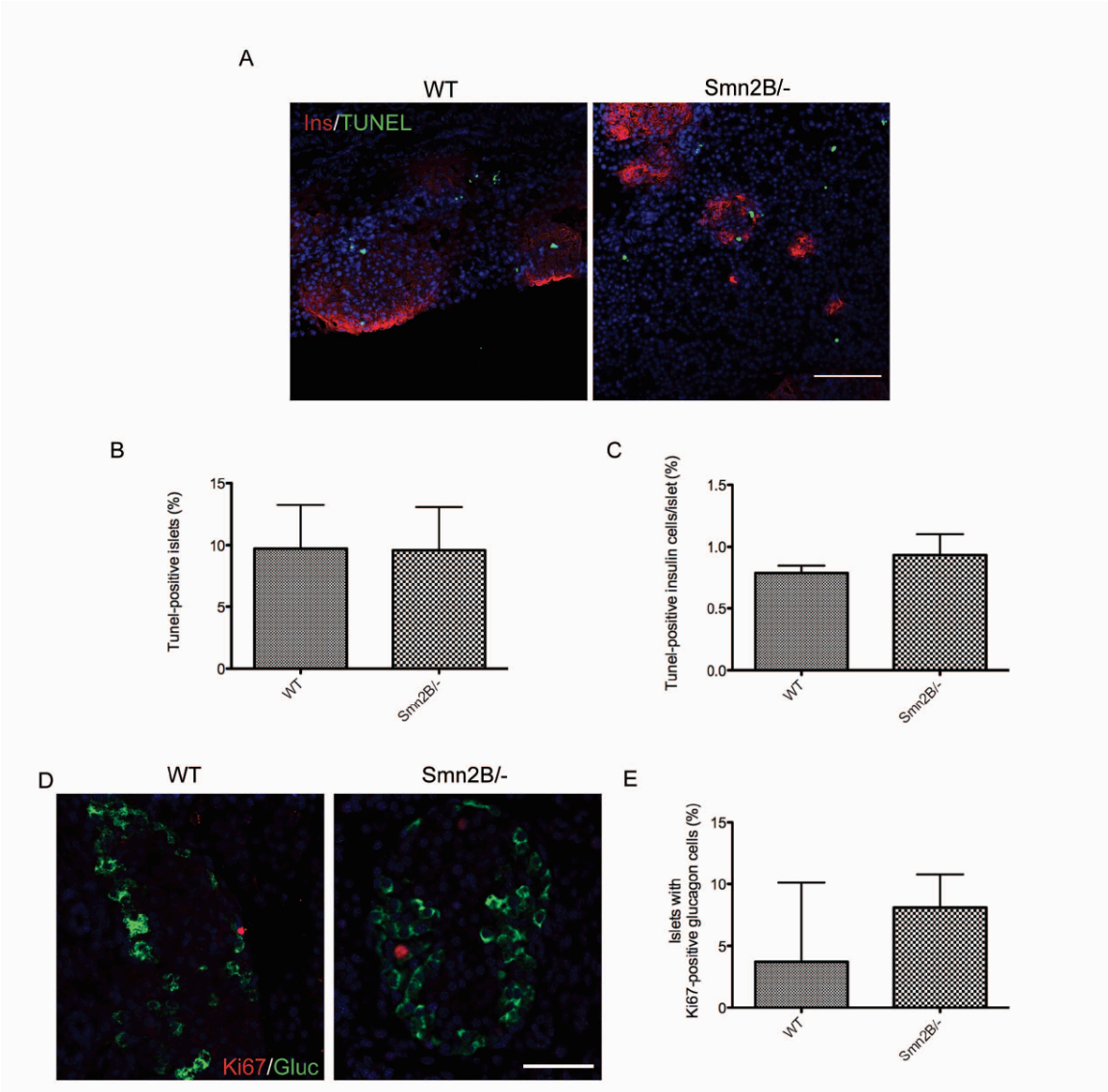

Figure 7.4. *Smn*$^{2B/-}$ islets do not show increased β cell apoptosis or α cell proliferation. A) Representative images of P10 pancreatic islets of wild type (WT) and *Smn*$^{2B/-}$ mice co-labeled for insulin (red; β cells), TUNEL (green) and Hoechst (blue; nuclei). Scale bar = 100 μm. B and C) Quantification of the percentage of TUNEL-positive islets (B) and the percentage of tunnel-positive insulin cells per islet (C) shows no difference between WT (n = 3 mice) and *Smn*$^{2B/-}$ (n = 3 mice) mice. (Data are mean +/- s.d.) D) Representative images of P10 pancreatic islets of WT and *Smn*$^{2B/-}$ mice co-labeled with Ki67 (red), glucagon (green; α cells) and Hoechst (blue;

nuclei). Scale bar = 50 μm. E) Quantification of the percentage of islets with Ki67-positive/glucagon-positive cells shows no difference between WT (n = 3 mice) and *Smn*$^{2B/-}$ (n = 3 mice) mice. (Data are mean +/- s.d.).

β cell identity transcription factors are unchanged in $Smn^{2B/-}$ islets

The results from the apoptosis and proliferation analysis suggest that there is another mechanism responsible for the gradual change in composition of $Smn^{2B/-}$ pancreatic islets. At P15, we observed cells co-labeling for insulin and glucagon (**Figure 7.2 A**, arrowhead), hinting at a temporal and progressive fate switch from β to α cell. To investigate this possibility, we examined the expression of various transcription factors responsible for the determination and maintenance of β cell identity (Rojas et al. 2010). RT-PCR was performed on RNA extracted from isolated pancreatic islets of P15 mice, an early phenotypic time-point for the $Smn^{2B/-}$ mice, both in terms of SMA as well as glucose tolerance and pancreatic defects. We did not observe any changes in mRNA expression of transcription factors responsible for the regulation of pancreatic progenitors (Pdx1), general growth and organization of pancreatic islets (Pax6), maturation and identity of β cells (NeuroD) and the function of differentiated β cells (Pdx1 and Islet1) (Rojas et al. 2010) (**Figure 7.5**). Insulin mRNA was also similar between WT and $Smn^{2B/-}$ islets (**Figure 7.5**), consistent with normoinsulinemic profile of the serum of P15 $Smn^{2B/-}$mice (**Figure 7.3 B**). Glucagon mRNA was slightly higher in $Smn^{2B/-}$ islets (**Figure 7.5**), also consistent with the hyperglucagonemia observed in P15 $Smn^{2B/-}$ serum (**Figure 7.3 A**).

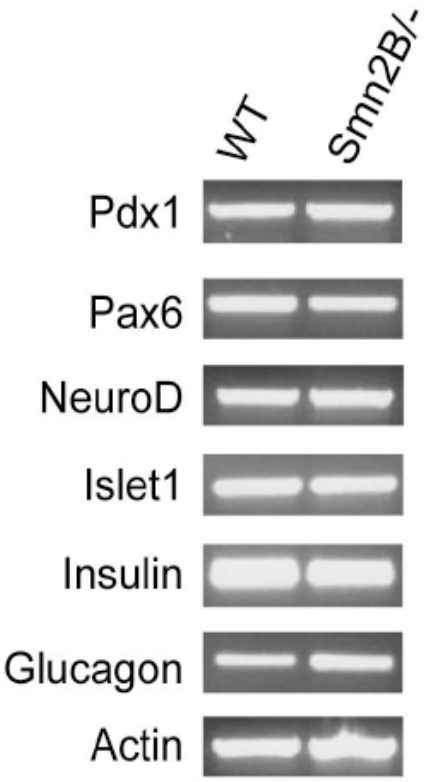

Figure 7.5. The expression profile of β cell identity transcription factors is unchanged in *Smn*$^{2B/-}$ islets. Representative RT-PCR results from RNA isolated from P15 pancreatic islets of wild type (WT) (n = 3, pooled) and *Smn*$^{2B/-}$ (n = 2, pooled) mice. Pdx1, Pax6, NeuroD and Islet 1 display similar mRNA levels in both WT and *Smn*$^{2B/-}$ islets. The mRNA levels for insulin were normal while levels for glucagon were increased. Actin transcripts were used as a loading control.

Metabolic abnormalities in human SMA subjects

All six infants from whom pancreas samples were collected at autopsy had been followed prospectively in our clinical outcomes study: "Clinical and genetic studies in SMA". The type I SMA patients were genetically confirmed by a homozygous deletion of *SMN1* and all of them possessed 2 *SMN2* copies. Clinical and laboratory records were examined for evidence of abnormal glucose levels, but no formal evaluation of glucose metabolism in the form of glucose tolerance testing was performed, nor were insulin or glucagon levels obtained. In two of six subjects (UT-SMA206 and UT-SMA217), point of care testing was performed on several occasions in the home, via glucometer, to assess for hypoglycemia that is often associated with an intolerance of gastric tube feeds. In this setting, glucose levels ranged from low (45 mg/dL, normal range > 60 mg/dL) to mild hyperglycemia (128 mg/dL, normal range < 108 mg/dL). We further reviewed all glucose levels obtained from all subjects during hospitalizations for illness or elective admissions, and during elective outpatient evaluations. One subject, UT-SMA177, underwent an elective surgical repair for coarctation of the aorta at 9 days of age, prior to her diagnosis of SMA at 3 months of age. A glucose reading obtained in the perioperative period was noted to be significantly elevated at 209 mg/dL (normal range 60-108 mg/dL). Of note, she was catabolic and had not received intravenous glucose or parenteral nutrition before or during the procedure. This same subject had at least two other mildly elevated glucose levels (113 and 111 mg/dL) during subsequent hospitalizations. At least 2 other subjects had at least one documented elevated glucose level. However, in the other 3 subjects, no abnormal glucose levels were documented, and in none of the 6 cases was glucose tolerance formally assessed.

Pancreas from human SMA displays abnormal islet composition

We next investigated whether SMA patients had similar pancreatic defects as those observed in the SMA mice. Pancreatic samples were not collected for any given observed abnormality or suggestive clinical history, and were grossly normal pathologically; rather, the tissue was obtained as part of a comprehensive collection of tissues in willing study participants, which included all major organs in addition to skin, muscle, nerve, spinal cord and brain. To this end we performed immunohistochemistry on six type 1 SMA pancreatic samples, co-labeling for insulin-producing β cells and glucagon-producing α cells (**Figure 7.6 A**). Astonishingly, every SMA pancreas contained islets predominantly composed of α cells and/or displaying an overall disorganized appearance (**Figure 7.6 A**). Indeed, quantification shows that pancreatic islets from type I SMA patients are composed of significantly more α cells compared to control islets (**Figure 7.6 B**). We further compared SMA patients individually and find that they display similar pancreatic islet compositions (**Figure 7.6 C**), suggesting, at least in the six samples analyzed herein, that the age at which type I SMA patients succumb to the disease does not influence islet pathology. It is important to note that human islets differ from rodent islets in that they do not display a core-mantle segregation of β and α cells (Bosco et al. 2010). Furthermore, human islets also contain fewer β cells since α cells localize along the mantle and internal vascular channels (Cabrera et al. 2006; Bosco et al. 2010). Nevertheless, the core of normal human islets is typically composed of more β cells than α cells (Bosco et al. 2010). Both SMA mice and human patients display pancreatic islets with an abnormal increase in α cell number, suggesting a conserved role for the SMN protein in normal pancreatic development.

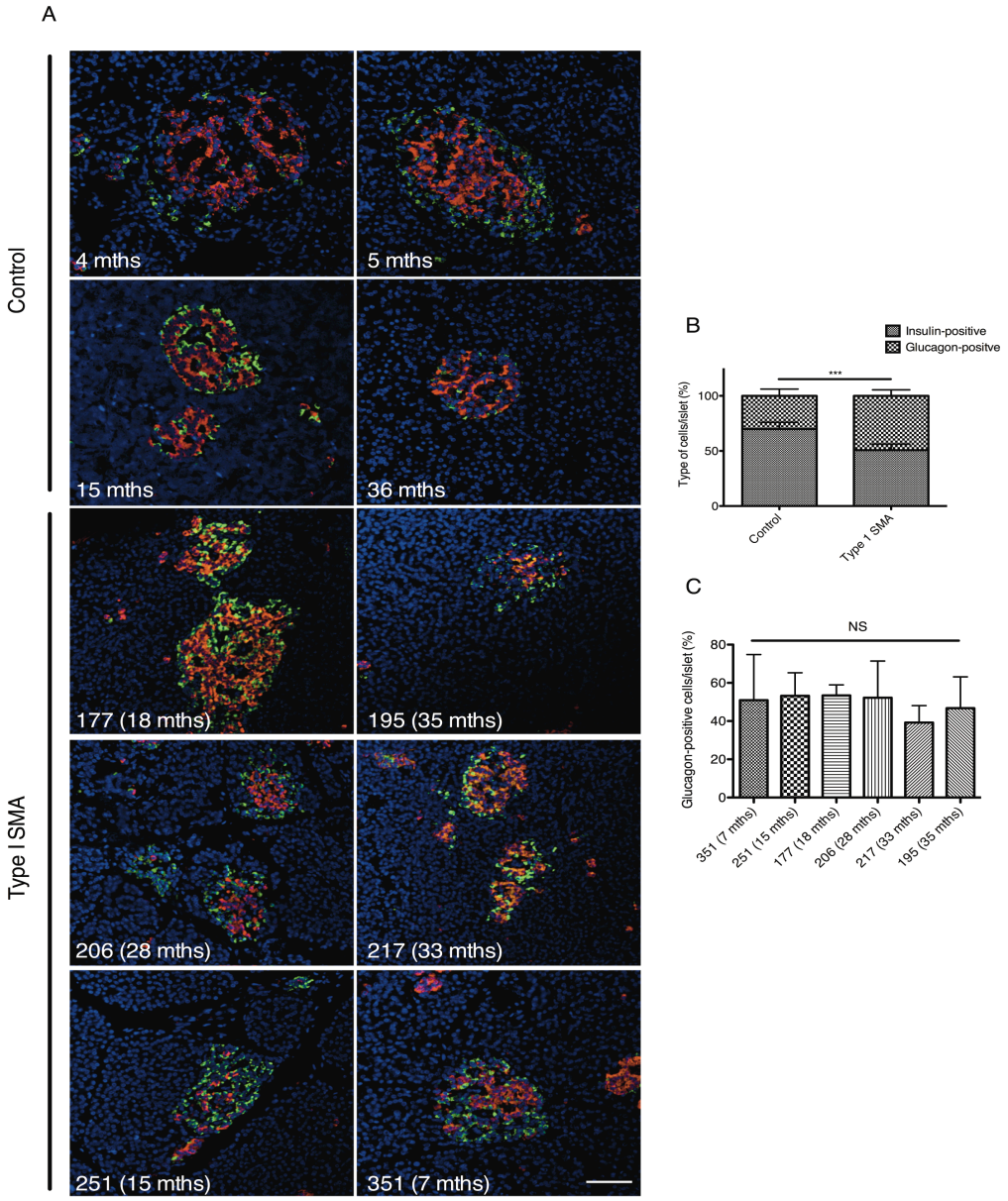

Figure 7.6. Human type I SMA pancreatic islets display an abnormal composition of insulin-secreting β cells and glucagon-secreting α cells. A) Representative pancreatic cross-sections from pediatric controls and type I SMA patients co-labeled for insulin (red; β cells), glucagon (green; α cells) and Hoechst (blue; nuclei). Scale bar = 50 μm. B) Quantification of islet composition shows that type I SMA islets display significantly more α cells and significantly

fewer β cells compared to control islets (Data are mean +/- s.d.; t-test; ***P = 0.0004). C) Comparison of the percentage of glucagon-positive cells per islet between type I SMA patients shows that their pancreatic islet composition are not significantly different (Data are mean +/- s.d.; NS = not significant).

DISCUSSION

Previous clinical reports have identified abnormal fatty acid metabolism (Tein et al. 1995; Crawford et al. 1999) and hyperlipoproteinemia (Quarfordt et al. 1970; Dahl et al. 1975) in SMA patients. Interestingly, all of these defects can originate from an inappropriate regulation of glucose metabolism. However, until now a specific defect in glucose metabolism or pancreatic islet cell function in mice or humans with SMA has not been recognized. In the present study, we demonstrate that pancreatic defects and as a consequence, alterations in glucose metabolism are associated with SMA. Indeed, SMA mice have fasting hyperglycemia, glucose intolerance, hypersensitivity to insulin and hyperglucagonemia. These metabolic defects are accompanied by a temporal shift in pancreatic islet composition, from the typical β cell core to an abnormal increase in α cell number. In addition, we demonstrate similar histopathologic abnormalities in autopsy specimens from SMA type I infants and children, with pancreatic islets that predominantly contain glucagon-producing α cells. Interestingly, while the age of death of the SMA patients ranged from 7 to 35 months, they displayed comparable pancreatic islet composition. A thorough examination of pancreas samples from type I, II and III SMA patients would most likely reveal a progressive increase in the severity of islet abnormalities.

Although we did not perform systematic studies of glucose metabolism in these children prior to their deaths, review of clinical records provides some evidence of potential abnormalities in glucose metabolism in at least 3 of the 6 subjects for whom we had pancreas samples from autopsy available for study. However, the relevance of such abnormalities, if any, to the clinical outcomes in these patients remains unclear at this time. In several other SMA type I children

enrolled in our studies, we have observed hyperglycemia in the setting of a catabolic state, particularly if the only source of calories provided is intravenous glucose. However, such abnormalities were attributed to their illness and severely reduced lean body mass, and neither formal glucose tolerance testing nor insulin or glucagon levels were examined prior to their deaths, which were invariably related to acute and/or chronic respiratory failure in the setting of severe muscle weakness. We have never clearly documented fasting hyperglycemia in SMA type I subjects. In general, we make every effort to limit fasting in this population, due to their severely diminished lean body mass and energy reserves, and prior anecdotal reports of hypoglycemia in this setting. However, several type II and type III SMA subjects enrolled in our research studies have been formally diagnosed with diabetes or glucose intolerance requiring medical treatment. Clearly, further systematic studies in human subjects are needed to clarify the relevance of these observations to SMA patients.

Other neurodegenerative diseases are also characterized by symptoms of metabolic disorders. Indeed, numerous studies suggest a role for impaired glucose uptake and insulin resistance in the pathology and progression of Alzheimer's disease (AD) (Dodart et al. 1999; de la Monte et al. 2008). Recently, an analysis of a mouse model of Prader Willi syndrome, a rare genetic neurodevelopmental disorder (Cassidy et al. 2011), revealed hypoinsulinemia and hypoglucagonemia due to increased apoptosis of α and β pancreatic cells (Stefan et al. 2011). Although the mechanisms that lead to the glucose homeostasis perturbations vary significantly between these various pathologies, their occurrences support the idea that the pathological

hallmarks of a specific disease may involve more than one organ and/or compartment, albeit with different severities and functional consequences.

The phenotypic picture painted herein, at least in the SMA mouse model, is one of a progressive pathology. Indeed, in pre-phenotype (P7) and early phenotype (P15) stages, random-fed SMA mice are normoglycemic while fasting SMA mice are hyperglycemic. At a later phenotypic stage (P21), random-fed *Smn*$^{2B/-}$ mice are hypoglycemic and continue to display fasting hyperglycemia. Furthermore, while P15 *Smn*$^{2B/-}$ mice have normal IPGTT curves, P21 *Smn*$^{2B/-}$ mice have become glucose intolerant. Interestingly, insulin levels in SMA mice remain normal and P21 *Smn*$^{2B/-}$ livers show signs of increased insulin sensitivity, suggesting that the defects in glucose metabolism are not due to hypoinsulinemia or insulin resistance. Rather, the observed metabolic abnormalities most likely stem from elevated glucagon levels, which subsequently enhance hepatic glucose output. In all probability, the increased glucagon release is a direct consequence of the increased number of α cells within *Smn*$^{2B/-}$ islets. It will therefore be of future interest to determine if preventing glucagon release, through the administration of glucagon receptor (GcgR) antagonist II (Yan et al. 2009; Liu et al. 2011), can benefit the glucose and pancreatic defects identified in the *Smn*$^{2B/-}$ mice.

Interestingly, the observed shift in islet composition in SMA mice does not appear to be a consequence of increased β cell apoptosis or α cell proliferation, which is what typically occurs in type 2 diabetes mellitus (T2DM) models (Pick et al. 1998; Liu et al. 2011). This finding suggests that the dramatic increase in the number of α cells within SMA islets may be due to a

time-dependent fate-switch. Future experiments should therefore focus on the identification of β and α cell lineage determinants modulated by the Smn protein. As the RT-PCR experiment does not reveal a general change in the transcription factor profiles, it is most likely that the developmental pancreatic defects in SMA stem specifically from one or a few essential components.

It is important to note that the cellular composition of pancreatic islets is species- and location-dependent (Kim et al. 2009; Bosco et al. 2010). Taking into account these factors, quantitative analyses were performed solely on intraspecies comparisons from islets that were localized throughout the entire pancreatic sections (tail, body and head). Furthermore, the increase in α cells in the islets of SMA mice is accompanied by hyperglucagonemia, highlighting a functional consequence of the observed change in cellular makeup. Thus, the progressive shift in SMA islet composition described in our study can be attributed to SMN loss and not pattern variability.

Our report identifies a novel role for the SMN protein in the pancreas, the loss of which results in pancreatic development and glucose metabolism defects in an SMA mouse model and human type I SMA patients. The ensuing question is whether this pathology is SMA-dependent or -independent. The pathological hallmarks in SMA are motor neuron loss and muscular atrophy (Crawford et al. 1996). Although not the primary targets, motor neuron innervation and degeneration occurs in late-stage diabetic models (Ramji et al. 2007; Zochodne et al. 2008). As for muscle, it is undeniably a central player in glucose metabolism via its role in insulin-

dependent glucose uptake (Huang et al. 2007). Furthermore, various neurodegenerative and neuromuscular disorders have been associated with pancreatic and glucose metabolism defects (Barris 1953; Sinnreich et al. 2004; Takeda et al. 2010). Thus, it is possible that the glucose and pancreas pathologies observed in the *Smn*$^{2B/-}$ mice are a direct consequence of the loss of functional motor neurons and compromised skeletal muscle. However, P7 *Smn*$^{2B/-}$ mice, which represent an SMA pre-phenotype stage, display fasting hyperglycemia and an increased number of pancreatic islet α cells. This suggests that glucose metabolism and pancreatic defects in the *Smn*$^{2B/-}$ mice are SMA-independent since they arise before disease onset and, therefore, occur as a direct consequence of SMN depletion and loss of its unique role in the pancreas.

While the defects in glucose metabolism and pancreatic development in the *Smn*$^{2B/-}$ mice are most likely independent of disease onset, their impact on the progression of SMA should not be underestimated. Indeed, various therapeutic strategies such as administration of insulin-like growth factor 1 (IGF1) to muscle, neuronal depletion of phosphatase and tensin homolog (PTEN) and systemic trichostatin A (TSA) administration, have shown beneficial effects in SMA mouse models and also act on glucose metabolism (Di Cola et al. 1997; Ranke 2005; Stiles et al. 2006; Avila et al. 2007; Sun et al. 2008; Ning et al. 2010; Bosch-Marce et al. 2011). Thus, while the SMA therapeutic strategies described above were aimed at motor neuron and muscle pathology, it is possible that the positive outcomes were due in part to improvements in glucose metabolism and pancreatic development. Furthermore, it has previously been reported that specific maternal rodent diets as well as neonatal nutritional support can increase the lifespan of SMA mice (Narver et al. 2008; Butchbach et al. 2010). Seeing that diet has a major influence on

glucose metabolism (Rivellese et al. 2002), these studies support the hypothesis that metabolism defects may indeed contribute to SMA pathology. Future development and assessment of SMA therapies should therefore also evaluate their effect on glucose metabolism and pancreatic abnormalities.

Finally, it would be of interest to perform a more in-depth characterization of the glucose defects in SMA patients and assess if they are linked to disease severity. A key component issuing from our work is that as SMA patients are surviving longer, either through mechanical or therapeutic strategies, additional tissue-specific pathologies are becoming apparent and impact the well being of these patients. Merging assessment and therapeutic intervention for metabolic impairments with existing clinical care management of SMA patients is therefore of paramount importance.

ACKNOWLEDGEMENTS

We are grateful to the Kothary laboratory for helpful discussions. This project was funded by a grant from the Canadian Institutes of Health Research (CIHR), and The Muscular Dystrophy Association to R.K. M.B. and J.P.M are recipients of a Frederick Banting and Charles Best CIHR Doctoral Research Award, and R.K. is a recipient of a University Health Research Chair from the University of Ottawa. R.A.S. holds the Canada Research Chair in Apoptotic Signaling.

CHAPTER 8: General discussion

SMN AND ACTIN DYNAMICS: IMPLICATIONS FOR SYNAPTIC STABILITY AND MAINTENANCE

Using cellular and animal models of SMA, we have identified and characterized a role for Smn in the regulation of actin cytoskeletal dynamics (Bowerman et al. 2007; Bowerman et al. 2009; Bowerman et al. 2010). Indeed, loss of Smn affects both downstream (profilin IIa, plastin 3) and upstream (RhoA, Cdc42) actin regulators. Importantly, our work is supported by the recent report confirming the molecular interaction of SMN, ROCK and profilin IIa (Nolle et al. 2011). Interestingly, most of the misregulated actin effectors uncovered in our work modulate pre-synaptic plasticity and could therefore be responsible for the NMJ defects recently described in SMA (Kariya et al. 2008; Murray et al. 2008; Kong et al. 2009; Bowerman et al. 2012a).

Consequential effects of increased profilin IIa expression at the NMJ

In recent years, profilin IIa, the predominantly expressed isoform of the neuronal-specific *profilin II* gene (Di Nardo et al. 2000; Lambrechts et al. 2000), has been identified as a key player in pre- and postsynaptic plasticity. High concentrations of profilin IIa results in increased stability of actin filaments, thus reducing the overall plasticity of actin cytoskeletal dynamics (Ackermann et al. 2003; Da Silva et al. 2003). In pre- and post-synaptic compartments, profilin IIa is thought to play a role in endocytosis and exocytosis. Studies performed in murine brains identified dynamin 1 and synapsin as profilin II-interactors (Witke et al. 1998; Gareus et al. 2006). Dynamin 1 is a large GTPase essential for the endocytosis and recycling of synaptic vesicles in nerve terminals (Scaife et al. 1990; van der Bliek et al. 1991; Marks et al. 2001). Overexpression of profilin II sequesters dynamin 1 and inhibits endocytosis (Gareus et al. 2006).

Synapsin is also associated with synaptic vesicle recycling and endocytosis (Bloom et al. 2003). Recently, Mondin *et al*. have characterized the role of profilin IIa in the exocytosis of the ionotropic kainate glutamate receptors (KGRs) (Coussen et al. 2005; Mondin et al. 2010), which mediate synaptic transmission and plasticity (reviewed in (Lerma 2003)). The authors show that profilin IIa binds the KAR subunit GluK2b, subsequently decreasing its exocytosis (Mondin et al. 2010). Interestingly, SMA has been associated with kainate-independent disturbed glutamate transport and regulation (Hayashi et al. 2002; Chan et al. 2003; Ling et al. 2010; Gogliotti et al. 2011). Thus, the increased profilin IIa expression and hyperphosphorylation observed in SMA (Bowerman et al. 2007; Bowerman et al. 2009; Nolle et al. 2011), might subsequently disrupt endocytosis and exocytosis pathways crucial for proper synaptic vesicle processing and transmission. Indeed, the *profilin II* knock-out mouse shows increased vesicle release and synaptic excitability of glutamergic neurons (Pilo Boyl et al. 2007), suggesting that abnormally high levels of profilin IIa may have the inverse effects.

Neuronal-specific profilin has also been implicated in the pathogenesis of other diseases. Fragile X syndrome is a genetic intellectual disability caused by the loss of the RNA-binding Fragile X mental retardation protein (FMRP) (Verkerk et al. 1991; Gibson et al. 1993). dFMRP is the *drosophila* homolog and *dfmr1* mutants are frequently used as a genetic model for Fragile X syndrome (Wan et al. 2000). Analysis of brain extracts from the *dfmr1* mutants identified that dFMRP binds to profilin mRNA and negatively regulates its expression and activity (Reeve et al. 2005). These findings are reminiscent of the increased profilin IIa expression observed in SMA models and of the suggestion that the function of the Smn-profilin IIa interaction is to regulate profilin IIa's inhibitory effects on actin dynamics (Sharma et al. 2005; Bowerman et al. 2007;

Bowerman et al. 2009). In the case of the neurodegenerative Huntington's disease (HD), caused by a polyglutamine expansion in the huntingtin (htt) protein (Group 1993), an inverse relationship with profilin II is found. Indeed, the htt-profilin interaction appears to attenuate htt toxicity (Burnett et al. 2008; Shao et al. 2008). Profilin protein levels and activity are significantly decreased in various models of HD and the overexpression of profilin rescues the aggregation of htt mutants (Burnett et al. 2008; Shao et al. 2008). Importantly, the activity and phosphorylation of profilin is mediated by ROCK and ROCK-inhibition via the Y-27632 synthetic compound has shown promising results as potential therapeutic strategy for HD (Bauer et al. 2009). This supports our hypothesis that the increased profilin IIa expression in SMA is a direct result of increased RhoA/ROCK activity (Bowerman et al. 2007; Bowerman et al. 2009; Bowerman et al. 2010). Together, these various reports highlight the importance of profilin in the regulation of actin dynamics and the overall maintenance of neuronal health.

Consequential effects of decreased activity of the Cdc42 pathway at the NMJ

Our PC12 study identifies a decrease in total expression and activity of the small Rho GTPase Cdc42 (Bowerman et al. 2007). Furthermore, we have preliminary data demonstrating that brain and spinal cord extracts from $Smn^{2B/-}$ mice display significantly less Cdc42-GTP than wild type littermates. While our attempts at modulating Cdc42 *in vivo* have so far been unsuccessful, its important role in NMJ development warrants that it should remain a potential therapeutic target for SMA. In the pre-synaptic compartment of the *drosophila* NMJ, Cdc42-dependent actin dynamics regulate synaptic growth through the endocytosis of activated growth signal receptors (Rodal et al. 2008). Cdc42 is also involved in postsynaptic organization of

acetylcholine receptors (AchRs) (Weston et al. 2000), an essential step in normal maturation and function of the endplate component of the NMJ (reviewed in (Sanes et al. 2001)). Indeed, inactivation of Cdc42 in muscle cells significantly decreased the clustering of AchRs (Weston et al. 2000). Thus, the impaired development, maturation and function of NMJs in SMA (Kariya et al. 2008; Murray et al. 2008; Kong et al. 2009; Bowerman et al. 2012a) may be the result, at least in part, of diminished pre- and postsynaptic Cdc42 activity.

Consequential effects of increased activity of the RhoA/ROCK pathway at the NMJ

One of our seminal discoveries is that the RhoA (RhoA-GTP)/ROCK pathway is significantly upregulated in Smn-depleted cellular and animal models (Bowerman et al. 2007; Bowerman et al. 2010). A recent study further identifies phosphorylation changes of ROCK downstream effectors in SMA cellular models (Nolle et al. 2011). The role of RhoA in neuronal outgrowth and differentiation has been extensively studied (Govek et al. 2005; Luo et al. 2005). However, examination of SMA models has shown that the motor axons are initially able to reach and form the NMJ, followed by a dying-back pathology (Murray et al. 2010b; Ling et al. 2011). It is thus most likely that the pathological effects of the upregulated RhoA/ROCK pathway impact NMJ stability and maintenance.

How RhoA and ROCK mediate NMJ formation and development is presently not fully understood. RhoA is activated by guanine nucleotide exchange factors (GEFs) and inactivated by GTPase-activating proteins (GAPs) and guanine nucleotide dissociation inhibitors (GDIs) (Schmidt et al. 2002; Bernards et al. 2004; DerMardirossian et al. 2005). The functional characterization of RhoA-GEFs, -GAPs and GDIs shows that activated RhoA generally plays an

inhibitory role at pre-synaptic compartment of the NMJ. In hippocampal neurons, the activation of RhoA via the GEF Ephexin 5 decreases synaptic number (Margolis et al. 2010) while p190RhoGAP attenuates RhoA's negative effect on synaptic stability (Sfakianos et al. 2007). In *C. elegans*, the RhoA-specific domain of UNC-73, RhoGEF-2, appears to play a unique role in the regulation of synaptic neurotransmission at the NMJ independently of axon guidance functions (Steven et al. 2005). Pre-synaptic functions of the RhoA/ROCK pathway can also be derived from studies of their downstream effectors. LIM kinase is phosphorylated by ROCK (Maekawa et al. 1999) and an investigation of *drosophila* NMJs demonstrates that increased p-LIMK results in stunted pre-synaptic terminals and a decrease in the number of synaptic boutons (Ang et al. 2006). Together, these results suggest that the activated RhoA/ROCK pathway in SMA may be an important player in the loss of synaptic function and stability observed at the NMJs of SMA models (Chang et al. 2008; Kariya et al. 2008; Murray et al. 2008; Kong et al. 2009).

Within the postsynaptic NMJ compartment, various reports propose conflicting roles for the RhoA/ROCK pathway. On one hand, RhoA activity appears to be required for normal postsynaptic formation, maintenance and AchR maturation from a plaque to pretzel morhphology (Ling et al. 2004; Shi et al. 2010). In contrast, increased p-cofilin expression, a downstream effector of ROCK (Sumi et al. 1999), significantly decreased vesicular trafficking and clustering of AchRs in *Xenopus* NMJs (Lee et al. 2009). Thus, present knowledge of RhoA/ROCK's function on postsynaptic NMJ development remains limited. The effects of RhoA and ROCK may be dependent on specific developmental stages and localization requirements. There also may be a need for the active cycling of RhoA-GDP and RhoA-GTP,

which may be inhibited in SMA, resulting in a permanent overexpression of RhoA-GTP (Bowerman et al. 2007; Bowerman et al. 2010). Clearly, a better understanding of the RhoA/ROCK pathway in the pre-synaptic and postsynaptic NMJ compartments and in SMA-afflicted tissues and cells is of utmost importance. Nevertheless, we have shown that targeting of the misregulated RhoA/ROCK pathway, via the ROCK inhibitors Y-27632 and Fasudil, is a valuable therapeutic strategy for SMA and supports the pathogenic role of this pathway in SMA (Bowerman et al. 2010; Bowerman et al. 2012b).

Consequential effects of the general perturbation of actin organization and localization at the NMJ

The common link between profilin IIa, plastin 3, Cdc42 and RhoA is that they all modulate actin cytoskeletal dynamics. Importantly, the normal organization and localization of actin is affected in various SMA models (Rossoll et al. 2003; Bowerman et al. 2007; van Bergeijk et al. 2007; Nolle et al. 2011), supporting our proposed model of a general misregulation of actin dynamics upon SMN loss (Bowerman et al. 2009). The perturbed regulation of actin could have dire effects on the synaptic stability and maintenance of SMA NMJs seeing that it is the most abundant cytoskeletal protein in the synapses of mature neurons. (Matus et al. 1982; Hirokawa et al. 1989). Furthermore, actin modulates various pre-synaptic pathways such as maintenance and regulation of synaptic vesicle pools, the mobility of vesicles, neurotransmitter release, and axonal vesicle trafficking (Cole et al. 2000; Sakaba et al. 2003; Dillon et al. 2005; Jordan et al. 2005; Shtrahman et al. 2005; Darcy et al. 2006). Interestingly, many of these pathways are negatively affected in SMA models (Kong et al. 2009; Akten et al.

2011; Dale et al. 2011; Torres-Benito et al. 2011). While the core of our work has focused on actin dynamics in neuronal cells, we have recently identified that actin cytoskeletal dynamics regulators are also misregulated in skeletal muscle (Bowerman et al. 2012b). The actin cytoskeleton is a key player in the stabilization and organization of AchRs in muscle (Dai et al. 2000) and its inappropriate modulation may be responsible for the immature morphology and composition of SMA endplates (Murray et al. 2008; Kong et al. 2009; Bowerman et al. 2012a).

In summary, we have identified multiple important actin regulators (profilin IIa, plastin 3, Cdc42 and RhoA) that are misregulated in SMA cellular and animal models (Bowerman et al. 2007; Bowerman et al. 2009; Bowerman et al. 2010). This could lead to a general deregulation of actin cytoskeletal dynamics in the pre- and postsynaptic compartments of the NMJ, followed by the loss of NMJ function and maintenance and eventually, motor neuron degeneration. Importantly, we have identified ROCK inhibitors as a beneficial and Smn-independent therapeutic strategy for SMA (Bowerman et al. 2010; Bowerman et al. 2012b).

SMN AND THE PANCREAS: IMPLICATIONS FOR SMA PATHOGENESIS

In Chapter 6, we describe the seminal discovery and characterization of a role for the SMN protein in pancreatic islet development and glucose homeostasis leading to morphological and functional consequences in SMA mice and type 1 SMA patients (Bowerman et al. 2012c). Interestingly, other neurodegenerative diseases are also characterized by symptoms of metabolic disorders. Indeed, numerous studies suggest a role for impaired glucose uptake and insulin resistance in the pathology and progression of Alzheimer's disease (AD) (Dodart et al. 1999; de la Monte et al. 2008). Recently, an analysis of a mouse model of Prader Willi syndrome, a rare

genetic neurodevelopmental disorder (Cassidy et al. 2011), revealed hypoinsulinemia and hypoglucagonemia due to increased apoptosis of α and β pancreatic cells (Stefan et al. 2011). Although the mechanisms that lead to the glucose homeostatis perturbations vary significantly between these various pathologies, their occurrences support the idea that the pathological hallmarks of a specific disease may involve more than one organ and/or compartment, albeit with different severities and functional consequences.

Our data suggests that the role of Smn in the pancreas is in the maintenance of β cell identity (Bowerman et al. 2012c), although the specific molecular pathways regulated by Smn remain to be identified and characterized. It is also not clear if the primary defect is the impaired glucose homeostasis or the dramatic increase in α cells. Indeed, glucagon secretion and glucagon receptor expression are influenced by glucose (Svoboda et al. 1999; Rorsman et al. 2008; Walker et al. 2011) while glucagon's major function is in hepatic glucose production (D'Alessio 2011). Finally, seeing that our understanding of SMN's role in the pancreas is at its mere beginning, it will be important to determine if the pancreatic and glucose metabolism defects are SMA-independent or -dependent. Future studies of SMA patients afflicted with ranging severities as well as of carriers of *SMN1* mutations and/or deletions will be crucial to decipher the relationship between SMN loss and pancreatic function.

The major theme throughout our work has been that SMN plays a role in the regulation of actin dynamics in the context of neuronal cells (**Figure 8.1**). The regulation of the actin cytoskeleton, however, is crucial to the functioning of all cells, including those within pancreatic islets (Howell et al. 1986). Cdc42 is expressed in β cells (Kowluru et al. 1994) and its activation

is an essential step in the glucose-stimulated actin reorganization in β cells required for insulin secretion (Nevins et al. 2003; Wang et al. 2007). In addition, Cdc42 mediates the vesicle fusion and exocytosis of insulin secretory granules (Nevins et al. 2005). RhoA is also present in β cells where the activation of the RhoA/ROCK inhibits glucose-stimulated insulin secretion and insulin gene transcription (Nakamura et al. 2006; Hammar et al. 2009). While the role of pancreatic profilin has not yet been defined, it was found to be significantly upregulated in pancreatic islets from the *lep/lep* obese mouse model characterized by impaired glucose metabolism such as hyperglycemia and glucose intolerance (Sanchez et al. 2002). Together, these data suggest that the regulation of actin cytoskeletal dynamics is very important for islet cell function. Although it still remains unclear if and how SMN depletion affect actin dynamics in the pancreas, it may influence, at least in part, the progressive increase in glucagon-producing α cells at the expense of insulin-producing β cells (**Figure 8.1**).

The idea that the SMN protein plays a role in pancreatic development and regulation of glucose metabolism is only at its beginning and future studies will be key to provide a better understanding of the molecular pathways modulated by SMN in pancreatic islets. Nevertheless, our study will doubtless ignite these experimental endeavors and benefit both the research fields of SMA and metabolism.

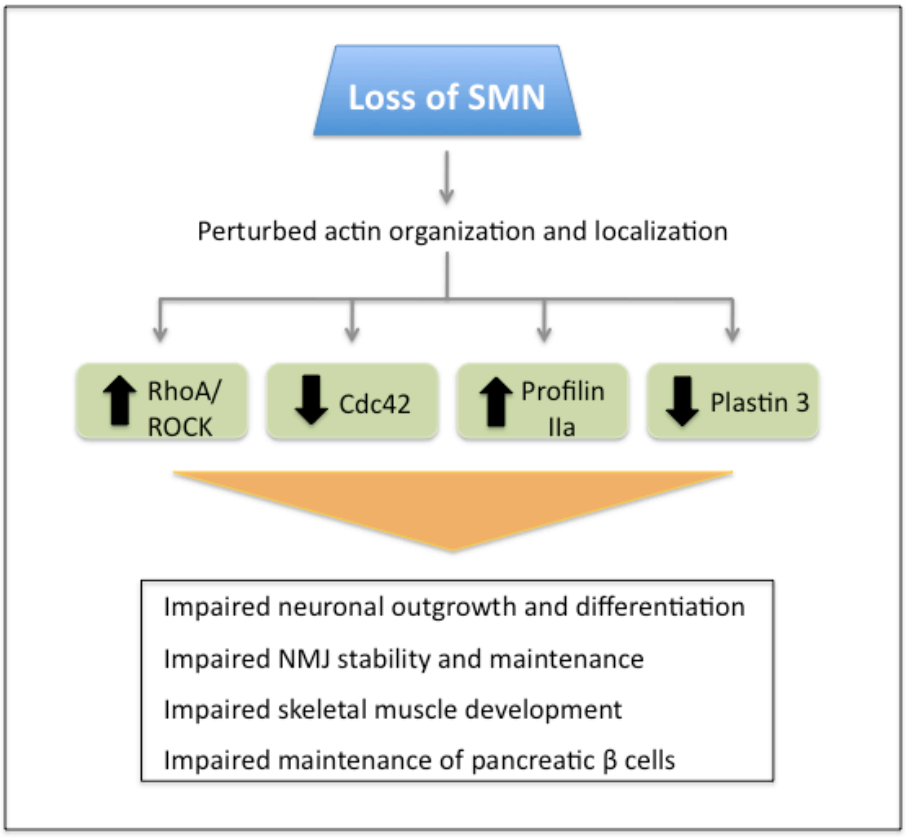

Figure 8.1. A proposed model of how SMN depletion affects upstream and downstream effectors of actin dynamics, subsequently impairing various cell types and compartments involved in SMA pathogenesis. Loss of SMN alters the general organization and localization of actin. Furthermore, SMN depletion results in increased activity of the RhoA/ROCK pathway, decreased activity of the Cdc42 pathway, increased profilin IIa expression and decreased plastin 3 expression. These defects in actin cytoskeletal dynamics could thus influence the functionality and maintenance motor neuron axons, NMJs, skeletal muscle and pancreatic β cells. Indeed, the actin cytoskeleton plays a crucial role in all these cells and/or tissues, which are severely affected in SMA.

REFERENCES

Aarts, L. H., L. H. Schrama, W. J. Hage, J. L. Bos, W. H. Gispen and P. Schotman (1998). "B-50/GAP-43-induced formation of filopodia depends on Rho-GTPase." *Mol Biol Cell* 9(6): 1279-92.

Ackermann, M. and A. Matus (2003). "Activity-induced targeting of profilin and stabilization of dendritic spine morphology." *Nat Neurosci* 6(11): 1194-200.

Akten, B., M. J. Kye, T. Hao le, M. H. Wertz, S. Singh, D. Nie, J. Huang, T. T. Merianda, J. L. Twiss, C. E. Beattie, J. A. Steen and M. Sahin (2011). "Interaction of survival of motor neuron (SMN) and HuD proteins with mRNA cpg15 rescues motor neuron axonal deficits." *Proc Natl Acad Sci U S A* 108(25): 10337-42.

Amano, M., M. Ito, K. Kimura, Y. Fukata, K. Chihara, T. Nakano, Y. Matsuura and K. Kaibuchi (1996). "Phosphorylation and activation of myosin by Rho-associated kinase (Rho-kinase)." *J Biol Chem* 271(34): 20246-9.

Amano, M., M. Nakayama and K. Kaibuchi (2010). "Rho-kinase/ROCK: A key regulator of the cytoskeleton and cell polarity." *Cytoskeleton (Hoboken)* 67(9): 545-54.

Anderson, K. N., D. Baban, P. L. Oliver, A. Potter and K. E. Davies (2004). "Expression profiling in spinal muscular atrophy reveals an RNA binding protein deficit." *Neuromuscul Disord* 14(11): 711-22.

Ang, L. H., W. Chen, Y. Yao, R. Ozawa, E. Tao, J. Yonekura, T. Uemura, H. Keshishian and H. Hing (2006). "Lim kinase regulates the development of olfactory and neuromuscular synapses." *Dev Biol* 293(1): 178-90.

Aoki, K., T. Nakamura and M. Matsuda (2004). "Spatio-temporal regulation of Rac1 and Cdc42 activity during nerve growth factor-induced neurite outgrowth in PC12 cells." *J Biol Chem* 279(1): 713-9.

Arber, S., F. A. Barbayannis, H. Hanser, C. Schneider, C. A. Stanyon, O. Bernard and P. Caroni (1998). "Regulation of actin dynamics through phosphorylation of cofilin by LIM-kinase." *Nature* 393(6687): 805-9.

Arnold, A. S., M. Gueye, S. Guettier-Sigrist, I. Courdier-Fruh, G. Coupin, P. Poindron and J. P. Gies (2004). "Reduced expression of nicotinic AChRs in myotubes from spinal muscular atrophy I patients." *Lab Invest* 84(10): 1271-8.

Avila, A. M., B. G. Burnett, A. A. Taye, F. Gabanella, M. A. Knight, P. Hartenstein, Z. Cizman, N. A. Di Prospero, L. Pellizzoni, K. H. Fischbeck and C. J. Sumner (2007). "Trichostatin A increases SMN expression and survival in a mouse model of spinal muscular atrophy." *J Clin Invest* 117(3): 659-71.

Azios, N. G., L. Krishnamoorthy, M. Harris, L. A. Cubano, M. Cammer and S. F. Dharmawardhane (2007). "Estrogen and resveratrol regulate Rac and Cdc42 signaling to the actin cytoskeleton of metastatic breast cancer cells." *Neoplasia* 9(2): 147-58.

Azzouz, M., T. Le, G. S. Ralph, L. Walmsley, U. R. Monani, D. C. Lee, F. Wilkes, K. A. Mitrophanous, S. M. Kingsman, A. H. Burghes and N. D. Mazarakis (2004). "Lentivector-mediated SMN replacement in a mouse model of spinal muscular atrophy." *J Clin Invest* 114(12): 1726-31.

Barris, R. W. (1953). "Hyperinsulinism and neuromuscular disorders; a consideration of the association of pancreatic adenoma with wasting states." *Calif Med* 78(3): 224-6.
Bauer, P. O., H. K. Wong, F. Oyama, A. Goswami, M. Okuno, Y. Kino, H. Miyazaki and N. Nukina (2009). "Inhibition of Rho kinases enhances the degradation of mutant huntingtin." *J Biol Chem* 284(19): 13153-64.
Baumer, D., S. Lee, G. Nicholson, J. L. Davies, N. J. Parkinson, L. M. Murray, T. H. Gillingwater, O. Ansorge, K. E. Davies and K. Talbot (2009). "Alternative splicing events are a late feature of pathology in a mouse model of spinal muscular atrophy." *PLoS Genet* 5(12): e1000773.
Bechade, C., P. Rostaing, C. Cisterni, R. Kalisch, V. La Bella, B. Pettmann and A. Triller (1999). "Subcellular distribution of survival motor neuron (SMN) protein: possible involvement in nucleocytoplasmic and dendritic transport." *Eur J Neurosci* 11(1): 293-304.
Benowitz, L. I. and A. Routtenberg (1997). "GAP-43: an intrinsic determinant of neuronal development and plasticity." *Trends Neurosci* 20(2): 84-91.
Bergin, A., G. Kim, D. L. Price, S. S. Sisodia, M. K. Lee and B. A. Rabin (1997). "Identification and characterization of a mouse homologue of the spinal muscular atrophy-determining gene, survival motor neuron." *Gene* 204(1-2): 47-53.
Bernal, S., E. Also-Rallo, R. Martinez-Hernandez, L. Alias, F. J. Rodriguez-Alvarez, J. M. Millan, C. Hernandez-Chico, M. Baiget and E. F. Tizzano (2011). "Plastin 3 expression in discordant spinal muscular atrophy (SMA) siblings." *Neuromuscul Disord* 21(6): 413-9.
Bernards, A. and J. Settleman (2004). "GAP control: regulating the regulators of small GTPases." *Trends Cell Biol* 14(7): 377-85.
Bevan, A. K., K. R. Hutchinson, K. D. Foust, L. Braun, V. L. McGovern, L. Schmelzer, J. G. Ward, J. C. Petruska, P. A. Lucchesi, A. H. Burghes and B. K. Kaspar (2010). "Early heart failure in the SMNDelta7 model of spinal muscular atrophy and correction by postnatal scAAV9-SMN delivery." *Hum Mol Genet* 19(20): 3895-905.
Bi, J., N. P. Tsai, H. Y. Lu, H. H. Loh and L. N. Wei (2007). "Copb1-facilitated axonal transport and translation of kappa opioid-receptor mRNA." *Proc Natl Acad Sci U S A* 104(34): 13810-5.
Birbach, A. (2008). "Profilin, a multi-modal regulator of neuronal plasticity." *Bioessays* 30(10): 994-1002.
Bloom, O., E. Evergren, N. Tomilin, O. Kjaerulff, P. Low, L. Brodin, V. A. Pieribone, P. Greengard and O. Shupliakov (2003). "Colocalization of synapsin and actin during synaptic vesicle recycling." *J Cell Biol* 161(4): 737-47.
Boda, B., C. Mas, C. Giudicelli, V. Nepote, F. Guimiot, B. Levacher, A. Zvara, M. Santha, I. LeGall and M. Simonneau (2004). "Survival motor neuron SMN1 and SMN2 gene promoters: identical sequences and differential expression in neurons and non-neuronal cells." *Eur J Hum Genet* 12(9): 729-37.
Boettner, B. and L. Van Aelst (2002). "The role of Rho GTPases in disease development." *Gene* 286(2): 155-74.
Boon, K. L., S. Xiao, M. L. McWhorter, T. Donn, E. Wolf-Saxon, M. T. Bohnsack, C. B. Moens and C. E. Beattie (2009). "Zebrafish survival motor neuron mutants exhibit presynaptic neuromuscular junction defects." *Hum Mol Genet* 18(19): 3615-25.

Bosch-Marce, M., C. D. Wee, T. L. Martinez, C. E. Lipkes, D. W. Choe, L. Kong, J. P. Van Meerbeke, A. Musaro and C. J. Sumner (2011). "Increased IGF-1 in muscle modulates the phenotype of severe SMA mice." *Hum Mol Genet* 20(9): 1844-53.

Bosco, D., M. Armanet, P. Morel, N. Niclauss, A. Sgroi, Y. D. Muller, L. Giovannoni, G. Parnaud and T. Berney (2010). "Unique arrangement of alpha- and beta-cells in human islets of Langerhans." *Diabetes* 59(5): 1202-10.

Bowerman, M., D. Shafey and R. Kothary (2007). "Smn depletion alters profilin II expression and leads to upregulation of the RhoA/ROCK pathway and defects in neuronal integrity." *J Mol Neurosci* 32(2): 120-31.

Bowerman, M., C. L. Anderson, A. Beauvais, P. P. Boyl, W. Witke and R. Kothary (2009). "SMN, profilin IIa and plastin 3: a link between the deregulation of actin dynamics and SMA pathogenesis." *Mol Cell Neurosci* 42(1): 66-74.

Bowerman, M., A. Beauvais, C. L. Anderson and R. Kothary (2010). "Rho-kinase inactivation prolongs survival of an intermediate SMA mouse model." *Hum Mol Genet* 19(8): 1468-78.

Bowerman, M., L. M. Murray, A. Beauvais, B. Pinheiro and R. Kothary (2012a). "A critical Smn threshold in mice dictates onset of an intermediate Spinal Muscular Atrophy phenotype associated with a distinct neuromuscular junction pathology." *Neuromus Dis* 22: 263-276.

Bowerman, M., L. M. Murray, J. G. Boyer, C. L. Anderson and R. Kothary (2012b). "Fasudil improves survival and promotes skeletal muscle development in a mouse model of spinal muscular atrophy." *BMC Med* 10(1): 24.

Bowerman, M., K. J. Swoboda, J. P. Michalski, G. S. Wang, C. Reeks, A. Beauvais, K. Murphy, J. Woulfe, R. A. Screaton, F. W. Scott and R. Kothary (2012c). "Glucose metabolism and pancreatic defects in Spinal Muscular Atrophy." *Ann Neurol*.

Boyer, J., M. Bowerman and R. Kothary (2010). "The many faces of SMN: deciphering the function critical to spinal muscular atrophy pathogenesis." *Future Neurology* 5(6): 873-890.

Bray, D. and K. Chapman (1985). "Analysis of microspike movements on the neuronal growth cone." *J Neurosci* 5(12): 3204-13.

Bretscher, A. (1981). "Fimbrin is a cytoskeletal protein that crosslinks F-actin in vitro." *Proc Natl Acad Sci U S A* 78(11): 6849-53.

Briese, M., B. Esmaeili and D. B. Sattelle (2005). "Is spinal muscular atrophy the result of defects in motor neuron processes?" *Bioessays* 27(9): 946-57.

Briese, M., D. U. Richter, D. B. Sattelle and N. Ulfig (2006). "SMN, the product of the spinal muscular atrophy-determining gene, is expressed widely but selectively in the developing human forebrain." *J Comp Neurol* 497(5): 808-16.

Briese, M., B. Esmaeili, S. Fraboulet, E. C. Burt, S. Christodoulou, P. R. Towers, K. E. Davies and D. B. Sattelle (2009). "Deletion of smn-1, the Caenorhabditis elegans ortholog of the spinal muscular atrophy gene, results in locomotor dysfunction and reduced lifespan." *Hum Mol Genet* 18(1): 97-104.

Buhler, D., V. Raker, R. Luhrmann and U. Fischer (1999). "Essential role for the tudor domain of SMN in spliceosomal U snRNP assembly: implications for spinal muscular atrophy." *Hum Mol Genet* 8(13): 2351-7.

Burgess, R. W., G. A. Cox and K. L. Seburn (2010). "Neuromuscular disease models and analysis." *Methods Mol Biol* 602: 347-93.
Burglen, L., R. Spiegel, J. Ignatius, J. M. Cobben, P. Landrieu, S. Lefebvre, A. Munnich and J. Melki (1995). "SMN gene deletion in variant of infantile spinal muscular atrophy." *Lancet* 346(8970): 316-7.
Burglen, L., S. Lefebvre, O. Clermont, P. Burlet, L. Viollet, C. Cruaud, A. Munnich and J. Melki (1996). "Structure and organization of the human survival motor neurone (SMN) gene." *Genomics* 32(3): 479-82.
Burlet, P., C. Huber, S. Bertrandy, M. A. Ludosky, I. Zwaenepoel, O. Clermont, J. Roume, A. L. Delezoide, J. Cartaud, A. Munnich and S. Lefebvre (1998). "The distribution of SMN protein complex in human fetal tissues and its alteration in spinal muscular atrophy." *Hum Mol Genet* 7(12): 1927-33.
Burnett, B. G., J. Andrews, S. Ranganathan, K. H. Fischbeck and N. A. Di Prospero (2008). "Expression of expanded polyglutamine targets profilin for degradation and alters actin dynamics." *Neurobiol Dis* 30(3): 365-74.
Butchbach, M. E., J. D. Edwards, K. R. Schussler and A. H. Burghes (2007). "A novel method for oral delivery of drug compounds to the neonatal SMNDelta7 mouse model of spinal muscular atrophy." *J Neurosci Methods* 161(2): 285-90.
Butchbach, M. E., F. F. Rose, Jr., S. Rhoades, J. Marston, J. T. McCrone, R. Sinnott and C. L. Lorson (2010). "Effect of diet on the survival and phenotype of a mouse model for spinal muscular atrophy." *Biochem Biophys Res Commun* 391(1): 835-40.
Cabrera, O., D. M. Berman, N. S. Kenyon, C. Ricordi, P. O. Berggren and A. Caicedo (2006). "The unique cytoarchitecture of human pancreatic islets has implications for islet cell function." *Proc Natl Acad Sci U S A* 103(7): 2334-9.
Cadotte, D. W. and M. G. Fehlings (2011). "Spinal cord injury: a systematic review of current treatment options." *Clin Orthop Relat Res* 469(3): 732-41.
Cao, L. G., G. G. Babcock, P. A. Rubenstein and Y. L. Wang (1992). "Effects of profilin and profilactin on actin structure and function in living cells." *J Cell Biol* 117(5): 1023-9.
Carissimi, C., L. Saieva, J. Baccon, P. Chiarella, A. Maiolica, A. Sawyer, J. Rappsilber and L. Pellizzoni (2006). "Gemin8 is a novel component of the survival motor neuron complex and functions in small nuclear ribonucleoprotein assembly." *J Biol Chem* 281(12): 8126-34.
Carlsson, L., L. E. Nystrom, I. Sundkvist, F. Markey and U. Lindberg (1977). "Actin polymerizability is influenced by profilin, a low molecular weight protein in non-muscle cells." *J Mol Biol* 115(3): 465-83.
Carrel, T. L., M. L. McWhorter, E. Workman, H. Zhang, E. C. Wolstencroft, C. Lorson, G. J. Bassell, A. H. Burghes and C. E. Beattie (2006). "Survival motor neuron function in motor axons is independent of functions required for small nuclear ribonucleoprotein biogenesis." *J Neurosci* 26(43): 11014-22.
Cartaud, A., F. Stetzkowski-Marden, A. Maoui and J. Cartaud (2011). "Agrin triggers the clustering of raft-associated acetylcholine receptors through actin cytoskeleton reorganization." *Biol Cell* 103(6): 287-301.

Cartegni, L. and A. R. Krainer (2002). "Disruption of an SF2/ASF-dependent exonic splicing enhancer in SMN2 causes spinal muscular atrophy in the absence of SMN1." *Nat Genet* 30(4): 377-84.

Cassidy, S. B., S. Schwartz, J. L. Miller and D. J. Driscoll (2011). "Prader-Willi syndrome." *Genet Med*.

Castellani, L., E. Salvati, S. Alema and G. Falcone (2006). "Fine regulation of RhoA and Rock is required for skeletal muscle differentiation." *J Biol Chem* 281(22): 15249-57.

Chan, C. C., K. Khodarahmi, J. Liu, D. Sutherland, L. W. Oschipok, J. D. Steeves and W. Tetzlaff (2005). "Dose-dependent beneficial and detrimental effects of ROCK inhibitor Y27632 on axonal sprouting and functional recovery after rat spinal cord injury." *Exp Neurol* 196(2): 352-64.

Chan, Y. B., I. Miguel-Aliaga, C. Franks, N. Thomas, B. Trulzsch, D. B. Sattelle, K. E. Davies and M. van den Heuvel (2003). "Neuromuscular defects in a Drosophila survival motor neuron gene mutant." *Hum Mol Genet* 12(12): 1367-76.

Chang, H. C., D. N. Dimlich, T. Yokokura, A. Mukherjee, M. W. Kankel, A. Sen, V. Sridhar, T. A. Fulga, A. C. Hart, D. Van Vactor and S. Artavanis-Tsakonas (2008). "Modeling spinal muscular atrophy in Drosophila." *PLoS One* 3(9): e3209.

Chari, A., M. M. Golas, M. Klingenhager, N. Neuenkirchen, B. Sander, C. Englbrecht, A. Sickmann, H. Stark and U. Fischer (2008). "An assembly chaperone collaborates with the SMN complex to generate spliceosomal SnRNPs." *Cell* 135(3): 497-509.

Charroux, B., L. Pellizzoni, R. A. Perkinson, J. Yong, A. Shevchenko, M. Mann and G. Dreyfuss (2000). "Gemin4. A novel component of the SMN complex that is found in both gems and nucleoli." *J Cell Biol* 148(6): 1177-86.

Chen, Q., S. D. Baird, M. Mahadevan, A. Besner-Johnston, R. Farahani, J. Xuan, X. Kang, C. Lefebvre, J. E. Ikeda, R. G. Korneluk and A. E. MacKenzie (1998). "Sequence of a 131-kb region of 5q13.1 containing the spinal muscular atrophy candidate genes SMN and NAIP." *Genomics* 48(1): 121-7.

Chuang, D. M., Y. Leng, Z. Marinova, H. J. Kim and C. T. Chiu (2009). "Multiple roles of HDAC inhibition in neurodegenerative conditions." *Trends Neurosci* 32(11): 591-601.

Cifuentes-Diaz, C., S. Nicole, M. E. Velasco, C. Borra-Cebrian, C. Panozzo, T. Frugier, G. Millet, N. Roblot, V. Joshi and J. Melki (2002). "Neurofilament accumulation at the motor endplate and lack of axonal sprouting in a spinal muscular atrophy mouse model." *Hum Mol Genet* 11(12): 1439-47.

Cingolani, L. A. and Y. Goda (2008). "Actin in action: the interplay between the actin cytoskeleton and synaptic efficacy." *Nat Rev Neurosci* 9(5): 344-56.

Cobben, J. M., G. van der Steege, P. Grootscholten, M. de Visser, H. Scheffer and C. H. Buys (1995). "Deletions of the survival motor neuron gene in unaffected siblings of patients with spinal muscular atrophy." *Am J Hum Genet* 57(4): 805-8.

Cole, J. C., B. R. Villa and R. S. Wilkinson (2000). "Disruption of actin impedes transmitter release in snake motor terminals." *J Physiol* 525 Pt 3: 579-86.

Coleman, M. (2005). "Axon degeneration mechanisms: commonality amid diversity." *Nat Rev Neurosci* 6(11): 889-98.

Coovert, D. D., T. T. Le, P. E. McAndrew, J. Strasswimmer, T. O. Crawford, J. R. Mendell, S. E. Coulson, E. J. Androphy, T. W. Prior and A. H. Burghes (1997). "The survival motor neuron protein in spinal muscular atrophy." *Hum Mol Genet* 6(8): 1205-14.
Corti, S., M. Nizzardo, M. Nardini, C. Donadoni, S. Salani, D. Ronchi, F. Saladino, A. Bordoni, F. Fortunato, R. Del Bo, D. Papadimitriou, F. Locatelli, G. Menozzi, S. Strazzer, N. Bresolin and G. P. Comi (2008). "Neural stem cell transplantation can ameliorate the phenotype of a mouse model of spinal muscular atrophy." *J Clin Invest* 118(10): 3316-30.
Coussen, F., D. Perrais, F. Jaskolski, S. Sachidhanandam, E. Normand, J. Bockaert, P. Marin and C. Mulle (2005). "Co-assembly of two GluR6 kainate receptor splice variants within a functional protein complex." *Neuron* 47(4): 555-66.
Crawford, T. O. and C. A. Pardo (1996). "The neurobiology of childhood spinal muscular atrophy." *Neurobiol Dis* 3(2): 97-110.
Crawford, T. O., J. T. Sladky, O. Hurko, A. Besner-Johnston and R. I. Kelley (1999). "Abnormal fatty acid metabolism in childhood spinal muscular atrophy." *Ann Neurol* 45(3): 337-43.
D'Alessio, D. (2011). "The role of dysregulated glucagon secretion in type 2 diabetes." *Diabetes Obes Metab* 13 Suppl 1: 126-32.
da Silva, J. S. and C. G. Dotti (2002). "Breaking the neuronal sphere: regulation of the actin cytoskeleton in neuritogenesis." *Nat Rev Neurosci* 3(9): 694-704.
Da Silva, J. S., M. Medina, C. Zuliani, A. Di Nardo, W. Witke and C. G. Dotti (2003). "RhoA/ROCK regulation of neuritogenesis via profilin IIa-mediated control of actin stability." *J Cell Biol* 162(7): 1267-79.
Dahl, D. S. and H. A. Peters (1975). "Lipid disturbances associated with spiral muscular atrophy. Clinical, electromyographic, histochemical, and lipid studies." *Arch Neurol* 32(3): 195-203.
Dai, Z., X. Luo, H. Xie and H. B. Peng (2000). "The actin-driven movement and formation of acetylcholine receptor clusters." *J Cell Biol* 150(6): 1321-34.
Dale, J. M., H. Shen, D. M. Barry, V. B. Garcia, F. F. Rose, Jr., C. L. Lorson and M. L. Garcia (2011). "The spinal muscular atrophy mouse model, SMADelta7, displays altered axonal transport without global neurofilament alterations." *Acta Neuropathol* 122(3): 331-41.
Dan, C., N. Nath, M. Liberto and A. Minden (2002). "PAK5, a new brain-specific kinase, promotes neurite outgrowth in N1E-115 cells." *Mol Cell Biol* 22(2): 567-77.
Darcy, K. J., K. Staras, L. M. Collinson and Y. Goda (2006). "Constitutive sharing of recycling synaptic vesicles between presynaptic boutons." *Nat Neurosci* 9(3): 315-21.
Das, K. P., T. M. Freudenrich and W. R. Mundy (2004). "Assessment of PC12 cell differentiation and neurite growth: a comparison of morphological and neurochemical measures." *Neurotoxicol Teratol* 26(3): 397-406.
de la Monte, S. M. and J. R. Wands (2008). "Alzheimer's disease is type 3 diabetes-evidence reviewed." *J Diabetes Sci Technol* 2(6): 1101-13.
de La Vega, L. A. and R. J. Stockert (1999). "The cytoplasmic coatomer protein COPI. A potential translational regulator." *J Biol Chem* 274(44): 31135-8.
DerMardirossian, C. and G. M. Bokoch (2005). "GDIs: central regulatory molecules in Rho GTPase activation." *Trends Cell Biol* 15(7): 356-63.

Dhawan, J. and D. M. Helfman (2004). "Modulation of acto-myosin contractility in skeletal muscle myoblasts uncouples growth arrest from differentiation." *J Cell Sci* 117(Pt 17): 3735-48.
Di Cola, G., M. H. Cool and D. Accili (1997). "Hypoglycemic effect of insulin-like growth factor-1 in mice lacking insulin receptors." *J Clin Invest* 99(10): 2538-44.
Di Nardo, A., R. Gareus, D. Kwiatkowski and W. Witke (2000). "Alternative splicing of the mouse profilin II gene generates functionally different profilin isoforms." *J Cell Sci* 113 Pt 21: 3795-803.
DiDonato, C. J., X. N. Chen, D. Noya, J. R. Korenberg, J. H. Nadeau and L. R. Simard (1997). "Cloning, characterization, and copy number of the murine survival motor neuron gene: homolog of the spinal muscular atrophy-determining gene." *Genome Res* 7(4): 339-52.
DiDonato, C. J., C. L. Lorson, Y. De Repentigny, L. Simard, C. Chartrand, E. J. Androphy and R. Kothary (2001). "Regulation of murine survival motor neuron (Smn) protein levels by modifying Smn exon 7 splicing." *Hum Mol Genet* 10(23): 2727-36.
DiDonato, C. J., R. J. Parks and R. Kothary (2003). "Development of a gene therapy strategy for the restoration of survival motor neuron protein expression: implications for spinal muscular atrophy therapy." *Hum Gene Ther* 14(2): 179-88.
DiDonato, C. J., Hammond, S., Bowerman, M.,Beauvais A., Kothary, R. (2007). SMN: How much is enough? 11th Annual International Spinal Muscular Atrophy Rsearch Group Meeting, Schaumburg.
Dillon, C. and Y. Goda (2005). "The actin cytoskeleton: integrating form and function at the synapse." *Annu Rev Neurosci* 28: 25-55.
Dobbins, G. C., B. Zhang, W. C. Xiong and L. Mei (2006). "The role of the cytoskeleton in neuromuscular junction formation." *J Mol Neurosci* 30(1-2): 115-8.
Dodart, J. C., C. Mathis, K. R. Bales, S. M. Paul and A. Ungerer (1999). "Early regional cerebral glucose hypometabolism in transgenic mice overexpressing the V717F beta-amyloid precursor protein." *Neurosci Lett* 277(1): 49-52.
Dreyfuss, G., M. J. Matunis, S. Pinol-Roma and C. G. Burd (1993). "hnRNP proteins and the biogenesis of mRNA." *Annu Rev Biochem* 62: 289-321.
Dubowitz, V. (1999). "Very severe spinal muscular atrophy (SMA type 0): an expanding clinical phenotype." *Eur J Paediatr Neurol* 3(2): 49-51.
Dutartre, H., J. Davoust, J. P. Gorvel and P. Chavrier (1996). "Cytokinesis arrest and redistribution of actin-cytoskeleton regulatory components in cells expressing the Rho GTPase CDC42Hs." *J Cell Sci* 109 (Pt 2): 367-77.
Eggert, C., A. Chari, B. Laggerbauer and U. Fischer (2006). "Spinal muscular atrophy: the RNP connection." *Trends Mol Med* 12(3): 113-21.
Fallini, C., G. J. Bassell and W. Rossoll (2010). "High-efficiency transfection of cultured primary motor neurons to study protein localization, trafficking, and function." *Mol Neurodegener* 5: 17.
Fan, L. and L. R. Simard (2002). "Survival motor neuron (SMN) protein: role in neurite outgrowth and neuromuscular maturation during neuronal differentiation and development." *Hum Mol Genet* 11(14): 1605-14.
Fifkova, E. and R. J. Delay (1982). "Cytoplasmic actin in neuronal processes as a possible mediator of synaptic plasticity." *J Cell Biol* 95(1): 345-50.

Fischer, U., Q. Liu and G. Dreyfuss (1997). "The SMN-SIP1 complex has an essential role in spliceosomal snRNP biogenesis." *Cell* 90(6): 1023-9.
Fortier, M., F. Comunale, J. Kucharczak, A. Blangy, S. Charrasse and C. Gauthier-Rouviere (2008). "RhoE controls myoblast alignment prior fusion through RhoA and ROCK." *Cell Death Differ* 15(8): 1221-31.
Fournier, A. E., B. T. Takizawa and S. M. Strittmatter (2003). "Rho kinase inhibition enhances axonal regeneration in the injured CNS." *J Neurosci* 23(4): 1416-23.
Foust, K. D., X. Wang, V. L. McGovern, L. Braun, A. K. Bevan, A. M. Haidet, T. T. Le, P. R. Morales, M. M. Rich, A. H. Burghes and B. K. Kaspar (2010). "Rescue of the spinal muscular atrophy phenotype in a mouse model by early postnatal delivery of SMN." *Nat Biotechnol* 28(3): 271-4.
Fox-Walsh, K. L. and K. J. Hertel (2009). "Splice-site pairing is an intrinsically high fidelity process." *Proc Natl Acad Sci U S A* 106(6): 1766-71.
Fu, A., A. C. Ng, C. Depatie, N. Wijesekara, Y. He, G. S. Wang, N. Bardeesy, F. W. Scott, R. M. Touyz, M. B. Wheeler and R. A. Screaton (2009). "Loss of Lkb1 in adult beta cells increases beta cell mass and enhances glucose tolerance in mice." *Cell Metab* 10(4): 285-95.
Fukumoto, Y., T. Matoba, A. Ito, H. Tanaka, T. Kishi, S. Hayashidani, K. Abe, A. Takeshita and H. Shimokawa (2005). "Acute vasodilator effects of a Rho-kinase inhibitor, fasudil, in patients with severe pulmonary hypertension." *Heart* 91(3): 391-2.
Gabanella, F., M. E. Butchbach, L. Saieva, C. Carissimi, A. H. Burghes and L. Pellizzoni (2007). "Ribonucleoprotein assembly defects correlate with spinal muscular atrophy severity and preferentially affect a subset of spliceosomal snRNPs." *PLoS ONE* 2(9): e921.
Gareus, R., A. Di Nardo, V. Rybin and W. Witke (2006). "Mouse profilin 2 regulates endocytosis and competes with SH3 ligand binding to dynamin 1." *J Biol Chem* 281(5): 2803-11.
Gaudreault, S. B., J. F. Blain, J. P. Gratton and J. Poirier (2005). "A role for caveolin-1 in post-injury reactive neuronal plasticity." *J Neurochem* 92(4): 831-9.
Gavrilina, T. O., V. L. McGovern, E. Workman, T. O. Crawford, R. G. Gogliotti, C. J. DiDonato, U. R. Monani, G. E. Morris and A. H. Burghes (2008). "Neuronal SMN expression corrects spinal muscular atrophy in severe SMA mice while muscle-specific SMN expression has no phenotypic effect." *Hum Mol Genet* 17(8): 1063-75.
Gennarelli, M., M. Lucarelli, F. Capon, A. Pizzuti, L. Merlini, C. Angelini, G. Novelli and B. Dallapiccola (1995). "Survival motor neuron gene transcript analysis in muscles from spinal muscular atrophy patients." *Biochem Biophys Res Commun* 213(1): 342-8.
Gertler, F. B., K. Niebuhr, M. Reinhard, J. Wehland and P. Soriano (1996). "Mena, a relative of VASP and Drosophila Enabled, is implicated in the control of microfilament dynamics." *Cell* 87(2): 227-39.
Giavazzi, A., V. Setola, A. Simonati and G. Battaglia (2006). "Neuronal-specific roles of the survival motor neuron protein: evidence from survival motor neuron expression patterns in the developing human central nervous system." *J Neuropathol Exp Neurol* 65(3): 267-77.

Gibson, T. J., P. M. Rice, J. D. Thompson and J. Heringa (1993). "KH domains within the FMR1 sequence suggest that fragile X syndrome stems from a defect in RNA metabolism." *Trends Biochem Sci* 18(9): 331-3.

Giesemann, T., S. Rathke-Hartlieb, M. Rothkegel, J. W. Bartsch, S. Buchmeier, B. M. Jockusch and H. Jockusch (1999). "A role for polyproline motifs in the spinal muscular atrophy protein SMN. Profilins bind to and colocalize with smn in nuclear gems." *J Biol Chem* 274(53): 37908-14.

Gifondorwa, D. J., M. B. Robinson, C. D. Hayes, A. R. Taylor, D. M. Prevette, R. W. Oppenheim, J. Caress and C. E. Milligan (2007). "Exogenous delivery of heat shock protein 70 increases lifespan in a mouse model of amyotrophic lateral sclerosis." *J Neurosci* 27(48): 13173-80.

Giganti, A., J. Plastino, B. Janji, M. Van Troys, D. Lentz, C. Ampe, C. Sykes and E. Friederich (2005). "Actin-filament cross-linking protein T-plastin increases Arp2/3-mediated actin-based movement." *J Cell Sci* 118(Pt 6): 1255-65.

Gillingwater, T. H. and R. R. Ribchester (2001). "Compartmental neurodegeneration and synaptic plasticity in the Wld(s) mutant mouse." *J Physiol* 534(Pt 3): 627-39.

Gillingwater, T. H. and R. R. Ribchester (2003). "The relationship of neuromuscular synapse elimination to synaptic degeneration and pathology: insights from WldS and other mutant mice." *J Neurocytol* 32(5-8): 863-81.

Gimona, M., K. Djinovic-Carugo, W. J. Kranewitter and S. J. Winder (2002). "Functional plasticity of CH domains." *FEBS Lett* 513(1): 98-106.

Girard, J. P., H. Lehtonen, M. Caizergues-Ferrer, F. Amalric, D. Tollervey and B. Lapeyre (1992). "GAR1 is an essential small nucleolar RNP protein required for pre-rRNA processing in yeast." *EMBO J* 11(2): 673-82.

Gladman, J. T., T. W. Bebee, C. Edwards, X. Wang, Z. Sahenk, M. M. Rich and D. S. Chandler (2010). "A humanized Smn gene containing the SMN2 nucleotide alteration in exon 7 mimics SMN2 splicing and the SMA disease phenotype." *Hum Mol Genet* 19(21): 4239-52.

Glenney, J. R., Jr., P. Kaulfus, P. Matsudaira and K. Weber (1981). "F-actin binding and bundling properties of fimbrin, a major cytoskeletal protein of microvillus core filaments." *J Biol Chem* 256(17): 9283-8.

Glinka, M., T. Herrmann, N. Funk, S. Havlicek, W. Rossoll, C. Winkler and M. Sendtner (2010). "The heterogeneous nuclear ribonucleoprotein-R is necessary for axonal beta-actin mRNA translocation in spinal motor neurons." *Hum Mol Genet* 19(10): 1951-66.

Gogliotti, R. G., C. Lutz, M. Jorgensen, K. Huebsch, S. Koh and C. J. Didonato (2011). "Characterization of a commonly used mouse model of SMA reveals increased seizure susceptibility and heightened fear response in FVB/N mice." *Neurobiol Dis* 43(1): 142-51.

Gonsalvez, G. B., L. Tian, J. K. Ospina, F. M. Boisvert, A. I. Lamond and A. G. Matera (2007). "Two distinct arginine methyltransferases are required for biogenesis of Sm-class ribonucleoproteins." *J Cell Biol* 178(5): 733-40.

Govek, E. E., S. E. Newey and L. Van Aelst (2005). "The role of the Rho GTPases in neuronal development." *Genes Dev* 19(1): 1-49.

Greene, L. A. and A. S. Tischler (1976). "Establishment of a noradrenergic clonal line of rat adrenal pheochromocytoma cells which respond to nerve growth factor." *Proc Natl Acad Sci U S A* 73(7): 2424-8.

Group, T. H. s. D. C. R. (1993). "A novel gene containing a trinucleotide repeat that is expanded and unstable on Huntington's disease chromosomes. The Huntington's Disease Collaborative Research Group." *Cell* 72(6): 971-83.

Gu, W., F. Pan, H. Zhang, G. J. Bassell and R. H. Singer (2002). "A predominantly nuclear protein affecting cytoplasmic localization of beta-actin mRNA in fibroblasts and neurons." *J Cell Biol* 156(1): 41-51.

Hahnen, E., R. Forkert, C. Marke, S. Rudnik-Schoneborn, J. Schonling, K. Zerres and B. Wirth (1995). "Molecular analysis of candidate genes on chromosome 5q13 in autosomal recessive spinal muscular atrophy: evidence of homozygous deletions of the SMN gene in unaffected individuals." *Hum Mol Genet* 4(10): 1927-33.

Hahnen, E., J. Schonling, S. Rudnik-Schoneborn, H. Raschke, K. Zerres and B. Wirth (1997). "Missense mutations in exon 6 of the survival motor neuron gene in patients with spinal muscular atrophy (SMA)." *Hum Mol Genet* 6(5): 821-5.

Hall, A. (1998). "Rho GTPases and the actin cytoskeleton." *Science* 279(5350): 509-14.

Hammar, E., A. Tomas, D. Bosco and P. A. Halban (2009). "Role of the Rho-ROCK (Rho-associated kinase) signaling pathway in the regulation of pancreatic beta-cell function." *Endocrinology* 150(5): 2072-9.

Hammond, S. M., R. G. Gogliotti, V. Rao, A. Beauvais, R. Kothary and C. J. Didonato (2010). "Mouse Survival Motor Neuron Alleles That Mimic SMN2 Splicing and Are Inducible Rescue Embryonic Lethality Early in Development but Not Late." *PLoS One* 5(12): e15887.

Hasty, P., A. Bradley, J. H. Morris, D. G. Edmondson, J. M. Venuti, E. N. Olson and W. H. Klein (1993). "Muscle deficiency and neonatal death in mice with a targeted mutation in the myogenin gene." *Nature* 364(6437): 501-6.

Hayashi, M., S. Araki, N. Arai, S. Kumada, M. Itoh, K. Tamagawa, M. Oda and Y. Morimatsu (2002). "Oxidative stress and disturbed glutamate transport in spinal muscular atrophy." *Brain Dev* 24(8): 770-5.

Heier, C. R., R. Satta, C. Lutz and C. J. DiDonato (2010). "Arrhythmia and cardiac defects are a feature of spinal muscular atrophy model mice." *Hum Mol Genet* 19(20): 3906-18.

Hinman, M. N. and H. Lou (2008). "Diverse molecular functions of Hu proteins." *Cell Mol Life Sci* 65(20): 3168-81.

Hirokawa, N., K. Sobue, K. Kanda, A. Harada and H. Yorifuji (1989). "The cytoskeletal architecture of the presynaptic terminal and molecular structure of synapsin 1." *J Cell Biol* 108(1): 111-26.

Hirose, M., T. Ishizaki, N. Watanabe, M. Uehata, O. Kranenburg, W. H. Moolenaar, F. Matsumura, M. Maekawa, H. Bito and S. Narumiya (1998). "Molecular dissection of the Rho-associated protein kinase (p160ROCK)-regulated neurite remodeling in neuroblastoma N1E-115 cells." *J Cell Biol* 141(7): 1625-36.

Howell, S. L. and M. Tyhurst (1986). "The cytoskeleton and insulin secretion." *Diabetes Metab Rev* 2(1-2): 107-23.

Hsieh-Li, H. M., J. G. Chang, Y. J. Jong, M. H. Wu, N. M. Wang, C. H. Tsai and H. Li (2000). "A mouse model for spinal muscular atrophy." *Nat Genet* 24(1): 66-70.
Huang, S. and M. P. Czech (2007). "The GLUT4 glucose transporter." *Cell Metab* 5(4): 237-52.
Ishizaki, T., M. Uehata, I. Tamechika, J. Keel, K. Nonomura, M. Maekawa and S. Narumiya (2000). "Pharmacological properties of Y-27632, a specific inhibitor of rho-associated kinases." *Mol Pharmacol* 57(5): 976-83.
Jablonka, S., B. Schrank, M. Kralewski, W. Rossoll and M. Sendtner (2000). "Reduced survival motor neuron (Smn) gene dose in mice leads to motor neuron degeneration: an animal model for spinal muscular atrophy type III." *Hum Mol Genet* 9(3): 341-6.
Jae, N., C. Preusser, T. Kruger, I. D. Tkacz, M. Engstler, S. Michaeli and A. Bindereif (2011). "snRNA-specific role of SMN in trypanosome snRNP biogenesis in vivo." *RNA Biol* 8(1): 90-100.
Javaherian, A. and H. T. Cline (2005). "Coordinated motor neuron axon growth and neuromuscular synaptogenesis are promoted by CPG15 in vivo." *Neuron* 45(4): 505-12.
Jones, K. W., K. Gorzynski, C. M. Hales, U. Fischer, F. Badbanchi, R. M. Terns and M. P. Terns (2001). "Direct interaction of the spinal muscular atrophy disease protein SMN with the small nucleolar RNA-associated protein fibrillarin." *J Biol Chem* 276(42): 38645-51.
Jordan, R., E. A. Lemke and J. Klingauf (2005). "Visualization of synaptic vesicle movement in intact synaptic boutons using fluorescence fluctuation spectroscopy." *Biophys J* 89(3): 2091-102.
Kapoukranidou, D., N. Gougoulias, A. Hatzisotiriou, D. Fardi, M. Albani and I. Kalpidis (2005). "Assessment of motoneuron death during development following neonatal nerve crush and Mg2+ treatment." *Med Sci Monit* 11(10): BR373-9.
Kariya, S., G. H. Park, Y. Maeno-Hikichi, O. Leykekhman, C. Lutz, M. S. Arkovitz, L. T. Landmesser and U. R. Monani (2008). "Reduced SMN protein impairs maturation of the neuromuscular junctions in mouse models of spinal muscular atrophy." *Hum Mol Genet* 17(16): 2552-69.
Kashima, T. and J. L. Manley (2003). "A negative element in SMN2 exon 7 inhibits splicing in spinal muscular atrophy." *Nat Genet* 34(4): 460-3.
Kholmanskikh, S. S., J. S. Dobrin, A. Wynshaw-Boris, P. C. Letourneau and M. E. Ross (2003). "Disregulated RhoGTPases and actin cytoskeleton contribute to the migration defect in Lis1-deficient neurons." *J Neurosci* 23(25): 8673-81.
Kim, A., K. Miller, J. Jo, G. Kilimnik, P. Wojcik and M. Hara (2009). "Islet architecture: A comparative study." *Islets* 1(2): 129-36.
Kishi, T., Y. Hirooka, A. Masumoto, K. Ito, Y. Kimura, K. Inokuchi, T. Tagawa, H. Shimokawa, A. Takeshita and K. Sunagawa (2005). "Rho-kinase inhibitor improves increased vascular resistance and impaired vasodilation of the forearm in patients with heart failure." *Circulation* 111(21): 2741-7.
Kishida, S., H. Yamamoto and A. Kikuchi (2004). "Wnt-3a and Dvl induce neurite retraction by activating Rho-associated kinase." *Mol Cell Biol* 24(10): 4487-501.
Knapp, J. R., J. K. Davie, A. Myer, E. Meadows, E. N. Olson and W. H. Klein (2006). "Loss of myogenin in postnatal life leads to normal skeletal muscle but reduced body size." *Development* 133(4): 601-10.

Kong, L., X. Wang, D. W. Choe, M. Polley, B. G. Burnett, M. Bosch-Marce, J. W. Griffin, M. M. Rich and C. J. Sumner (2009). "Impaired synaptic vesicle release and immaturity of neuromuscular junctions in spinal muscular atrophy mice." *J Neurosci* 29(3): 842-51.

Kowluru, A., M. E. Rabaglia, K. E. Muse and S. A. Metz (1994). "Subcellular localization and kinetic characterization of guanine nucleotide binding proteins in normal rat and human pancreatic islets and transformed beta cells." *Biochim Biophys Acta* 1222(3): 348-59.

Kraemer, W. J. Z., Vladimir M. (2006). Science and practice of strength training. Il, Champaign.

Kranenburg, O., M. Poland, M. Gebbink, L. Oomen and W. H. Moolenaar (1997). "Dissociation of LPA-induced cytoskeletal contraction from stress fiber formation by differential localization of RhoA." *J Cell Sci* 110 (Pt 19): 2417-27.

Lambrechts, A., A. Braun, V. Jonckheere, A. Aszodi, L. M. Lanier, J. Robbens, I. Van Colen, J. Vandekerckhove, R. Fassler and C. Ampe (2000). "Profilin II is alternatively spliced, resulting in profilin isoforms that are differentially expressed and have distinct biochemical properties." *Mol Cell Biol* 20(21): 8209-19.

Le, T. T., D. D. Coovert, U. R. Monani, G. E. Morris and A. H. Burghes (2000). "The survival motor neuron (SMN) protein: effect of exon loss and mutation on protein localization." *Neurogenetics* 3(1): 7-16.

Le, T. T., L. T. Pham, M. E. Butchbach, H. L. Zhang, U. R. Monani, D. D. Coovert, T. O. Gavrilina, L. Xing, G. J. Bassell and A. H. Burghes (2005). "SMNDelta7, the major product of the centromeric survival motor neuron (SMN2) gene, extends survival in mice with spinal muscular atrophy and associates with full-length SMN." *Hum Mol Genet* 14(6): 845-57.

Le, T. T., V. L. McGovern, I. E. Alwine, X. Wang, A. Massoni-Laporte, M. M. Rich and A. H. Burghes (2011). "Temporal requirement for high SMN expression in SMA mice." *Hum Mol Genet* 20(18): 3578-91.

Lee, C. W., J. Han, J. R. Bamburg, L. Han, R. Lynn and J. Q. Zheng (2009). "Regulation of acetylcholine receptor clustering by ADF/cofilin-directed vesicular trafficking." *Nat Neurosci* 12(7): 848-56.

Lefebvre, S., L. Burglen, S. Reboullet, O. Clermont, P. Burlet, L. Viollet, B. Benichou, C. Cruaud, P. Millasseau, M. Zeviani and et al. (1995). "Identification and characterization of a spinal muscular atrophy-determining gene." *Cell* 80(1): 155-65.

Lefebvre, S., P. Burlet, Q. Liu, S. Bertrandy, O. Clermont, A. Munnich, G. Dreyfuss and J. Melki (1997). "Correlation between severity and SMN protein level in spinal muscular atrophy." *Nat Genet* 16(3): 265-9.

Lefebvre, S., P. Burlet, L. Viollet, S. Bertrandy, C. Huber, C. Belser and A. Munnich (2002). "A novel association of the SMN protein with two major non-ribosomal nucleolar proteins and its implication in spinal muscular atrophy." *Hum Mol Genet* 11(9): 1017-27.

Lerma, J. (2003). "Roles and rules of kainate receptors in synaptic transmission." *Nat Rev Neurosci* 4(6): 481-95.

Li, L., L. J. Houenou, W. Wu, M. Lei, D. M. Prevette and R. W. Oppenheim (1998). "Characterization of spinal motoneuron degeneration following different types of peripheral nerve injury in neonatal and adult mice." *J Comp Neurol* 396(2): 158-68.

Lin, C. S., R. H. Aebersold, S. B. Kent, M. Varma and J. Leavitt (1988). "Molecular cloning and characterization of plastin, a human leukocyte protein expressed in transformed human fibroblasts." *Mol Cell Biol* 8(11): 4659-68.

Lin, W., R. W. Burgess, B. Dominguez, S. L. Pfaff, J. R. Sanes and K. F. Lee (2001). "Distinct roles of nerve and muscle in postsynaptic differentiation of the neuromuscular synapse." *Nature* 410(6832): 1057-64.

Ling, K. K., N. L. Siow, R. C. Choi, A. K. Ting, L. W. Kong and K. W. Tsim (2004). "ATP potentiates agrin-induced AChR aggregation in cultured myotubes: activation of RhoA in P2Y1 nucleotide receptor signaling at vertebrate neuromuscular junctions." *J Biol Chem* 279(30): 31081-8.

Ling, K. K., M. Y. Lin, B. Zingg, Z. Feng and C. P. Ko (2010). "Synaptic defects in the spinal and neuromuscular circuitry in a mouse model of spinal muscular atrophy." *PLoS One* 5(11): e15457.

Ling, K. K., R. M. Gibbs, Z. Feng and C. P. Ko (2011). "Severe neuromuscular denervation of clinically relevant muscles in a mouse model of spinal muscular atrophy." *Hum Mol Genet*.

Liu, H., A. Beauvais, A. N. Baker, C. Tsilfidis and R. Kothary (2010a). "Smn deficiency causes neuritogenesis and neurogenesis defects in the retinal neurons of a mouse model of spinal muscular atrophy." *Dev Neurobiol* 71(2): 153-69.

Liu, H., D. Shafey, J. N. Moores and R. Kothary (2010b). "Neurodevelopmental consequences of Smn depletion in a mouse model of spinal muscular atrophy." *J Neurosci Res* 88(1): 111-22.

Liu, Q. and G. Dreyfuss (1996). "A novel nuclear structure containing the survival of motor neurons protein." *EMBO J* 15(14): 3555-65.

Liu, Q., U. Fischer, F. Wang and G. Dreyfuss (1997). "The spinal muscular atrophy disease gene product, SMN, and its associated protein SIP1 are in a complex with spliceosomal snRNP proteins." *Cell* 90(6): 1013-21.

Liu, Z., W. Kim, Z. Chen, Y. K. Shin, O. D. Carlson, J. L. Fiori, L. Xin, J. K. Napora, R. Short, J. O. Odetunde, Q. Lao and J. M. Egan (2011). "Insulin and glucagon regulate pancreatic alpha-cell proliferation." *PLoS One* 6(1): e16096.

Lorson, C. L. and E. J. Androphy (1998a). "The domain encoded by exon 2 of the survival motor neuron protein mediates nucleic acid binding." *Hum Mol Genet* 7(8): 1269-75.

Lorson, C. L., J. Strasswimmer, J. M. Yao, J. D. Baleja, E. Hahnen, B. Wirth, T. Le, A. H. Burghes and E. J. Androphy (1998b). "SMN oligomerization defect correlates with spinal muscular atrophy severity." *Nat Genet* 19(1): 63-6.

Lorson, C. L., E. Hahnen, E. J. Androphy and B. Wirth (1999). "A single nucleotide in the SMN gene regulates splicing and is responsible for spinal muscular atrophy." *Proc Natl Acad Sci U S A* 96(11): 6307-11.

Luo, L., L. Y. Jan and Y. N. Jan (1997). "Rho family GTP-binding proteins in growth cone signalling." *Curr Opin Neurobiol* 7(1): 81-6.

Luo, L. (2002). "Actin cytoskeleton regulation in neuronal morphogenesis and structural plasticity." *Annu Rev Cell Dev Biol* 18: 601-35.

Luo, L. and D. D. O'Leary (2005). "Axon retraction and degeneration in development and disease." *Annu Rev Neurosci* 28: 127-56.

MacLeod, M. J., J. E. Taylor, P. W. Lunt, C. G. Mathew and S. A. Robb (1999). "Prenatal onset spinal muscular atrophy." *Eur J Paediatr Neurol* 3(2): 65-72.

Maekawa, M., T. Ishizaki, S. Boku, N. Watanabe, A. Fujita, A. Iwamatsu, T. Obinata, K. Ohashi, K. Mizuno and S. Narumiya (1999). "Signaling from Rho to the actin cytoskeleton through protein kinases ROCK and LIM-kinase." *Science* 285(5429): 895-8.

Margolis, S. S., J. Salogiannis, D. M. Lipton, C. Mandel-Brehm, Z. P. Wills, A. R. Mardinly, L. Hu, P. L. Greer, J. B. Bikoff, H. Y. Ho, M. J. Soskis, M. Sahin and M. E. Greenberg (2010). "EphB-mediated degradation of the RhoA GEF Ephexin5 relieves a developmental brake on excitatory synapse formation." *Cell* 143(3): 442-55.

Marks, B., M. H. Stowell, Y. Vallis, I. G. Mills, A. Gibson, C. R. Hopkins and H. T. McMahon (2001). "GTPase activity of dynamin and resulting conformation change are essential for endocytosis." *Nature* 410(6825): 231-5.

Martinez-Hernandez, R., C. Soler-Botija, E. Also, L. Alias, L. Caselles, I. Gich, S. Bernal and E. F. Tizzano (2009). "The developmental pattern of myotubes in spinal muscular atrophy indicates prenatal delay of muscle maturation." *J Neuropathol Exp Neurol* 68(5): 474-81.

Masumoto, A., M. Mohri, H. Shimokawa, L. Urakami, M. Usui and A. Takeshita (2002). "Suppression of coronary artery spasm by the Rho-kinase inhibitor fasudil in patients with vasospastic angina." *Circulation* 105(13): 1545-7.

Matera, A. G., R. M. Terns and M. P. Terns (2007). "Non-coding RNAs: lessons from the small nuclear and small nucleolar RNAs." *Nat Rev Mol Cell Biol* 8(3): 209-20.

Mattaj, I. W. (1988). U snRNP assembly and transport. Structure and Function of Major and Minor Small Nuclear Ribonucleoprotein Particles. M. Birnstiel. Berlin/New York, Springer Verlag**:** 100114.

Mattis, V. B., M. Bowerman, R. Kothary and C. L. Lorson (2008). "A SMNDelta7 read-through product confers functionality to the SMNDelta7 protein." *Neurosci Lett* 442(1): 54-8.

Matus, A., M. Ackermann, G. Pehling, H. R. Byers and K. Fujiwara (1982). "High actin concentrations in brain dendritic spines and postsynaptic densities." *Proc Natl Acad Sci U S A* 79(23): 7590-4.

McGovern, V. L., T. O. Gavrilina, C. E. Beattie and A. H. Burghes (2008). "Embryonic motor axon development in the severe SMA mouse." *Hum Mol Genet* 17(18): 2900-9.

McWhorter, M. L., U. R. Monani, A. H. Burghes and C. E. Beattie (2003). "Knockdown of the survival motor neuron (Smn) protein in zebrafish causes defects in motor axon outgrowth and pathfinding." *J Cell Biol* 162(5): 919-31.

Meister, G., D. Buhler, R. Pillai, F. Lottspeich and U. Fischer (2001a). "A multiprotein complex mediates the ATP-dependent assembly of spliceosomal U snRNPs." *Nat Cell Biol* 3(11): 945-9.

Meister, G., C. Eggert, D. Buhler, H. Brahms, C. Kambach and U. Fischer (2001b). "Methylation of Sm proteins by a complex containing PRMT5 and the putative U snRNP assembly factor pICln." *Curr Biol* 11(24): 1990-4.

Meister, G., C. Eggert and U. Fischer (2002). "SMN-mediated assembly of RNPs: a complex story." *Trends Cell Biol* 12(10): 472-8.

Menke, L. A., B. T. Poll-The, S. A. Clur, C. M. Bilardo, A. C. van der Wal, H. H. Lemmink and J. M. Cobben (2008). "Congenital heart defects in spinal muscular atrophy type I: a

clinical report of two siblings and a review of the literature." *Am J Med Genet A* 146A(6): 740-4.

Miguel-Aliaga, I., E. Culetto, D. S. Walker, H. A. Baylis, D. B. Sattelle and K. E. Davies (1999). "The Caenorhabditis elegans orthologue of the human gene responsible for spinal muscular atrophy is a maternal product critical for germline maturation and embryonic viability." *Hum Mol Genet* 8(12): 2133-43.

Miguel-Aliaga, I., Y. B. Chan, K. E. Davies and M. van den Heuvel (2000). "Disruption of SMN function by ectopic expression of the human SMN gene in Drosophila." *FEBS Lett* 486(2): 99-102.

Moller, P., N. Moe, O. D. Saugstad, K. Skullerud, M. Velken, K. Berg, S. Nitter-Hauge and A. L. Borresen (1990). "Spinal muscular atrophy type I combined with atrial septal defect in three sibs." *Clin Genet* 38(2): 81-3.

Monani, U. R., C. L. Lorson, D. W. Parsons, T. W. Prior, E. J. Androphy, A. H. Burghes and J. D. McPherson (1999a). "A single nucleotide difference that alters splicing patterns distinguishes the SMA gene SMN1 from the copy gene SMN2." *Hum Mol Genet* 8(7): 1177-83.

Monani, U. R., J. D. McPherson and A. H. Burghes (1999b). "Promoter analysis of the human centromeric and telomeric survival motor neuron genes (SMNC and SMNT)." *Biochim Biophys Acta* 1445(3): 330-6.

Monani, U. R., D. D. Coovert and A. H. Burghes (2000a). "Animal models of spinal muscular atrophy." *Hum Mol Genet* 9(16): 2451-7.

Monani, U. R., M. Sendtner, D. D. Coovert, D. W. Parsons, C. Andreassi, T. T. Le, S. Jablonka, B. Schrank, W. Rossoll, T. W. Prior, G. E. Morris and A. H. Burghes (2000b). "The human centromeric survival motor neuron gene (SMN2) rescues embryonic lethality in Smn(-/-) mice and results in a mouse with spinal muscular atrophy." *Hum Mol Genet* 9(3): 333-9.

Mondin, M., M. Carta, E. Normand, C. Mulle and F. Coussen (2010). "Profilin II regulates the exocytosis of kainate glutamate receptors." *J Biol Chem* 285(51): 40060-71.

Mouaikel, J., C. Verheggen, E. Bertrand, J. Tazi and R. Bordonne (2002). "Hypermethylation of the cap structure of both yeast snRNAs and snoRNAs requires a conserved methyltransferase that is localized to the nucleolus." *Mol Cell* 9(4): 891-901.

Mouaikel, J., U. Narayanan, C. Verheggen, A. G. Matera, E. Bertrand, J. Tazi and R. Bordonne (2003). "Interaction between the small-nuclear-RNA cap hypermethylase and the spinal muscular atrophy protein, survival of motor neuron." *EMBO Rep* 4(6): 616-22.

Mueller, B. K. (1999). "Growth cone guidance: first steps towards a deeper understanding." *Annu Rev Neurosci* 22: 351-88.

Munsat, T. L. and K. E. Davies (1992). "International SMA consortium meeting. (26-28 June 1992, Bonn, Germany)." *Neuromuscul Disord* 2(5-6): 423-8.

Murray, L. M., L. H. Comley, D. Thomson, N. Parkinson, K. Talbot and T. H. Gillingwater (2008). "Selective vulnerability of motor neurons and dissociation of pre- and post-synaptic pathology at the neuromuscular junction in mouse models of spinal muscular atrophy." *Hum Mol Genet* 17(7): 949-62.

Murray, L. M., S. Lee, D. Baumer, S. H. Parson, K. Talbot and T. H. Gillingwater (2009). "Pre-symptomatic development of lower motor neuron connectivity in a mouse model of severe spinal muscular atrophy." *Hum Mol Genet* 19(3): 420-33.

Murray, L. M., T. H. Gillingwater and S. H. Parson (2010a). "Using mouse cranial muscles to investigate neuromuscular pathology in vivo." *Neuromuscul Disord*.

Murray, L. M., S. Lee, D. Baumer, S. H. Parson, K. Talbot and T. H. Gillingwater (2010b). "Pre-symptomatic development of lower motor neuron connectivity in a mouse model of severe spinal muscular atrophy." *Hum Mol Genet* 19(3): 420-33.

Murray, L. M., K. Talbot and T. H. Gillingwater (2010c). "Review: neuromuscular synaptic vulnerability in motor neurone disease: amyotrophic lateral sclerosis and spinal muscular atrophy." *Neuropathol Appl Neurobiol* 36(2): 133-56.

Murray, L. M., L. H. Comley, T. H. Gillingwater and S. H. Parson (2011). "The response of neuromuscular junctions to injury is developmentally regulated." *FASEB J*.

Mutsaers, C. A., T. M. Wishart, D. J. Lamont, M. Riessland, J. Schreml, L. H. Comley, L. M. Murray, S. H. Parson, H. Lochmuller, B. Wirth, K. Talbot and T. H. Gillingwater (2011). "Reversible molecular pathology of skeletal muscle in spinal muscular atrophy." *Hum Mol Genet*.

Nakagawa, O., K. Fujisawa, T. Ishizaki, Y. Saito, K. Nakao and S. Narumiya (1996). "ROCK-I and ROCK-II, two isoforms of Rho-associated coiled-coil forming protein serine/threonine kinase in mice." *FEBS Lett* 392(2): 189-93.

Nakamura, Y., H. Kaneto, T. Miyatsuka, T. A. Matsuoka, M. Matsuhisa, K. Node, M. Hori and Y. Yamasaki (2006). "Marked increase of insulin gene transcription by suppression of the Rho/Rho-kinase pathway." *Biochem Biophys Res Commun* 350(1): 68-73.

Nakayama, Y. and Y. Aoki (2000). "Mechanism responsible for the formation of focal swellings on injured neuronal processes using a novel in vitro model of axonal injury." *Forensic Sci Int* 113(1-3): 245-9.

Narayanan, U., J. K. Ospina, M. R. Frey, M. D. Hebert and A. G. Matera (2002). "SMN, the spinal muscular atrophy protein, forms a pre-import snRNP complex with snurportin1 and importin beta." *Hum Mol Genet* 11(15): 1785-95.

Narayanan, U., T. Achsel, R. Luhrmann and A. G. Matera (2004). "Coupled in vitro import of U snRNPs and SMN, the spinal muscular atrophy protein." *Mol Cell* 16(2): 223-34.

Narver, H. L., L. Kong, B. G. Burnett, D. W. Choe, M. Bosch-Marce, A. A. Taye, M. A. Eckhaus and C. J. Sumner (2008). "Sustained improvement of spinal muscular atrophy mice treated with trichostatin A plus nutrition." *Ann Neurol* 64(4): 465-70.

Negishi, M. and H. Katoh (2002). "Rho family GTPases as key regulators for neuronal network formation." *J Biochem (Tokyo)* 132(2): 157-66.

Nevins, A. K. and D. C. Thurmond (2003). "Glucose regulates the cortical actin network through modulation of Cdc42 cycling to stimulate insulin secretion." *Am J Physiol Cell Physiol* 285(3): C698-710.

Nevins, A. K. and D. C. Thurmond (2005). "A direct interaction between Cdc42 and vesicle-associated membrane protein 2 regulates SNARE-dependent insulin exocytosis." *J Biol Chem* 280(3): 1944-52.

Ning, K., C. Drepper, C. F. Valori, M. Ahsan, M. Wyles, A. Higginbottom, T. Herrmann, P. Shaw, M. Azzouz and M. Sendtner (2010). "PTEN depletion rescues axonal growth

defect and improves survival in SMN-deficient motor neurons." *Hum Mol Genet* 19(16): 3159-68.
Nishiyama, T., I. Kii and A. Kudo (2004). "Inactivation of Rho/ROCK signaling is crucial for the nuclear accumulation of FKHR and myoblast fusion." *J Biol Chem* 279(45): 47311-9.
Nolle, A., A. Zeug, J. van Bergeijk, L. Tonges, R. Gerhard, H. Brinkmann, S. Al Rayes, N. Hensel, Y. Schill, D. Apkhazava, S. Jablonka, J. Omer, R. K. Srivastav, A. Baasner, P. Lingor, B. Wirth, E. Ponimaskin, R. Niedenthal, C. Grothe and P. Claus (2011). "The Spinal Muscular Atrophy disease protein SMN is linked to the Rho-kinase pathway via profilin." *Hum Mol Genet*.
Nusser, N., E. Gosmanova, Y. Zheng and G. Tigyi (2002). "Nerve growth factor signals through TrkA, phosphatidylinositol 3-kinase, and Rac1 to inactivate RhoA during the initiation of neuronal differentiation of PC12 cells." *J Biol Chem* 277(39): 35840-6.
Ono, S., N. Minami, H. Abe and T. Obinata (1994). "Characterization of a novel cofilin isoform that is predominantly expressed in mammalian skeletal muscle." *J Biol Chem* 269(21): 15280-6.
Oprea, G. E., S. Krober, M. L. McWhorter, W. Rossoll, S. Muller, M. Krawczak, G. J. Bassell, C. E. Beattie and B. Wirth (2008). "Plastin 3 is a protective modifier of autosomal recessive spinal muscular atrophy." *Science* 320(5875): 524-7.
Pagliardini, S., A. Giavazzi, V. Setola, C. Lizier, M. Di Luca, S. DeBiasi and G. Battaglia (2000). "Subcellular localization and axonal transport of the survival motor neuron (SMN) protein in the developing rat spinal cord." *Hum Mol Genet* 9(1): 47-56.
Pascale, A., P. A. Gusev, M. Amadio, T. Dottorini, S. Govoni, D. L. Alkon and A. Quattrone (2004). "Increase of the RNA-binding protein HuD and posttranscriptional up-regulation of the GAP-43 gene during spatial memory." *Proc Natl Acad Sci U S A* 101(5): 1217-22.
Passini, M. A. and S. H. Cheng (2011). "Prospects for the gene therapy of spinal muscular atrophy." *Trends Mol Med* 17(5): 259-65.
Paushkin, S., B. Charroux, L. Abel, R. A. Perkinson, L. Pellizzoni and G. Dreyfuss (2000). "The survival motor neuron protein of Schizosacharomyces pombe. Conservation of survival motor neuron interaction domains in divergent organisms." *J Biol Chem* 275(31): 23841-6.
Paushkin, S., A. K. Gubitz, S. Massenet and G. Dreyfuss (2002). "The SMN complex, an assemblyosome of ribonucleoproteins." *Curr Opin Cell Biol* 14(3): 305-12.
Pearn, J. (1978a). "Genetic studies of acute infantile spinal muscular atrophy (SMA type I). An analysis of sex ratios, segregation ratios, and sex influence." *J Med Genet* 15(6): 414-7.
Pearn, J. (1978b). "Incidence, prevalence, and gene frequency studies of chronic childhood spinal muscular atrophy." *J Med Genet* 15(6): 409-13.
Pearn, J. (1980). "Classification of spinal muscular atrophies." *Lancet* 1(8174): 919-22.
Pellizzoni, L., N. Kataoka, B. Charroux and G. Dreyfuss (1998). "A novel function for SMN, the spinal muscular atrophy disease gene product, in pre-mRNA splicing." *Cell* 95(5): 615-24.
Pellizzoni, L., B. Charroux and G. Dreyfuss (1999). "SMN mutants of spinal muscular atrophy patients are defective in binding to snRNP proteins." *Proc Natl Acad Sci U S A* 96(20): 11167-72.

Pellizzoni, L., J. Baccon, B. Charroux and G. Dreyfuss (2001a). "The survival of motor neurons (SMN) protein interacts with the snoRNP proteins fibrillarin and GAR1." *Curr Biol* 11(14): 1079-88.

Pellizzoni, L., B. Charroux, J. Rappsilber, M. Mann and G. Dreyfuss (2001b). "A functional interaction between the survival motor neuron complex and RNA polymerase II." *J Cell Biol* 152(1): 75-85.

Pellizzoni, L., J. Yong and G. Dreyfuss (2002). "Essential role for the SMN complex in the specificity of snRNP assembly." *Science* 298(5599): 1775-9.

Peter, C. J., M. Evans, V. Thayanithy, N. Taniguchi-Ishigaki, I. Bach, A. Kolpak, G. J. Bassell, W. Rossoll, C. L. Lorson, Z. Z. Bao and E. J. Androphy (2011). "The COPI vesicle complex binds and moves with survival motor neuron within axons." *Hum Mol Genet* 20(9): 1701-11.

Piccoli, G., U. Rutishauser and J. L. Bruses (2004). "N-cadherin juxtamembrane domain modulates voltage-gated Ca2+ current via RhoA GTPase and Rho-associated kinase." *J Neurosci* 24(48): 10918-23.

Pick, A., J. Clark, C. Kubstrup, M. Levisetti, W. Pugh, S. Bonner-Weir and K. S. Polonsky (1998). "Role of apoptosis in failure of beta-cell mass compensation for insulin resistance and beta-cell defects in the male Zucker diabetic fatty rat." *Diabetes* 47(3): 358-64.

Pilo Boyl, P., A. Di Nardo, C. Mulle, M. Sassoe-Pognetto, P. Panzanelli, A. Mele, M. Kneussel, V. Costantini, E. Perlas, M. Massimi, H. Vara, M. Giustetto and W. Witke (2007). "Profilin2 contributes to synaptic vesicle exocytosis, neuronal excitability, and novelty-seeking behavior." *Embo J* 26(12): 2991-3002.

Putz, U., C. Harwell and E. Nedivi (2005). "Soluble CPG15 expressed during early development rescues cortical progenitors from apoptosis." *Nat Neurosci* 8(3): 322-31.

Quarfordt, S. H., D. C. DeVivo, W. K. Engel, R. I. Levy and D. S. Fredrickson (1970). "Familial adult-onset proximal spinal muscular atrophy. Report of a family with type II hyperlipoproteinemia." *Arch Neurol* 22(6): 541-9.

Rajendra, T. K., G. B. Gonsalvez, M. P. Walker, K. B. Shpargel, H. K. Salz and A. G. Matera (2007). "A Drosophila melanogaster model of spinal muscular atrophy reveals a function for SMN in striated muscle." *J Cell Biol* 176(6): 831-41.

Ramakers, G. J. (2002). "Rho proteins, mental retardation and the cellular basis of cognition." *Trends Neurosci* 25(4): 191-9.

Ramji, N., C. Toth, J. Kennedy and D. W. Zochodne (2007). "Does diabetes mellitus target motor neurons?" *Neurobiol Dis* 26(2): 301-11.

Ranke, M. B. (2005). "Insulin-like growth factor-I treatment of growth disorders, diabetes mellitus and insulin resistance." *Trends Endocrinol Metab* 16(4): 190-7.

Reeve, S. P., L. Bassetto, G. K. Genova, Y. Kleyner, M. Leyssen, F. R. Jackson and B. A. Hassan (2005). "The Drosophila fragile X mental retardation protein controls actin dynamics by directly regulating profilin in the brain." *Curr Biol* 15(12): 1156-63.

Rehfeldt, C., G. Ott, D. E. Gerrard, L. Varga, W. Schlote, J. L. Williams, U. Renne and L. Bunger (2005). "Effects of the compact mutant myostatin allele Mstn (Cmpt-dl1Abc) introgressed into a high growth mouse line on skeletal muscle cellularity." *J Muscle Res Cell Motil* 26(2-3): 103-12.

Riessland, M., L. Brichta, E. Hahnen and B. Wirth (2006). "The benzamide M344, a novel histone deacetylase inhibitor, significantly increases SMN2 RNA/protein levels in spinal muscular atrophy cells." *Hum Genet* 120(1): 101-10.

Rivellese, A. A., C. De Natale and S. Lilli (2002). "Type of dietary fat and insulin resistance." *Ann N Y Acad Sci* 967: 329-35.

Rochette, C. F., N. Gilbert and L. R. Simard (2001). "SMN gene duplication and the emergence of the SMN2 gene occurred in distinct hominids: SMN2 is unique to Homo sapiens." *Hum Genet* 108(3): 255-66.

Rodal, A. A., R. N. Motola-Barnes and J. T. Littleton (2008). "Nervous wreck and Cdc42 cooperate to regulate endocytic actin assembly during synaptic growth." *J Neurosci* 28(33): 8316-25.

Rojas, A., A. Khoo, J. R. Tejedo, F. J. Bedoya, B. Soria and F. Martin (2010). "Islet cell development." *Adv Exp Med Biol* 654: 59-75.

Rorsman, P., S. A. Salehi, F. Abdulkader, M. Braun and P. E. MacDonald (2008). "K(ATP)-channels and glucose-regulated glucagon secretion." *Trends Endocrinol Metab* 19(8): 277-84.

Rose, F. F., Jr., V. B. Mattis, H. Rindt and C. L. Lorson (2009). "Delivery of recombinant follistatin lessens disease severity in a mouse model of spinal muscular atrophy." *Hum Mol Genet* 18(6): 997-1005.

Rosner, H., W. Moller, T. Wassermann, J. Mihatsch and M. Blum (2007). "Attenuation of actinomyosinII contractile activity in growth cones accelerates filopodia-guided and microtubule-based neurite elongation." *Brain Res* 1176: 1-10.

Rossoll, W., A. K. Kroning, U. M. Ohndorf, C. Steegborn, S. Jablonka and M. Sendtner (2002). "Specific interaction of Smn, the spinal muscular atrophy determining gene product, with hnRNP-R and gry-rbp/hnRNP-Q: a role for Smn in RNA processing in motor axons?" *Hum Mol Genet* 11(1): 93-105.

Rossoll, W., S. Jablonka, C. Andreassi, A. K. Kroning, K. Karle, U. R. Monani and M. Sendtner (2003). "Smn, the spinal muscular atrophy-determining gene product, modulates axon growth and localization of beta-actin mRNA in growth cones of motoneurons." *J Cell Biol* 163(4): 801-12.

Rudnik-Schoneborn, S., R. Heller, C. Berg, C. Betzler, T. Grimm, T. Eggermann, K. Eggermann, R. Wirth, B. Wirth and K. Zerres (2008). "Congenital heart disease is a feature of severe infantile spinal muscular atrophy." *J Med Genet* 45(10): 635-8.

Sakaba, T. and E. Neher (2003). "Involvement of actin polymerization in vesicle recruitment at the calyx of Held synapse." *J Neurosci* 23(3): 837-46.

Sanchez, J. C., V. Converset, A. Nolan, G. Schmid, S. Wang, M. Heller, M. V. Sennitt, D. F. Hochstrasser and M. A. Cawthorne (2002). "Effect of rosiglitazone on the differential expression of diabetes-associated proteins in pancreatic islets of C57Bl/6 lep/lep mice." *Mol Cell Proteomics* 1(7): 509-16.

Sanes, J. R. and J. W. Lichtman (1999). "Development of the vertebrate neuromuscular junction." *Annu Rev Neurosci* 22: 389-442.

Sanes, J. R. and J. W. Lichtman (2001). "Induction, assembly, maturation and maintenance of a postsynaptic apparatus." *Nat Rev Neurosci* 2(11): 791-805.

Sarner, S., R. Kozma, S. Ahmed and L. Lim (2000). "Phosphatidylinositol 3-kinase, Cdc42, and Rac1 act downstream of Ras in integrin-dependent neurite outgrowth in N1E-115 neuroblastoma cells." *Mol Cell Biol* 20(1): 158-72.

Satoh, K., Y. Fukumoto and H. Shimokawa (2011). "Rho-kinase: important new therapeutic target in cardiovascular diseases." *Am J Physiol Heart Circ Physiol* 301(2): H287-96.

Scaife, R. and R. L. Margolis (1990). "Biochemical and immunochemical analysis of rat brain dynamin interaction with microtubules and organelles in vivo and in vitro." *J Cell Biol* 111(6 Pt 2): 3023-33.

Schaefer, A. W., V. T. Schoonderwoert, L. Ji, N. Mederios, G. Danuser and P. Forscher (2008). "Coordination of actin filament and microtubule dynamics during neurite outgrowth." *Dev Cell* 15(1): 146-62.

Schmidt, A. and A. Hall (2002). "Guanine nucleotide exchange factors for Rho GTPases: turning on the switch." *Genes Dev* 16(13): 1587-609.

Schnell, E. and R. A. Nicoll (2001). "Hippocampal synaptic transmission and plasticity are preserved in myosin Va mutant mice." *J Neurophysiol* 85(4): 1498-501.

Schrank, B., R. Gotz, J. M. Gunnersen, J. M. Ure, K. V. Toyka, A. G. Smith and M. Sendtner (1997). "Inactivation of the survival motor neuron gene, a candidate gene for human spinal muscular atrophy, leads to massive cell death in early mouse embryos." *Proc Natl Acad Sci U S A* 94(18): 9920-5.

Sebok, A., N. Nusser, B. Debreceni, Z. Guo, M. F. Santos, J. Szeberenyi and G. Tigyi (1999). "Different roles for RhoA during neurite initiation, elongation, and regeneration in PC12 cells." *J Neurochem* 73(3): 949-60.

Sfakianos, M. K., A. Eisman, S. L. Gourley, W. D. Bradley, A. J. Scheetz, J. Settleman, J. R. Taylor, C. A. Greer, A. Williamson and A. J. Koleske (2007). "Inhibition of Rho via Arg and p190RhoGAP in the postnatal mouse hippocampus regulates dendritic spine maturation, synapse and dendrite stability, and behavior." *J Neurosci* 27(41): 10982-92.

Shababi, M., J. Habibi, H. T. Yang, S. M. Vale, W. A. Sewell and C. L. Lorson (2010a). "Cardiac defects contribute to the pathology of spinal muscular atrophy models." *Hum Mol Genet* 19(20): 4059-71.

Shababi, M., V. B. Mattis and C. L. Lorson (2010b). "Therapeutics that directly increase SMN expression to treat spinal muscular atrophy." *Drug News Perspect* 23(8): 475-82.

Shafey, D., P. D. Cote and R. Kothary (2005). "Hypomorphic Smn knockdown C2C12 myoblasts reveal intrinsic defects in myoblast fusion and myotube morphology." *Exp Cell Res* 311(1): 49-61.

Shafey, D., A. E. MacKenzie and R. Kothary (2008). "Neurodevelopmental abnormalities in neurosphere-derived neural stem cells from SMN-depleted mice." *J Neurosci Res* 86(13): 2839-47.

Shafey, D., J. G. Boyer, K. Bhanot and R. Kothary (2010). "Identification of novel interacting protein partners of SMN using tandem affinity purification." *J Proteome Res* 9(4): 1659-69.

Shanik, M. H., Y. Xu, J. Skrha, R. Dankner, Y. Zick and J. Roth (2008). "Insulin resistance and hyperinsulinemia: is hyperinsulinemia the cart or the horse?" *Diabetes Care* 31 Suppl 2: S262-8.

Shao, J., W. J. Welch, N. A. Diprospero and M. I. Diamond (2008). "Phosphorylation of profilin by ROCK1 regulates polyglutamine aggregation." *Mol Cell Biol* 28(17): 5196-208.

Sharma, A., A. Lambrechts, T. Hao le, T. T. Le, C. A. Sewry, C. Ampe, A. H. Burghes and G. E. Morris (2005). "A role for complexes of survival of motor neurons (SMN) protein with gemins and profilin in neurite-like cytoplasmic extensions of cultured nerve cells." *Exp Cell Res* 309(1): 185-97.

Shi, L., B. Butt, F. C. Ip, Y. Dai, L. Jiang, W. H. Yung, M. E. Greenberg, A. K. Fu and N. Y. Ip (2010). "Ephexin1 is required for structural maturation and neurotransmission at the neuromuscular junction." *Neuron* 65(2): 204-16.

Shimokawa, H., K. Hiramori, H. Iinuma, S. Hosoda, H. Kishida, H. Osada, T. Katagiri, K. Yamauchi, Y. Yui, T. Minamino, M. Nakashima and K. Kato (2002). "Anti-anginal effect of fasudil, a Rho-kinase inhibitor, in patients with stable effort angina: a multicenter study." *J Cardiovasc Pharmacol* 40(5): 751-61.

Shtrahman, M., C. Yeung, D. W. Nauen, G. Q. Bi and X. L. Wu (2005). "Probing vesicle dynamics in single hippocampal synapses." *Biophys J* 89(5): 3615-27.

Shupliakov, O., O. Bloom, J. S. Gustafsson, O. Kjaerulff, P. Low, N. Tomilin, V. A. Pieribone, P. Greengard and L. Brodin (2002). "Impaired recycling of synaptic vesicles after acute perturbation of the presynaptic actin cytoskeleton." *Proc Natl Acad Sci U S A* 99(22): 14476-81.

Sinnreich, M., E. J. Sorenson and C. J. Klein (2004). "Neurologic course, endocrine dysfunction and triplet repeat size in spinal bulbar muscular atrophy." *Can J Neurol Sci* 31(3): 378-82.

Somers, E., Z. Stencel, T. M. Wishart, T. H. Gillingwater and S. H. Parson (2011). "Density, calibre and ramification of muscle capillaries are altered in a mouse model of severe spinal muscular atrophy." *Neuromuscul Disord*.

Stefan, M., R. A. Simmons, S. Bertera, M. Trucco, F. Esni, P. Drain and R. D. Nicholls (2011). "Global deficits in development, function, and gene expression in the endocrine pancreas in a deletion mouse model of Prader-Willi syndrome." *Am J Physiol Endocrinol Metab* 300(5): E909-22.

Steven, R., L. Zhang, J. Culotti and T. Pawson (2005). "The UNC-73/Trio RhoGEF-2 domain is required in separate isoforms for the regulation of pharynx pumping and normal neurotransmission in C. elegans." *Genes Dev* 19(17): 2016-29.

Stiles, B. L., C. Kuralwalla-Martinez, W. Guo, C. Gregorian, Y. Wang, J. Tian, M. A. Magnuson and H. Wu (2006). "Selective deletion of Pten in pancreatic beta cells leads to increased islet mass and resistance to STZ-induced diabetes." *Mol Cell Biol* 26(7): 2772-81.

Stratigopoulos, G., P. Lanzano, L. Deng, J. Guo, P. Kaufmann, B. Darras, R. Finkel, R. Tawil, M. P. McDermott, W. Martens, D. C. Devivo and W. K. Chung (2010). "Association of plastin 3 expression with disease severity in spinal muscular atrophy only in postpubertal females." *Arch Neurol* 67(10): 1252-6.

Su, J. L., M. T. Lin, C. C. Hong, C. C. Chang, S. G. Shiah, C. W. Wu, S. T. Chen, Y. P. Chau and M. L. Kuo (2005). "Resveratrol induces FasL-related apoptosis through Cdc42 activation of ASK1/JNK-dependent signaling pathway in human leukemia HL-60 cells." *Carcinogenesis* 26(1): 1-10.

Suetsugu, S., H. Miki and T. Takenawa (1998). "The essential role of profilin in the assembly of actin for microspike formation." *Embo J* 17(22): 6516-26.
Sumi, T., K. Matsumoto, Y. Takai and T. Nakamura (1999). "Cofilin phosphorylation and actin cytoskeletal dynamics regulated by rho- and Cdc42-activated LIM-kinase 2." *J Cell Biol* 147(7): 1519-32.
Sumner, C. J., C. D. Wee, L. C. Warsing, D. W. Choe, A. S. Ng, C. Lutz and K. R. Wagner (2009). "Inhibition of myostatin does not ameliorate disease features of severe spinal muscular atrophy mice." *Hum Mol Genet* 18(17): 3145-52.
Sun, C. and J. Zhou (2008). "Trichostatin A improves insulin stimulated glucose utilization and insulin signaling transduction through the repression of HDAC2." *Biochem Pharmacol* 76(1): 120-7.
Suzuki, M., J. McHugh, C. Tork, B. Shelley, A. Hayes, I. Bellantuono, P. Aebischer and C. N. Svendsen (2008). "Direct muscle delivery of GDNF with human mesenchymal stem cells improves motor neuron survival and function in a rat model of familial ALS." *Mol Ther* 16(12): 2002-10.
Svoboda, M., L. Portois and W. J. Malaisse (1999). "Glucose regulation of the expression of the glucagon receptor gene." *Mol Genet Metab* 68(2): 258-67.
Szkudelski, T. and K. Szkudelska (2011). "Anti-diabetic effects of resveratrol." *Ann N Y Acad Sci* 1215: 34-9.
Tadesse, H., J. Deschenes-Furry, S. Boisvenue and J. Cote (2008). "KH-type splicing regulatory protein interacts with survival motor neuron protein and is misregulated in spinal muscular atrophy." *Hum Mol Genet* 17(4): 506-24.
Takano, H., I. Komuro, T. Oka, I. Shiojima, Y. Hiroi, T. Mizuno and Y. Yazaki (1998). "The Rho family G proteins play a critical role in muscle differentiation." *Mol Cell Biol* 18(3): 1580-9.
Takeda, S., N. Sato, K. Uchio-Yamada, K. Sawada, T. Kunieda, D. Takeuchi, H. Kurinami, M. Shinohara, H. Rakugi and R. Morishita (2010). "Diabetes-accelerated memory dysfunction via cerebrovascular inflammation and Abeta deposition in an Alzheimer mouse model with diabetes." *Proc Natl Acad Sci U S A* 107(15): 7036-41.
Talbot, K., C. P. Ponting, A. M. Theodosiou, N. R. Rodrigues, R. Surtees, R. Mountford and K. E. Davies (1997). "Missense mutation clustering in the survival motor neuron gene: a role for a conserved tyrosine and glycine rich region of the protein in RNA metabolism?" *Hum Mol Genet* 6(3): 497-500.
Taniguchi, C. M., B. Emanuelli and C. R. Kahn (2006). "Critical nodes in signalling pathways: insights into insulin action." *Nat Rev Mol Cell Biol* 7(2): 85-96.
Tein, I., A. E. Sloane, E. J. Donner, D. C. Lehotay, D. S. Millington and R. I. Kelley (1995). "Fatty acid oxidation abnormalities in childhood-onset spinal muscular atrophy: primary or secondary defect(s)?" *Pediatr Neurol* 12(1): 21-30.
Todd, A. G., R. Morse, D. J. Shaw, S. McGinley, H. Stebbings and P. J. Young (2010a). "SMN, Gemin2 and Gemin3 associate with beta-actin mRNA in the cytoplasm of neuronal cells in vitro." *J Mol Biol* 401(5): 681-9.
Todd, A. G., R. Morse, D. J. Shaw, H. Stebbings and P. J. Young (2010b). "Analysis of SMN-neurite granules: Core Cajal body components are absent from SMN-cytoplasmic complexes." *Biochem Biophys Res Commun* 397(3): 479-85.

Todd, A. G., D. J. Shaw, R. Morse, H. Stebbings and P. J. Young (2010c). "SMN and the Gemin proteins form sub-complexes that localise to both stationary and dynamic neurite granules." *Biochem Biophys Res Commun* 394(1): 211-6.

Torres-Benito, L., M. F. Neher, R. Cano, R. Ruiz and L. Tabares (2011). "SMN Requirement for Synaptic Vesicle, Active Zone and Microtubule Postnatal Organization in Motor Nerve Terminals." *PLoS One* 6(10): e26164.

Tsai, L. K., M. S. Tsai, C. H. Ting and H. Li (2008). "Multiple therapeutic effects of valproic acid in spinal muscular atrophy model mice." *J Mol Med* 86(11): 1243-54.

Tyc, K. and J. A. Steitz (1989). "U3, U8 and U13 comprise a new class of mammalian snRNPs localized in the cell nucleolus." *EMBO J* 8(10): 3113-9.

Uehata, M., T. Ishizaki, H. Satoh, T. Ono, T. Kawahara, T. Morishita, H. Tamakawa, K. Yamagami, J. Inui, M. Maekawa and S. Narumiya (1997). "Calcium sensitization of smooth muscle mediated by a Rho-associated protein kinase in hypertension." *Nature* 389(6654): 990-4.

van Bergeijk, J., K. Haastert, C. Grothe and P. Claus (2006). "Valproic acid promotes neurite outgrowth in PC12 cells independent from regulation of the survival of motoneuron protein." *Chem Biol Drug Des* 67(3): 244-7.

van Bergeijk, J., K. Rydel-Konecke, C. Grothe and P. Claus (2007). "The spinal muscular atrophy gene product regulates neurite outgrowth: importance of the C terminus." *FASEB J* 21(7): 1492-502.

van der Bliek, A. M. and E. M. Meyerowitz (1991). "Dynamin-like protein encoded by the Drosophila shibire gene associated with vesicular traffic." *Nature* 351(6325): 411-4.

Verkerk, A. J., M. Pieretti, J. S. Sutcliffe, Y. H. Fu, D. P. Kuhl, A. Pizzuti, O. Reiner, S. Richards, M. F. Victoria, F. P. Zhang and et al. (1991). "Identification of a gene (FMR-1) containing a CGG repeat coincident with a breakpoint cluster region exhibiting length variation in fragile X syndrome." *Cell* 65(5): 905-14.

Waerhaug, O. and H. Korneliussen (1974). "Morphological types of motor nerve terminals in rat hindlimb muscles, possibly innervating different muscle fiber types." *Z Anat Entwicklungsgesch* 144(3): 237-47.

Walker, J. N., R. Ramracheya, Q. Zhang, P. R. Johnson, M. Braun and P. Rorsman (2011). "Regulation of glucagon secretion by glucose: paracrine, intrinsic or both?" *Diabetes Obes Metab* 13 Suppl 1: 95-105.

Walker, M. P., T. K. Rajendra, L. Saieva, J. L. Fuentes, L. Pellizzoni and A. G. Matera (2008). "SMN complex localizes to the sarcomeric Z-disc and is a proteolytic target of calpain." *Hum Mol Genet* 17(21): 3399-410.

Wan, L., T. C. Dockendorff, T. A. Jongens and G. Dreyfuss (2000). "Characterization of dFMR1, a Drosophila melanogaster homolog of the fragile X mental retardation protein." *Mol Cell Biol* 20(22): 8536-47.

Wan, L., D. J. Battle, J. Yong, A. K. Gubitz, S. J. Kolb, J. Wang and G. Dreyfuss (2005). "The survival of motor neurons protein determines the capacity for snRNP assembly: biochemical deficiency in spinal muscular atrophy." *Mol Cell Biol* 25(13): 5543-51.

Wang, L., L. Xue, H. Yan, J. Li and Y. Lu (2009). "Effects of ROCK inhibitor, Y-27632, on adhesion and mobility in esophageal squamous cell cancer cells." *Mol Biol Rep*.

Wang, Z., E. Oh and D. C. Thurmond (2007). "Glucose-stimulated Cdc42 signaling is essential for the second phase of insulin secretion." *J Biol Chem* 282(13): 9536-46.
Wehner, K. A., L. Ayala, Y. Kim, P. J. Young, B. A. Hosler, C. L. Lorson, S. J. Baserga and J. W. Francis (2002). "Survival motor neuron protein in the nucleolus of mammalian neurons." *Brain Res* 945(2): 160-73.
Weston, C., B. Yee, E. Hod and J. Prives (2000). "Agrin-induced acetylcholine receptor clustering is mediated by the small guanosine triphosphatases Rac and Cdc42." *J Cell Biol* 150(1): 205-12.
Wierzbowska, J., J. Robaszkiewicz, M. Figurska and A. Stankiewicz (2010). "Future possibilities in glaucoma therapy." *Med Sci Monit* 16(11): RA252-9.
Will, C. L. and R. Luhrmann (2001). "Spliceosomal UsnRNP biogenesis, structure and function." *Curr Opin Cell Biol* 13(3): 290-301.
Williams, J. H., R. C. Schray, C. A. Patterson, S. O. Ayitey, M. K. Tallent and G. J. Lutz (2009). "Oligonucleotide-mediated survival of motor neuron protein expression in CNS improves phenotype in a mouse model of spinal muscular atrophy." *J Neurosci* 29(24): 7633-8.
Willmann, R., J. Dubach and K. Chen (2011). "Developing standard procedures for pre-clinical efficacy studies in mouse models of spinal muscular atrophy: report of the expert workshop "Pre-clinical testing for SMA", Zurich, March 29-30th 2010." *Neuromuscul Disord* 21(1): 74-7.
Winkler, C., C. Eggert, D. Gradl, G. Meister, M. Giegerich, D. Wedlich, B. Laggerbauer and U. Fischer (2005). "Reduced U snRNP assembly causes motor axon degeneration in an animal model for spinal muscular atrophy." *Genes Dev* 19(19): 2320-30.
Wirth, B., M. Herz, A. Wetter, S. Moskau, E. Hahnen, S. Rudnik-Schoneborn, T. Wienker and K. Zerres (1999). "Quantitative analysis of survival motor neuron copies: identification of subtle SMN1 mutations in patients with spinal muscular atrophy, genotype-phenotype correlation, and implications for genetic counseling." *Am J Hum Genet* 64(5): 1340-56.
Wirth, B. (2000). "An update of the mutation spectrum of the survival motor neuron gene (SMN1) in autosomal recessive spinal muscular atrophy (SMA)." *Hum Mutat* 15(3): 228-37.
Witke, W., A. V. Podtelejnikov, A. Di Nardo, J. D. Sutherland, C. B. Gurniak, C. Dotti and M. Mann (1998). "In mouse brain profilin I and profilin II associate with regulators of the endocytic pathway and actin assembly." *EMBO J* 17(4): 967-76.
Yamaguchi, H., M. Kasa, M. Amano, K. Kaibuchi and T. Hakoshima (2006). "Molecular mechanism for the regulation of rho-kinase by dimerization and its inhibition by fasudil." *Structure* 14(3): 589-600.
Yamaguchi, Y., H. Katoh, H. Yasui, K. Mori and M. Negishi (2001). "RhoA inhibits the nerve growth factor-induced Rac1 activation through Rho-associated kinase-dependent pathway." *J Biol Chem* 276(22): 18977-83.
Yan, H., W. Gu, J. Yang, V. Bi, Y. Shen, E. Lee, K. A. Winters, R. Komorowski, C. Zhang, J. J. Patel, D. Caughey, G. S. Elliott, Y. Y. Lau, J. Wang, Y. S. Li, T. Boone, R. A. Lindberg, S. Hu and M. M. Veniant (2009). "Fully human monoclonal antibodies antagonizing the glucagon receptor improve glucose homeostasis in mice and monkeys." *J Pharmacol Exp Ther* 329(1): 102-11.

Yang, C., M. Huang, J. DeBiasio, M. Pring, M. Joyce, H. Miki, T. Takenawa and S. H. Zigmond (2000). "Profilin enhances Cdc42-induced nucleation of actin polymerization." *J Cell Biol* 150(5): 1001-12.

Yang, X., S. Arber, C. William, L. Li, Y. Tanabe, T. M. Jessell, C. Birchmeier and S. J. Burden (2001). "Patterning of muscle acetylcholine receptor gene expression in the absence of motor innervation." *Neuron* 30(2): 399-410.

Young, P. J., T. T. Le, N. thi Man, A. H. Burghes and G. E. Morris (2000a). "The relationship between SMN, the spinal muscular atrophy protein, and nuclear coiled bodies in differentiated tissues and cultured cells." *Exp Cell Res* 256(2): 365-74.

Young, P. J., N. T. Man, C. L. Lorson, T. T. Le, E. J. Androphy, A. H. Burghes and G. E. Morris (2000b). "The exon 2b region of the spinal muscular atrophy protein, SMN, is involved in self-association and SIP1 binding." *Hum Mol Genet* 9(19): 2869-77.

Zhang, H., L. Xing, W. Rossoll, H. Wichterle, R. H. Singer and G. J. Bassell (2006). "Multiprotein complexes of the survival of motor neuron protein SMN with Gemins traffic to neuronal processes and growth cones of motor neurons." *J Neurosci* 26(33): 8622-32.

Zhang, H. L., F. Pan, D. Hong, S. M. Shenoy, R. H. Singer and G. J. Bassell (2003). "Active transport of the survival motor neuron protein and the role of exon-7 in cytoplasmic localization." *J Neurosci* 23(16): 6627-37.

Zhang, Z., F. Lotti, K. Dittmar, I. Younis, L. Wan, M. Kasim and G. Dreyfuss (2008). "SMN deficiency causes tissue-specific perturbations in the repertoire of snRNAs and widespread defects in splicing." *Cell* 133(4): 585-600.

Zochodne, D. W., N. Ramji and C. Toth (2008). "Neuronal targeting in diabetes mellitus: a story of sensory neurons and motor neurons." *Neuroscientist* 14(4): 311-8.